



University of Kentucky
UKnowledge

Theses and Dissertations--Chemical and
Materials Engineering

Chemical and Materials Engineering

2014

THERMO-CHEMICAL CONVERSION OF COAL-BIOMASS BLENDS: KINETICS MODELING OF PYROLYSIS, MOVING BED GASIFICATION AND STABLE CARBON ISOTOPE ANALYSIS

Abhijit Bhagavatula
University of Kentucky, abhijitbv@gmail.com

[Right click to open a feedback form in a new tab to let us know how this document benefits you.](#)

Recommended Citation

Bhagavatula, Abhijit, "THERMO-CHEMICAL CONVERSION OF COAL-BIOMASS BLENDS: KINETICS MODELING OF PYROLYSIS, MOVING BED GASIFICATION AND STABLE CARBON ISOTOPE ANALYSIS" (2014). *Theses and Dissertations--Chemical and Materials Engineering*. 43.
https://uknowledge.uky.edu/cme_etds/43

This Doctoral Dissertation is brought to you for free and open access by the Chemical and Materials Engineering at UKnowledge. It has been accepted for inclusion in Theses and Dissertations--Chemical and Materials Engineering by an authorized administrator of UKnowledge. For more information, please contact UKnowledge@lsv.uky.edu.

STUDENT AGREEMENT:

I represent that my thesis or dissertation and abstract are my original work. Proper attribution has been given to all outside sources. I understand that I am solely responsible for obtaining any needed copyright permissions. I have obtained needed written permission statement(s) from the owner(s) of each third-party copyrighted matter to be included in my work, allowing electronic distribution (if such use is not permitted by the fair use doctrine) which will be submitted to UKnowledge as Additional File.

I hereby grant to The University of Kentucky and its agents the irrevocable, non-exclusive, and royalty-free license to archive and make accessible my work in whole or in part in all forms of media, now or hereafter known. I agree that the document mentioned above may be made available immediately for worldwide access unless an embargo applies.

I retain all other ownership rights to the copyright of my work. I also retain the right to use in future works (such as articles or books) all or part of my work. I understand that I am free to register the copyright to my work.

REVIEW, APPROVAL AND ACCEPTANCE

The document mentioned above has been reviewed and accepted by the student's advisor, on behalf of the advisory committee, and by the Director of Graduate Studies (DGS), on behalf of the program; we verify that this is the final, approved version of the student's thesis including all changes required by the advisory committee. The undersigned agree to abide by the statements above.

Abhijit Bhagavatula, Student

Dr. Naresh Shah, Major Professor

Dr. Thomas Dziubla, Director of Graduate Studies

THERMO-CHEMICAL CONVERSION OF COAL-BIOMASS BLENDS:
KINETICS MODELING OF PYROLYSIS, MOVING BED GASIFICATION AND
STABLE CARBON ISOTOPE ANALYSIS

DISSERTATION

A dissertation submitted in partial fulfillment of the
requirements for the degree of Doctor of Philosophy in the
College of Engineering
at the University of Kentucky

By

Abhijit Bhagavatula
Lexington, Kentucky

Co-Directors: Dr. Naresh Shah, Professor of Chemical and Materials Engineering
and Dr. Gerald P. Huffman, Professor of Chemical and Materials Engineering

Lexington, Kentucky

Copyright © Abhijit Bhagavatula 2014

ABSTRACT OF DISSERTATION

THERMO-CHEMICAL CONVERSION OF COAL-BIOMASS BLENDS: KINETICS MODELING OF PYROLYSIS, MOVING BED GASIFICATION AND STABLE CARBON ISOTOPE ANALYSIS

The past few years have seen an upsurge in the use of renewable biomass as a source of energy due to growing concerns over greenhouse gas emissions caused by the combustion of fossil fuels and the need for energy independence due to depleting fossil fuel resources. Although coal will continue to be a major source of energy for many years, there is still great interest in replacing part of the coal used in energy generation with renewable biomass. Combustion converts inherent chemical energy of carbonaceous feedstock to only thermal energy. On the other hand, partial oxidation processes like gasification convert chemical energy into thermal energy as well as synthesis gas which can be easily stored or transported using existing infrastructure for downstream chemical conversion to higher value specialty chemicals as well as production of heat, hydrogen, and power.

Devolatilization or pyrolysis plays an important role during gasification and is considered to be the starting point for all heterogeneous gasification reactions. Pyrolysis kinetic modeling is, therefore, an important step in analyzing interactions between blended feedstocks. The thermal evolution profiles of different coal-biomass blends were investigated at various heating rates using thermogravimetric analysis. Using MATLAB, complex models for devolatilization of the blends were solved for obtaining and predicting the global kinetic parameters. Parallel first order reactions model, distributed activation energy model and matrix inversion algorithm were utilized and compared for this purpose. Using these global kinetic parameters, devolatilization rates of unknown fuel blends gasified at unknown heating rates can be accurately predicted using the matrix inversion method.

A unique laboratory scale auto-thermal moving bed gasifier was also designed and constructed for studying the thermochemical conversion of coal-biomass blends. The effect of varying operating parameters was analyzed for optimizing syngas production. In addition, stable carbon isotope analysis using Gas Chromatography-Combustion-Isotope

Ratio Mass Spectrometry (GC-C-IRMS) was used for qualitatively and quantitatively measuring individual contributions of coal and biomass feedstocks for generation of carbonaceous gases during gasification. The predictive models utilized and experimental data obtained via these methods can provide valuable information for analyzing synergistic interactions between feedstocks and also for process modeling and optimization.

KEYWORDS: Coal-Biomass Blends, Thermogravimetric Analysis, Kinetics Modeling, Moving Bed Gasification, Stable Carbon Isotope Analysis

Abhijit Bhagavatula

Student's Signature

November 10th, 2014

Date

THERMO-CHEMICAL CONVERSION OF COAL-BIOMASS BLENDS: KINETICS
MODELING OF PYROLYSIS, MOVING BED GASIFICATION AND STABLE
CARBON ISOTOPE ANALYSIS

By

Abhijit Bhagavatula

Dr. Naresh Shah

Co-Director of Dissertation

Dr. Gerald P. Huffman

Co-Director of Dissertation

Dr. Thomas Dziubla

Director of Graduate Studies

November 10th, 2014

Date

DEDICATED TO MY GRANDPARENTS

ACKNOWLEDGEMENTS

I have always believed that pursuing a doctoral degree is akin to undertaking a daunting expedition to ascend the pinnacle of planet Earth, Mt. Everest or an Olympian who trains tirelessly for long years to achieve "THAT" one medal. In my opinion, none of these endeavors can be accomplished single-handedly. The society tends to remember those for their success but forgets to applaud the efforts of the people that stood by and aided the individuals in achieving what they had aimed for. Now, as I reach the summit, I have a lot of people to thank, acknowledge and be indebted for making this journey a memorable experience. Without these people, I would not have achieved whatever miniscule I have achieved over the past four years and beyond.

First and foremost, I would like to express my deep and sincere gratitude for my research advisor and Committee Chair, Dr. Naresh Shah, for his constant support, guidance and encouragement during the course of this work and without whom this work would not have been possible. I cannot thank him enough for always being available despite being extremely busy. The excellent discussions that he has had with me over the years, not only pertaining to the subject but also sharing his experiences in general have been a constant motivation for me to think independently and perform better. I will be ever grateful to Dr. Shah for guiding me throughout, despite the terrain being bumpy along the way.

I am also extremely grateful to Dr. Gerald P. Huffman, head of CFFS and the Co-Chair of my doctoral advisory committee, for providing me with the initial financial support and allowing me to work at the CFFS laboratory. An extremely patient and encouraging professor, I thank him whole-heartedly for giving me the freedom to work independently and placing trust in my abilities.

Another important member of my advisory committee whose contribution I can never forget is Dr. Ricky Q. Honaker. I will always be indebted to him, not only because he provided me work and financial support during the second half of my PhD, but also for placing extreme trust, being ever helpful and always instilling confidence that was sometimes lacking within me. The faith and confidence that he placed brought about a huge wave of positiveness in me. I cannot express in words how much I am indebted to him for giving me the opportunity to work on research activities beyond this dissertation and beyond the realm of my expertise. Working with Dr. Honaker has truly been an enriching experience and helped me discover that an engineer working on his PhD is capable to work and excel in areas beyond his expertise.

In addition, I would like to extend my sincere gratitude to Dr. Douglass S. Kalika, Dr. Czarena L. Crofcheck and Dr. Jeffrey R. Seay for readily accepting to be a part of my doctoral advisory committee and providing me with valuable suggestions, guidance and sharing their insights at various stages of the program. I would also like to express my gratitude to Dr. Thomas Novak for agreeing to be the external examiner for my final examination.

Although not a part of my doctoral advisory committee, I would like to sincerely thank and acknowledge Dr. Christopher S. Romanek for introducing me to stable carbon isotope analysis and permitting me to use his laboratory and IRMS equipment at the Earth and Environmental Sciences Department, University of Kentucky. In addition, his contribution towards publishing this unique work is immense. Also, I would like to specially mention and whole-heartedly appreciate the guidance provided by Dr. Frank E. Huggins and Mr. Nicholas Cprek during the construction phase of the lab-scale gasifier at

the CFFS laboratory and helping me out whenever I hit a roadblock. I would also like to take this opportunity to thank all the faculty, staff and my fellow graduate students at the Department of Chemical and Materials Engineering for making this an enriching experience.

I would also particularly appreciate my buddies, Sumesh Sukumara, Venkat Narayan and Suvid Joshi, for always sharing their valuable insights and helping me broaden my knowledge base. A big thank you to all my friends in Lexington for making this ride so memorable that I would never forget a moment of this phase of my life. It would not be fair if I do not mention the support that I have had from my best buddies, Rahul, Vijay Sai, Rajiv and Aditi, for always taking time off from their busy lives and helping me out during stressful times. Above all, special words of appreciation for Saket Fadnavis and Nisha Kishor for putting up with me, being with me at all times and treating me like a member of their own respective families. I can and will never forget all that you have ever done for me.

This segment would be incomplete without me acknowledging the role played by the most important people in my life. Of paramount and supreme importance among them are my late grandparents, who have been great pillars of strength for me, who have nurtured and instilled great values in me during my formative years. Words fall short for me to describe how much I love and miss them. I know that I will always be blessed by them wherever they are. My sincere gratitude to my parents and sister who have always supported me, encouraged me and stood by me in whatever I have done through my life. I would not have made it this far without the hard work and sacrifices made by my parents. Last but not the least, my deepest and sincere thanks to my parents-in-law and my loving

and caring wife, Mayuri Mukka, for being extremely patient with me and providing all the support and encouragement that I needed during times of stress and distress. These experiences that I have had, truly speaking, would hold me in good stead as I further my professional career and move along in my personal life.

TABLE OF CONTENTS

ACKNOWLEDGEMENTS	III
LIST OF FIGURES	XI
LIST OF TABLES	XVII
CHAPTER 1: INTRODUCTION AND BACKGROUND	1
1.1 Global Energy Concerns	1
1.2 Biomass as a Source for Energy	3
1.2.1 Classification of Biomass	6
1.2.2 Resource Assessment of Biomass.....	7
1.3 Gasification.....	9
1.4 Co-Gasification of Coal and Biomass.....	13
1.5 Downstream Processing of Syngas.....	16
1.6 Types of Gasifiers and Applications.....	17
1.6.1 Moving Bed Gasifier.....	18
1.6.2 Fluidized Bed Gasifier	20
1.6.3 Entrained Bed Gasifier.....	21
1.7 Gasification Processes	22
1.7.1 Pyrolysis or Devolatilization.....	23
1.7.2 Reaction of Volatiles.....	24
1.7.3 Char Gasification	25
1.8 Chemical Reactions During Gasification.....	26
1.9 Kinetic Modeling	30
1.10 Research Objectives.....	36

CHAPTER 2: THERMOGRAVIMETRIC ANALYSIS OF COAL-BIOMASS BLENDS	39
2.1 Introduction.....	39
2.2 Materials, Experimental Apparatus and Operation.....	41
2.3 Results and Discussion	43
2.3.1 Thermal Evolution Profiles: Blends with Corn Stover	43
2.3.2 Thermal Evolution Profiles: Blends with Switchgrass	50
2.3.3 Single Fuels: Effect of Heating Rates	53
2.3.4 Analysis of Synergistic Interactions in Blends	58
 CHAPTER 3: KINETICS MODELING OF PYROLYSIS	 67
3.1 Parallel First Order Reactions Model: Approximation of Temperature Integral.....	67
3.2 Distributed Activation Energy Model: Gaussian Distribution of Activation Energy	74
3.3 Matrix Inversion Method	83
3.4 Results and Discussion: Matrix Inversion Method.....	88
3.4.1 Kinetics of DECS-38 Sub-Bituminous Coal Devolatilization.....	88
3.4.2 Kinetics of Corn Stover Devolatilization: Matrix Inversion Method	96
3.4.3 Devolatilization Kinetics of 10CS90SB Blend.....	100
3.5 Reactivity in CO ₂ Atmosphere.....	105
3.5.1 Kinetics of Boudouard Reaction: Single Reaction Model.....	107
3.5.2 Kinetics of Boudouard Reaction: Matrix Inversion Algorithm	112
3.6 Conclusions.....	115

CHAPTER 4: EXPERIMENTAL MOVING BED GASIFICATION OF COAL-BIOMASS BLENDS	117
4.1 Laboratory Moving Bed Gasifier: Design and Operation.....	117
4.2 Gasification with Varying Oxygen/Steam Ratio	123
4.2.1 Quartz Insulation.....	123
4.2.2 Stainless Steel Reactor: Gasification of Coal Feedstocks.....	128
4.2.3 Stainless Steel Reactor: Blends with Corn Stover	131
4.2.4 Stainless Steel Reactor: Blends with Switchgrass	139
4.3 Gasification with Varying Oxygen Partial Pressure	144
4.4 Gasification of Briquettes	152
4.4.1 Product Gas Analysis: Briquette Gasification	154
 CHAPTER 5: SOURCE APPORTIONMENT OF CARBON USING STABLE CARBON ISOTOPE ANALYSIS.....	 166
5.1 Introduction.....	166
5.2 Theory	167
5.3 Experimental	170
5.3.1 Materials	170
5.3.2 Process Parameters and Reactions	171
5.3.3 Apparatus	173
5.4 Results and Discussion	178
5.4.1 Blends with Corn Stover.....	180
5.4.2 Blends with Switchgrass	185
5.5 Statistical Significance of Experimental Data	189
5.6 Isotope Equilibrium	192
5.7 Carbon Sourcing	195

CHAPTER 6: CONCLUSIONS AND FUTURE WORK.....	198
6.1 Conclusions.....	198
6.2 Recommendations for Future Work.....	205
APPENDIX A: MATLAB CODES USED FOR ESTIMATING KINETIC PARAMETERS	208
A.1 Distributed Activation Energy Model: Gaussian Distribution of Activation Energy	208
A.2 Matrix Inversion Algorithm	211
REFERENCES	227
VITA.....	238

LIST OF FIGURES

Figure 1.2.1: Available corn stover residues in the United States of America at less than \$50/Dry Ton.....	8
Figure 1.2.2: Availability of switchgrass in the United States of America at less than \$50/Dry Ton.....	9
Figure 1.3.1 (a): Flowchart illustrating the process of converting solid coal/biomass into gaseous and liquid fuel.....	11
Figure 1.3.1 (b): Flowchart illustrating the processes utilized in biomass conversion and the advantages of gasification over other conventional processes.....	12
Figure 1.3.2: Ternary diagram demonstrating the formation of different products in a gasifier.....	13
Figure 1.6.1: Diagram of a generic moving bed reactor	18
Figure 1.6.2: Diagram of a generic fluidized bed gasifier	21
Figure 1.6.3: Diagram of a generic entrained bed gasifier	22
Figure 1.7.1: Schematic representing the process of pyrolysis in coal or biomass.	24
Figure 1.8.1: Stages of gasification in a moving bed reactor.....	29
Figure 2.3.1 (a): Weight loss curves on an as-received basis during the pyrolysis of DECS-38 Sub-Bituminous coal, corn stover and their blends at 5 °C/min.....	44
Figure 2.3.1 (b): Weight loss curves on an as-received basis during the pyrolysis of DECS-25 Lignite coal, corn stover and their blends at 5 °C/min.	45
Figure 2.3.2 (a): Differential thermogravimetric curves of pyrolysis of SB-CS blends at 5 °C/min.....	47
Figure 2.3.2 (b): Differential thermogravimetric curves of pyrolysis of LG-CS blends at 5 °C/min.....	48
Figure 2.3.3: Weight loss curves and DTG profiles during the pyrolysis of DECS-38 sub-bituminous coal, switchgrass and their blends at 20 °C/min.	51
Figure 2.3.4: Weight loss curves and DTG profiles during the pyrolysis of DECS-25 lignite coal, switchgrass and their blends at 20 °C/min.	52
Figure 2.3.5: Weight loss profiles and DTG curves of pyrolysis of DECS-38 sub-bituminous coal at four different heating rates ranging from 5 °C/min to 40 °C/min.....	54

Figure 2.3.6: Weight loss profiles and DTG curves of pyrolysis of DECS-25 lignite coal at four different heating rates ranging from 5 °C/min to 40 °C/min.	55
Figure 2.3.7: Weight loss profiles and DTG curves of pyrolysis of Corn Stover at four different heating rates ranging from 5 °C/min to 40 °C/min.	56
Figure 2.3.8: Weight loss profiles and DTG curves of pyrolysis of switchgrass at four different heating rates ranging from 5 °C/min to 40 °C/min.	57
Figure 2.3.9: Disparity in the experimental and predicted curves during the release of volatile matter with increasing concentration of corn stover.	60
Figure 2.3.10: Comparison of the experimental and predicted weight loss curves for, (a) Blends of DECS-38 Sub-Bituminous Coal and Corn Stover, (b) Blends of DECS-25 Lignite Coal and Corn Stover.	61
Figure 2.3.11: Comparison of the experimental and predicted DTG curves for, (a) 10% CS + 90% SB blend, (b) 20% CS + 80% SB blend, (c) 30% CS + 70% SB blend.	62
Figure 2.3.12: Comparison of the experimental and predicted DTG curves for, (a) 10% CS + 90% LG blend, (b) 20% CS + 80% LG blend, (c) 30% CS + 70% LG blend.	63
Figure 2.3.13: Disparity in the experimental and predicted curves during the release of volatile matter with increasing concentration of switchgrass.	64
Figure 2.3.14: Comparison of the experimental and predicted weight loss and DTG curves for, (a) 10% SG + 90% SB blend, (b) 30% SG + 70% SB blend.	65
Figure 2.3.15: Comparison of the experimental and predicted weight loss and DTG curves for, (a) 10% SG + 90% LG blend, (b) 30% SG + 70% LG blend.	66
Figure 3.1.1: Analysis of the thermal evolution profiles and temperature ranges for pyrolysis of, (a) DECS-38 sub-bituminous coal, (b) Corn Stover and (c) 10% CS and 90% SB blend.	71
Figure 3.1.2: Estimation of kinetic parameters (activation energy and Arrhenius constant) for pyrolysis of (a) DECS-38 sub-bituminous coal, (b) Corn Stover and (c) 10% CS and 90% SB blend.	72
Figure 3.2.1: Plot for estimating the activation energy and Arrhenius constant for pyrolysis of DECS-38 sub-bituminous coal at various heating rates and conversion points using DAEM.	78
Figure 3.2.2: Plot for estimating the relationship between V/V _f and activation energy for pyrolysis of DECS-38 sub-bituminous coal using DAEM.	79
Figure 3.2.3: Plot for estimating the relationship between f (E) and activation energy for pyrolysis of DECS-38 sub-bituminous coal using DAEM.	80

Figure 3.2.4: Plot for estimating the relationship between Arrhenius constant and activation energy for pyrolysis of DECS-38 sub-bituminous coal using DAEM.	81
Figure 3.4.1: Mass fraction of fuel associated with each reaction during devolatilization of DECS-38 sub-bituminous coal.	90
Figure 3.4.2: Plot of activation energy vs mass fraction remaining for pyrolysis of DECS-38 sub-bituminous coal describing the values of activation energy for each parallel reaction.....	91
Figure 3.4.3: Plot of pre-exponential factor vs mass fraction remaining for pyrolysis of DECS-38 sub-bituminous coal describing the values of pre-exponential factor for each parallel reaction.....	92
Figure 3.4.4: Comparison of experimental and predicted values for devolatilization of DECS-38 sub-bituminous coal for two heating rates (10 °C/min and 20 °C/min) used in the matrix inversion algorithm. (a) weight loss vs temperature, (b) derivative weight loss vs temperature.....	93
Figure 3.4.5: Comparison of experimental and predicted values for devolatilization of DECS-38 sub-bituminous coal for two heating rates (5 °C/min and 40 °C/min) not used in the matrix inversion algorithm. (a) weight loss vs temperature, (b) derivative weight loss vs temperature.....	94
Figure 3.4.6: Mass fraction of fuel associated with each reaction during devolatilization of corn stover.....	96
Figure 3.4.7: Plot of activation energy vs mass fraction remaining for pyrolysis of corn stover describing the values of activation energy for each parallel reaction.	97
Figure 3.4.8: Comparison of experimental and predicted values for devolatilization of corn stover for two heating rates (20 °C/min and 40 °C/min) used in the matrix inversion algorithm. (a) weight Loss vs temperature, (b) derivative weight loss vs temperature.	98
Figure 3.4.9: Comparison of experimental and predicted values for devolatilization of corn stover for the heating Rate (5 °C/min) not used in the matrix inversion algorithm. (a) weight Loss vs temperature, (b) derivative weight loss vs temperature.....	99
Figure 3.4.10: Mass fraction of fuel associated with each reaction during devolatilization of 10% corn stover blended with 90% DECS-38 sub-bituminous coal.....	100
Figure 3.4.11: Plot of activation energy vs mass fraction remaining for pyrolysis of 10% corn stover-90% DECS-38 Sub-Bituminous coal describing the values of activation energy for each parallel reaction.....	101
Figure 3.4.12: Comparison of experimental and predicted values for devolatilization of 10% corn stover-90% DECS-38 sub-bituminous coal for two heating rates (10 °C/min and	

20 °C/min) used in the matrix inversion algorithm. (a) weight loss vs temperature, (b) derivative weight loss vs temperature.	102
Figure 3.4.13: Comparison of experimental and predicted values for devolatilization of 10% corn stover-90% DECS-38 sub-bituminous coal blend for heating rates (5 °C/min and 40 °C/min) not used in the matrix inversion algorithm. (a) weight loss vs temperature, (b) derivative weight loss vs temperature.	103
Figure 3.5.1: Weight loss profiles (Left Y-Axis) and DTG curves (Right Y-Axis) of sub-bituminous coal, corn stover and SB-CS blends at a 5 °C/min heating rate in a CO ₂ atmosphere.	106
Figure 3.5.2: Weight loss profiles (Left Y-Axis) and DTG curves (Right Y-Axis) of lignite coal, corn stover and LG-CS blends at a 5 °C/min heating rate in a CO ₂ atmosphere. ...	106
Figure 3.5.3: Plot for estimating the activation energy for Boudouard Reaction of DECS-38 sub-bituminous coal, corn stover and blends of sub-bituminous coal with corn stover at various heating rates.	108
Figure 3.5.4: Plot for estimating the activation energy for Boudouard Reaction of DECS-25 lignite coal, corn stover and blends of lignite coal with corn stover at various heating rates.	109
Figure 3.5.5: Variation in activation energy of Boudouard reaction with increasing percentage of corn stover in blends with sub-bituminous and lignite coals.	111
Figure 3.5.6: Stem plot of mass fraction of fuel associated with each reaction occurring during decomposition of DECS-38 sub-bituminous coal in CO ₂ atmosphere obtained using DAEM (matrix inversion algorithm).	113
Figure 3.5.7: Comparison of experimental and predicted weight loss curves using the DAEM matrix inversion algorithm for the decomposition of DECS-38 sub-bituminous coal in a CO ₂ atmosphere at heating rates of 5 °C/min and 10 °C/min.	114
Figure 4.1.1 (a): Schematic of the laboratory scale moving bed gasification system.	119
Figure 4.1.1 (b): Pictures of the laboratory scale moving bed gasification system designed and constructed for gasifying coal-biomass blends.	120
Figure 4.1.1 (c): Schematic representation of the change in reactor design: (i) original design with inner quartz lining. (ii) modified reactor design with inner stainless steel tube for better heat utilization.	121
Figure 4.2.1: Average compositions of the product gases obtained during gasification of sub-bituminous coal with varying steam to oxygen ratios.	125
Figure 4.2.2: Average ratios of the product gases obtained during gasification of sub-bituminous coal with varying steam to oxygen ratios.	126

Figure 4.2.3: Maximum ratios of the product gases and efficiency obtained during gasification of sub-bituminous coal with varying steam to oxygen ratios.....	127
Figure 4.2.4 (a): Effect of increasing percentage of corn stover on the product gas compositions in its blends with DECS-38 Sub-Bituminous coal (Steam/O ₂ = 2).....	137
Figure 4.2.4 (b): Effect of increasing percentage of corn stover on the desired product gas ratios and efficiency in its blends with DECS-38 Sub-Bituminous coal (Steam/O ₂ = 2).....	138
Figure 4.3.1: Average carbon monoxide concentration in exit stream obtained during gasification of sub-bituminous coal with varying oxygen partial pressures.....	147
Figure 4.3.2: Average carbon dioxide concentration in exit stream during gasification of sub-bituminous coal with varying oxygen partial pressures.....	148
Figure 4.3.3: Average CO:CO ₂ ratios in the exit gas stream obtained during gasification of sub-bituminous coal with varying oxygen partial pressures.....	149
Figure 4.3.4: Average hydrogen concentration obtained during gasification of sub-bituminous coal with varying oxygen partial pressures.....	150
Figure 4.3.5: Energy conversion efficiency obtained during gasification of sub-bituminous coal with varying oxygen partial pressures.....	151
Figure 4.4.1: Average compositions of the product gases obtained during gasification of EM-SD briquettes with varying steam to oxygen ratios.....	157
Figure 4.4.2: Average ratios of the product gases obtained during gasification of EM-SD briquettes with varying steam to oxygen ratios.	158
Figure 4.4.3: Average compositions of the product gases obtained during gasification of EM-SD briquettes with varying steam to oxygen ratios at a constant air flow rate of 1400 ml/min.....	159
Figure 4.4.4: Average ratios of the product gases obtained during gasification of EM-SD briquettes with varying steam to oxygen ratios.	160
Figure 4.4.5: Comparison of cold gas efficiencies for gasification of EM-SD briquettes.....	161
Figure 5.4.1: Typical GC-C-IRMS Chromatogram of the Gasification Products. CO elutes at t = 318 s followed by CH ₄ at 606 s and CO ₂ at 1350 s.....	179
Figure 5.4.2: Effect of increasing percentage of corn stover and varying oxygen/steam ratios on the isotopic signatures of product gases in its blends with DECS-38 Sub-Bituminous coal. (A) Isotopic Signature of CO, (B) Isotopic Signature of CO ₂	183

Figure 5.4.3: Effect of increasing percentage of corn stover and varying oxygen/steam ratios on the isotopic signatures of product gases in its blends with DECS-25 Lignite coal. (A) Isotopic Signature of CO, (B) Isotopic Signature of CO₂.184

Figure 5.4.4: Effect of increasing percentage of switchgrass and varying oxygen/steam ratios on the isotopic signatures of product gases in its blends with DECS-38 sub-bituminous coal. (A) Isotopic Signature of CO, (B) Isotopic Signature of CO₂.186

Figure 5.4.5: Effect of increasing percentage of switchgrass and varying oxygen/steam ratios on the isotopic signatures of product gases in its blends with DECS-25 lignite coal. (A) Isotopic Signature of CO, (B) Isotopic Signature of CO₂.187

Figure 5.4.6: Comparison of isotopic signatures at an O₂:steam ratio of 2:1, (A) and (B): Blends with Corn Stover, (C) and (D): Blends with Switchgrass.....188

Figure 5.7.1: Individual contribution of each biomass source towards generation of product gases at different O₂/steam ratios. (A) Contribution in the generation of CO in blends with sub-bituminous coal, (B) Contribution in the generation of CO₂ in blends with sub-bituminous coal, (C) Contribution in the generation of CO in blends with lignite coal, and (D) Contribution in the generation of CO₂ in blends with lignite coal.197

LIST OF TABLES

Table 1.2.1: Classification of different biomass types.....	6
Table 2.2.1: Proximate and Elemental Analysis of Feedstocks.....	42
Table 2.3.1: Pyrolysis Temperature Range, Maximum Weight Loss Rates and Peak Temperatures of all Feedstocks Determined by TGA	46
Table 2.3.2: Maximum Weight Loss Rates and Peak Temperatures Attained During the Devolatilization of Individual Feedstocks at Different Heating Rates	58
Table 3.1.1: Obtained pyrolysis kinetic parameters, temperature and conversion ranges for all feedstocks at a heating rate of 5 °C/min.	73
Table 3.2.1: Obtained pyrolysis kinetic parameters for single fuels and blended feedstocks using distributed activation energy model (Gaussian distribution of activation energies) 83	
Table 3.4.1: Pyrolysis kinetic parameters and number of devolatilization reactions obtained for various feedstocks using matrix inversion algorithm.....	104
Table 3.5.1: Peak temperatures at various heating rates and activation energies for heat treatment of coal-corn stover blends in a CO ₂ atmosphere obtained using thermogravimetric analysis.....	110
Table 4.2.1: Average composition of product gases obtained during gasification of DECS-38 sub-bituminous coal with varying oxygen to steam ratios.....	123
Table 4.2.2: Calculated energy efficiency during gasification of DECS-38 sub-bituminous coal with varying oxygen to steam ratios.	124
Table 4.2.3 (a): Average composition of product gases obtained during gasification of sub-bituminous coal at varying O ₂ /steam ratios in the stainless steel moving bed gasifier. ..	128
Table 4.2.3 (b): Average ratios of desired product gases and calculated energy efficiency during gasification of sub-bituminous coal at varying O ₂ /steam ratios in the stainless steel moving bed gasifier.....	129
Table 4.2.3 (c): Average composition of product gases obtained during gasification of lignite coal at varying O ₂ /steam ratios in the stainless steel moving bed gasifier.	130
Table 4.2.3 (d): Average ratios of product gases and energy efficiency during gasification of lignite coal at varying O ₂ /steam ratios in the stainless steel moving bed gasifier.....	131
Table 4.2.4: Average composition of product gases and energy efficiency obtained during gasification of blends of sub-bituminous coal and corn stover at varying O ₂ /steam ratios in the lab scale stainless steel moving bed gasifier.	133

Table 4.2.4 (contd.): Average composition of product gases and energy efficiency obtained during gasification of blends of sub-bituminous coal and corn stover at varying O ₂ /steam ratios in the lab scale stainless steel moving bed gasifier.	134
Table 4.2.5: Average composition of product gases and energy efficiency obtained during gasification of blends of lignite coal and corn stover at varying O ₂ /steam ratios in the lab scale stainless steel moving bed gasifier.	135
Table 4.2.5 (contd.): Average composition of product gases and energy efficiency obtained during gasification of blends of lignite coal and corn stover at varying O ₂ /steam ratios in the lab scale stainless steel moving bed gasifier.	136
Table 4.2.6: Average composition of product gases obtained during gasification of blends of sub-bituminous coal and switchgrass at varying O ₂ /steam ratios in the lab scale stainless steel moving bed gasifier.	140
Table 4.2.6 (contd.): Average composition of product gases obtained during gasification of blends of sub-bituminous coal and switchgrass at varying O ₂ /steam ratios in the lab scale stainless steel moving bed gasifier.	141
Table 4.2.7: Average composition of product gases obtained during gasification of blends of lignite coal and switchgrass at varying O ₂ /steam ratios in the lab scale stainless steel moving bed gasifier.	142
Table 4.2.7 (contd.): Average composition of product gases obtained during gasification of blends of lignite coal and switchgrass at varying O ₂ /steam ratios in the lab scale stainless steel moving bed gasifier.	143
Table 4.3.1: Average composition of product gases obtained during gasification of sub-bituminous coal with varying oxygen partial pressures.	145
Table 4.3.2: Calculated energy efficiency during gasification of sub-bituminous coal with varying oxygen partial pressures.	146
Table 4.4.1: Average Composition of Product Gases Obtained During Gasification of EM-SD Briquettes with Varying Oxygen to Steam Ratios.	156
Table 4.4.2: Average Composition of Product Gases Obtained During Gasification of EM-SD-G97 Briquettes with Varying Oxygen to Steam Ratios.	162
Table 4.4.3: Average Composition of Product Gases Obtained During Gasification of EB-CS Briquettes with Varying Oxygen to Steam Ratios.	163
Table 4.4.4.: Average Composition of Product Gases Obtained During Gasification of EB-CS-G97 Briquettes with Varying Oxygen to Steam Ratios.	164
Table 5.3.1: Product Gas Compositions for CO and CO ₂ Produced During the Gasification of Various Coal/Biomass Blends at Different O ₂ /Steam Ratios.	175

Table 5.3.1 (contd.): Product Gas Compositions for CO and CO ₂ Produced During the Gasification of Various Coal/Biomass Blends at Different O ₂ /Steam Ratios	176
Table 5.3.2: δ ¹³ C values of various feedstock materials.....	176
Table 5.3.3: Carbon Isotope Ratios for CO and CO ₂ Produced During the Gasification of Various Coal/Biomass Blends at Different O ₂ /Steam Ratios	177
Table 5.5.1: Analysis of Variance (ANOVA) for Models Generated Based on Experimental Data and Estimating the Statistical Significance (P-Values) Between Treatment Factors and Response Variables.	190
Table 5.5.1 (contd.): Analysis of Variance (ANOVA) for Models Generated Based on Experimental Data and Estimating the Statistical Significance (P-Values) Between Treatment Factors and Response Variables.....	191
Table 5.6.1: Comparison of Isotopic Equilibrium Temperatures of CO ₂ -CO Product Gases and Experimental Gasifier Temperatures	194

CHAPTER 1: INTRODUCTION AND BACKGROUND

Carbon(C) is an abundant non-metallic element. It is distributed widely in nature. As a free element, carbon forms different bonds with itself, the result of which is the formation of allotropes such as diamond and graphite. Carbon is the major source for organic life. Carbon combines with oxygen to produce carbon dioxide which is useful for plant growth. Carbon also forms flammable compounds called hydrocarbons when combined with hydrogen. These compounds are essential components of fossil fuels. Finally, carbon forms many complex molecules such as carbohydrates, sugars, esters, celluloses, DNA, RNA, etc. which are important groups of biological compounds. Thus, carbon is rightly referred to as the building block of life. Carbon is a major constituent of fossil fuels which include coal, oil and natural gas. These fossil fuels were formed millions of years ago due to the decay of dead plant and animal matter under conditions of high pressure and temperature inside the Earth's crust. Fossil fuels, on combustion in the presence of oxygen, produce an enormous amount of energy, and thus, are of great importance in the present-day world. Fossil fuels, on combustion in the presence of oxygen, produce an enormous amount of energy, and thus, are of great importance in the present-day world [1].

1.1 Global Energy Concerns

Worldwide energy consumption and escalating energy crisis in recent years, due to the global growth in industrialization, economy, population and most importantly, the depletion in fossil fuel resources has resulted in the global energy demand to increase exponentially [2-4]. This increasing rate will become more rapid in the future. Currently, heavy exploitation and extensive use of fossil fuels are the reasons leading towards their

foreseeable depletion within the next few decades [5, 6]. Despite continuous development of the exploration technology and frequent reports on the discovery of new reserves of oil and gas, the increased production cannot meet the world's energy demand and thus a gap exists between the demand and the supply of these two fuel resources [3, 7, 8]. More importantly, extensive use of fossil fuels has contributed to climate change due to Green House Gas emissions. The energy shortage and the negative impact on the environment have created an opportunity for developing alternative, renewable energy resources as substitutes for the oil and the natural gas.

Kentucky produces about 10% of the total coal mined annually in the United States [9]. The fluctuating prices of crude oil along with a major decline in the domestic crude stocks, has accentuated the importance of alternate sources of fuel and chemical feedstocks. On a security point of view, large proportions of oil and gas reserves are concentrated in politically unstable regions, therefore, increasing the diversity in energy sources is important for many nations to secure a reliable and constant supply of energy [10]. Therefore, the production of liquid fuel from solid carbon feedstock is a major area of research.

Liquid fuels produced from coal, by using either direct or indirect liquefaction, can potentially replace imported oil. Direct liquefaction, the direct reaction between coal and hydrogen, involves the conversion of coal to refinable crude hydrocarbons, from which liquid fuels such as gasoline, diesel, kerosene, etc., can be produced. Direct liquefaction of coal, an example of which is the Bergius process, is a high-pressure, high-temperature process with pressures ranging from 200 to 700 atm. and temperatures ranging from 360 °C to 480 °C. In this process, the hydrogenation reaction is done in the presence of a solvent

and a catalyst. The liquids thus produced typically contain a large fraction of aromatic hydrocarbons. Lower operating temperatures and pressures are desirable for direct liquefaction since higher operating conditions tend to promote the cracking of molecules and thus produce more gaseous and solid products.

Indirect liquefaction first utilizes the process of gasification to produce hydrogen and carbon monoxide and then catalytically combines them to produce liquid fuels. It involves the process of gasification combined with downstream processes such as Fischer-Tropsch synthesis to produce diesel or methanol synthesis to produce gasoline. During this process, the principal product of the first stage is syngas which leaves behind most of the mineral matter in coal and is one its major advantages as it is easier to control the build-up of small molecular components than controlling the breakdown of the coal structure [1].

1.2 Biomass as a Source for Energy

Energy is the cornerstone to economic stability and development. Since the industrial revolution, fossil fuels have stimulated economic growth especially in the developed world. Only recently have we realized that this accelerated economic growth has not occurred without a penalty. Carbon dioxide emissions from fossil fuels combustion, combined with land-use changes, have driven the concentration of this most significant greenhouse gas (GHG) to levels in our atmosphere not seen for at least 800,000 years, and probably many millions of years [11, 12]. Although somewhat controversial, the scientific evidence of global warming and climate change and their link to anthropogenic activities has been established. The concentration of GHG in the atmosphere and its consequences is expected to be exacerbated given the high rate of world population growth as well as economic development expected in developing countries with a direct effect on

competition for energy resources. The quest for substitutes to fossil fuels, the need to mitigate the negative environmental effects of fossil fuels utilization and the necessity to safely and economically dispose wastes have encouraged the development of alternative sources of energy and promotion of low quality fuels. Co-conversion of coal and biomass/wastes for energy purposes and chemicals are among these alternatives.

Coal fired power plants are still the largest source of electricity generation in the United States (contributing to about 42% of net electricity generation), and will keep their lead until 2040 [13]. According to the International Energy Agency (IEA), coal will continue to be a global energy solution throughout the 21st century [14]. The world's coal stock is still enormous. Coal has a low cost and a high energy density. It is expected to contribute significantly in the future energy needs in many nations [15, 16], especially in fast-developing countries such as China and India. China alone uses nearly twice as much coal as all countries from the Organization for Economic Co-operation and Development (OECD) combined, while India has since 2011 become the third largest coal consumer in the world after China and the United States [16]. Conversion of coal-to-liquids and chemicals could become significant in the petrochemical industry. However, coal has a major drawback: it is responsible for the emission of environmentally harmful compounds [sulfur, nitrogen (N) and heavy metals]. Combustion of fossil fuels, which accounts for about 75% of total GHG emissions, together with land-use change is the main source of anthropogenic GHG emissions [17-20]. Combustion of coal alone accounts for 30% to 40% of the share of GHGs from fossil fuels combustion [21, 22]; therefore, coal utilization deserves special attention given the likelihood of continued use for electricity generation and the potential for coal to partially replace petroleum for chemicals and transportation

fuels as has recently occurred in China. In short, fueled by the following factors, the past few years have seen an upsurge in interest in gasification of biomass [20]:

1. Reduction in greenhouse gas emissions caused due to the combustion of fossil fuels.
2. Need for energy independence emerging due to the depleting resources and fluctuating prices of oil and natural gas.
3. Developing interest in renewable and locally available energy resources.

If grown in a regenerative manner, biomass systems and respective biofuels as sub-systems can be considered to be renewable as their combustion does not produce any net CO₂ emissions (CO₂ neutral) [23, 24]. Therefore, the use of biomass as a renewable source of energy has been increasingly gaining importance in the recent past and extensive research is being done to partially replace fossil fuels with renewable sources of energy for thermochemical processes [25]. One method of reducing CO₂ emissions from coal-fired power plants is to substitute part of the coal feed with a renewable fuel such as biomass or waste fuels. Hence many countries have initiated incentives in recent years to encourage the co-utilization of biomass for energy production [26].

By definition, bio-renewable resources are sustainable natural resources implying that the resource renews itself at such a rate that it will be available for future use, that is, the rate of consumption is equal to or less than the rate at which it is generated. These bio-renewable resources can be converted into bioenergy. Adding sustainably grown and harvested biomass to the coal feedstock would allow an increase in domestic fuel supply while reducing total greenhouse gas emissions in two ways. Firstly, the emission of carbon during the burning of fuels that are produced from biomass will be countered through the

removal of carbon from the atmosphere by the biomass through the process of photosynthesis during its growth. Secondly, the CO₂ that is produced during the conversion of biomass and coal to liquid fuels can be captured and stored [27].

1.2.1 Classification of Biomass

The term biomass is used to encompass any plant-derived organic matter available on a renewable basis. This includes dedicated energy crops and trees, agricultural food and feed crops, agricultural crop waste and residues, aquatic plants, animal wastes, municipal wastes and other waste materials [12, 23-25, 28-30]. A general classification of biomass varieties that can be utilized as solid fuel resources is listed in Table 1.2.1. The classification is according to their distinct biological diversity, source and origin.

Table 1.2.1: Classification of different biomass types [23, 31, 32]

Biomass Groups	Varieties and Species
Wood and woody biomass	Coniferous or deciduous; soft or hard; stems, branches, foliage, bark, chips, lumps, pellets, briquettes, sawdust, etc.
Herbaceous and agricultural biomass	(a) Grasses or energy crops (alfalfa, arundo, cane, miscanthus, switchgrass, etc.) (b) Straws (barley, corn, wheat, rice, etc.) (c) Other residues (fruits, shells, husks, grains, seeds, cobs, kernels, etc.)
Animal wastes	Chicken litter, various manures, etc.
Aquatic biomass	Marine or freshwater algae, seaweed, etc.
Non-agricultural biomass wastes	Municipal solid waste, refuse-derived fuel, sewage sludge, etc.
Biomass mixtures	Blends of above varieties

The properties of biomass fuels differ significantly from those of typical coals and there is a greater variation in these properties compared to coal. The heating values of

biomass are typically half that of coal. The bulk densities are also considerably less than coal. The ash content of biomass can range from 1% to over 20%. The moisture content of biomass is generally much higher than coal and can range from over 25% to even over 50%. The nitrogen content in biomass can vary from 0.1% to over 1% but the sulfur content of biomass is usually very low because of the lack of pyrite impurities [23]. A sustainable biomass supply requires that the resource base be assessed systematically to address multiple environmental, public and private sector concerns in parallel. Additional measures to grow bio-feedstocks need to be taken for avoiding competition with food supply [33-35].

1.2.2 Resource Assessment of Biomass

Of all the varieties of biomass discussed in Section 1.2.1 (Table 1.2.1), the potential of agricultural residues like corn stover and energy crops such as switchgrass has been widely recognized [31, 32]. The availability of these biomass resources in the U.S. and their potential energy generation capability are shown in Figures 1.2.1 and 1.2.2. Agriculture is a major economic activity in the U.S and corn stover and wheat straw are the primary agricultural residues used in energy production. Although more states produce wheat than corn, the country's total MW-generation potential is significantly less from wheat straw than from corn stover because wheat straw has a lower energy content than corn stover and fewer tons of wheat straw can be collected per acre than corn stover. Corn stover has an energy content of 5,290 Btu/lb (wet) and 7,560 Btu/lb (dry). Wheat straw has an energy content of 5,470 Btu/lb (wet) and 6,840 Btu/lb (dry). Most recent USDA census lists that agricultural residues and wastes that are available at less than \$50/dry ton are about 244 million dry tons currently and may increase up to 404 million dry tons by 2030.

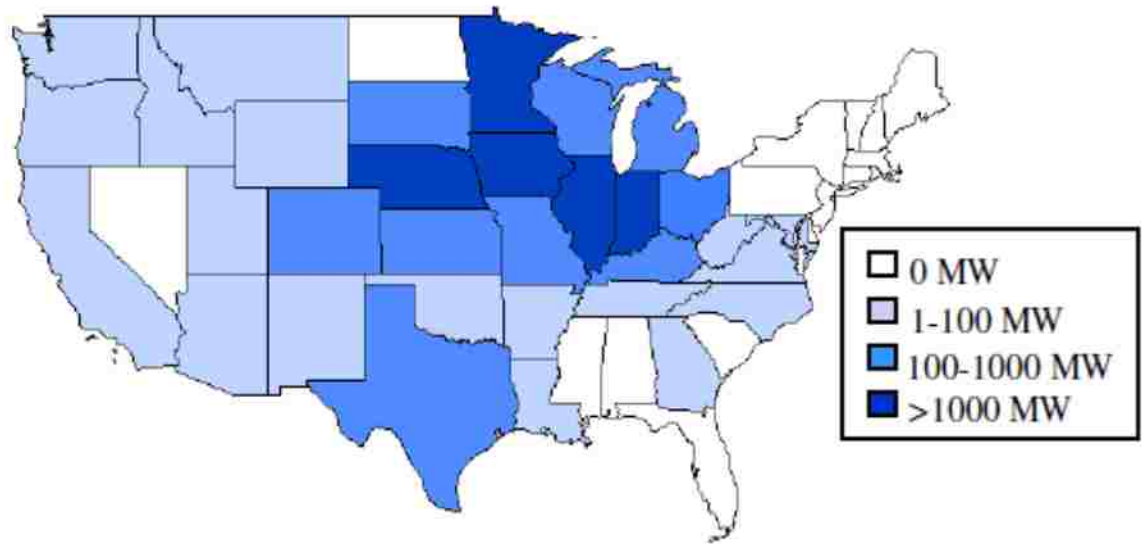


Figure 1.2.1: Available corn stover residues in the United States of America at less than \$50/Dry Ton [32].

Energy crops like switchgrass are also being considered as a huge potential source of biomass feedstock. Although these crops are currently not being grown commercially in the U.S, they are still estimated to account for about 540 million dry tons by 2030. These crops are estimated to provide about 37% of the total available biomass by 2030. Harvesting costs for switchgrass are similar to most forage crops because switchgrass can be cut and baled with conventional mowers and balers, which make this energy crop the easiest and cheapest to harvest. The advantages of using crops specifically grown for energy production is consistency in moisture content, heat content, and processing characteristics. Disadvantages include relatively higher overall costs than many fossil fuels, higher-value alternative land uses that further drive up costs, added expenses associated with harvesting and processing, and farmers’ and power plant owners’ unfamiliarity with energy crops.

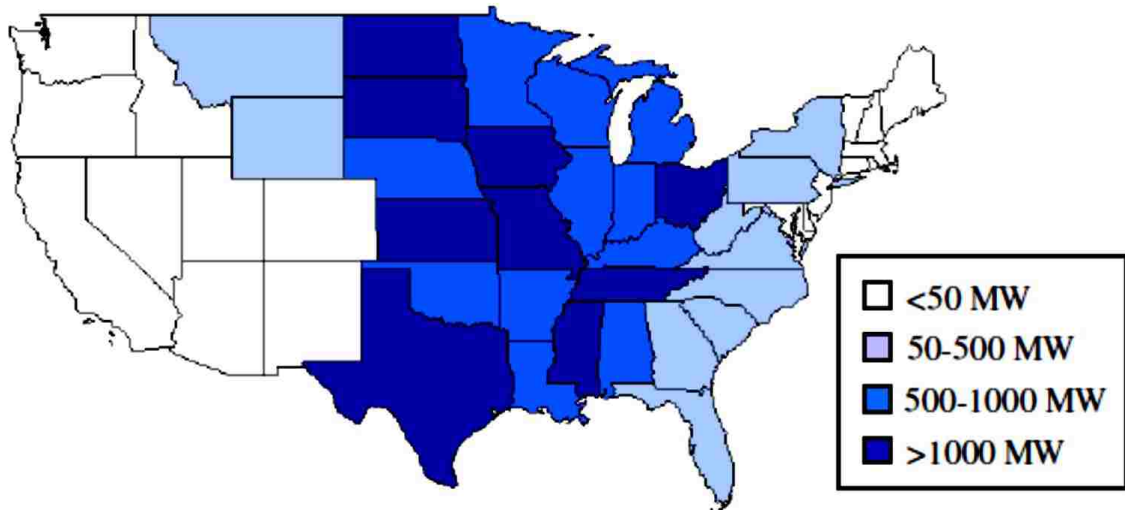


Figure 1.2.2: Availability of switchgrass in the United States of America at less than \$50/Dry Ton [32].

1.3 Gasification

Gasification is the thermochemical process of converting a low-value solid carbonaceous source such as coal, biomass, coke and other organic wastes into synthesis gas, a high-value gaseous mixture comprising hydrogen and carbon monoxide in varying ratios, which is used as a feedstock for producing fuels and chemicals. Gasification, generally done in the presence of mixtures of air/pure oxygen and steam at temperatures ranging between 600 °C and 900 °C, produces a gaseous mixture of hydrogen, carbon monoxide, steam, methane and light hydrocarbons along with some undesirable effluents such as inorganic particulates and condensable organic vapors or tars, as they are commonly known. Gasification is an extremely effective technology that can be used for providing an alternative energy source for crude oil and natural gas. A flowchart illustrating the process of converting solid coal/biomass into gaseous and liquid fuel is shown in Figure 1.3.1 (a) and the advantages of gasification over other conventional processes is shown in Figure 1.3.1 (b).

Gasification is the most important step and also the bottleneck during the thermochemical conversion of solid carbonaceous feed to liquid and gaseous fuels. Therefore, a thorough investigation of this process is necessary for producing valuable products using downstream processes like Fischer-Tropsch synthesis and water gas shift reaction. Coal gasification is an established technology which has been used over the years to convert coal partially or completely to syngas [18]. The oxidizing agent can be chosen as air, oxygen, steam, or a mixture of these. The resulting gas has a low calorific value (3.8-5.6 MJ/Nm³ versus 38 MJ/Nm³ of natural gas) when air is used. This can be increased (10-18 MJ/Nm³) by using oxygen or steam but in the latter case sufficient heat should be provided because steam gasification is an endothermic process. In some cases, steam is added to air to increase the level of hydrogen in the syngas [34]. Oxygen, though primarily used for the process of combustion, is a popular gasifying agent. It may be supplied to a gasifier either in pure form or through air.

The heating value and the composition of the gas produced in a gasifier are strong functions of the nature and amount of the gasifying/oxidizing agent used. A ternary diagram of carbon, hydrogen, and oxygen demonstrating the conversion paths of formation of different products in a gasifier is shown in Figure 1.3.2. As shown in Figure 1.3.2, the use of oxygen as a gasifying agent results in the formation of products like carbon monoxide and carbon dioxide while also lowering the hydrogen content in the product gas since the conversion path shifts towards the oxygen corner. Contrary to this, the use of steam as a gasifying agent results in the conversion path shifting towards the hydrogen corner, thereby producing a product gas with higher H/C ratio.

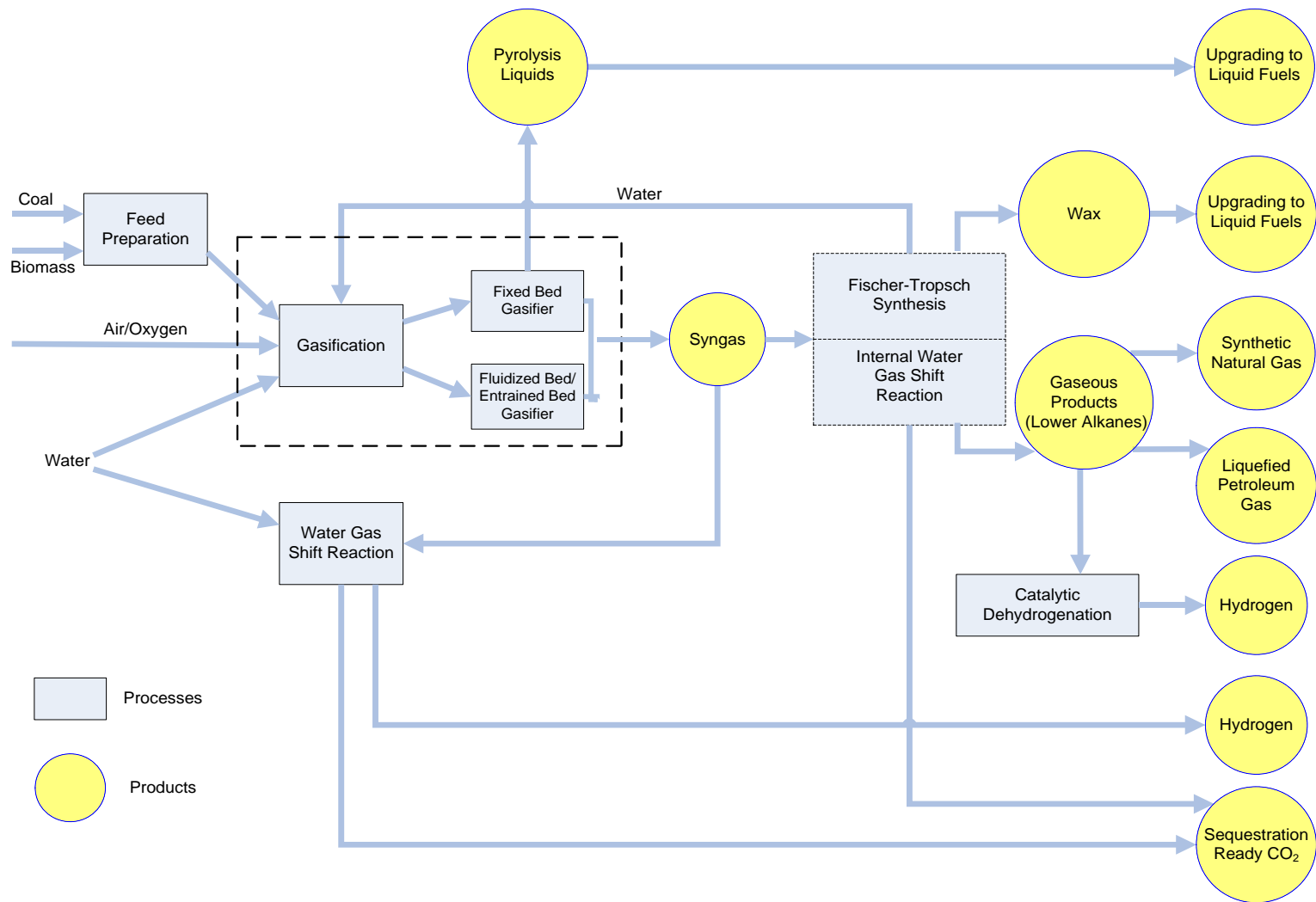


Figure 1.3.1 (a): Flowchart illustrating the process of converting solid coal/biomass into gaseous and liquid fuel.

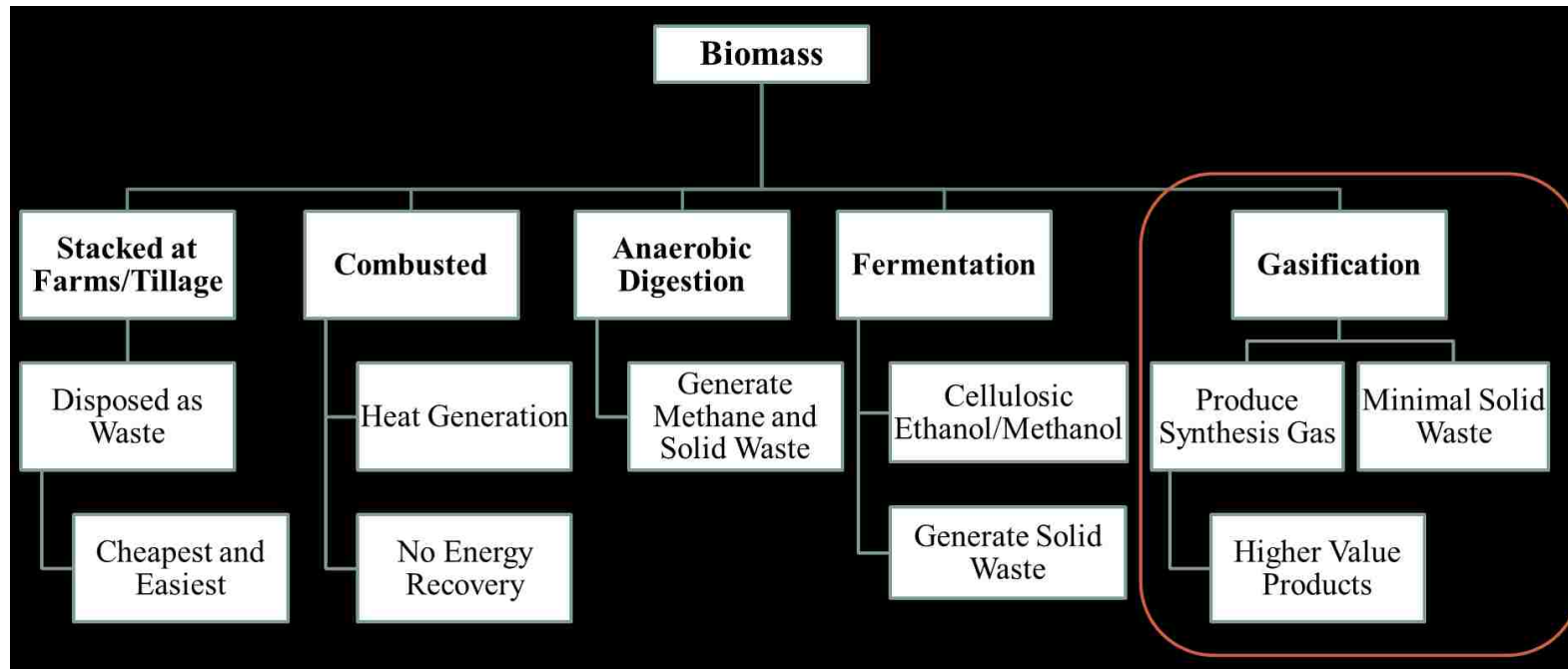


Figure 1.3.1 (b): Flowchart illustrating the processes utilized in biomass conversion and the advantages of gasification over other conventional processes.

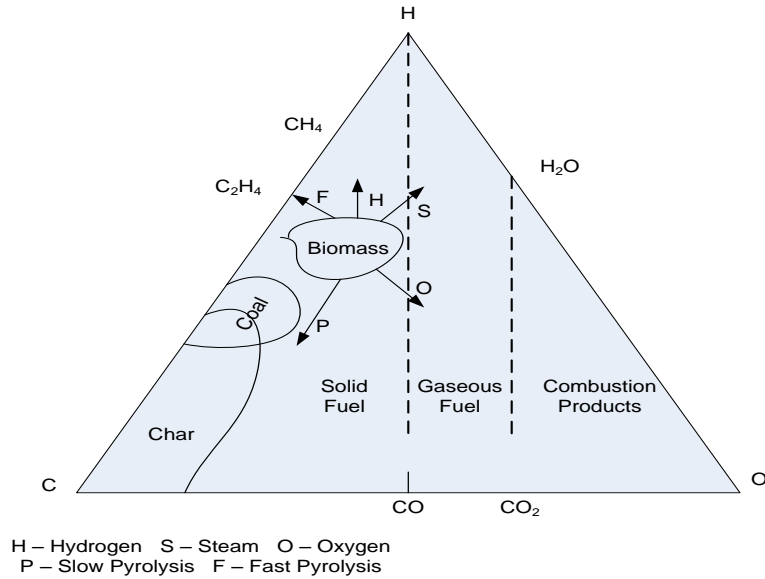


Figure 1.3.2: Ternary diagram demonstrating the formation of different products in a gasifier [20].

Thermochemical conversion of any carbonaceous source is a complex chemical process which includes both homogeneous as well as heterogeneous reactions. Gasification is different from combustion in the sense that during combustion, coal is burnt in excess oxygen to ensure complete combustion while in gasification partial oxidation occurs, that is, the amount of oxygen varies from one-fifth to one-third of the theoretical requirement for complete combustion, thus producing syngas (CO and H₂) rather than CO₂ and H₂O [19].

1.4 Co-Gasification of Coal and Biomass

A lot of similarities exist between the gasification of coal and biomass. The temperature required for complete thermal gasification of biomass is similar to that of coal which is around 800 °C – 900 °C. However, a number of differences are also present owing to the fact that their fuel properties are different. In comparison to coal, which is used in most commercial gasification processes, biomass is more reactive and can be effectively

gasified at lower temperatures. Being a renewable source as discussed in Section 1.2.1, the use of biomass alone as the gasification feed greatly reduces the net production of greenhouse gases. However, the process involves higher operating costs and also produces higher amount of tar when compared to that of coal.

Biomass in general has a high content of hydrogen (H), making it suitable as a blend to compensate the often-low H content of coal. Biomass as gasification feedstock, although giving a high hydrogen yield, has the disadvantage of low energy density because of its high oxygen and moisture content.

This shortcoming is compensated for when blended with a higher energy content coal. Other challenges such as the seasonal limitation of biomass are somewhat mitigated through co-conversion with coal. The higher tar release (due to excessive volatile release and low gasification temperature from biomass gasification) is also reduced as blending with coal increases the temperature, enhancing tar cracking. Blending biomass and coal as feedstock can reduce the shortcomings of each fuel and boost the efficacy of the overall system. The high tar content of product gases from biomass gasification is a major and widely recognized problem. These high tar contents arise mainly from the lower temperatures and shorter residence times in gasifiers constructed for biomass processing compared to those designed for coal gasification. Tar yields from ligno-cellulosic biomass materials tend to be considerably higher than tar yields from coals [33, 34].

Prins et al. reported that fuels with higher oxygen to carbon ratios have larger energy losses due to their high ratio of available chemical energy to heating value [36]. Also, such fuels are over-oxidized in the gasifier in order to reach the required gasification temperature. Therefore, it can be said that highly oxygenated fuels are not ideal for gasifiers

keeping in view the energy losses that can be incurred and hence, solid biomass can be more readily gasified if it is co-gasified with coal [26]. Therefore, co-gasification of blends of coal and biomass to produce syngas ($\text{CO} + \text{H}_2$), which in turn can be used as feedstock for processes such as Fischer-Tropsch Synthesis used for producing liquid fuels, is a major area of research.

One of the major advantages of co-gasification is that it can utilize a much larger variety of available feedstock [37]. For the coal plants, partly gasifying biomass enables them to potentially obtain credits for the use of a renewable fuel and also lower the economics since biomass is a low cost feedstock. As stated earlier, co-converting blends of coal and biomass can potentially reduce the GHG emissions and environmental pollution due to the fact that biomass is carbon neutral if produced sustainably and also because of the fact that the concentration of nitrogen, sulfur and heavy metals are much lower when compared to that of coal. Also, co-conversion of coal-biomass blends is relatively cost effective when compared to carbon capture and storage (CCS) which has a high energy penalty ranging between 15 % and 40 % and therefore, CCS would not be able to meet the emissions reduction targets suggested by International Panel on Climate Change (IPCC) [12, 38, 39].

However, several technical issues arise which need to be addressed for co-gasifying coal and biomass [27]. Biomass has much lower bulk density, almost one-fifth that of coal; and higher moisture content than that of coal. Also, biomass has higher inherent oxygen content which, though increases the reactivity, also decreases the energy density [26, 40]. The heating values and particle densities of biomass are about half as much as that of coal. The overall energy density of biomass is about one-tenth that of coal. Therefore, a large

volumetric flow of biomass is needed for mixing even a small percentage of biomass with coal for co-gasification. Due to these differences in the physical properties of the two fuels, delivery, storage and handling costs for biomass are much higher as compared with coal [26, 41].

The different compositions of coal and biomass also affect the thermodynamic efficiency of the co-gasification process. Biomass generally contains higher oxygen to carbon ratio which is useful for gasification as it increases the reactivity at lower temperatures and also lowers the amount of oxygen that is required to be added for the process. Various thermodynamic models have been developed in the past to describe the performance of gasifiers and to assess the maximum efficiency that can be attained when gasifying different fuels [26, 36]. In general, thermodynamic models assume perfect mixing and uniform temperatures in the gasifier. Another common assumption is that the reactions occurring during gasification are fast enough with sufficiently long residence times to reach equilibrium.

1.5 Downstream Processing of Syngas

Syngas generated from gasification can be used for producing pure hydrogen which can be used directly as a fuel or as an intermediate in the production of chemicals such as ammonia. Syngas can also be used to produce useful industrial chemicals such as methanol which can be used as a substitute for gasoline. Methanol is also an important intermediate in chemical industries and almost a tenth of the world's methanol production comes from gasification of coal and heavy residues. Production of ultra-clean synthetic fuels from these diverse feedstocks can supplement world fuel supplies as well as mitigate the dependence on traditional crude oil [42, 43].

Fischer-Tropsch synthesis, catalyzed most commonly by Iron or Cobalt based catalysts, is the process used for converting syngas to liquid fuels. It is a mildly exothermic polymerization reaction with CH_2 as monomer, producing primarily saturated n-alkanes, ranging from methane to high molecular weight waxes. The wax products obtained from Fischer-Tropsch synthesis can then be upgraded by hydrocracking the heavy wax products or catalytic dewaxing/hydro-isomerization to produce various fuels like gasoline, diesel and jet fuel while the gaseous products are a combination of synthetic natural gas and liquefied petroleum gas [21, 42].

The equation shown below is a general representation of Fischer-Tropsch Synthesis [44].



The clean synthesis gas obtained from gasification is used as feed for the Fischer-Tropsch synthesis, where most of the clean gas is converted into zero-sulfur liquid hydrocarbon fuels. Fischer-Tropsch synthesis produces a wide array of hydrocarbon products in addition to some oxygenates. The array of products depends on the chain growth probability relative to chain termination. The probability function can be theoretically modeled using Anderson-Schultz-Flory distribution, in which the parameter alpha determines the shape of the probability curve; the higher the value of alpha, the longer the hydrocarbon chains [27, 44, 45].

1.6 Types of Gasifiers and Applications

There are three main types of reactors that are used for the process of gasification: moving bed gasifier, fluidized bed gasifier and entrained bed gasifier. These reactor schemes differ from each other with respect to the type of feedstocks that can be used,

particle size distribution, residence time, reaction temperature and pressure as well as the flow patterns of the reactants and products.

1.6.1 Moving Bed Gasifier

A moving bed gasifier or a fixed bed gasifier, as it is sometimes referred to, follows a counter current type of operation in which the solid feed such as coal or biomass is fed from the top while the gasifying agent is fed from the bottom. In a moving bed gasifier, relatively large lumps of coal move down slowly through the bed while reacting with gases moving upwards. This type of gasifier, whose residence time is typically 30 minutes to 60 minutes, is normally designed to operate for pressures ranging from 1 atm to 100 atm. A picture depicting the moving bed gasifier and the temperature profile inside the bed is shown in Figure 1.6.1.

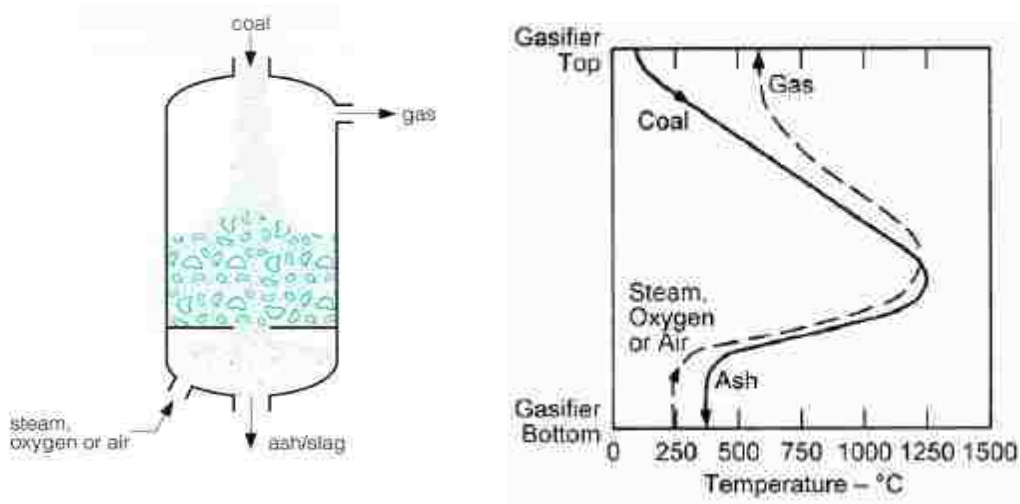


Figure 1.6.1: Diagram of a generic moving bed reactor [19, 26].

The main advantage of using a fixed/moving bed reactor is because of the fact that in such a reactor high carbon conversion, longer solid residence times, low ash carry over and high thermal efficiency can be obtained. Moving bed gasifiers have high cold gas efficiency as

compared with other gasifiers as a large proportion of the heating value of the solid feed appears as chemical energy in the gas rather than thermal energy. Another advantage of the moving bed gasifier over other gasifier technologies is heterogeneity of reactions within the gasifier. In the pyrolysis zone, volatile matter present in the coal feed is driven out of the coal matrix as a mobile phase in vapor form leaving behind a solid char matrix. Since this reaction occurs in the non-oxidizing zone of the moving bed gasifier, the mobile phase does not convert to synthesis gas and can be collected and condensed separately as liquid fuel. In power generation units, including pulverized coal combustors and integrated gasification combined cycle (IGCC) gasifiers, the volatile matter is simply combusted for its heat content. In a moving bed gasifier, analogous to direct liquefaction, this volatile matter is collected as a separate fuel while the remaining char is subsequently converted to synthesis gas which can be further converted to liquid fuels via indirect liquefaction. In the past, ash removal was one of the major problems in this type of gasifier but the usage of rotating grates at the bottom of the gasifier more recently has negated the problems caused during ash removal. The temperatures in the gasifier may exceed the ash melting point if less steam is used, thus causing the gasifier to be slagging.

Inside a moving bed gasifier, the solid feed that is fed from the top is sequentially dried, devolatilized, gasified and combusted. In the drying or feeding zone at the top of the gasifier, the coal is heated and dried while the product gas is cooled before leaving the reactor. The coal is further heated as it descends and begins to devolatilize. Once devolatilized, the coal is gasified with steam and CO₂. The combustion zone is at the bottom of the reactor where the oxygen reacts with the remaining char and highest

temperatures are attained. Due to this reason, there is a large temperature gradient within the bed in this type of gasifier as shown in Figure 1.6.1.

Moving bed gasifiers have limited tolerance to the presence of fines as these tend to be blown away from the top due to the high flow rate of the gases coming through. Also, the presence of excess amount of fines in the solid feed hinders the path of the up-flowing syngas resulting in clogging of the gasifier. In addition, the moisture content of the feed affects the discharge temperature. In the case of reactor technology, fixed beds have a wide temperature distribution. This includes possibilities for hot spots with ash fusion, low specific capacity, long periods for heat-up and a limited scale-up potential. For plants with high power requirement the limited scale-up includes higher investment costs for a cascade of single fixed beds. To avoid channeling the feedstock has to be as uniform as possible [46].

1.6.2 Fluidized Bed Gasifier

In a fluidized bed gasifier, the solid feed is gasified in a bed of hot non-combustible particles suspended by an upward flow of fluidizing gas. They can either use bubbling bed or circulating bed technology. The bed is formed of a mixture of sand, coke, char, sorbent or ash. Crushed feed, in the size range 0.5-5 mm, enters the side of the reactor while the steam and air or oxygen enter mainly at the bottom and fluidize the bed. The residence time of the feed in the gasifier is typically in the range 10-100 s but can be much longer. High levels of back mixing ensure a uniform temperature distribution in the gasifier. These gasifiers operate at temperatures below ash fusion temperatures of 900-1050 °C to prevent ash melting, to avoid clinker formation and the loss of fluidity in the bed. They are usually air based. The low operating temperatures can result in incomplete gasification and the

char particles entrained in the raw gas leaving the gasifier are usually recovered by a cyclone and recycled back to the gasifier.

A typical fluidized bed is shown in Figure 1.6.2. Fluidized beds have good heat and material transfer between the gas and solid phases with the best temperature distribution, high specific capacity and fast heat-up. They tolerate wide variations in fuel quality and a broad particle size distribution. Disadvantages of fluidized beds are high dust content in the gas phase and the conflict between high reaction temperatures with good conversion efficiency and low melting points of ash components [46].

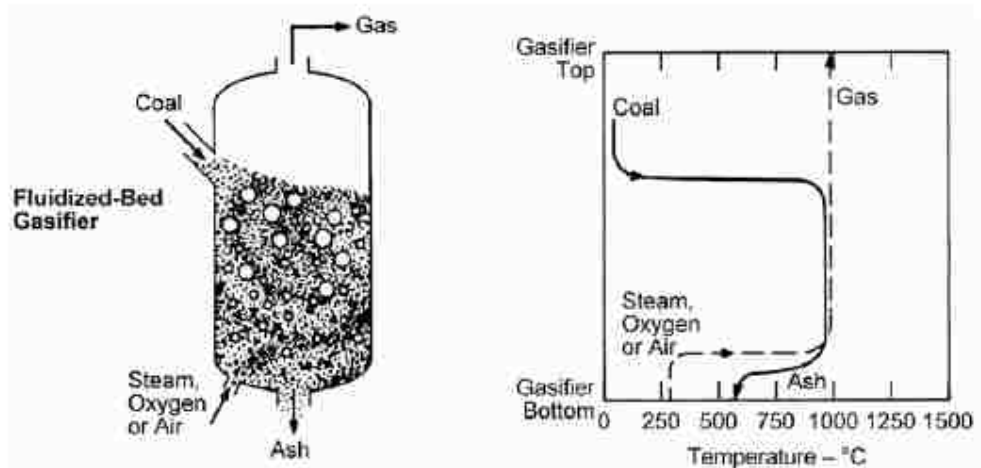


Figure 1.6.2: Diagram of a generic fluidized bed gasifier [19, 26].

1.6.3 Entrained Bed Gasifier

In entrained flow gasifiers, fine coal particles react concurrently with steam and oxygen or air. The solid feed that is fed into the gasifier can be either dry or wet. These gasifiers operate at high temperatures between 1200 °C and 1600 °C and pressures in the range of 20 atm to 80 atm. The temperature must be maintained above the slagging temperature so that ash behaves as a liquid. Otherwise, the ash becomes sticky and agglomerates, thereby causing fouling of the gasifier. A typical entrained flow gasifier

along with its temperature distribution is shown in Figure 1.6.3. The residence time of an entrained flow gasifier is very low and is of the order of seconds. Hence, to achieve high carbon conversion, these gasifiers must operate at high temperatures. Generic characteristics of entrained flow gasifiers include: high temperature slugging operation, entrainment of molten slag in the raw syngas, large oxidant requirements, ability to gasify all coal regardless of rank, caking characteristics or amount of fines.

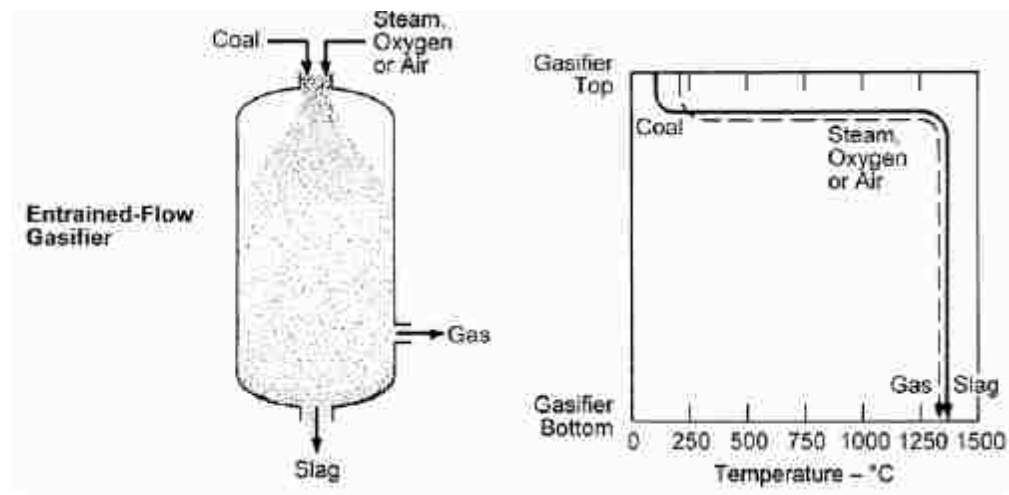


Figure 1.6.3: Diagram of a generic entrained bed gasifier [19, 26].

1.7 Gasification Processes

Gasification is a combination of several processes that occur at distinct temperature regimes or zones within a gasifier. Gasification packs energy in chemical bonds in the product gases while adding hydrogen and stripping off carbon from the feedstock to produce gases with higher hydrogen to carbon ratio. A simplified reaction sequence for coal or biomass gasification in a moving bed reactor can be described by the following stages from top to bottom of the reactor [18, 20, 37, 47].

1. Elimination of moisture or drying.
2. Pyrolysis process during which volatile matter such as condensable tar, and gases like carbon monoxide, methane and hydrogen are released.
3. Homogeneous reaction of volatiles in the gas phase.
4. Heterogeneous reaction of char and gas phase species such as steam and carbon dioxide.
5. Oxidation of the carbonaceous source to produce carbon dioxide and heat.
6. Release of mineral matter and transformation.

The amount of moisture present in coal varies depending on the type and rank of coal. Generally, the moisture content decreases as the rank of coal increases, i.e. lignite has the highest percentage of moisture while bituminous coals have the lowest. The combustion of volatiles provides the heat required for the evaporation of the moisture present in coal, typically between the temperatures of 100 °C and 150 °C. This energy used for vaporizing the moisture is non-recoverable. However, the evaporated moisture can also act as a gasifying agent during the later stages of the process, thus decreasing the steam requirement in some cases.

1.7.1 Pyrolysis or Devolatilization

Pyrolysis or devolatilization (used interchangeably) is the first zone of the gasification process. The chemical components in the raw coal decompose by heating to a relatively low temperature (350-800°C) in the absence of oxygen. Coal/biomass can be considered as a complex polymer network consisting of aromatic clusters and aliphatic bridges. During the process of pyrolysis, the complex structure of coal is broken down into several small fragments whose vapor pressure is high enough to form volatile matter. The duration of evolution of volatiles is relatively shorter for biomass than coal [48]. The

products include: pyrolysis gases (CO , H_2 , CH_4 and H_2O), tar, oil, naphtha and residual solid char. A schematic diagram representing the process of pyrolysis is shown in Figure 1.7.1. A complete description of the characteristics of pyrolysis is complicated, but for a given sample, the pyrolysis behavior depends on the heating rate, final decomposition temperature, vapor residence time, the environment under which the pyrolysis takes place, pressure, coal particle size and coal rank [49]. The structure and the composition of the char obtained are also greatly affected by the pyrolysis conditions. This can be considered as the starting point for all heterogeneous gasification reactions.

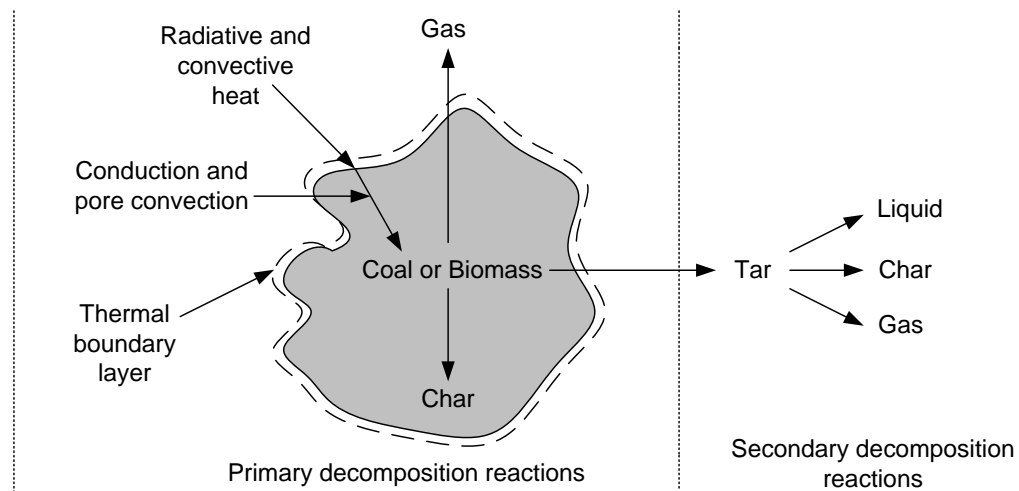


Figure 1.7.1: Schematic representing the process of pyrolysis in coal or biomass.

1.7.2 Reaction of Volatiles

The volatiles formed during the pyrolysis process mainly contain carbon monoxide, methane, hydrogen, hydrocarbon liquids and tars. In the presence of an oxidant surrounding the coal particles, these volatiles react exothermically in gas phase releasing significant amount of heat, thereby increasing the temperature of product gases. However, during

gasification, volatile combustion will not reach completion, particularly in those feedstocks having high volatile content, due to the low oxygen to coal ratio. Mass transport limitation between phases is negligible during this process since volatile combustion is a gas phase homogeneous reaction. There is, however, a mass transfer resistance due to gas phase mixing of combustible gases and oxidizers. In general, volatile combustion is much faster than the pyrolysis process, which in turn is much faster than the char gasification process.

1.7.3 Char Gasification

In any gasifier, char gasification takes place following coal pyrolysis. The remaining carbonaceous solids from the pyrolysis reactions are further oxidized to syngas through heterogeneous reactions with carbon dioxide, carbon monoxide, steam, oxygen and hydrogen. The reactivity of chars in gaseous atmospheres is a complicated physicochemical process depending on the temperature, particle structure, carbon source and thermal history of the char. Char gasification is the slowest step occurring in a gasifier and hence, is the rate controlling step. The reactivity of coal chars depends on a number of factors such as the minerals present in coal, the conditions at which pyrolysis occurs to form char and the gasification conditions which convert the char to gases [19].

While developing the char gasification rates and mechanisms, coal is always assumed to be pure carbon reacting with other components in the gasifier. Additionally, the overall rate of char gasification may be affected not only by chemical kinetics but also by intraparticle and external mass transfer resistances [50]. Therefore, any description of the kinetics of the gasification reactions must include its intrinsic chemical rate and the effects of mass transfer. The gasification of char by steam or carbon dioxide proceeds by the formation of carbon-oxygen complexes on active sites. One of the most important steps in developing kinetic models for char gasification is desorption of CO and CO₂ from the

active sites. Therefore, it is important to understand the chemistry of the surface on which the carbon-oxygen complexes form and desorbs [51].

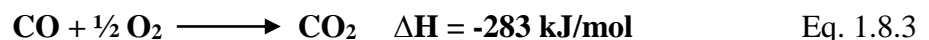
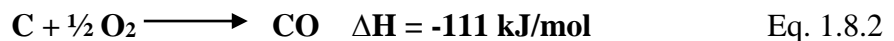
1.8 Chemical Reactions During Gasification

As discussed earlier, during the gasification of solid carbon, the principle chemical reactions are those involving carbon, carbon monoxide, carbon dioxide, hydrogen, steam and methane. Since this research is focused on moving bed gasifiers, those reactions that occur during the process of gasification in a moving bed gasifier will be described as an example.

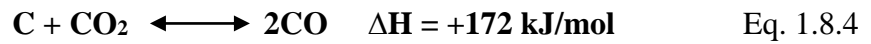
As described in the prior section on moving bed gasifiers, the gasifying medium enters the reactor from the bottom and meets unconverted char descending from the top. The temperature in the bottom layer is much higher than the ignition temperature of carbon and therefore, a highly exothermic combustion reaction, shown in Equation 1.8.1, takes place in the presence of excess oxygen. The heat thus released during this process helps in heating the upward moving gas as well as the descending solids.



As the combustion reaction is extremely fast, most of the oxygen is consumed during this process. Hence, as the oxygen contained in the upward moving gas is reduced further, the combustion reaction is converted to partial combustion, releasing carbon monoxide and moderate amount of heat. The carbon monoxide thus formed, combines with remaining oxygen to release carbon dioxide exothermically.



The hot gas which is a mixture of CO, CO₂ and steam from the feed and gasifying medium, moves further up into the gasifying zone, where char from the top of the bed is gasified with carbon dioxide. The carbon dioxide concentration is high in the combustion zone, but once oxygen is depleted, CO₂ enters the gasifying zone and reacts with char to form carbon monoxide. This reaction, known as the Boudouard reaction, is endothermic in nature and results in a decline in the CO₂ concentration in the gasification zone.



Apart from the Boudouard reaction, the char also reacts with steam that enters the gasification zone to produce carbon monoxide and hydrogen. This reaction, popularly known as the water gas reaction, is also endothermic like the Boudouard reaction and results in further increasing the concentration of carbon monoxide in the gasification zone.



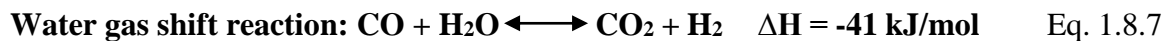
This reaction is favored by high temperatures and reduced pressures and in the absence of a catalyst occurs slowly around 900 °C. This reaction is faster than the Boudouard reaction under same conditions. It should be noted that gasification with steam produces two molecules of synthesis gas per atom of carbon whereas the partial combustion reaction with oxygen produces only one. Sensible heating of the hot gas provides the heat required for the two endothermic gasification reactions given by Equations 1.8.4 and 1.8.5. These are responsible for most of the gasification products like hydrogen and carbon monoxide. Due

to the endothermic nature of these reactions, the temperature of the product gas reduces. Figure 1.8.1 gives an insight into the various stages occurring in a moving bed gasifier.

Apart from the major reactions described above, few other reactions occur during gasification. These are as follows:



The reaction of char with hydrogen proceeds at a very slow rate except at very high pressures.



The water gas shift reaction is an exothermic reaction and has an effect on the H₂/CO ratio of the gasification product. The H₂/CO ratio is very important when the gas is used for synthesis in the downstream processes such as Fischer-Tropsch synthesis.

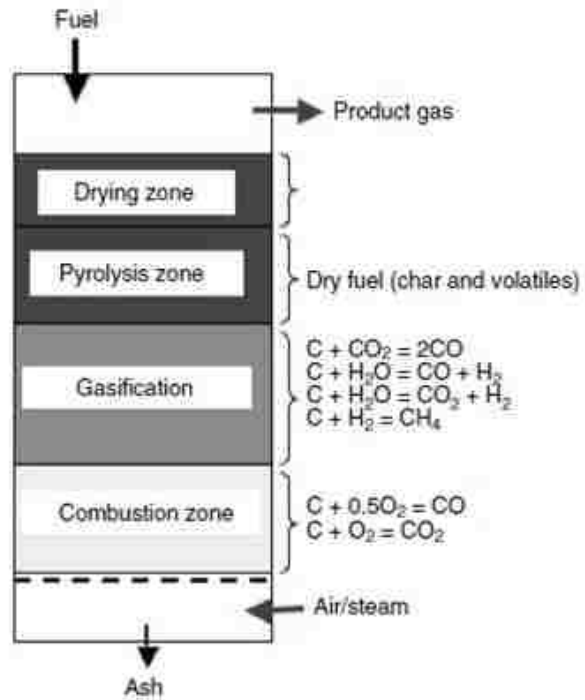
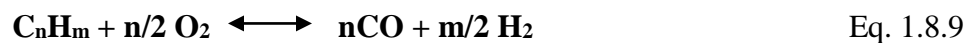


Figure 1.8.1: Stages of gasification in a moving bed reactor.



The methanation reaction increases the heating value of the product gas since methane has a high heat of combustion but proceeds at a very slow rate in the absence of catalysts except at high pressures. In general, for real fuels, the overall reaction can be written as:



Where,

- For gas, such as pure methane, $m = 4$ and $n = 1$.
- For oil, $m/n \approx 2$
- For coal, $m/n \approx 1$

Due to the high temperatures in the gasification process, no hydrocarbon other than methane is present in appreciable quantity in the outlet of the gasifier.

1.9 Kinetic Modeling

One of the main objectives of this research is to establish the synergistic effects of coal-biomass blends in making co-gasification a useful and economical process. Kinetic modeling of the devolatilization behavior of coal and biomass is an important step to assess the contribution of single materials and their interactions during the devolatilization stage. The understanding of kinetics of pyrolysis of blends of biomass and coals is far from clear and it is important in design and operation of co-gasification processes.

Thermogravimetric analysis (TGA) can be used to investigate thermal events and kinetics of pyrolysis and oxidation of the solid raw materials. Thermogravimetric analysis provides a measurement of weight loss of the sample as a function of time and temperature. The kinetics of the thermal events can then be determined by the application of the Arrhenius equation corresponding to the separate slopes of constant mass degradation in each thermal event with different reaction order, activation energy and frequency factor. Thermogravimetric analysis experiments can be carried out either isothermally, where the sample is heated at a constant temperature, or non-isothermally, where the sample is heated at a constant rate. Isothermal experiments are cumbersome due to the fact that the sample might take a long time to reach even 50 % conversion at relatively low temperatures of 500 °C or less apart from the fact that multiple experiments are required for predicting the kinetic parameters. On the contrary, the kinetic parameters can be predicted using only a single experimental run in the non-isothermal mode apart from achieving close to complete conversion in a much shorter period of time.

As described earlier, coal devolatilization is a process involving complex decomposition and the exact description of the kinetics involved is not yet available. Several authors have approximated the overall process as a first-order decomposition occurring uniformly throughout the particle [17, 52-54]. Therefore, the pyrolysis reaction equation can be conveniently represented as:

$$dX/dt = k(1 - X) \quad \text{Eq. 1.9.1}$$

$$X = \left(\frac{W_0 - W_t}{W_0 - W_f} \right) \quad \text{Eq. 1.9.2}$$

And, $k = A \exp(-E/RT)$ Eq. 1.9.3

where X is the pyrolysis conversion, k is the reaction rate constant, W₀ is the original mass of the test sample, W_t is the mass of the test sample at time t, W_f is the final mass at the end of pyrolysis, E is the activation energy, T is the temperature, A is the pre-exponential factor and R is the universal gas constant.

Solution of Equation 1.9.1, via integration subject to the condition that conversion is zero at initial time, yields the following result:

$$-\ln(1 - X) = kt \quad \text{Eq. 1.9.4}$$

Hence, the rate constant k can be determined from the slope of a plot of $-\ln(1-X)$ versus time. Subsequently, the values of activation energy and pre-exponential factor can be estimated from the slope and intercept, respectively, of an Arrhenius plot $\ln k$ versus $1/T$

represented by Equation 1.9.3. Equations 1.9.1 through 1.9.4 represent the pyrolysis reaction as a global one step kinetic chemical reaction model under isothermal conditions.

For pyrolysis or oxidation reactions under non-isothermal conditions, the heating rate H plays a very important role in determining the kinetic parameters [54-56]. For a first-order reaction at constant heating rate, $H = dT/dt$, a combination of Equations 1.9.1 and 1.9.3 yields the following result:

$$dX/dT = [A(1 - X)/H] \exp(-E/RT) \quad \text{Eq. 1.9.5}$$

As in the case of isothermal analysis, solution of Equation 1.8.5, via integration subject to the condition that conversion is zero at initial temperature, T_0 , yields the following result:

$$\ln(1 - X) = -(A/H) \int_{T_0}^T \exp(-E/RT) dT \quad \text{Eq. 1.9.6}$$

Since, there is no conversion at initial temperature, T_0 , the limits of the integral in Equation 1.9.6 can be conventionally changed to $\int_0^T \exp(-E/RT)$, thereby introducing a new function as represented in Equation 1.9.7.

$$f(y) = \int_y^\infty (e^{-y}/y^2) dy \quad \text{Eq. 1.9.7}$$

Where, $y = (-E/RT)$

Therefore, Equation 1.9.6 reduces to,

$$\ln(1 - X) = -(A/H) f(y) \quad \text{Eq. 1.9.8}$$

Since Equation 1.9.7 cannot be solved analytically, the function $f(y)$ can be approximated using two theories: Doyle's approximation and Coats-Redfern approximation. The use of these approximations would help in transforming Equation 1.9.7 into simple linear forms and thus obtaining the activation energy, E and pre-exponential factor, A as shown in Equations 1.9.9 through 1.9.13.

In Doyle's approximation, $f(y)$ is obtained by assuming a linear relationship between $\ln f(y)$ and y as shown in Equation 1.9.8 while in Coats-Redfern approximation an asymptotic expansion of $f(y)$ is assumed where in only the first term is utilized.

Doyle's Approximation:

$$f(y) \cong \exp(-5.33 - y) \quad \text{Eq. 1.9.9}$$

And, $\ln[\ln(1 - X)] = \ln(-AE/HR) - 5.33 - 1.052(E/RT)$ Eq. 1.9.10

Coats-Redfern Approximation:

$$f(y) = e^{-y}/y^2 \left[1 - (2!/y) + (3!/y^2) - (4!/y^3) + \dots \right] \quad \text{Eq. 1.9.11}$$

Or, $f(y) \approx e^{-y}/y^2$ Eq. 1.9.12

And, $\ln \left[-\ln(1 - X)/T^2 \right] = \ln(AR/HE) - E/RT$ Eq. 1.9.13

The theory presented using Equations 1.9.1 through 1.9.13 models the pyrolysis and oxidation reactions assuming them to be first-order decomposition reactions. However, in reality, these reactions need to be modeled for an unknown reaction order. For an n^{th} order

reaction, a similar theory as to the one presented above can be utilized to determine the kinetic parameters [57, 58], where in Equation 1.9.13 can be modified as:

$$\ln \left[\frac{(1 - (1 - X)^{1-n})}{(1 - n)T^2} \right] = \ln(AR/HE) + E/RT \quad \text{Eq. 1.9.14}$$

Kinetic parameters obtained using the single first order reaction models are actually a starting point in the devolatilization modeling. More accurate and specific models are required to meet the experimental results of each material, one model being the distributed activation energy model [52, 53]. The distributed activation energy model treats the thermal decomposition process as a large number of independent, parallel rate processes. The thermal decomposition of a single organic species can be described as an irreversible first-order reaction with respect to the amount of unreacted material remaining. Thus, the rate at which the volatiles are produced by a particular reaction can be defined according to the mass balance on the reactant species.

$$dV_i/dt = k_i(V_i^\infty - V_i) \quad \text{Eq. 1.9.15}$$

$$V_i^\infty - V_i = V_i^\infty \exp \left(-At \exp(-E/RT) \right)_i \quad \text{Eq. 1.9.16}$$

Where V_i^∞ is the final quantity of volatile matter for the generic species, i , and k_i is the rate constant of the reaction expressed according to the Arrhenius law.

This type of kinetic model requires that the amount of volatiles and kinetic parameters known for all the single reactions. To estimate these parameters from experimental data for all the reactions is practically not possible. The problem can be simplified if it is assumed that the rate constants for all the reactions differ only in the

activation energy. The number of reactions is large enough so that the activation energy can be expressed as a continuous Gaussian distribution function $f(E)$ and $f(E)dE$ representing the potential loss of volatile fraction with activation energy between the intervals E and $E + dE$.

$$\text{Thus, } V_i^\infty = dV^\infty = V^\infty f(E)dE \quad \text{Eq. 1.9.17}$$

The total amount of volatile material unreleased is obtained by summing the contribution from each reaction, that is, by integrating Equation 1.9.16 over all values of E using Equation 1.9.17. Finally, the yield of volatiles can be calculated using Equation 1.9.18.

$$(V^\infty - V)/V^\infty = \left[\int_0^\infty \exp\left(-\int_0^t k dt\right) f(E)dE \right] \quad \text{Eq. 1.9.18}$$

and,
$$f(E) = (\sigma(2\pi)^{0.5})^{-1} \exp\left[-(E - E_0)^2/2\sigma^2\right] \quad \text{Eq. 1.9.19}$$

where V^∞ is the global volatile quantity of the material, E_0 is the mean activation energy and σ is the standard deviation of the activation energy.

This approach avoids the low values of the activation energies which result when a single first-order reaction model is applied to fit a temperature dependence that arises from the occurrence of different reactions in different temperature intervals [17]. The theories presented in this chapter would form a basis for analyzing the experimental data discussed in the chapters that follow.

1.10 Research Objectives

For thermochemical conversion of coal and biomass to gaseous and liquid fuel, the most important steps are pyrolysis and gasification. This research examined the devolatilization characteristics using thermogravimetric analysis at various heating rates and co-gasification characteristics of different blends of coal and biomass in a moving bed reactor under varying reaction conditions. It is important to develop a versatile technology that can benefit from different fuel compositions. Although, there is a large scientific knowledge on separate gasification of coal and biomass, the application of co-gasification technology is still under development. The research objectives are broken down into the following individual tasks:

1. **Variation in feed material:** To evaluate the gasification properties for a variety of feed materials which include different coals, biomasses and their selected blends. The feed materials utilized in this research work include two different rank coals: DECS-38 Sub- Bituminous coal and DECS-25 Lignite coal; and two biomass feedstocks consisting of agricultural crop residues like corn stover and energy crops like switchgrass. The two coals were blended with each of the biomass materials up to a maximum of 30% by weight of biomass respectively.
2. **Synergy in Coal-biomass blends:** Potential synergistic effects between blends of coal and biomass on the production of liquid and gaseous fuels was examined based on the experimental results using thermogravimetric data and actual product gas composition obtained at various operating conditions using the laboratory scale moving bed gasifier.

3. **Kinetics of pyrolysis:** Non-isothermal thermogravimetric analysis were performed on all the feed materials to establish the effect of heating rates on devolatilization. The thermogravimetric analysis was performed at four different heating rates of 5 °C/min, 10 °C/min, 20 °C/min and 40 °C/min in an inert nitrogen atmosphere. These experiments were carried out at temperatures within the devolatilization interval of each material.
4. **Kinetics of Boudouard reaction:** Non-isothermal thermogravimetric analysis of carbonaceous feed material in carbon dioxide atmosphere was also performed at relatively higher temperatures to study the effects of heating rates and temperatures on the Boudouard reaction.
5. **Kinetic modeling of pyrolysis and Boudouard reaction:** Kinetic modeling of the obtained thermogravimetric analysis data was evaluated for the feed materials. Three models, namely, single first-order reaction model, distributed activation energy model and model-free matrix inversion algorithm were used for determining the kinetic parameters like activation energy and pre-exponential factor.
6. **Effect of Steam/Oxygen/Air ratio:** For the experiments on the laboratory scale moving bed reactor, gasification on the feed materials was performed by varying the steam:oxygen (or air) ratio from 0 to 2.5:1. The effect of steam and O₂ (or air) content in the inlet gas stream on the gasification products and overall efficiency was thus analyzed.
7. **Oxygen partial pressure:** The effect of partial pressure of oxygen on the gasification products was also studied by varying the oxygen percentage in the inlet

gas stream. Five different concentrations of air were utilized: 20 %, 40 %, 60 % and 80 % and 100 % that is, from pure air to pure oxygen. It was important to perform research task 6 to obtain the operating conditions that give the best possible H₂:CO ratio, syngas:CO₂ ratio and efficiency.

8. **Effect of addition of biomass:** As stated in Research Task 1, sub-bituminous coal and lignite coal were blended individually with up to 30 % by weight of corn stover and switchgrass respectively. The blended feedstocks were then gasified at operating conditions specified in Research Task 6 and the product gas compositions and gasification characteristics were compared with that of pure coals.
9. **Isotope Ratio Mass Spectrometry:** Stable carbon isotope analysis, a unique analytical technique, has been utilized for distinguishing and quantifying the individual contributions of coal and biomass feedstock materials in the generation of carbon containing gases during the gasification of their blends and check for the existence of isotopic equilibrium during moving bed gasification.

CHAPTER 2: THERMOGRAVIMETRIC ANALYSIS OF COAL-BIOMASS BLENDS

The thermal evolution profiles and kinetic parameters for the pyrolysis of two coals (DECS-38 Sub- Bituminous coal and DECS-25 Lignite coal), one biomass sample (corn stover) and their blends (10%, 20% and 30% by weight of corn stover) have been investigated at a heating rate of 5 °C/min in an inert nitrogen atmosphere, using thermogravimetric analysis. The weight loss profiles observed illustrate that the thermal evolution profiles of the single fuels are different from that of the blends. The thermal evolution profiles of DECS-38 Sub-Bituminous coal (SB) and DECS-25 Lignite coal (LG) display only one major peak over a wide temperature distribution, ~ 152-814 °C for SB and ~ 175-818 °C for LG whereas the thermal decomposition profile for corn stover (CS) falls in a much narrower band than that of the coals, ~ 226-608 °C. The non-linearity in the evolution of volatile matter with increasing percentage of corn stover in the blends verifies the possibility of synergistic behavior in the blends with sub-bituminous coal where deviations from the predicted yield ranging between 2% -7% were observed whereas very little deviations (1% - 3%) from predicted yield were observed in blend with lignite coal indicating no significant interactions with corn stover.

2.1 Introduction

Pyrolysis or devolatilization (used interchangeably) is the first zone of the gasification process as described in Chapter 1. The chemical components in the raw coal decompose by heating to a relatively low temperature (350-800°C) in the absence of oxygen. Coal can be considered as a complex polymer network consisting of aromatic clusters and aliphatic bridges. During the process of pyrolysis, the complex structure of

coal is broken down into several small fragments whose vapor pressure is high enough to form volatile matter. The duration of evolution of volatiles is relatively shorter for biomass than coal [48]. The products include: pyrolysis gases (CO, H₂, CH₄ and H₂O), tar, oil, naphtha and residual solid char [18, 20, 37, 59]. A complete description of the characteristics of pyrolysis is complicated, but for a given sample, the pyrolysis behavior depends on the heating rate, final decomposition temperature, vapor residence time, the environment under which the pyrolysis takes place, pressure, coal particle size and coal rank [49]. The structure and the composition of the char obtained are also greatly affected by the pyrolysis conditions. This can be considered as the starting point for all heterogeneous gasification reactions.

Kinetic modeling of the devolatilization behavior of coal and biomass is, therefore, an important step in assessing the contribution of single materials and their interactions during the devolatilization stage. The understanding of kinetics of co-pyrolysis of blends of biomass and coals, particularly the mixtures of Montana coals, corn stover and switchgrass used in this study, is far from clear and, hence, it is important in design and operation of co-gasification processes.

Thermogravimetric analysis (TGA) can be used to investigate thermal events and kinetics of pyrolysis and oxidation of the solid raw materials. TGA analysis provides a measurement of weight loss of the sample as a function of time and temperature. The kinetics of the thermal events can then be determined by the application of the Arrhenius equation corresponding to the separate slopes of constant mass degradation in each thermal event with different reaction order, activation energy, and frequency factor. TGA experiments can be carried out either isothermally, where the sample is heated at a constant

temperature, or non-isothermally, where the temperature of the sample is increased at a constant rate. Isothermal experiments are typically slower since the sample might take a long time to reach even 50 % conversion at temperatures of 500 °C or less and multiple experiments are required for determining the kinetic parameters. On the contrary, the kinetic parameters can be determined using only a single experimental run in the non-isothermal mode which can achieve complete conversion in a much shorter period of time [55]. As described earlier, the devolatilization of coal-biomass blends is a complex process and the exact description of the kinetics is not yet available.

2.2 Materials, Experimental Apparatus and Operation

The thermal behavior of pure coal, biomass which includes corn stover (CS) and switchgrass (SG) and their blends using thermogravimetric analysis will be discussed extensively in this chapter. For the purpose of this work, biomass (CS and SG) was blended individually up to 30 % by weight with two different ranks of coals, namely, sub-bituminous coal (SB) and lignite coal (LG). The samples were crushed and sieved to 150 μm before blending to limit the effects of intra-particle heat transfer. The coal-biomass blends were prepared in appropriate proportions and homogenized by constant stirring in the sample holders to ensure sufficient dispersion. Subsequently, their non-isothermal weight loss profiles were evaluated and co-pyrolysis kinetic parameters were determined. The various methods utilized for determining the kinetic parameters for co-pyrolysis are described extensively in Chapter 3. These coals were chosen based on economic considerations, their low sulfur content, and relatively high percentage of carbon present since the ultimate goal is to gasify these blends in a moving bed reactor for the production of syngas that can be used as feedstock for downstream processes such as Fischer-Tropsch Synthesis used for producing liquid fuels. Also, keeping in view of the overall gasification

process, blends of higher percentages of biomass (in excess of 30 % by weight) was not possible for the conditions at which the gasifier was operated since biomass is a low density, low heating value fuel and addition of more biomass would make the gasification process less efficient. Hence, a maximum of 30 % by weight of biomass was chosen for this study. The proximate and elemental analyses of the single fuels are presented in Table 2.2.1.

Table 2.2.1: Proximate and Elemental Analysis of Feedstocks

Feedstock	Proximate Analysis (As Received Basis)				Elemental Analysis (As Received Basis)				
	% Moisture	% Fixed Carbon	% Volatile Matter	% Ash	% C	% H	% N	% S	% O
DECS-38 Sub- Bituminous Coal	22.01	39.66	34.58	3.75	56.82	3.95	0.98	0.44	12.36
DECS-25 Lignite Coal	34.91	27.32	30.05	7.71	42.80	2.99	0.61	0.47	10.50
Corn Stover	5.66	10.32	76.15	7.87	42.33	6.71	0.73	0.30	42.06
Switchgrass	4.87	9.35	83.62	2.16	45.76	8.09	0.32	0.08	42.87

As a part of this, pyrolysis of the different feedstocks was carried out in non-isothermal mode using a TA-SDT-Q600 thermogravimetric analyzer. The weight of the samples used for these experiments was about 30 mg for the coal samples and about 10 mg for the biomass samples on an as received basis (which is approximately 25 mg for coal samples and 8 mg for biomass on a dry basis). Pure nitrogen was used as the purge gas. Flow of pure nitrogen through the system negates sample oxidation and also removes the volatile pyrolysis products, thus ensuring an inert atmosphere during the run. In the non-

isothermal mode, once the sample is inserted into the furnace, the temperature of the furnace was increased from room temperature to 127 °C and held at that temperature for 15 minutes to ensure drying. Subsequently, the furnace temperature was raised to 900 °C at constant heating rates ranging between 5 °C/min and 40 °C/min. An inert nitrogen atmosphere was employed throughout the process and the nitrogen flow rate was maintained constant at 100 ml/min. Upon reaching a temperature of 900 °C, air was introduced into the furnace to burn off the remaining char and obtain the percentage of ash in the respective samples. Also, the heat transfer limitations may be ignored due to the fact that the furnace heats up slowly combined with a low weight of the sample being pyrolyzed. The process was repeated four times to ensure reproducibility of the weight loss profiles for each sample (error < 5 % for all samples).

2.3 Results and Discussion

2.3.1 Thermal Evolution Profiles: Blends with Corn Stover

The weight loss curves (dry ash free basis) during the non-isothermal pyrolysis at a heating rate of 5 °C/min for all the feedstocks containing corn stover are shown in Figures 2.3.1 (a) and 2.3.1(b). The weight loss increases with increasing reaction temperature for all samples. Also, the weight loss profiles of the coal-biomass blends fall between those of the isolated single fuels. Figures 2.3.2 (a) and 2.3.2 (b) depict the differential thermogravimetric (DTG) curves of the samples used in this work, as a function of pyrolysis temperature, at a heating rate of 5 °C/min. It can be seen that the samples display one peak at temperatures less than 150 °C representing the removal of moisture from the samples [60].

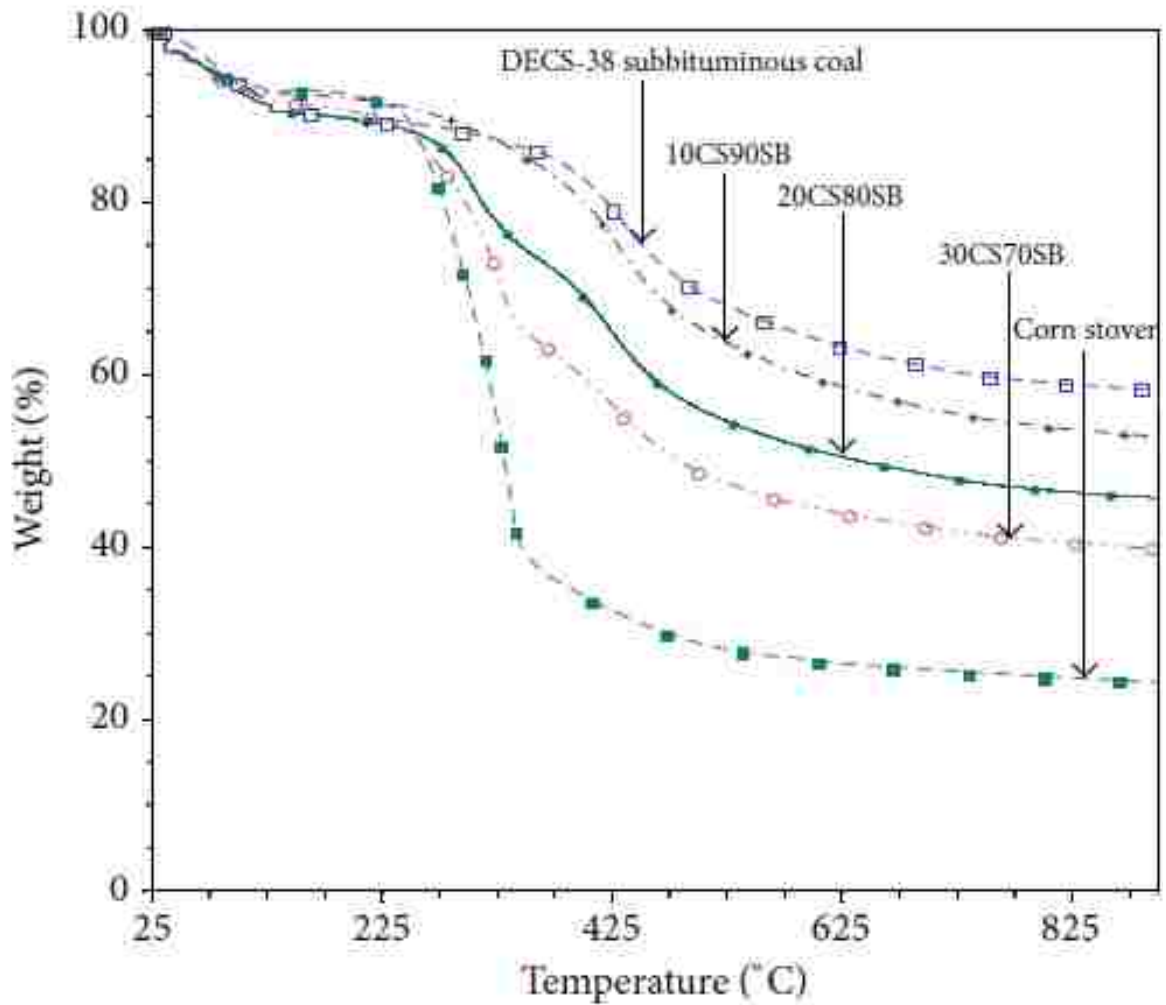


Figure 2.3.1 (a): Weight loss curves on an as-received basis during the pyrolysis of DECS-38 Sub-Bituminous coal, corn stover and their blends at 5 °C/min.

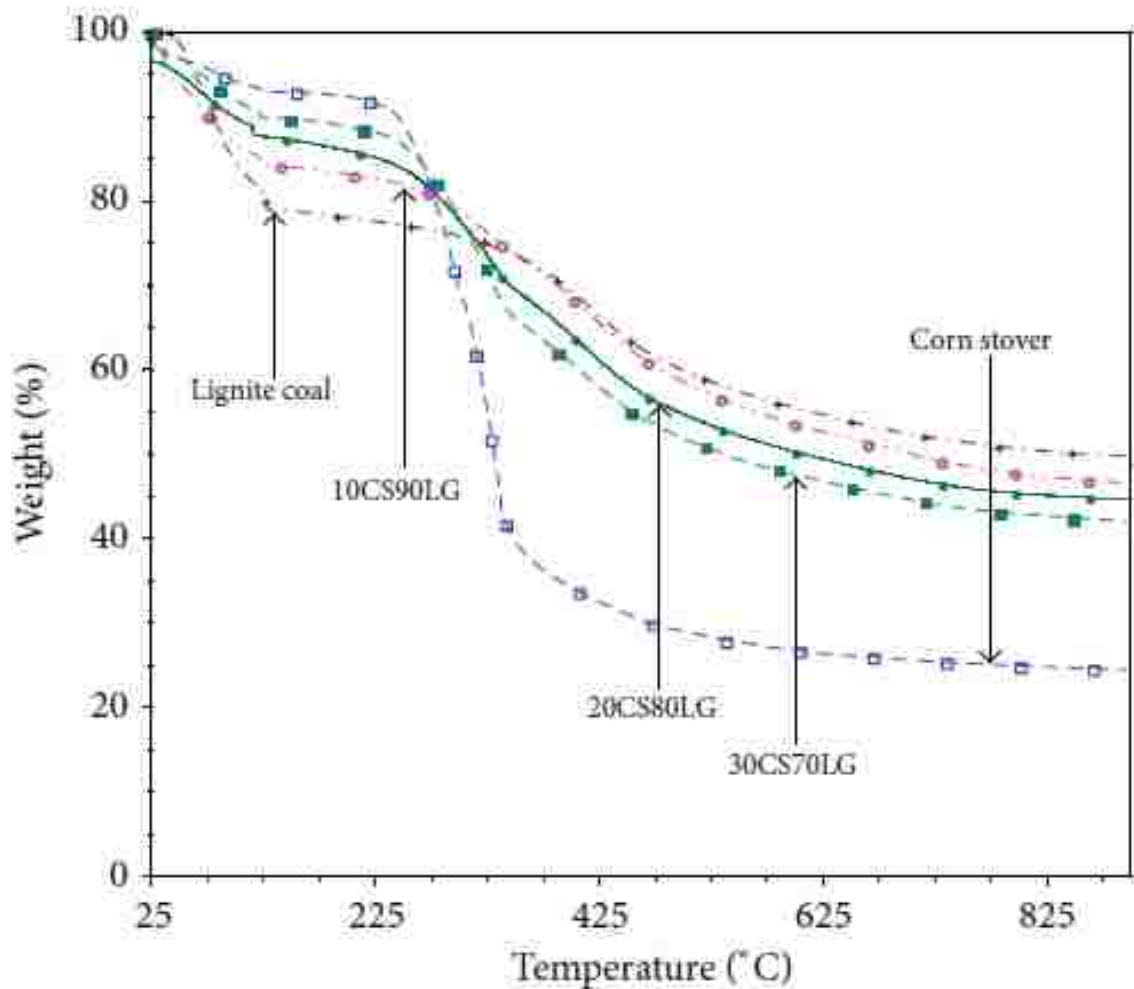


Figure 2.3.1 (b): Weight loss curves on an as-received basis during the pyrolysis of DECS-25 Lignite coal, corn stover and their blends at 5 °C/min.

Above this temperature, varied peaks are observed for the coals, corn stover and their blends. Table 2.3.1 summarizes some of the pyrolysis parameters which include, pyrolysis temperature range (T_i is the temperature of initial weight loss and T_f is the temperature at the end of the reaction), maximum weight loss rates and corresponding maximum DTG peak temperatures.

Table 2.3.1: Pyrolysis Temperature Range, Maximum Weight Loss Rates and Peak Temperatures of all Feedstocks Determined by TGA

Feedstock Materials	Pyrolysis T Range, °C		Maximum Weight Loss Rate, (%/min) _{max}		Peak Temperature, T _{max} , °C	
	T _i	T _f	Peak 1 (CS)	Peak 2 (Coal)	T _{max,1}	T _{max,2}
DECS-38 Sub-Bituminous Coal (SB)	152	814	-	0.889	-	433
DECS-25 Lignite Coal (LG)	175	818	-	0.668	-	419
Corn Stover (CS)	226	608	4.492	-	331	-
10% CS + 90% SB	207	787	0.251	0.819	330	430
20% CS + 80% SB	204	765	1.492	0.500	326	419
30% CS + 70% SB	190	755	2.332	0.561	330	427
10% CS + 90% LG	176	815	0.550	0.603	318	423
20% CS + 80% LG	201	785	0.941	0.599	327	411
30% CS + 70% LG	199	755	1.550	0.552	336	413

The thermal evolution profiles of Sub- Bituminous coal (SB) and Lignite coal (LG) display only one major peak over a wide temperature distribution, ~ 152-814 °C for SB and ~ 175-818 °C for LG. This peak represents the release of carbon containing volatile matter from both coals [60]. The maximum peak temperature for this major peak is approximately 433 °C and 419 °C, respectively, for SB and LG. It is worth noting that the maximum weight loss rate of LG is much lower than that of SB. This can attributed to the fact that the volatile

matter or the immobile phase present in LG coal are bonded together with much higher molecular bond energy than that of SB coal and hence will be removed with a slower rate at similar temperatures apart from the fact that LG contains much lower amount of volatile matter than SB as shown in Table 2.2.1.

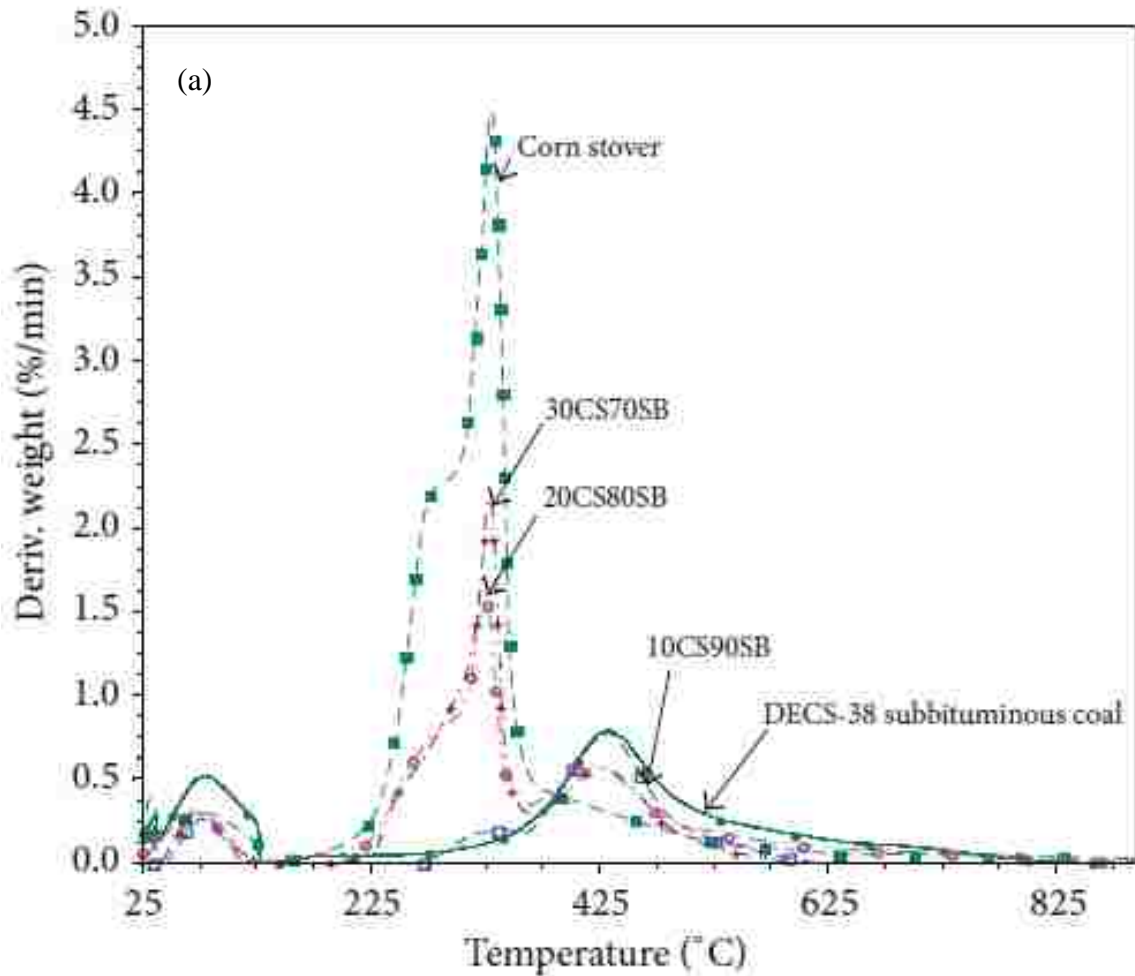


Figure 2.3.2 (a): Differential thermogravimetric curves of pyrolysis of SB-CS blends at 5 °C/min.

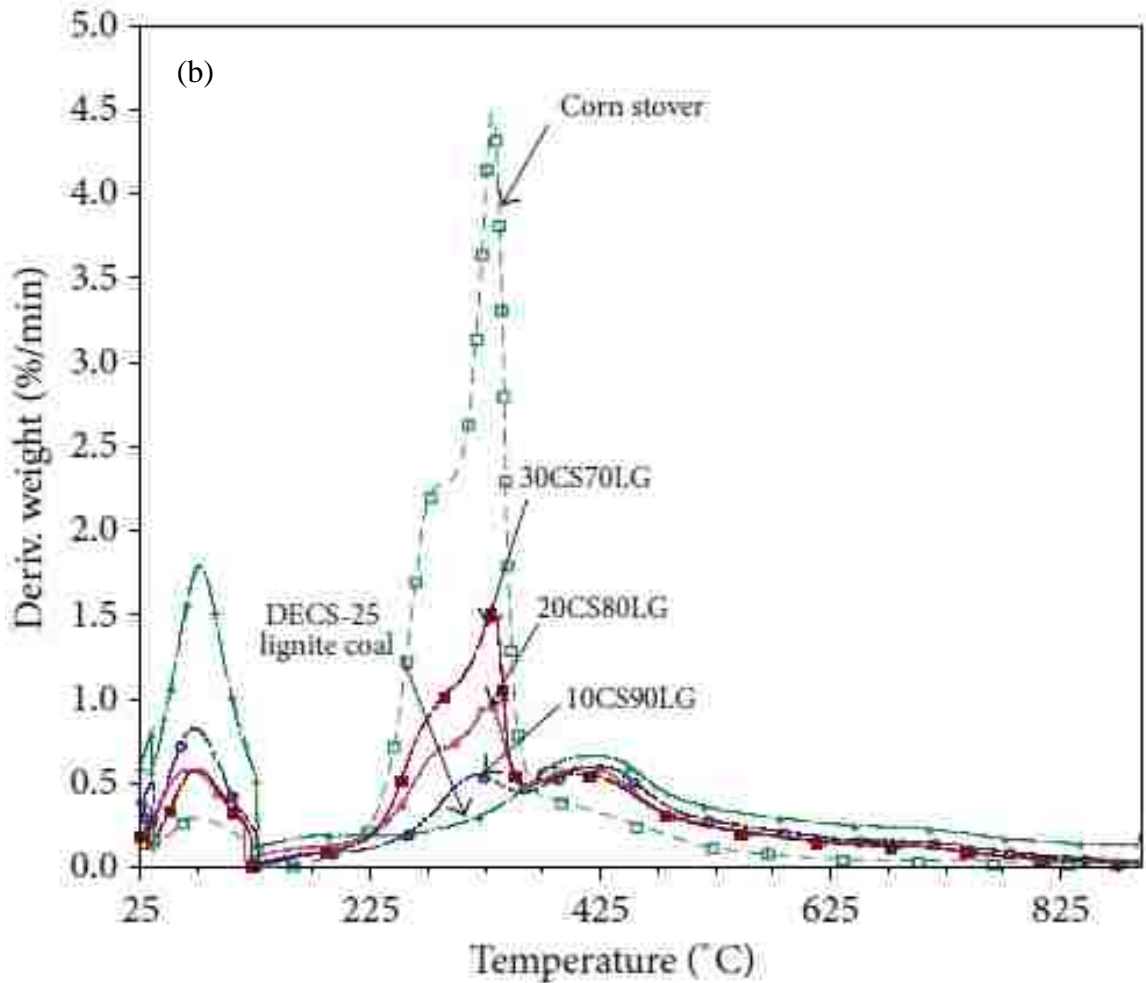


Figure 2.3.2 (b): Differential thermogravimetric curves of pyrolysis of LG-CS blends at 5 °C/min

Also, the maximum weight loss rates for the coals occur in a temperature range of 400-500 °C corresponding to the data reported by Sun et al [61]. In the case of corn stover (CS), the thermal evolution profiles can be divided into three more stages apart from moisture removal corresponding to the removal of hemicellulose, cellulose and lignin components of corn stover. The decomposition of the hemicellulose and cellulose components of corn stover can also be termed as the active pyrolysis zone while the slow decomposition of the lignin component represents the passive pyrolysis zone. This is generally the case for all ligno-cellulosic materials [62]. As it can be seen, the thermal decomposition profile for CS

falls in a much narrower band than that of the coals, ~ 226-608 °C. This is mainly due to the high volatile content and lower fixed carbon content of CS as compared with that of the coals.

This difference is also attributed to the strength of the molecular structure of the fuels. The immobile phase present in coal structure comprises dense polycyclic aromatic hydrocarbons linked together by aromatic rings with very high bond energy of about 1000 kJ/mol [63]. In contrast, the polymers of hemicellulose, cellulose and lignin which constitute the macromolecular structure of biomass and other woody materials are linked together by relatively weak bonds with a bond energy of about 380-420 kJ/mol [64]. These bonds are less resistant to heat at low temperatures. As a consequence, a much higher mass loss rate results in biomass samples as compared with coal as can be seen from Table 2.3.1. The maximum weight loss rate of CS is almost an order of magnitude higher than both coals. As observed, the DTG profile of CS results in a split peak in the temperature range of ~ 226-375 °C. The lower temperature shoulder represents the decomposition of the hemicellulose component with a peak temperature of ~ 286 °C and a weight loss rate of 2.278 %/min while the higher temperature peak represents the decomposition of the cellulose component with a maximum weight loss rate of 4.492 %/min at a temperature of 331 °C. This decomposition continues up to a temperature of approximately 375 °C. Above this temperature, the slow decomposition of the lignin component begins continuing up to a temperature of about 608 °C beyond which very little change in the weight occurs.

As for the blends of both coals with corn stover, the DTG curves are represented in Figure 2.3.2. The DTG evolution profiles for different blends of CS with SB and LG showed two distinct peaks in the temperature range of approximately 176-815 °C. For

blends of CS and SB, the first peak occurs at a maximum peak temperature of approximately 326-330 °C representing the devolatilization of CS (evolution of hemicellulose and cellulose components) while the second peak occurs at a maximum peak temperature of 419-430 °C representing the devolatilization of SB. Similar trends are observed for blends of CS and LG with maximum peak temperatures ranging from 318-336 °C for the devolatilization of CS and 411-423 °C for the devolatilization of LG. Also, it can be observed that the maximum weight loss rate (%/min) for the CS devolatilization profile increased with increasing concentration of CS in the blends and vice versa for the coal devolatilization profile, without an apparent change in the shape and position of the peaks when compared to that of the single fuels. This may be attributed to the fact that the release of volatiles containing oxygenated components during the devolatilization of CS, generally, does not affect the devolatilization of coal at higher temperatures [60, 65, 66]. However, it must be noted here that the change in the maximum devolatilization rate is not linear with the increase in corn stover percentage indicating the possibility of interactions between the blended fuels.

2.3.2 Thermal Evolution Profiles: Blends with Switchgrass

The thermal evolution profiles of switchgrass and blends of both coals with switchgrass during devolatilization at a heating rate of 20 °C/min are shown in Figures 2.3.3 and 2.3.4 respectively.

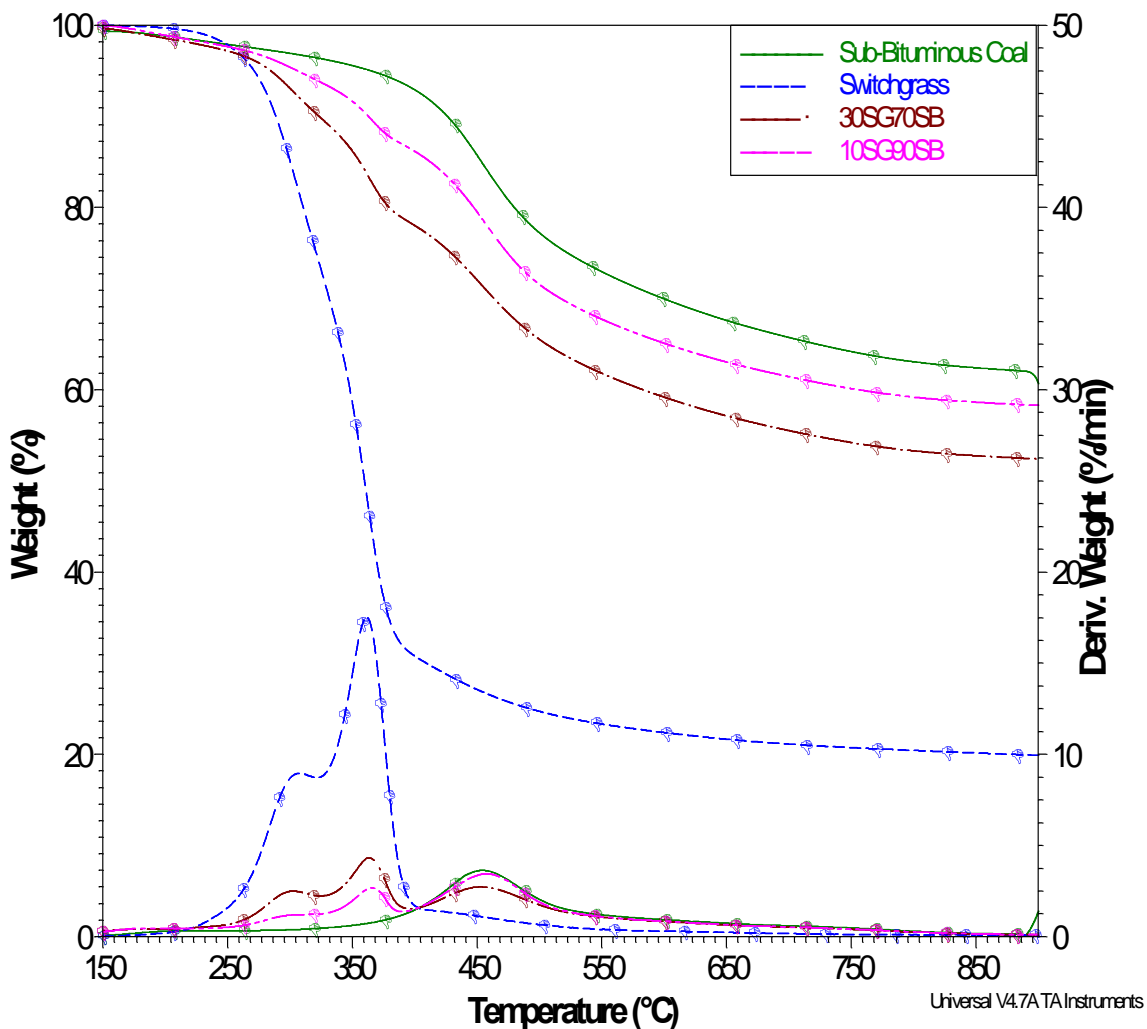


Figure 2.3.3: Weight loss curves and DTG profiles during the pyrolysis of DECS-38 sub-bituminous coal, switchgrass and their blends at 20 °C/min.

The weight loss curves, seen in Figures 2.3.3 and 2.3.4, follow a similar pattern as that of blends with corn stover described in the previous section. The devolatilization interval for switchgrass starts around 175 °C with the decomposition of hemicellulose and ends around 650 °C with the slow decomposition of lignin. The low temperature shoulder, attributed towards the peak hemicellulose decomposition, occurs at 305 °C. The region between 305 °C and 405 °C is attributed towards the decomposition of the cellulose component of switchgrass, with peak decomposition occurring around 360 °C.

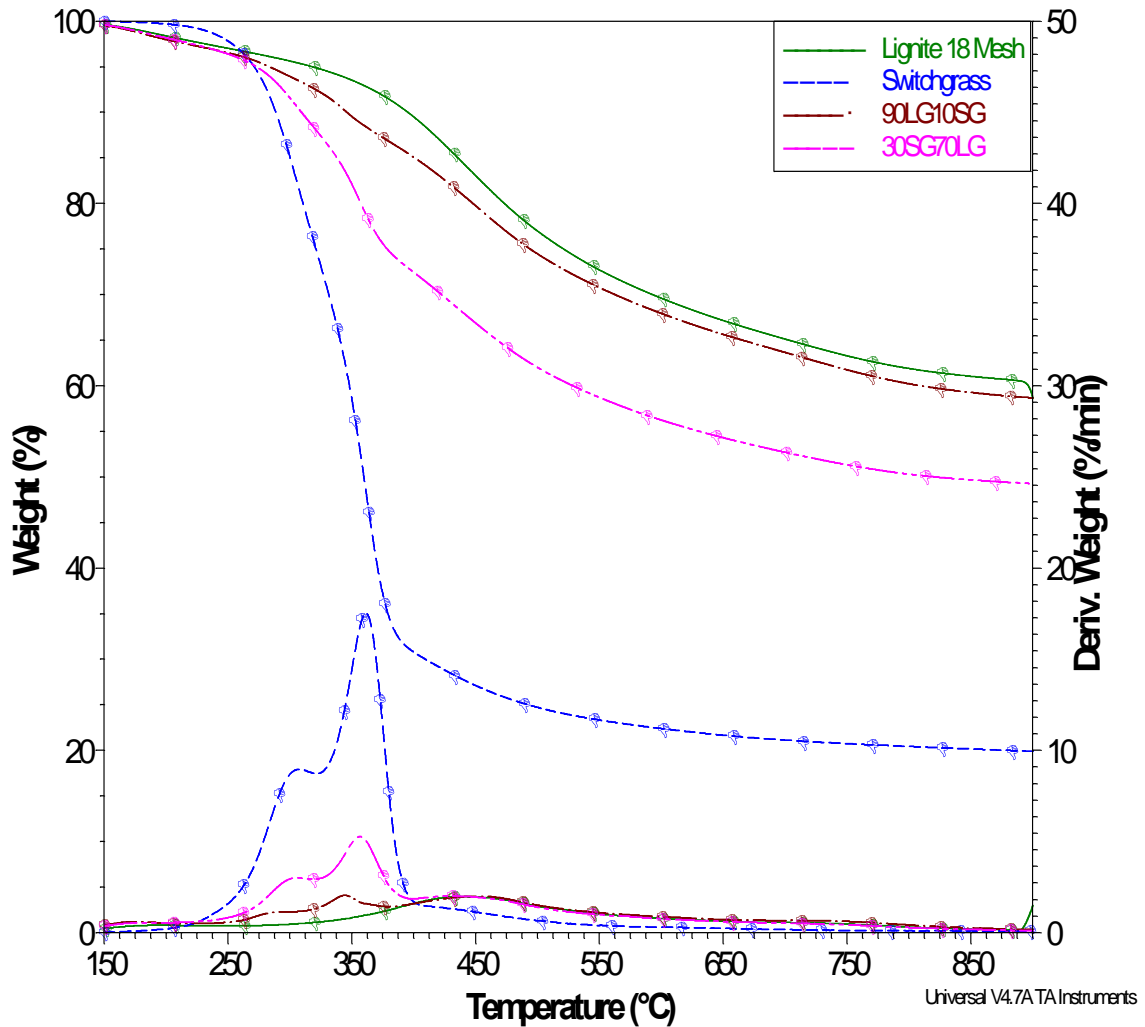


Figure 2.3.4: Weight loss curves and DTG profiles during the pyrolysis of DECS-25 lignite coal, switchgrass and their blends at 20 °C/min.

When compared with blends of corn stover, a clear distinction in the DTG profiles can be observed. For these blends of coals and switchgrass, three different peaks are clearly observed, where the low temperature peaks can be attributed to the decomposition of switchgrass while the high temperature peak is for the decomposition of coals. This is different from those observed in blends with corn stover, where the two low temperature peaks merge which is an indication that some components in coal are interacting with corn stover in the low temperature range of around 220–380 °C. Since there is a clear distinction

in the hemicellulose and cellulose peaks when switchgrass is blended with coal, suggests the fact that no significant interactions are occurring and that the two components are decomposing separately.

2.3.3 Single Fuels: Effect of Heating Rates

The effect of various heating rates ranging from 5 °C/min to 40 °C/min on the devolatilization of single fuels (Figures 2.3.5 through 2.3.8) will be described in this section. The values of T_{\max} and maximum peak heights at various heating rates for all the single feedstocks are shown in Table 2.3.2. Evidently, the maximum peak height and the temperatures at which maximum devolatilization occurs increases with increasing heating rates. In other words, an increase in reactivity of devolatilization is observed with increasing heating rates. Different temperatures affect the point coordinates and thus the slope and intercept of the linear fit represented in Equation 1.9.14 of Chapter 1. This in turn affects the activation energy, E , and the pre-exponential factor, k_0 . It may be inferred from the weight loss profiles and DTG curves of various feedstocks that a possible reason for this shift in temperatures could be because of the fact that less heat is required for the cracking of solid fuel particles into products. At higher heating rates, this process occurs later at slightly higher temperatures due to the fact that heat transfer is not as effective as it were at lower heating rates, where the solid fuel particles are more gradually heated resulting in an effective transfer of heat to the inner portions and within the particles themselves. Therefore, heating rates and temperatures play a crucial role during devolatilization processes.

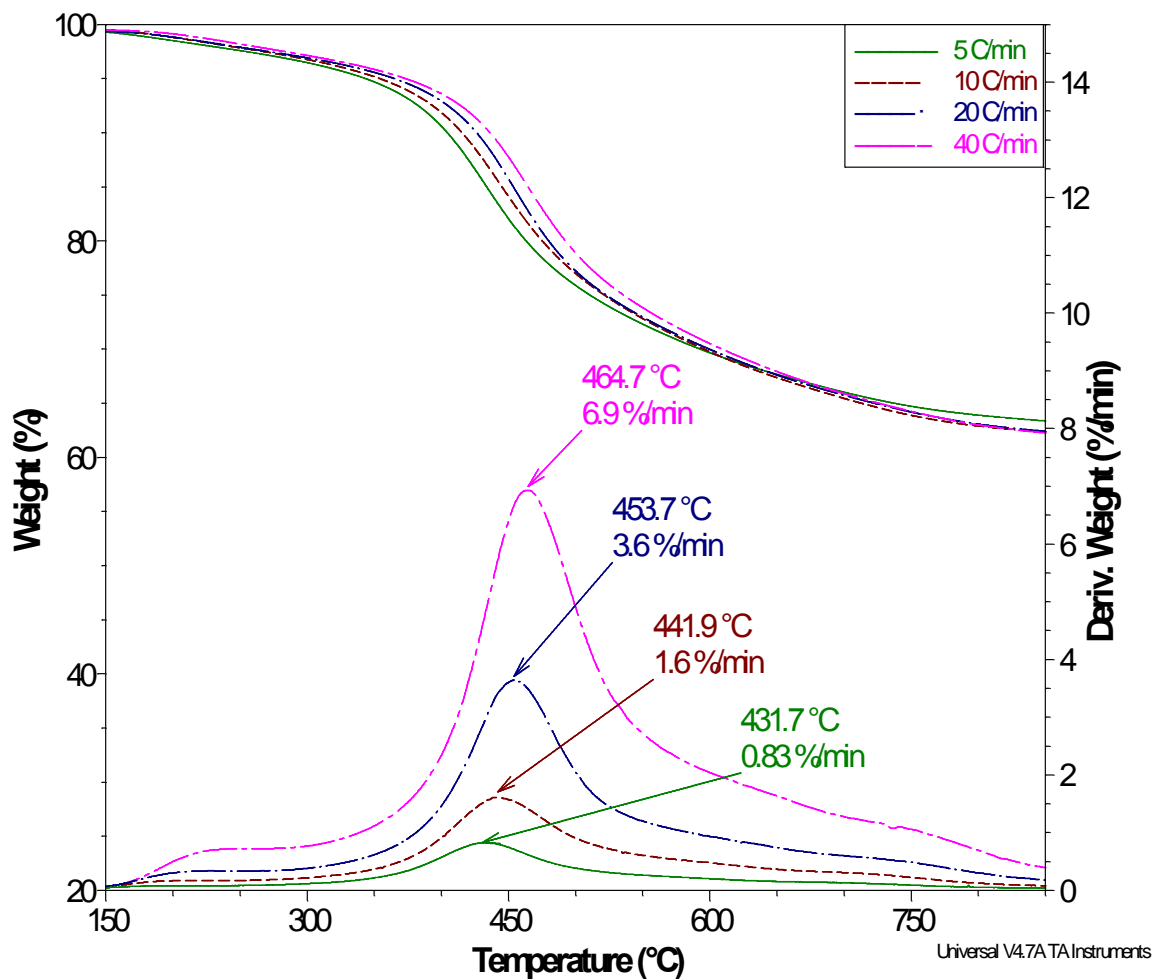


Figure 2.3.5: Weight loss profiles and DTG curves of pyrolysis of DECS-38 sub-bituminous coal at four different heating rates ranging from 5 °C/min to 40 °C/min.

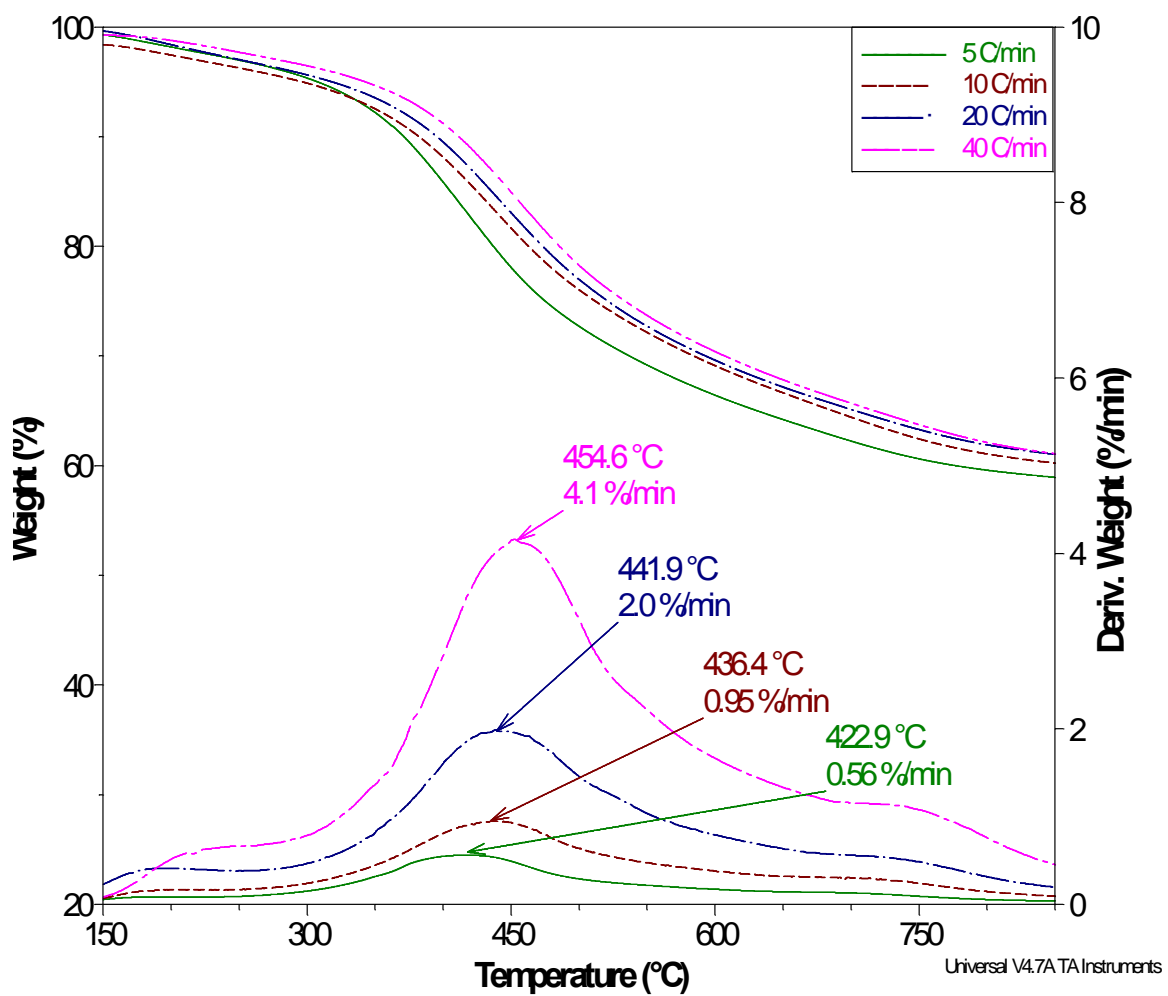


Figure 2.3.6: Weight loss profiles and DTG curves of pyrolysis of DECS-25 lignite coal at four different heating rates ranging from 5 °C/min to 40 °C/min.

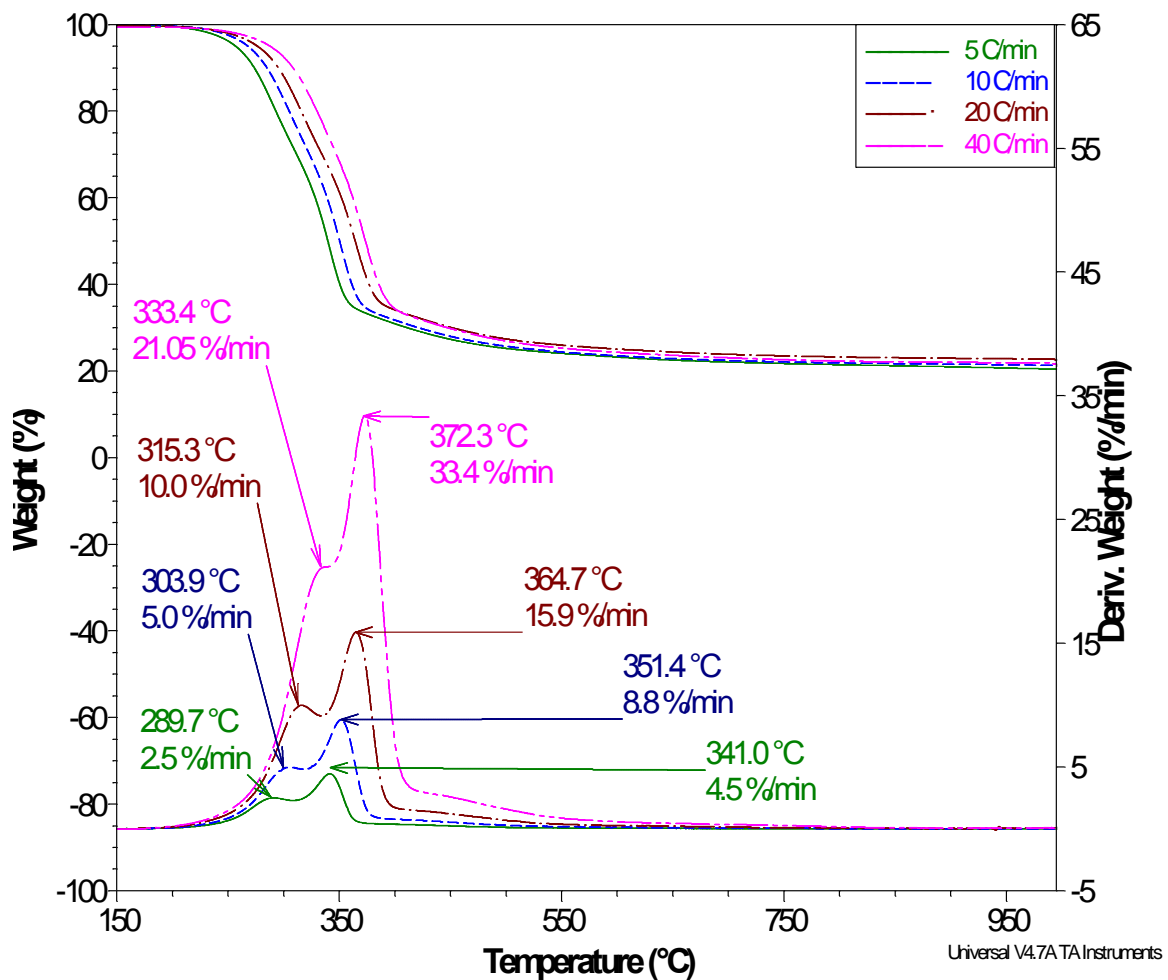


Figure 2.3.7: Weight loss profiles and DTG curves of pyrolysis of Corn Stover at four different heating rates ranging from 5 °C/min to 40 °C/min.

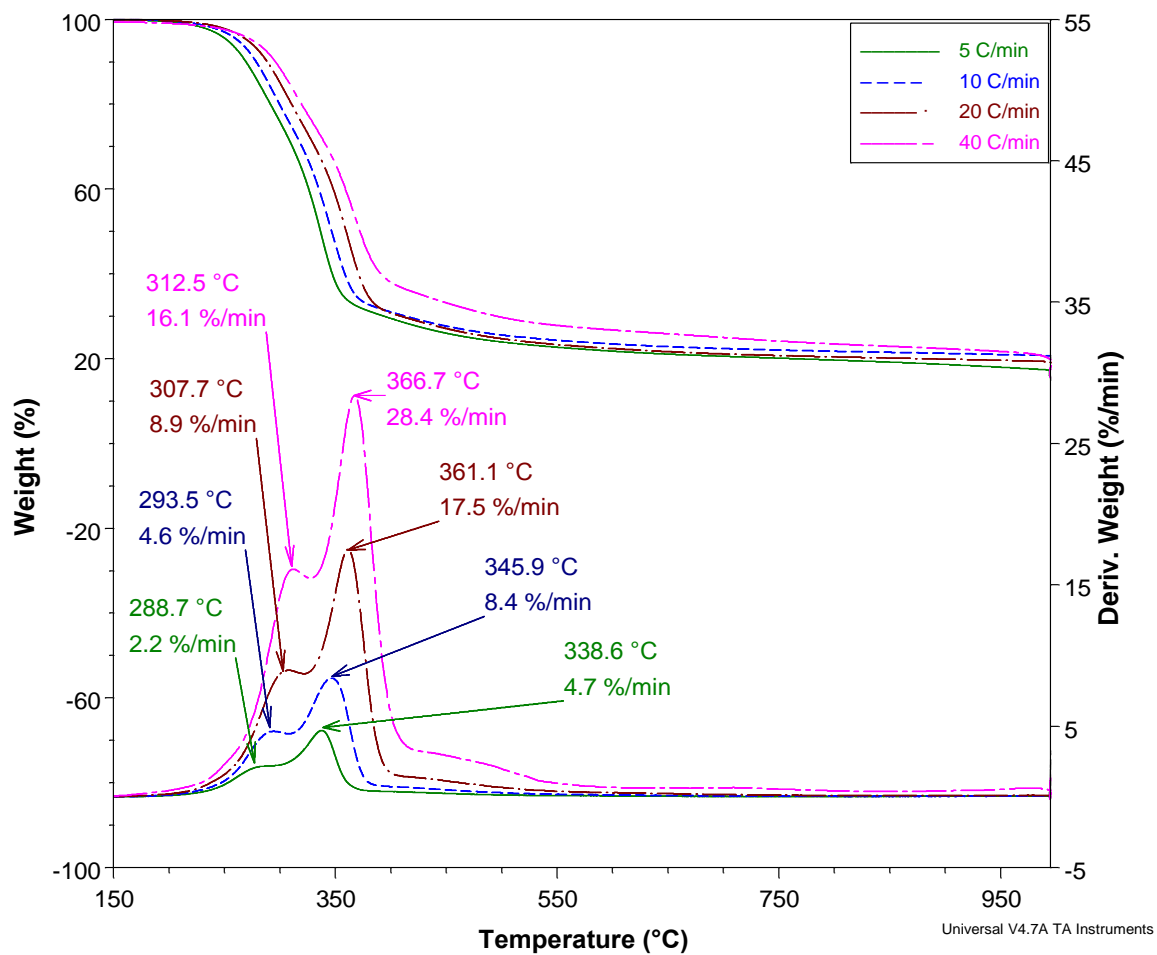


Figure 2.3.8: Weight loss profiles and DTG curves of pyrolysis of switchgrass at four different heating rates ranging from 5 °C/min to 40 °C/min

Table 2.3.2: Maximum Weight Loss Rates and Peak Temperatures Attained During the Devolatilization of Individual Feedstocks at Different Heating Rates

Feedstock Materials	Heating Rates °C/min	Maximum Weight Loss Rate, (%/min) _{max}		Peak Temperature, T _{max} , °C	
		Peak 1	Peak 2	T _{max, 1}	T _{max, 2}
DECS-38 Sub-Bituminous Coal (SB)	5	0.83		432	
	10	1.60		442	
	20	3.60		454	
	40	6.90		465	
DECS-25 Lignite Coal (LG)	5	0.56		423	
	10	0.95		436	
	20	2.00		442	
	40	4.10		454	
Corn Stover (CS)		Peak 1	Peak 2	T _{max, 1}	T _{max, 2}
	5	2.50	4.50	290	341
	10	5.00	8.80	304	351
	20	10.00	15.90	315	365
	40	21.05	33.40	333	372
Switchgrass (SG)	5	2.20	4.70	289	339
	10	4.60	8.40	294	346
	20	8.90	17.50	308	361
	40	16.10	28.40	313	367

2.3.4 Analysis of Synergistic Interactions in Blends

For investigating the synergistic behavior between coal and biomass in the blended feedstocks, the disparity in the amount of volatile matter released was evaluated between the experimental and calculated curves as shown in Figures 2.3.9 and 2.3.10. To better analyze the synergistic behavior between the blended fuels, an additional experimental run consisting of 40 % biomass was also performed. The predicted amount of volatile matter released was calculated using a simple additive relationship [57, 67] as shown in Equation

2.3.1. Here, for the pyrolysis of blends of coal and biomass, if the interaction between the two blended feedstocks shows a faster reaction rate than the sum of the rate of each pure feedstock individually (weighted according to their mixture mass ratio) accounting for experimental uncertainty, then a positive synergistic effect or synergy is noted between the pair. On the contrary, if the interaction of two chars shows no effect on the reaction rate or shows a slower reaction rate than the sum of the weighted rates based on the individual chars, a negative synergistic effect is demonstrated.

$$VM_{Calc, Blend} = X_{Coal} * VM_{Coal, Obs} + X_{CS} * VM_{CS, Obs} \quad (\text{Eq 2.3.1})$$

Where, X_i , refers to the fraction of each material in the blend and VM is the % of volatile matter evolved.

As shown in Figure 2.3.9, for the TGA experimental runs performed, the percentage of volatile matter evolved increases with an increase in the percentage of corn stover in the blend which is an expected result due to the fact that corn stover has higher volatile content inherently.

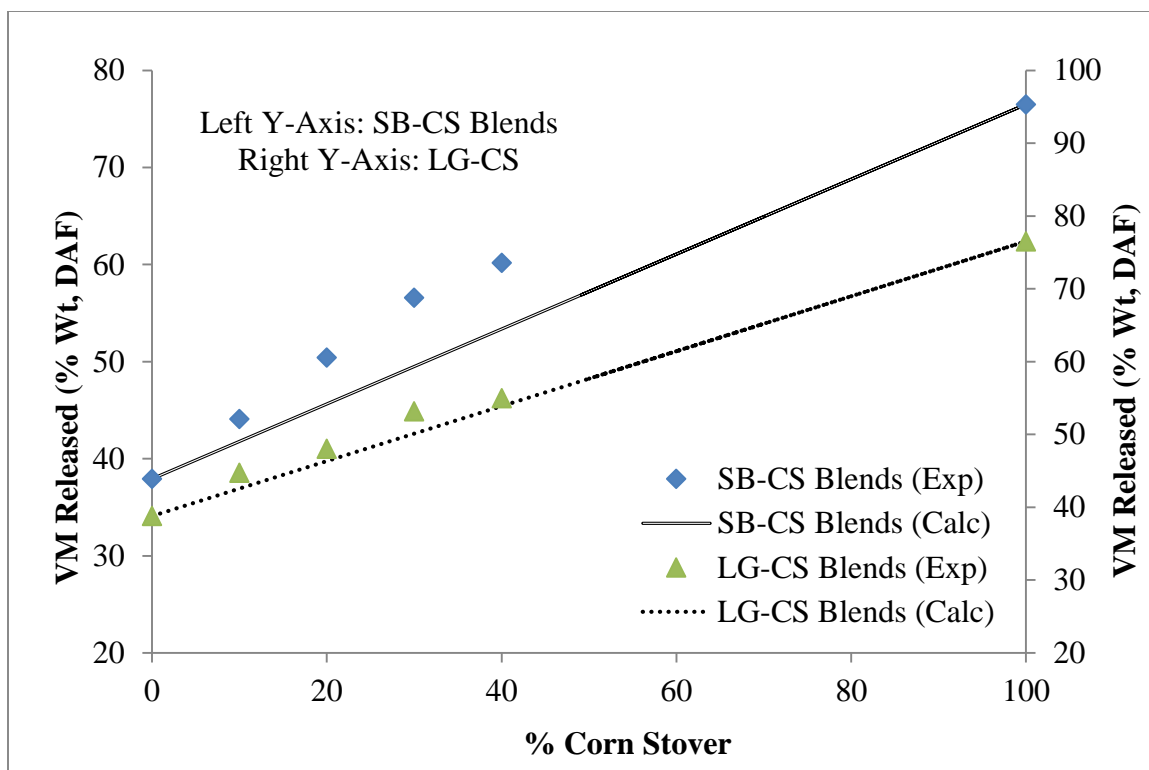


Figure 2.3.9: Disparity in the experimental and predicted curves during the release of volatile matter with increasing concentration of corn stover.

However, it is noteworthy that this increase in volatile matter with increasing corn stover concentration in the blends of corn stover with sub-bituminous coal is not linear with deviations from the predicted yield ranging between 2% -7%, indicating some kind of positive synergistic behavior between the blended materials unlike some previous works indicated in literature [64, 68]. On the contrary, for blends of corn stover with lignite coal, the deviations from the predicted yield are much lower (1% - 3%), implying, very little synergistic interactions between corn stover and lignite coal. To further verify this assumption and delve deeper into the synergistic behavior between the materials, the calculated and experimental DTG curves were plotted as shown in Figure 2.3.11 and Figure 2.3.12. The calculated DTG curves were estimated using an equation similar to Equation

2.3.1 by replacing the % of volatile matter evolved with the weight loss rate of the material. The DTG curves for SB and CS blends show that the predicted and experimental curves match closely at temperatures above 500 °C indicating that synergy between the materials exists at lower temperatures (~ 230-450 °C). Also, increasing the percentage of CS in the blend lowers the temperature (~ 380 °C) until when synergistic behavior is observed. In the case of CS and LG blends, the disparity in the predicted and experimental DTG curves is quite apparent at lower concentrations of CS. The synergistic behavior for 10% CS and 90% LG starts at about 320 °C continuing until the end of pyrolysis. However, increasing the CS percentage to 30% drastically reduces the synergistic behavior. This can be observed only at higher temperatures (~ 380-680 °C), albeit, with very less deviations in both curves.

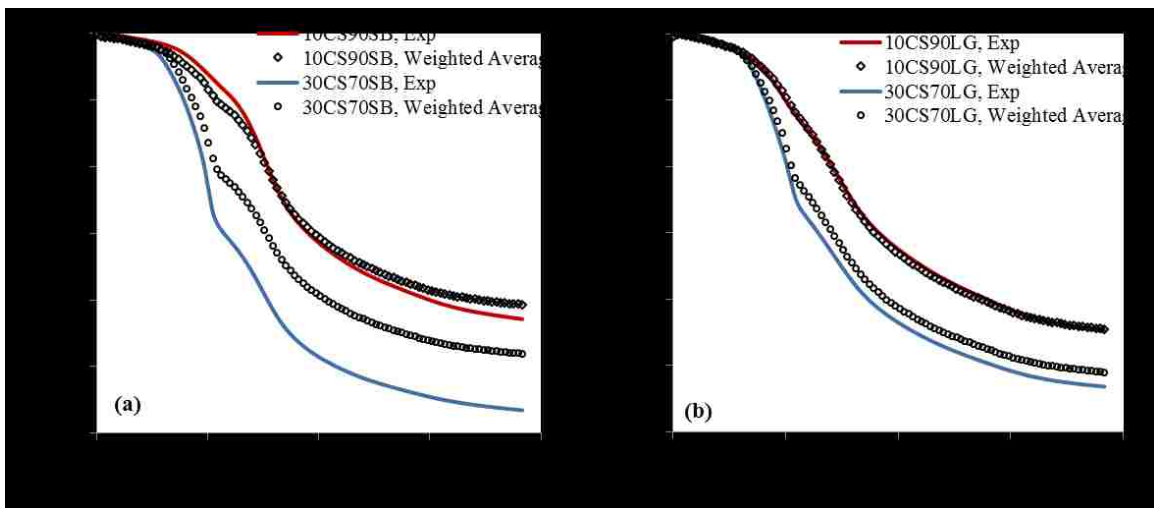


Figure 2.3.10: Comparison of the experimental and predicted weight loss curves for, (a) Blends of DECS-38 Sub-Bituminous Coal and Corn Stover, (b) Blends of DECS-25 Lignite Coal and Corn Stover

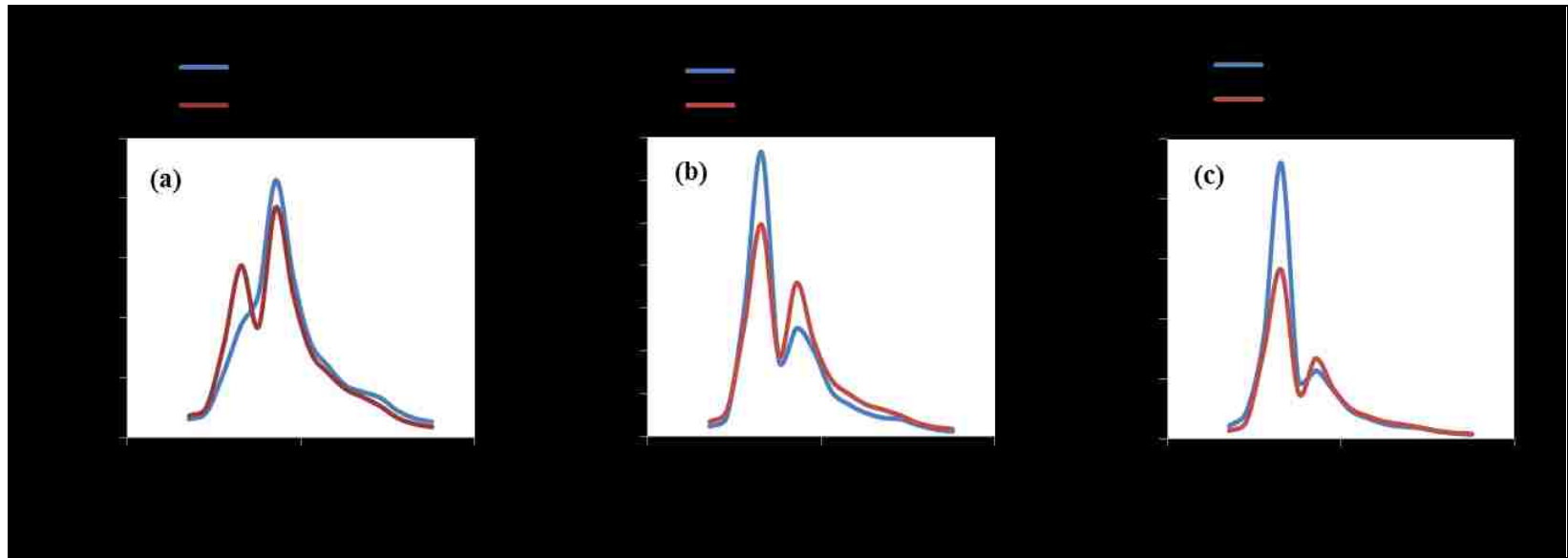


Figure 2.3.11: Comparison of the experimental and predicted DTG curves for, (a) 10% CS + 90% SB blend, (b) 20% CS + 80% SB blend, (c) 30% CS + 70% SB blend

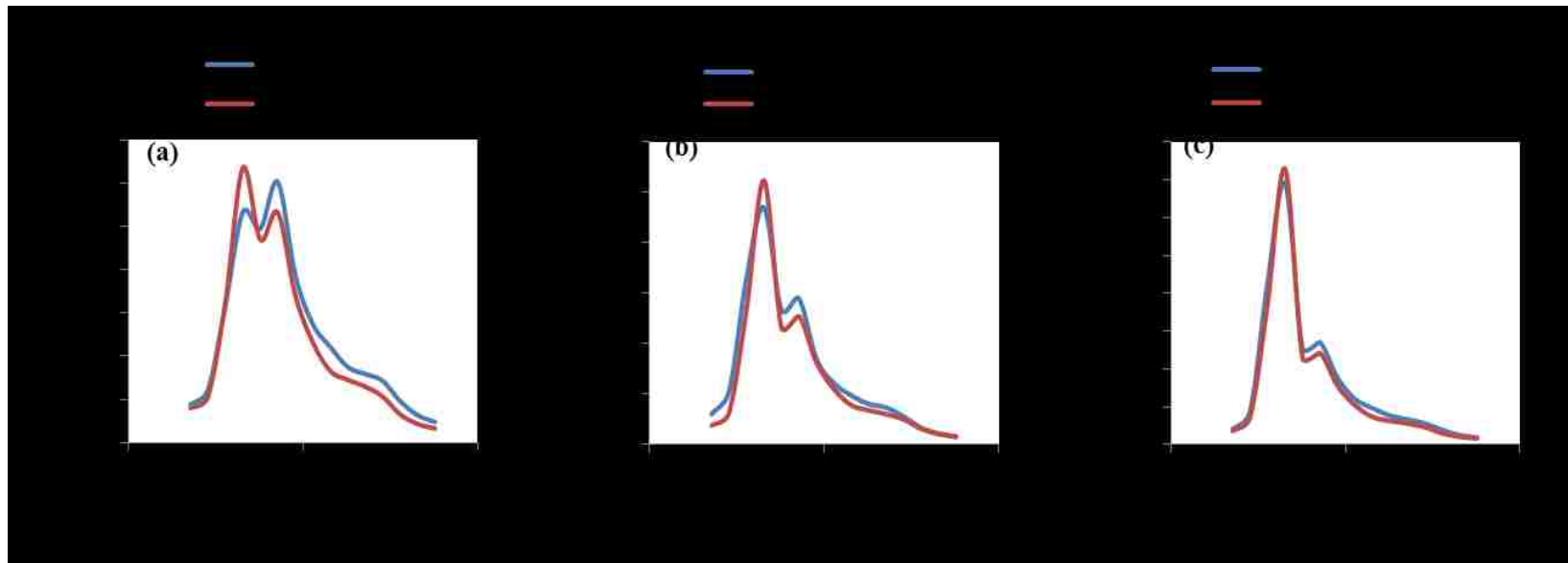


Figure 2.3.12: Comparison of the experimental and predicted DTG curves for, (a) 10% CS + 90% LG blend, (b) 20% CS + 80% LG blend, (c) 30% CS + 70% LG blend

Similar to corn stover blends, the blends containing switchgrass also show an increase in the amount of volatile matter with increasing percentage of switchgrass in the blend. However, clearly, from Figure 2.3.13, it can be stated that the deviations from the predicted and experimental yield is minimal suggesting that no significant interactions are present during devolatilization of blends of coals and switchgrass.

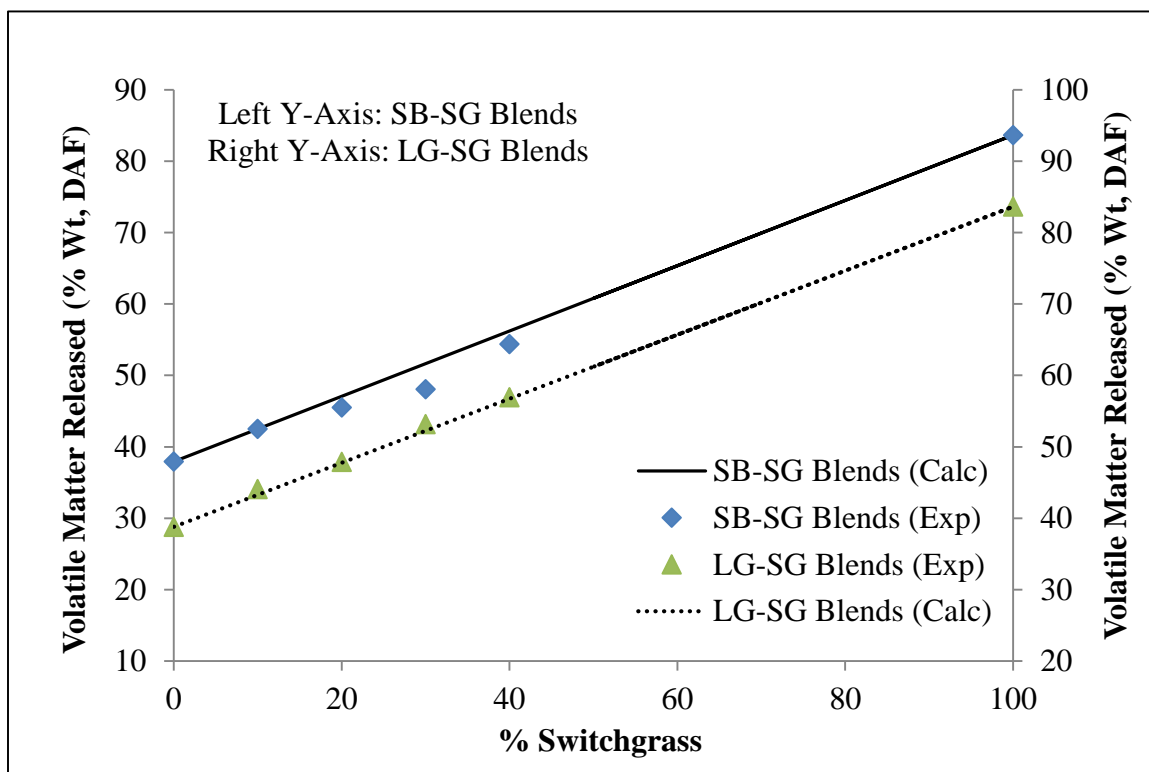


Figure 2.3.13: Disparity in the experimental and predicted curves during the release of volatile matter with increasing concentration of switchgrass.

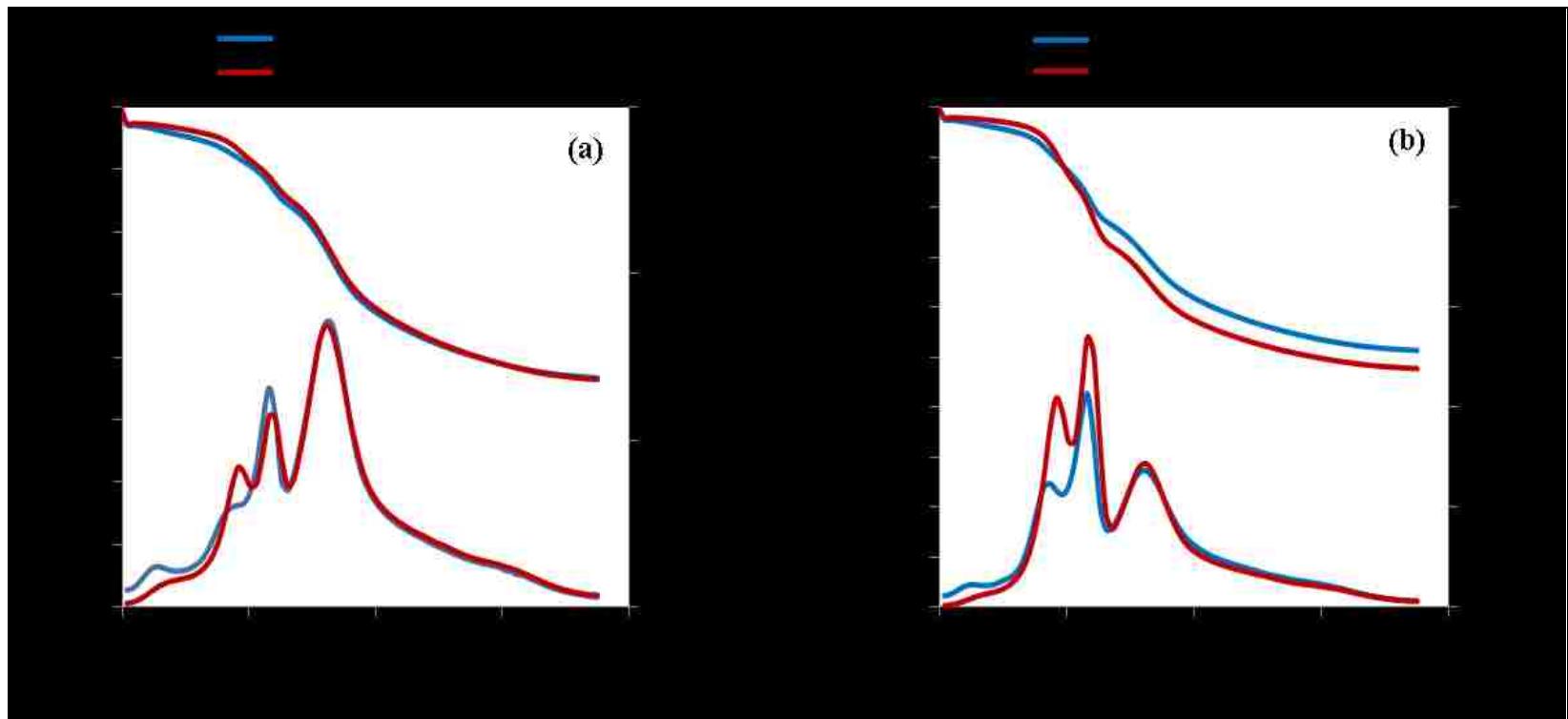


Figure 2.3.14: Comparison of the experimental and predicted weight loss and DTG curves for, (a) 10% SG + 90% SB blend, (b) 30% SG + 70% SB blend

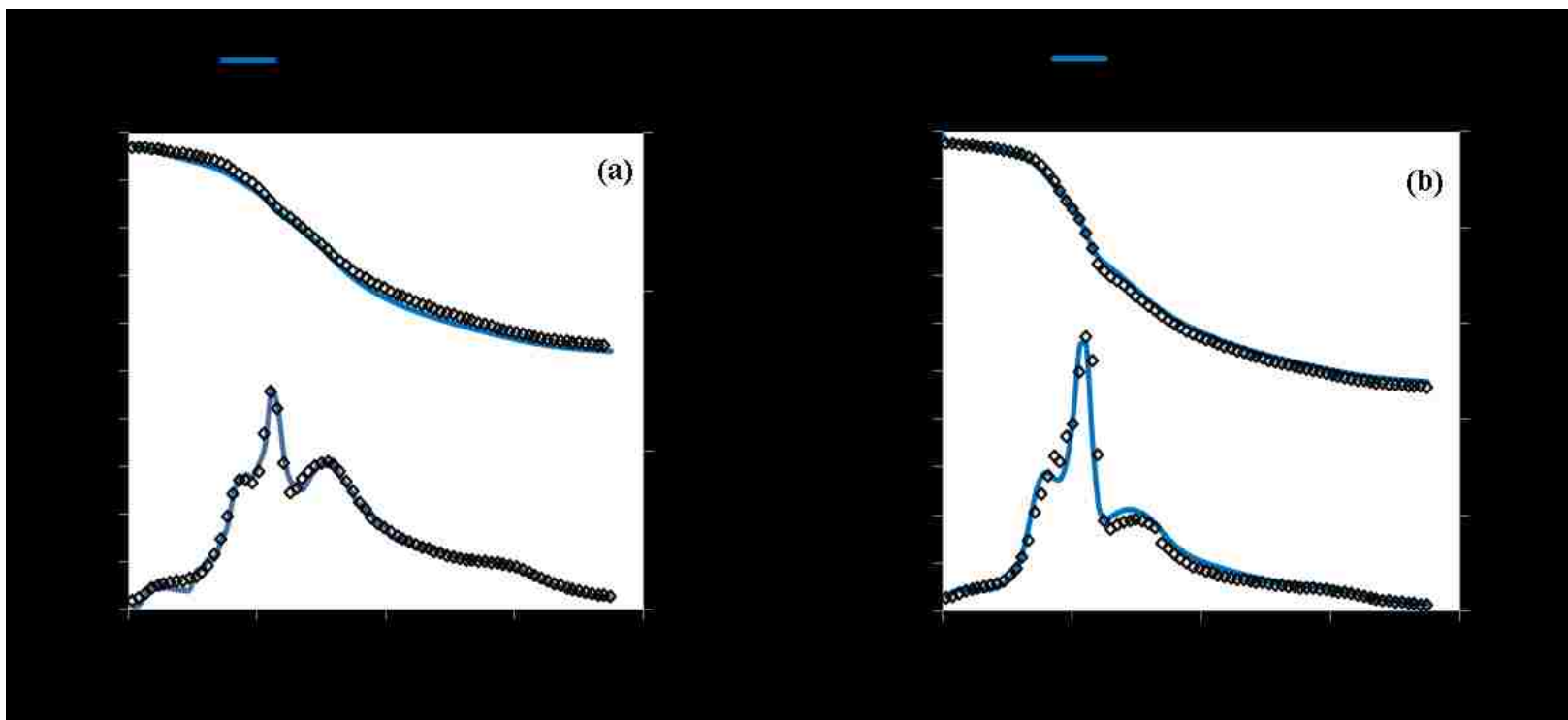


Figure 2.3.15: Comparison of the experimental and predicted weight loss and DTG curves for, (a) 10% SG + 90% LG blend, (b) 30% SG + 70% LG blend

CHAPTER 3: KINETICS MODELING OF PYROLYSIS

In this chapter, a single first order reaction model using the Coats-Redfern approximation was utilized to predict the kinetic parameters of the pyrolysis reaction. The kinetic analysis indicated that each thermal evolution profile may be represented as a single first order reaction. Three temperature regimes were identified of each of the coals while corn stover and the blends were analyzed using two and four temperature regimes respectively. The kinetic parameters were also obtained through two other distributed activated energy models and the results were compared effectively. Ultimately, it has been shown that using the distributed activation energy models, matrix inversion algorithm in particular, is extremely effective and robust in predicting devolatilization kinetics than just using single first order models.

3.1 Parallel First Order Reactions Model: Approximation of Temperature Integral

Several authors have approximated the overall process of pyrolysis as a first-order decomposition occurring uniformly throughout the coal and biomass particles [17, 54, 56, 69-73]. For pyrolysis or oxidation reactions under non-isothermal conditions, the heating rate H plays a very important role in determining the kinetic parameters [54-56, 58, 73]. For a first-order reaction at constant heating rate, $H = dT/dt$:

$$dX/dT = [A(1 - X)/H] \exp(-E/RT) \quad \text{Eq. 3.1.1}$$

Where, A is pre-exponential factor and E is the activation energy.

Integration of the above equation subject to the condition that conversion is zero at initial temperature, T_0 , leads to the following result:

$$\ln(1 - X) = -(A/H) \int_{T_0}^T \exp(-E/RT) dT \quad \text{Eq. 3.1.2}$$

Since, there is no conversion at initial temperature, T_0 , the limits of the integral in Equation 3.1.2 can be conventionally changed to $\int_0^T \exp(-E/RT)$, thereby introducing a new function as represented in Equation 3.1.3.

$$f(y) = \int_y^\infty (e^{-y}/y^2) dy \quad \text{Eq. 3.1.3}$$

Where, $y = (-E/RT)$

Therefore, Equation 3.1.2 reduces to,

$$\ln(1 - X) = -(A/H) f(y) \quad \text{Eq. 3.1.4}$$

Since Equation 3.1.3 cannot be solved analytically, several authors have used different approaches to solve the function $f(y)$ [56, 74-76]. Coats-Redfern approximation [55, 56, 77-79] has been used in this study to determine the approximate value of the temperature integral because of the fact that this method provides the best linearity of the data as opposed to other analytical model-fitting methods [55, 78, 79]. This method is widely used and accepted for the calculation of kinetic parameters. The use of this approximation would help in transforming Equation 3.1.3 into simple linear forms and thus obtaining the activation energy, E and pre-exponential factor, A as shown in Equations 3.1.5 through 3.1.7. In this approximation, $f(y)$ is obtained by assuming an asymptotic expansion where in only the first two terms are utilized.

Coats-Redfern Approximation

$$f(y) = e^{-y}/y^2 \left[1 - (2!/y) + (3!/y^2) - (4!/y^3) + \dots \right] \quad \text{Eq. 3.1.5}$$

Or,
$$f(y) \approx e^{-y}/y^2 \left(1 - \frac{2}{y} \right) \quad \text{Eq. 3.1.6}$$

And,
$$\ln \left[\frac{-\ln(1-X)}{T^2} \right] = \ln \left[\left(1 - \frac{2RT}{E} \right) AR/HE \right] - E/RT \quad \text{Eq. 3.1.7}$$

As described in Equations 3.1.1 through 3.1.7, using Coats-Redfern approximation, the kinetic parameters, activation energy and pre-exponential factor, were determined for both single fuels as well as the blends. From the pyrolysis data obtained, it is evident that different constituents of the sample pyrolyze at different temperatures and each temperature regime may be represented with a specific set of kinetic parameters. Each zone or temperature regime was estimated through inflection points or tangents drawn along the weight loss curves once moisture has been removed. The points corresponding to the tangents were marked as the beginning of a particular temperature zone of the total pyrolysis regime. Figure 3.1.1 shows the first order plot of $\ln [-\ln(1-X)/T^2]$ versus $1/T$. The activation energy can be estimated from the slope of this plot while the pre-exponential factor can be estimated from the intercept by taking the temperature at which $W_t = (W_0 + W_f)/2$.

The pyrolysis of DECS-38 Sub-Bituminous coal may be described as a process with three consecutive first order reactions. For applying Equation 3.1.7, the conversion was recalculated for each zone separately to determine the kinetic parameters for the respective zones. A similar procedure was carried out for estimating the kinetic parameters of DECS-25 Lignite coal and blends of both coals with corn stover. Lignite coal also has

three zones where the first-order analysis can be applied while the corn stover has two independent zones and the blends contain at least four different zones [80]. As an illustration, Figure 3.1.2 depicts the kinetic analysis for the pyrolysis of DECS-38 sub-bituminous coal, corn stover, and 10% CS and 90% SB blend. Thus, the coal devolatilization process can be divided into three stages [63, 64, 73]. For DECS-38 sub-bituminous coal, in the first stage, for temperatures less than 360 °C or until a conversion level of approximately 16 %, only the peripheral parts and the mobile phase of the macromolecular structure of coal decompose. This zone will have relatively lower activation energy as shown in Table 3.1.1. In the second stage, for temperatures between 360 °C and 460 °C (conversion between 16% and 53%), pyrolysis liquids and gases are the main products. As explained earlier, this zone mainly comprises the immobile phase of the coal structure which is more resistant to heat. Therefore, only a small amount of fragmented polycyclic aromatic compounds are produced during this phase. Hence, the activation energy of this phase is much higher than that of the first phase. In the last stage, for temperatures greater than 460 °C, the remaining macromolecular structure of coal is further decomposed. The activation energy in this case is much lower than that of the second phase indicating that during the third stage, repolymerization or cross-linking reaction resulting in the formation of char as the pyrolysis product occurs more easily since most of the volatiles or oxygen containing functional groups have been removed in the previous stages. In addition, it can be observed that the kinetic zones for the coal-biomass blend are slightly different from that of coals.

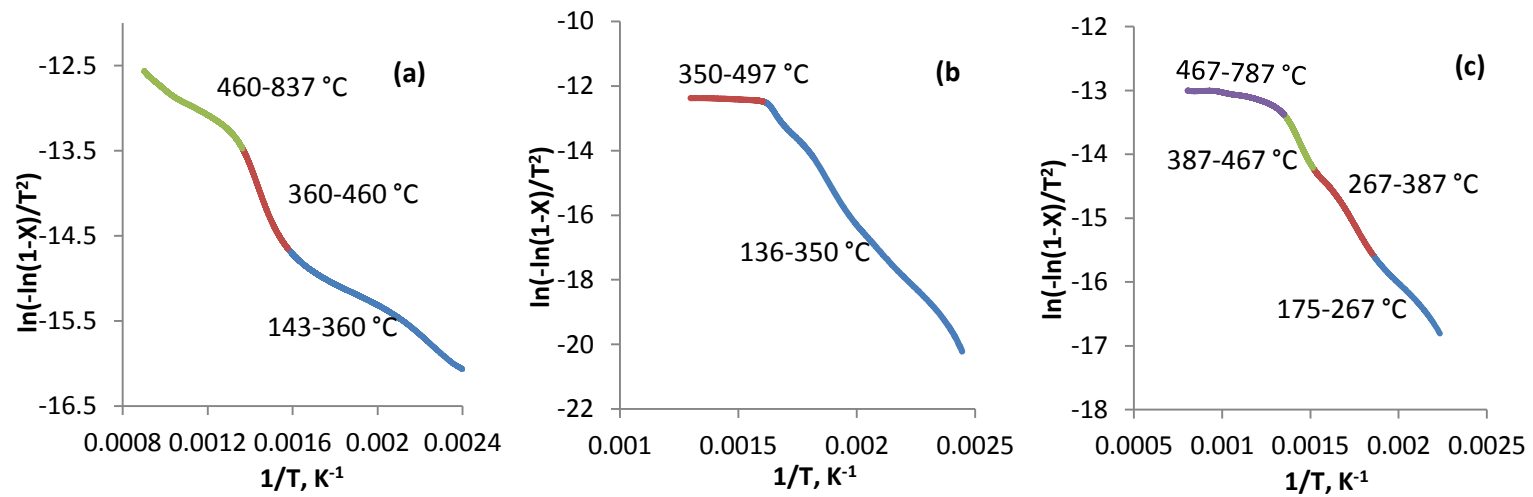


Figure 3.1.1: Analysis of the thermal evolution profiles and temperature ranges for pyrolysis of, (a) DECS-38 sub-bituminous coal, (b) Corn Stover and (c) 10% CS and 90% SB blend.

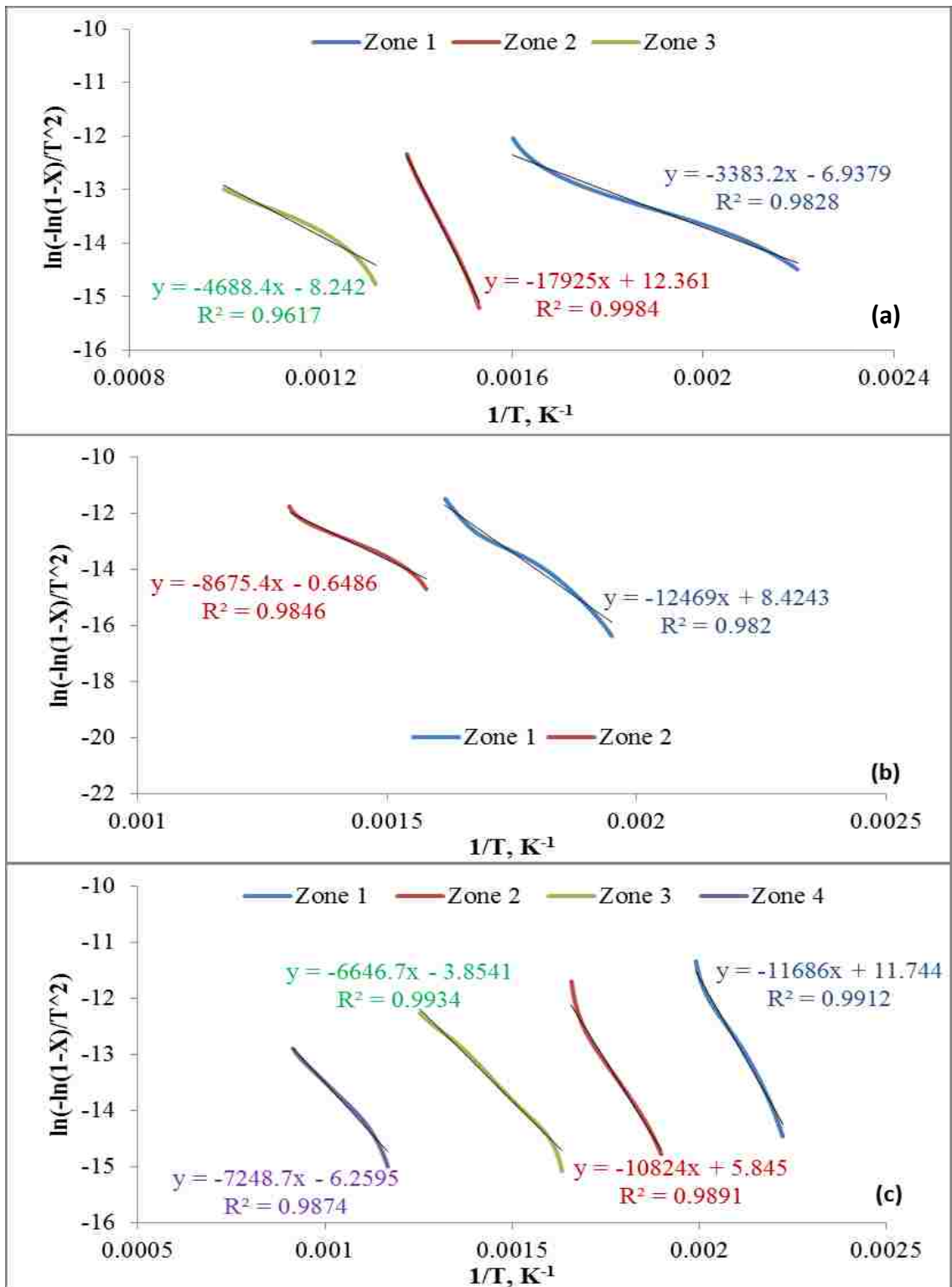


Figure 3.1.2: Estimation of kinetic parameters (activation energy and Arrhenius constant) for pyrolysis of (a) DECS-38 sub-bituminous coal, (b) Corn Stover and (c) 10% CS and 90% SB blend.

Table 3.1.1: Obtained pyrolysis kinetic parameters, temperature and conversion ranges for all feedstocks at a heating rate of 5 °C/min.

Feedstock Materials	Temperature °C	Conversion Range, %	Activation Energy E, KJ/mol	Arrhenius Constant, min⁻¹
DECS-38 Sub-Bituminous Coal (SB)	143 - 360	2-16	28.13	2.46E+01
	360 - 460	16 - 53	149.03	2.27E+10
	460 - 837	53-98	38.98	9.55E+00
DECS-25 Lignite Coal (LG)	175-281	2-9	56.96	8.37E+04
	281-457	9-55	78.15	1.13E+05
	457-791	55-97	41.75	1.40E+01
Corn Stover (CS)	136 - 350	3-77	103.67	3.13E+08
	350 - 497	77-92	72.13	2.69E+04
10% CS + 90% SB	175-267	1-5	67.90	1.36E+06
	267-387	5-25	82.47	1.20E+06
	387-467	25-57	179.16	3.37E+12
	467-787	57-97	25.69	1.18E+00
20% CS + 80% SB	150-244	1-5	57.39	1.92E+05
	244-360	5-38	107.69	6.30E+08
	360-496	38-75	107.07	9.69E+06
	496-843	75-97	45.85	1.88E+01
30% CS + 70% SB	166-231	1-5	97.16	8.02E+09
	231-332	5-43	89.99	2.09E+07
	332-550	43-86	55.26	8.89E+02
	550-854	86-97	60.27	9.31E+01
10% CS + 90% LG	156-265	1-7	53.61	9.52E+04
	265-338	7-22	138.82	9.92E+11
	338-451	20-53	100.42	1.29E+07
	451-853	53-98	28.71	3.63E+00
20% CS + 80% LG	156-224	2-6	64.59	2.69E+06
	224-308	6-18	126.01	2.06E+11
	308-437	18-61	96.90	3.02+03
	437-835	61-97	30.37	1.53E+00
30% CS + 70% LG	171-245	1-5	87.10	2.85E+08
	245-342	5-45	99.15	1.22E+08
	342-455	45-71	93.14	1.81E+06
	455-880	71-98	34.98	4.53E+00

For coal-biomass blends, four independent reactions are used to describe the co-pyrolysis process. It can be noted that the conversion range for the first stage is only up to ~ 7 % indicating that the main decomposition of the coal-biomass blend occurs at higher temperatures. As seen from Table 3.1.1, the kinetic parameters for the different thermal evolution profiles during the co-pyrolysis of coal and corn stover blends have been predicted. The good correlation factor indicates that each thermal evolution profile may be represented as a single first order reaction.

3.2 Distributed Activation Energy Model: Gaussian Distribution of Activation Energy

Kinetic parameters obtained using the single first order reaction models are actually a starting point in the devolatilization modeling. Although simple and used as a starting point for more complex models, a single first order reaction model utilized for estimating the devolatilization kinetics of complex materials is only applicable over a limited range of experimental conditions. The kinetic parameters obtained through such a model may not be used as global parameters and that the parameters such as activation energy and pre-exponential factor change for different heating rates, i.e, the parameters obtained through one experimental condition may not be extrapolated to an unknown heating rate. More accurate and specific models are required to meet the experimental results of each material, one model being the distributed activation energy model [[52](#), [53](#)].

Since coal and biomass are complex fuels with a wide variety of chemical groups, the distributed activation energy model treats the thermal decomposition process as a large number of independent, parallel rate processes or decomposition of many different chemical groups where each group is characterized uniquely by its activation energy. The thermal decomposition of a single organic species can be described as an irreversible first-

order reaction with respect to the amount of unreacted material remaining. Thus, the rate at which the volatiles are produced by a particular reaction can be defined according to the mass balance on the reactant species.

$$\frac{dV_i}{dt} = k_i(V_i^* - V_i) \quad \text{Eq. 3.2.1}$$

$$V_i^* - V_i = V_i^* \exp\left(-At \exp\left(-\frac{E}{RT}\right)\right)_i \quad \text{Eq. 3.2.2}$$

Where V_i^* is the final quantity of volatile matter for the generic species, i , and k_i is the rate constant of the reaction expressed according to the Arrhenius law.

This type of kinetic model requires that the amount of volatiles and kinetic parameters known for all the single reactions. To estimate these parameters from experimental data for all the reactions is practically not possible. The problem can be simplified if it is assumed that the rate constants for all the reactions differ only in the activation energy. The number of reactions is large enough so that the activation energy can be expressed as a continuous Gaussian distribution function $f(E)$ and $f(E)dE$ representing the potential loss of volatile fraction with activation energy between the intervals E and $E + dE$. Thus,

$$V_i^* = dV^* = V^* f(E)dE \quad \text{Eq. 3.2.3}$$

The total amount of volatile material unreleased is obtained by summing the contribution from each reaction, that is, by integrating Equation 3.2.2 over all values of E using Equation 3.2.3. Finally, the yield of volatiles can be calculated using Equation 3.2.4.

$$\frac{(V^* - V)}{V^*} = \left[\int_0^\infty \exp\left(-\left(\int_0^t k dt\right) f(E)dE\right) \right] \quad \text{Eq. 3.2.4}$$

Where, $k = A \text{Exp} \left(-E/RT \right)$ Eq. 3.2.5

And, $f(E) = (\sigma(2\pi)^{0.5})^{-1} \exp \left[-(E - E_0)^2 / 2\sigma^2 \right]$ Eq. 3.2.6

Where, V^* is the global volatile quantity of the material, E_0 is the mean activation energy and σ is the standard deviation of the activation energy. This approach avoids the low values of the activation energies which result when a single first-order reaction model is applied to fit a temperature dependence that arises from the occurrence of different reactions in different temperature intervals [17].

In this work, Miura's method is used to estimate $f(E)$ and A values [81] for all the feedstock materials. Both $f(E)$ and A are obtained from at least three thermogravimetric experiments using different heating profiles without assuming any functional forms for $f(E)$ and A [82].

The procedure used to estimate $f(E)$ and A is summarized as [81, 82]:

- (1) Measure V/V^* vs. T using at least three different heating rates on a dry and ash-free basis.
- (2) Calculate the values of $\ln(H/T^2)$ and $1/(RT)$ at the same V/V^* , where H is the heating rate.
- (3) Plot $\ln(H/T^2)$ and $1/(RT)$ at the selected V/V^* ratio and then determine the activation energies E from the slopes and A from the intercept as shown in Equation 3.2.7.

$$\ln \left(\frac{H}{T^2} \right) = \ln \left(\frac{AR}{E} \right) + 0.6075 - \frac{E}{RT}$$
 Eq. 3.2.7

- (4) Plot V/V^* and E and differentiate the V/V^* vs. E relationship by E to obtain $f(E)$.

(5) Pre-exponential factor, A, can be expressed as a function of activation energy using the following expression:

$$A = \alpha \text{Exp}(E\beta) \quad \text{Eq. 3.2.8}$$

Where, α and β are constants dependent on the reacting material.

For illustration of the distributed activated energy model (DAEM), Figures 3.2.1 through 3.2.4 describe the method for establishing the kinetic parameters during the pyrolysis of DECS-38 sub-bituminous coal. For different heating rates ranging from 5 °C/min to 40 °C/min, Figure 3.2.1 describes the linear relationship between $\ln(H/T^2)$ and $1/T$ at various conversions. The idea is that, with increase in heating rates, the temperature required to attain a particular conversion increases and hence, the kinetic parameters can be determined at each conversion point. Once the activation energies at selected conversions are determined, the relationship between conversion (V/V_f) and activation energies needs to be established through a plot of V/V_f vs E as shown in Figure 3.2.2. The relationship between V/V_f and E is fitted using a logistic distribution curve using Equation 3.2.9:

$$\frac{V}{V_f} = A_2 + \frac{(A_1 - A_2)}{\left(1 + \left(\frac{E}{E_0}\right)^p\right)} \quad \text{Eq 3.2.9}$$

where A_1 and A_2 are the initial and final conversion points, E_0 is the mean activation energy and p is a constant. The values of these constant are obtained by fitting the experimental data with Equation 3.2.9.

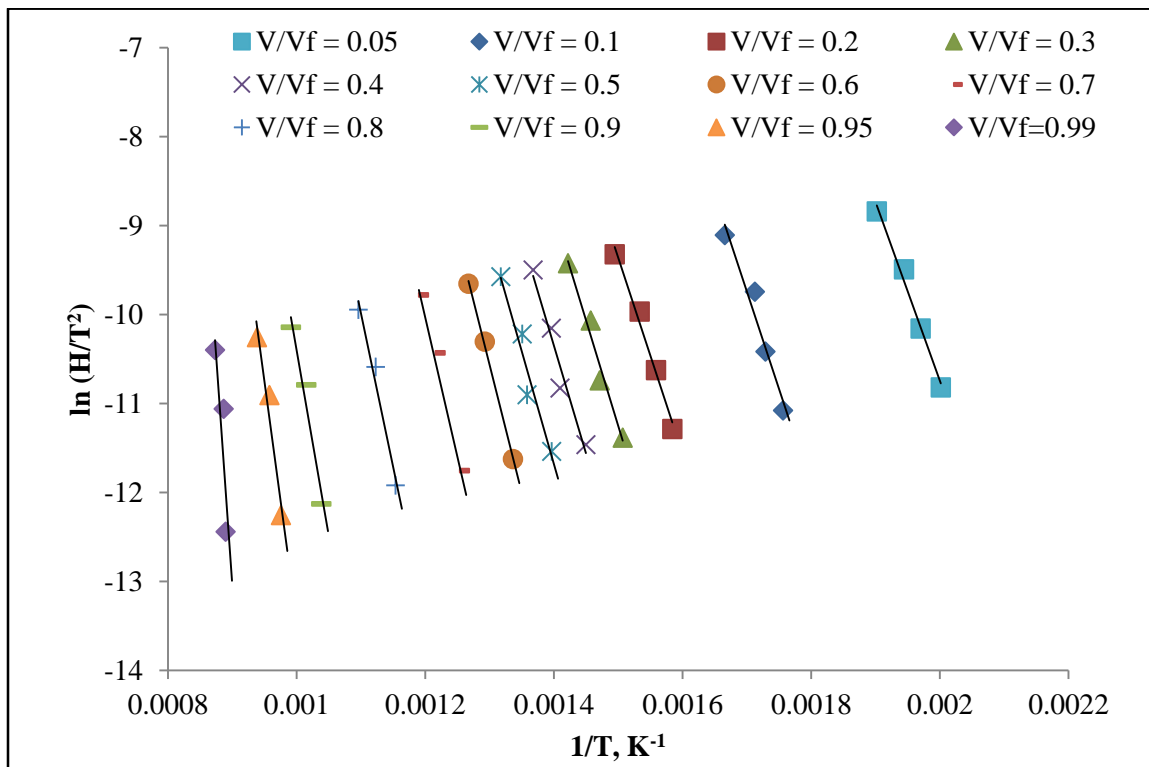


Figure 3.2.1: Plot for estimating the activation energy and Arrhenius constant for pyrolysis of DECS-38 sub-bituminous coal at various heating rates and conversion points using DAEM.

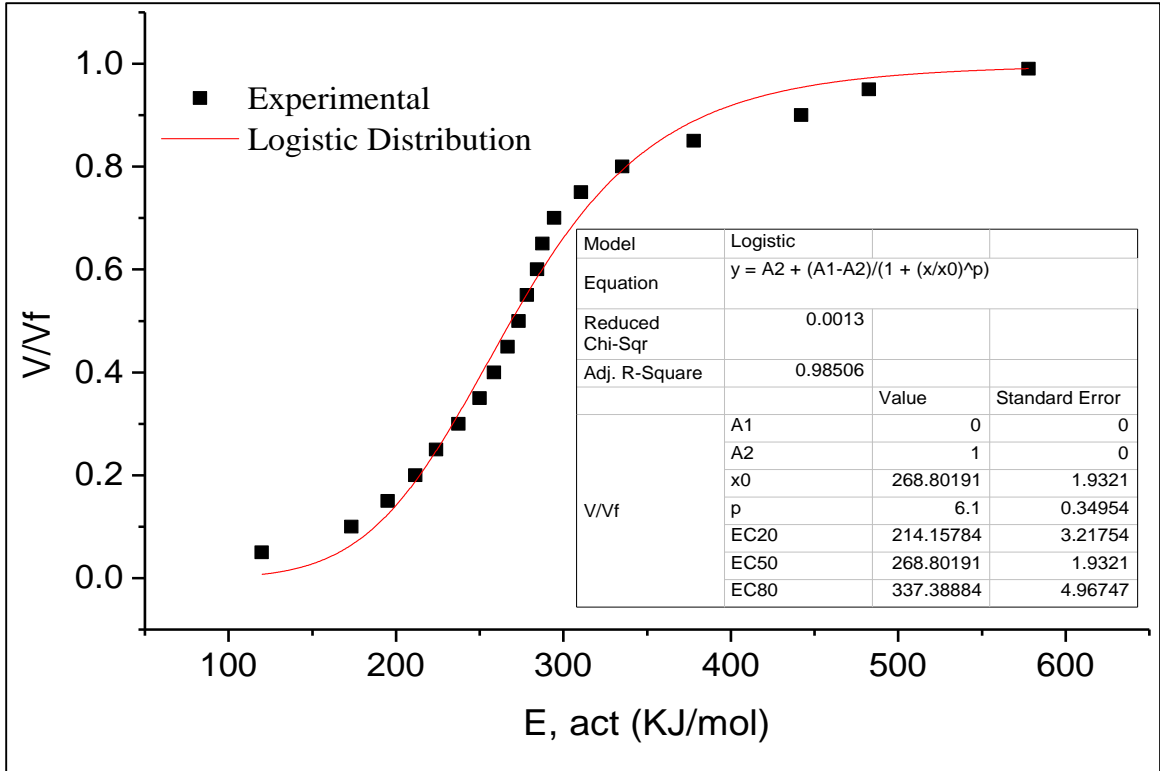


Figure 3.2.2: Plot for estimating the relationship between V/V_f and activation energy for pyrolysis of DECS-38 sub-bituminous coal using DAEM.

Once the relationship between V/V_f and E is established and the unknown constants obtained, Equation 3.2.9 can be differentiated with respect to E to obtain the values for the function $f(E)$. Finally, a plot of the obtained $f(E)$ values with respect to the activation energy shown in Figure 3.2.3, can be fitted using a Gaussian distribution function and that the complex devolatilization reaction kinetics of carbonaceous materials may not be represented by only a single first order reaction but, the reaction is made up of several parallel reactions occurring simultaneously with increasing temperatures.

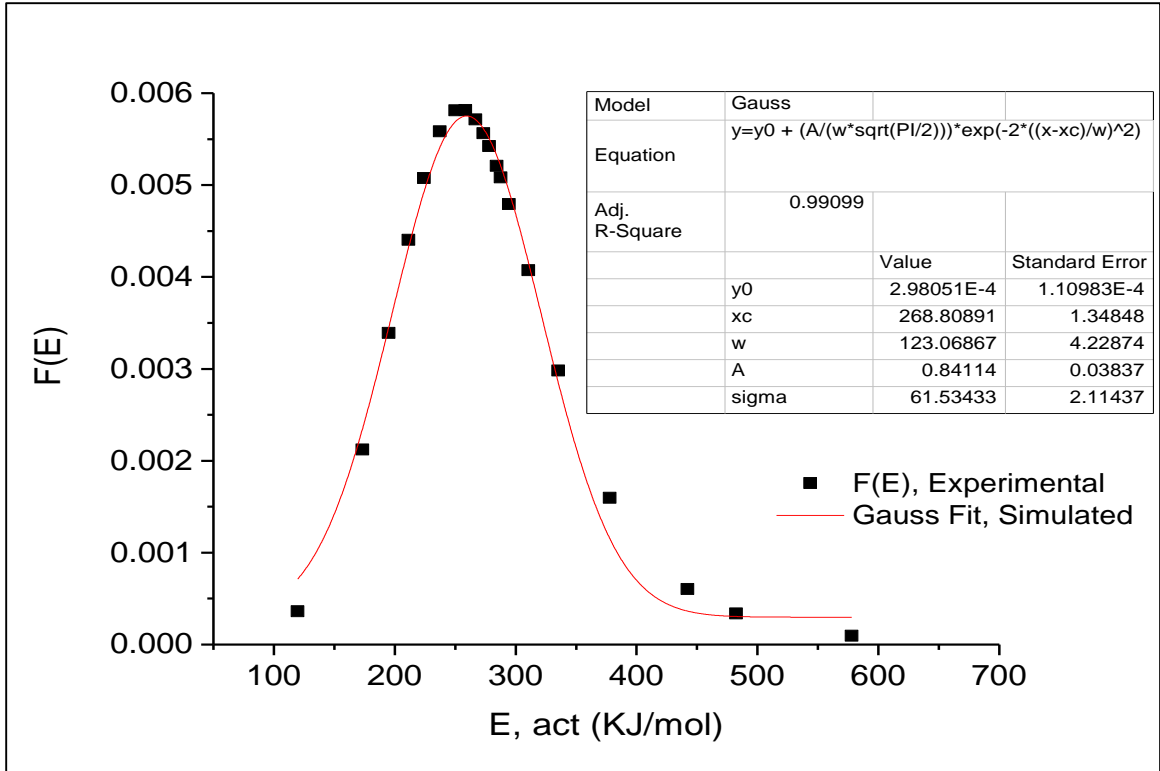


Figure 3.2.3: Plot for estimating the relationship between f (E) and activation energy for pyrolysis of DECS-38 sub-bituminous coal using DAEM.

As seen from Figure 3.2.3, for DECS-38 sub-bituminous coal, the peak of f (E) occurs at 0.00575 KJ/mol corresponding to an activation energy of approximately 269 KJ/mol and the distribution of activation energies follows an approximate Gaussian function ($R^2 = 0.99$). The range of activation energies is between 120-578 KJ/mol within the devolatilization conversion interval of 5-99%.

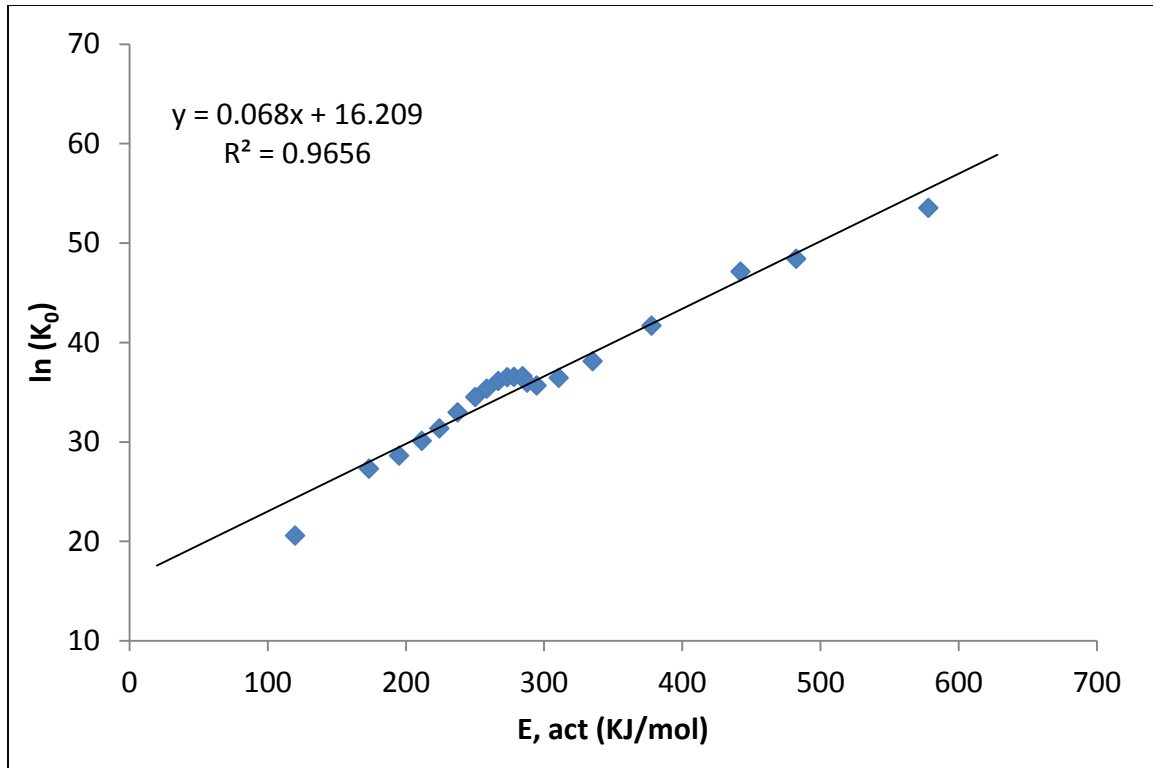


Figure 3.2.4: Plot for estimating the relationship between Arrhenius constant and activation energy for pyrolysis of DECS-38 sub-bituminous coal using DAEM.

From Figure 3.2.4, it may be observed that a linear relationship with reasonable correlation coefficient ($R^2 = 0.97$) exists between $\ln k_0$ and activation energy. For the devolatilization interval, the values of k_0 range between $e^{20} - e^{53} \text{ min}^{-1}$ for DECS-38 sub-bituminous coal corresponding well to the values available in literature for coals with similar properties [81, 82].

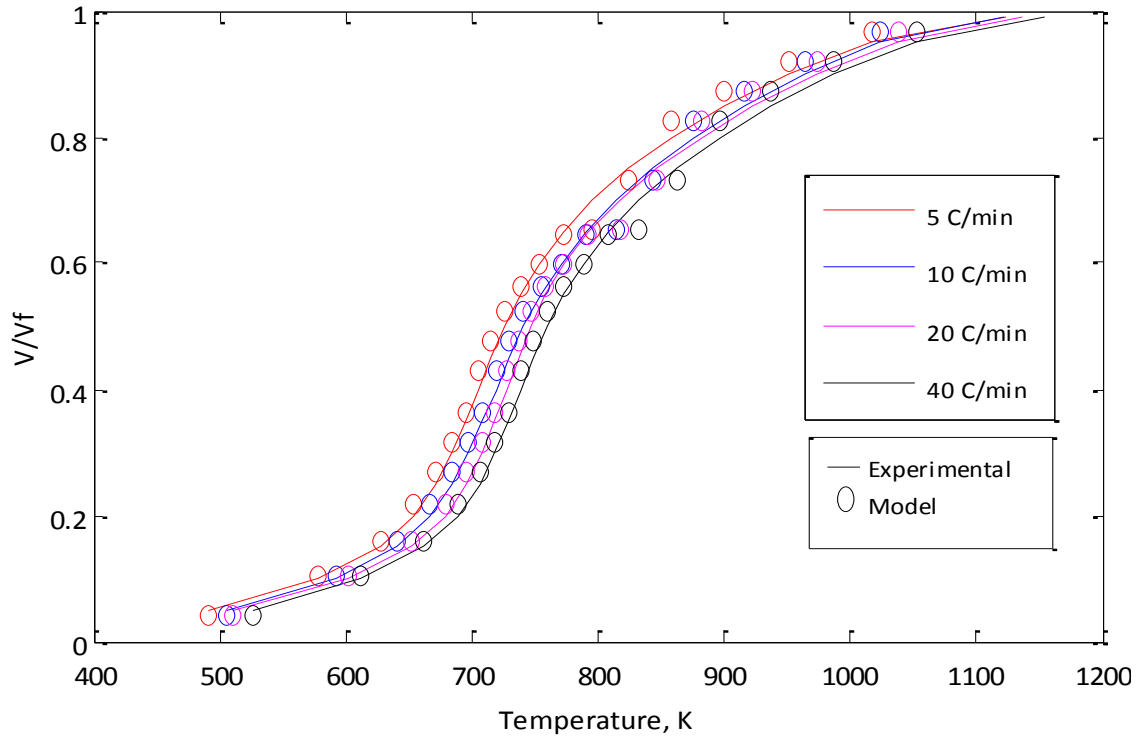


Figure 3.2.5: Comparison between experimental and calculated devolatilization weight loss of DECS-38 sub-bituminous coal with increasing temperature using DAEM.

Using the kinetic parameters thus obtained, Equation 3.2.4 is then solved using the quadrature function of MATLAB to predict the weight loss or conversion profiles during devolatilization at all heating rates and compared with the experimental data as shown in Figure 3.2.5. From Figure 3.2.5, it can be observed that the weight loss profiles can be predicted with greater accuracy when compared with that of Method 1. Similar procedure has been utilized for analyzing the devolatilization kinetic parameters of all the feedstock materials and these values are shown in Table 3.2.1.

Table 3.2.1: Obtained pyrolysis kinetic parameters for single fuels and blended feedstocks using distributed activation energy model (Gaussian distribution of activation energies)

Feedstock Materials	Activation Energy Range KJ/mol	Peak f (E), KJ/mol	Peak Activation Energy, KJ/mol	Arrhenius Constant Range, min⁻¹
DECS-38 Sub-Bituminous Coal (SB)	120-578	0.00575	269	$e^{20} - e^{53}$
DECS-25 Lignite Coal (LG)	100-446	0.00936	210	$e^{19} - e^{43}$
Corn Stover (CS)	91-256	0.00859	171	$e^{14} - e^{40}$
10% CS + 90% SB	118-374	0.0042	220	$e^{23} - e^{46}$
30% CS + 70% SB	110-350	0.0061	175	$e^{17} - e^{46}$
10% CS + 90% LG	95-396	0.0047	226	$e^{27} - e^{42}$
30% CS + 70% LG	92-320	0.00875	154	$e^{17} - e^{26}$

3.3 Matrix Inversion Method

As described in Section 3.2, the devolatilization mass loss of a complex carbonaceous material can be uniquely characterized within an activation energy interval of E and $E + dE$ at any particular time t [83-85]. If the decomposition is considered to be first order, then Equation 3.2.4 can be re-written in the following form:

$$m(E, t) = m_0(E) \Psi (E, t) \quad \text{Eq. 3.3.1}$$

And,
$$\Psi (E, t) = \text{Exp} \left[-A(E) \int_0^t \text{Exp} \left(-E/RT \right) dt \right]$$

Where, $m (E, t)$ is the mass density function of the volatile material at any time t and $m_0 (E)$ is the initial mass of volatile material within the interval E and $E + dE$.

Since $m (E, t)$ cannot be measured quantitatively, integrating Equation 3.3.1 over all activation energies enables the calculation of total amount of material decomposed, $M_v (t)$, at any time t .

$$\frac{M_v (t)}{M_{v0}} = \frac{M_{v0} - V (t)}{M_{v0}} = \int_0^\infty g (E) \Psi (E, t) dE \quad \text{Eq. 3.3.2}$$

And,
$$g (E) = \frac{m_0 (E)}{\int_0^\infty m_0 (E) dE}$$

Where, $M_v (t)$ is the mass of volatiles at any time t , M_{v0} is the initial mass of volatile matter, $V (t)$ is the yield of volatiles and $g (E)$ is the underlying initial distribution of activation energies.

Since, $g (E)$ is unknown, calculation of activation energies and pre-exponential factors for each parallel reaction is more complex. To overcome this complexity, a mathematical inversion method which does not rely on any assumption of the initial distribution of activation energies is utilized in this research for estimating the kinetic parameters. This method was successfully tested by Scott et al. [84, 85] for evaluating the kinetic parameters of pyrolysis of sewage sludge. This method, which is virtually an extension of Miura's method, is used for determining the number of reactions occurring

during the process of devolatilization, in addition to determining the values of activation energies and pre-exponential factors.

If it is assumed that a volatile component of the fuel with an initial mass fraction of $f_{i,0}$ reacts with an activation energy of E_i and pre-exponential factor of A_i , Equation 16 can then be expressed as:

$$f_i = f_{i,0} \Psi_i \quad \text{Eq. 3.3.3}$$

Where, f_i is the fraction of the i^{th} component remaining as the fuel is devolatilized and Ψ_i is the double exponential term. For a material decomposing via several parallel first-order reactions, Equation 3.3.3 can therefore be expressed as:

$$\frac{M(t)}{M_0} = W + \sum_{All\ Reactions,i} f_{i,0} \Psi_i \quad \text{Eq. 3.3.4}$$

and, W is the fraction of inert material.

The problem is therefore to estimate $f_{i,0}$, E_i and A_i . The distributed activation energy model can be stated to be a special case of this general problem which can be generated by increasing the number of reactions to infinity with a constraint that each of the reactions is uniquely characterized by its activation energy. It is to be noted that while the DAEM is ill-posed when the number of reactions is finite and the reactions do not overlap, the problem stated above is well-posed and can be solved. This is because of the fact that during the conversion process, there will be a point when a particular reaction is dominant and hence, its values of E and A can be directly evaluated without interference from other reactions. Equation 3.3.4, therefore, would be a linear problem so that the mass of solid fuel remaining at a given time would be the sum of the masses of each of the components remaining. Therefore, Equation 3.3.4 can be interpreted in a matrix form as follows:

$$\frac{1}{M_0} \begin{bmatrix} M(t_0) \\ M(t_1) \\ M(t_2) \\ \vdots \\ M(t_n) \end{bmatrix} = \begin{bmatrix} \Psi_1(t_0) & \Psi_2(t_0) & \cdots & \Psi_n(t_0) & 1 \\ \Psi_1(t_1) & \Psi_2(t_1) & \cdots & \Psi_n(t_1) & 1 \\ \Psi_1(t_2) & \Psi_2(t_2) & \cdots & \Psi_n(t_2) & 1 \\ \vdots & \vdots & \cdots & \vdots & 1 \\ \Psi_1(t_n) & \Psi_2(t_n) & \cdots & \Psi_n(t_n) & 1 \end{bmatrix} \times \begin{bmatrix} f_{1,0} \\ f_{2,0} \\ f_{3,0} \\ \vdots \\ W \end{bmatrix} \quad \text{Eq. 3.3.5}$$

Equation 3.3.5 can therefore be termed as a modified form of the distributed activation energy model. For a constant heating rate experiment, i.e. $dT/dt = H$ and initial temperature T_0 , the double exponential term, Ψ can be expressed as:

$$\Psi_i(t) = \Psi_i(T) = \text{Exp} \left[-\frac{A_i}{H} \int_{T_0}^T \text{Exp} \left(-\frac{E_i}{RT} \right) dT \right] \quad \text{Eq. 3.3.6}$$

And, $f_i(T) = f_{i,0} \Psi_i(T)$ Eq. 3.3.7

Thermogravimetric experiments conducted at two different heating rates, H_1 and H_2 , can be used for calculating the values of E_i and A_i . Assuming that the i^{th} reaction is the only reaction occurring at the same conversion in both experiments, then,

$$f_i(H_1, T_1) = f_i(H_2, T_2) \quad \text{Eq. 3.3.8}$$

And subsequently, $\Psi_i(H_1, T_1) = \Psi_i(H_2, T_2)$ Eq. 3.3.9

Substituting for Ψ_i from equation 3.3.6 and taking natural logarithms on each side yields:

$$\frac{1}{H_1} \left[T_0 \text{Exp} \left(-\frac{E_i}{RT_0} \right) - \frac{-E_i}{R} \int_{\frac{E}{RT_0}}^{\infty} \frac{\text{Exp}(-u)}{u} du - T_1 \text{Exp} \left(-\frac{E_i}{RT_1} \right) + \frac{E_i}{R} \int_{\frac{E}{RT_1}}^{\infty} \frac{\text{Exp}(-u)}{u} du \right] =$$

$$\frac{1}{H_2} \left[T_0 \text{Exp} \left(-\frac{E_i}{RT_0} \right) - \frac{-E_i}{R} \int_{\frac{E}{RT_0}}^{\infty} \frac{\text{Exp}(-u)}{u} du - T_2 \text{Exp} \left(-\frac{E_i}{RT_2} \right) + \frac{E_i}{R} \int_{\frac{E}{RT_2}}^{\infty} \frac{\text{Exp}(-u)}{u} du \right] \quad \text{Eq. 3.3.10}$$

Equation 3.3.10 is a non-linear equation, which can be solved analytically for estimating unknown E_i . This calculated value of activation energy using Equation 3.3.10 will be accurate due to the fact that only one reaction would be dominating the overall mass loss at a chosen conversion point. Deviations in activation energy are observed, when several reactions occur simultaneously at the same conversion. Once the activation energy, E_i , is determined, pre-exponential factor, A_i , can be calculated by assuming that the conversion of the individual component i of the dominating reaction reaches a particular conversion. For this method, it is assumed that the conversion is:

$$X_i = 1 - e^{-1} \Rightarrow \Psi_i = e^{-1} \Rightarrow \ln(\Psi_i) = -1 \quad \text{Eq. 3.3.11}$$

Also, this value of Ψ_i corresponds to the conversion at which the rate of decomposition is at a maximum, i.e. $d^2 f_i / dt^2 = 0$. Combining Equations 3.3.6 and 3.3.10, A_i can then be estimated.

The matrix inversion method is thus different from Method 2 in the sense that this method does not require that each reaction be uniquely characterized by its activation energy and does not use a step function approximation, which is central to Method 2 (Miura's method) for estimating the amount of each reaction occurring. The procedure for solving Equation 3.3.4 can thus be summarized as follows:

1. Perform at least two thermogravimetric experiments at different constant rates of heating and measure the values of mass as a function of temperature.
2. Consider n points of conversion during the decomposition temperature interval where the kinetic parameters, E_i and A_i , are to be evaluated.

3. At each conversion point, evaluate E_i and A_i using a combination of Equations 3.3.6 and 3.3.10 to obtain n values of the kinetic parameters.
4. Using the set of n reactions with known values of E_i and A_i , create the matrix Ψ in Equation 3.3.5.
5. Once the matrix Ψ is created, the mass fraction of each reaction, f_i , can be evaluated by inverting Equation 3.3.5: $f_i = \Psi^{-1} m$

This type of analysis has been used before for the determination of pyrolysis characteristics of dried sewage sludge [84] and high ash, inertinite-rich, medium rank C South African coal [86]. In this work, the modified distributed activated energy model has been extended for determining the kinetic parameters of single fuels as well as blends of coal and biomass.

3.4 Results and Discussion: Matrix Inversion Method

3.4.1 Kinetics of DECS-38 Sub-Bituminous Coal Devolatilization

The results of the real TGA devolatilization experiments using the Matrix Inversion method are presented and discussed in this section. Figures 3.4.1 through 3.4.3 describe the inversion algorithm results for DECS-38 sub-bituminous coal. The inversion algorithm was applied to the TGA data at various heating rates and kinetic parameters were obtained at various conversions. The obtained kinetic parameters were then used to model the reactions at unknown heating rates that were not used in the algorithm. The obtained weight loss data was then compared with real TGA data for comparison and accuracy of the method.

As discussed earlier, this inversion algorithm is advantageous over Miura's method due to the fact that only two TGA curves are required and less data needs to be processed overall, thereby, significantly reducing the processing times and also the ability to predict

the reaction curves at unknown heating rates. For DECS-38 sub-bituminous coal, TGA data for heating rates 10 °C/min and 20 °C/min were used in the inversion algorithm for determining the kinetic parameters and the obtained parameters were then used to predict the weight loss curves at 5 °C/min and 40 °C/min.

MATLAB codes used for calculations in this method are presented in Appendix A. The weight loss data sets from TGA experiments were reduced by linear interpolation to further simplify the computation. From these reduced data sets, a total of 50 conversions were chosen where the kinetic parameters were to be calculated. One candidate reaction is generated at each value of conversion and for cases where more than one real reaction occurs at a particular conversion, the values of E and A generated (using Step 3) would be incorrect. Therefore, using the second stage of the algorithm (Steps 4 and 5), the values of $f_{i,0}$ of such unrealistic reactions can be set to zero, thereby determining the total number of reactions during devolatilization.

Figure 3.4.1 shows the values of $f_{i,0}$ for DECS-38 sub-bituminous coal. Upon examination of these values, 35 parallel reactions have been identified which are deemed to be occurring during the devolatilization of DECS-38 sub-bituminous coal. Increasing the number of conversion points to a number greater than 50 would not make a difference because the total number of parallel reactions occurring in this case falls within the number of conversion points chosen. For example, when the number of conversion points were increased from 50 to 100, the number of parallel reactions occurring was still the same and no change in the activation energy range was observed. It should be noted here that only the decomposition reactions, starting with removal of moisture, are taken into consideration during this method and hence, fixed carbon content and ash content are not included in

Figures 3.4.1 through 3.4.3. The values of activation energy and pre-exponential factor for each reaction are shown in Figures 3.4.2 and 3.4.3.

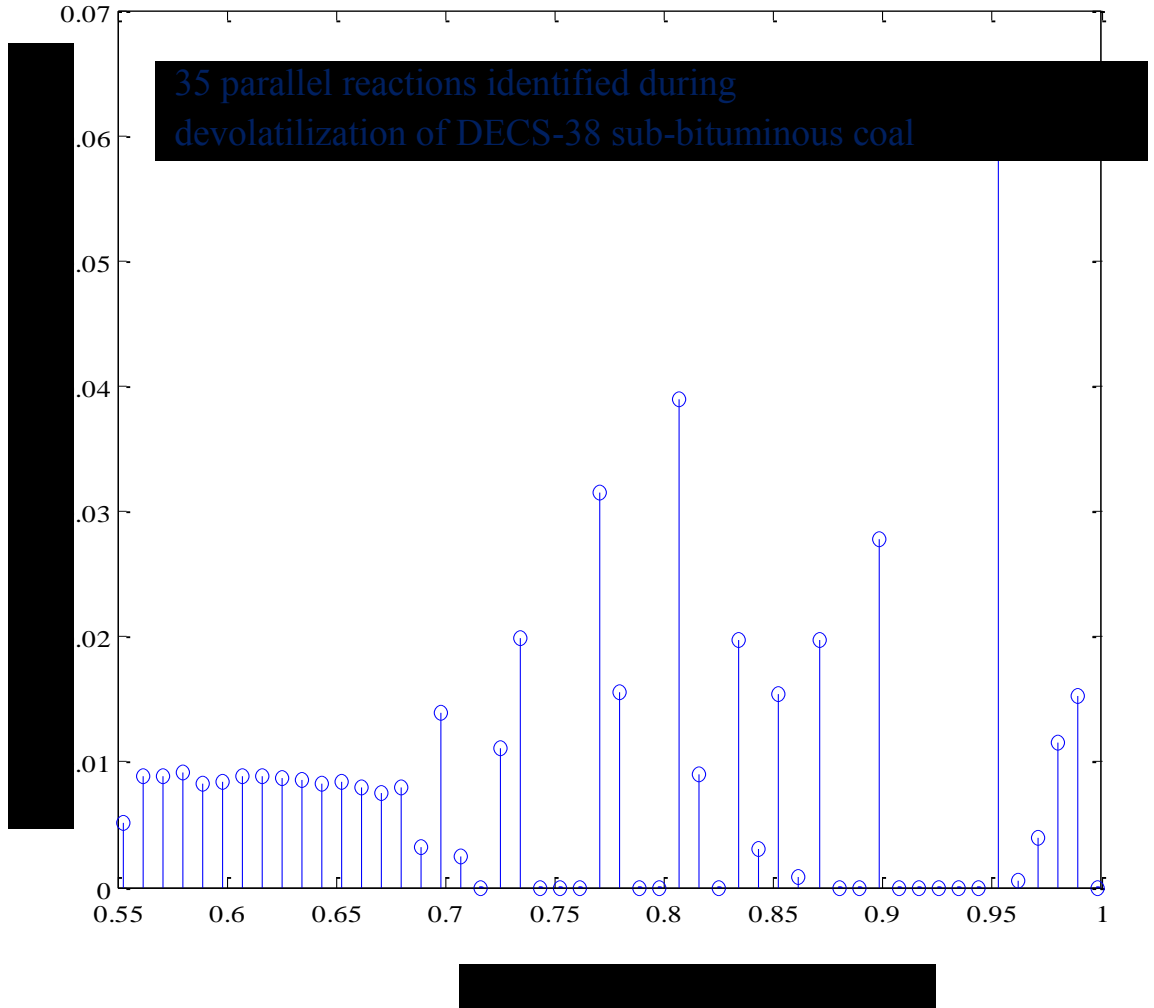


Figure 3.4.1: Mass fraction of fuel associated with each reaction during devolatilization of DECS-38 sub-bituminous coal.

It can be observed from Figure 3.4.2 and 3.4.3 that the values of kinetic parameters increase with increasing weight loss until a maxima is achieved when the mass fraction of the fuel (sub-bituminous coal) remaining is approximately 55 % indicating the completion of the devolatilization process.

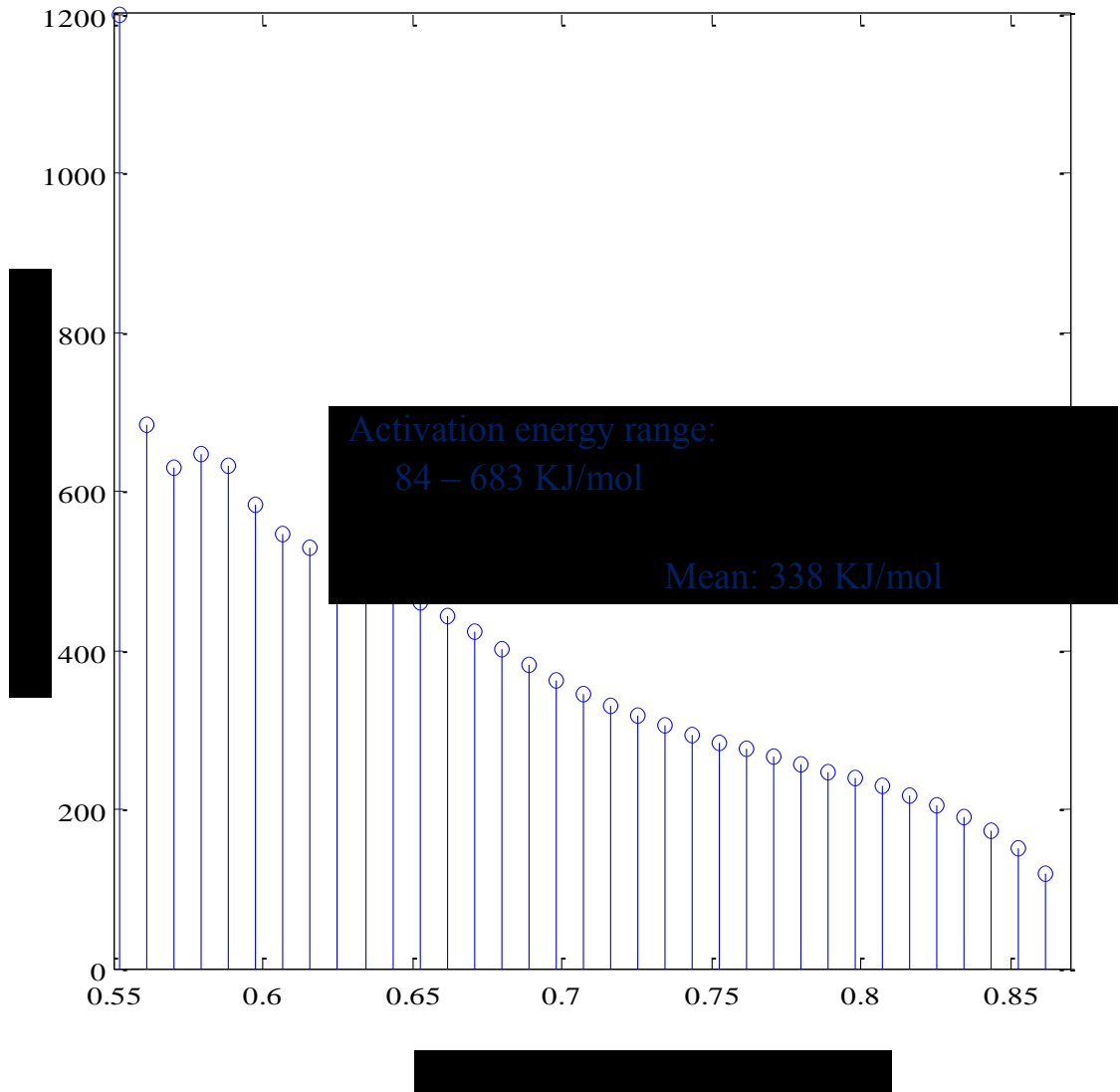


Figure 3.4.2: Plot of activation energy vs mass fraction remaining for pyrolysis of DECS-38 sub-bituminous coal describing the values of activation energy for each parallel reaction.

Activation energy values occurring during pyrolysis of DECS-38 sub-bituminous coal have a range between 84 - 683 KJ/mol with a mean activation energy of approximately 338 KJ/mol while the values of pre-exponential factor are not constant for all reactions but have a large range between $9E+5 \text{ min}^{-1}$ and $5E+32 \text{ min}^{-1}$.

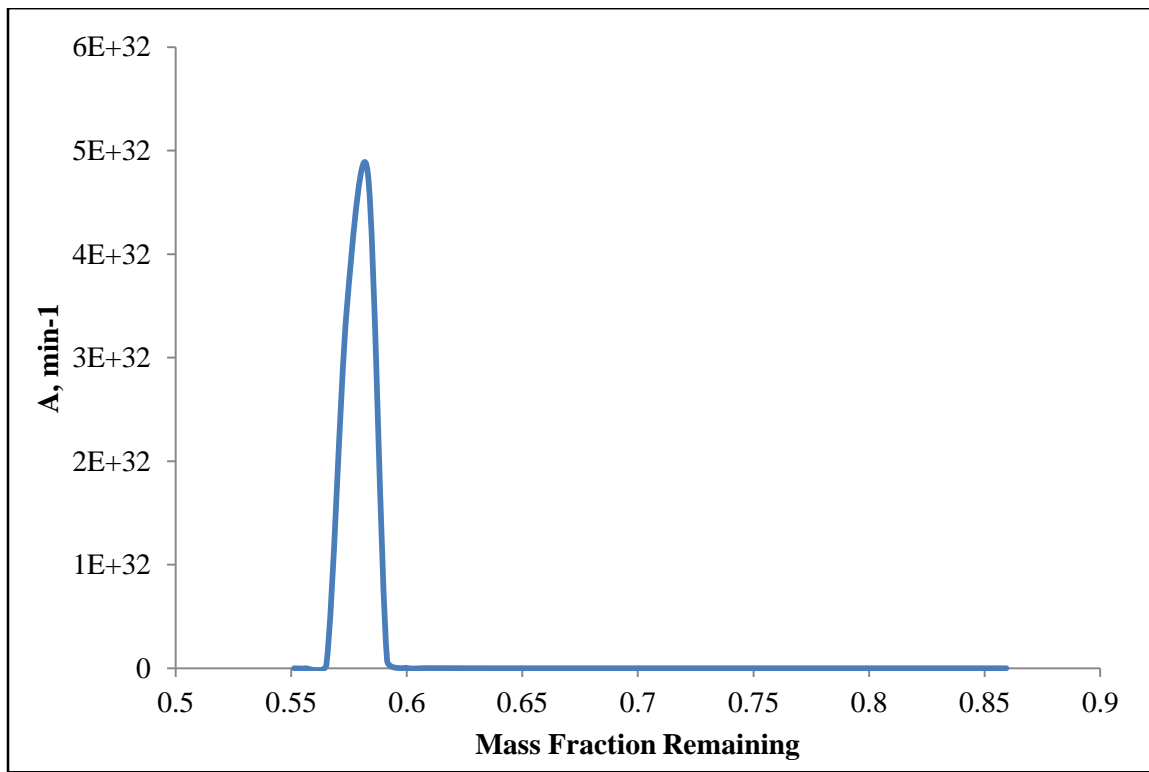


Figure 3.4.3: Plot of pre-exponential factor vs mass fraction remaining for pyrolysis of DECS-38 sub-bituminous coal describing the values of pre-exponential factor for each parallel reaction.

The kinetic parameters thus obtained were used to model the TGA curves. A comparison of the actual TGA curves and the predicted curves are shown in Figures 3.4.4 and 3.4.5.

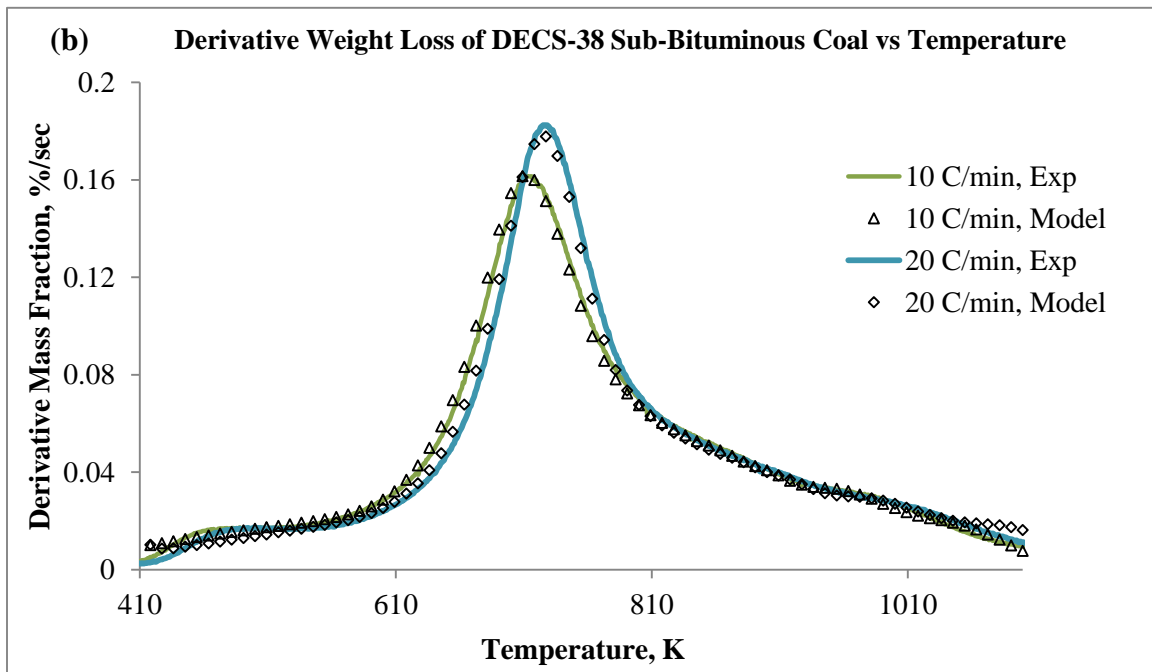
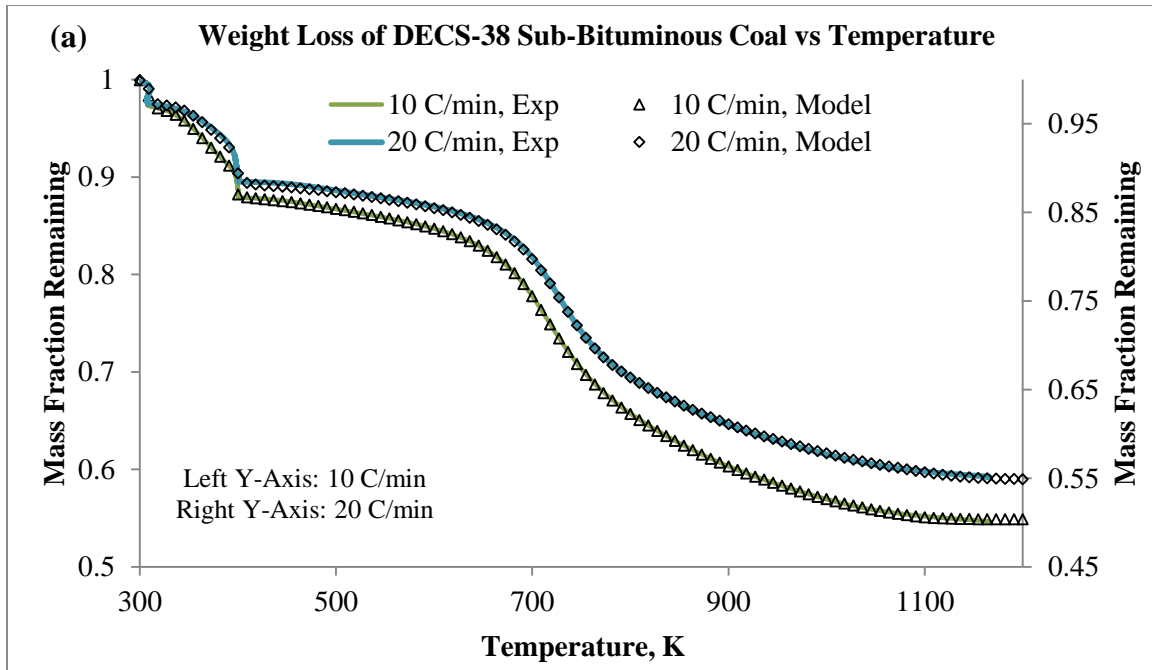


Figure 3.4.4: Comparison of experimental and predicted values for devolatilization of DECS-38 sub-bituminous coal for two heating rates (10 °C/min and 20 °C/min) used in the matrix inversion algorithm. (a) weight loss vs temperature, (b) derivative weight loss vs temperature.

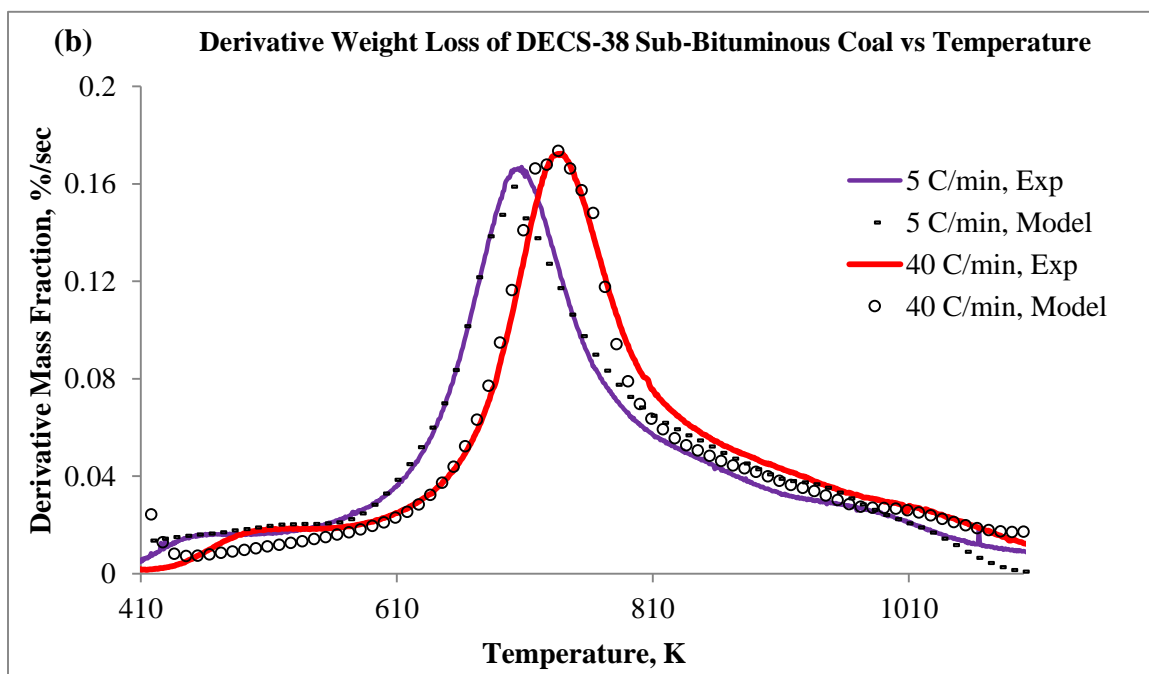
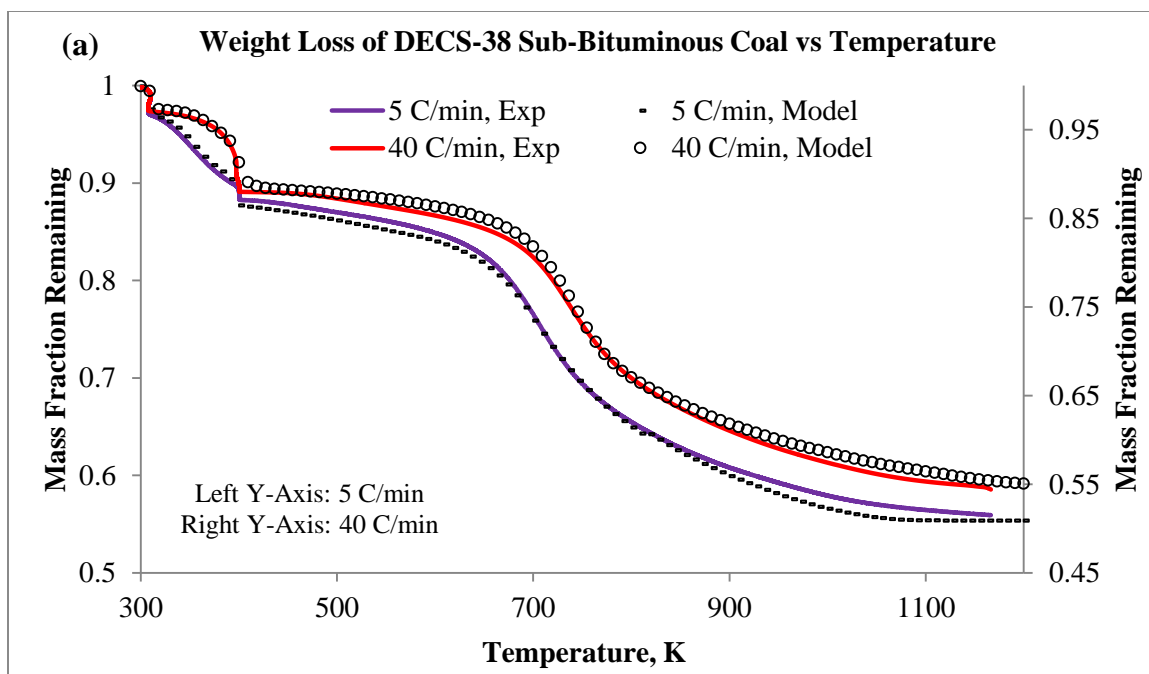


Figure 3.4.5: Comparison of experimental and predicted values for devolatilization of DECS-38 sub-bituminous coal for two heating rates (5 °C/min and 40 °C/min) not used in the matrix inversion algorithm. (a) weight loss vs temperature, (b) derivative weight loss vs temperature.

From Figure 3.4.4, it can be clearly seen that for the two heating rates used in the algorithm, the model predicts the weight loss data and derivative weight loss data excellently with standard error of less than 0.5 % between the experimental and predicted values.

The kinetic parameters obtained were then used for modeling the devolatilization reaction at two heating rates, 5 °C/min and 40 °C/min, not used in the algorithm to verify if the model could be extrapolated to unknown heating rates. This is important to verify since the process of devolatilization occurs instantaneously at the top of a moving bed reactor during gasification where the heating rates tend to be much higher, in the order of 100 °C/sec. For the thermogravimetric analyzer used in this work (TA SDT Q600), a linear increase in furnace temperature was not possible at heating rates higher than 40 °C/min. Hence, it must be noted here that the maximum heating rates utilized in this work is 40 °C/min.

It can be observed from Figure 3.4.5, that the model can be utilized for predicting weight loss data for unknown heating rates also. As seen from Figure 3.4.5, the predicted weight loss values and derivative weight loss values fall within 1 % of the actual experimental curves suggesting that this model can be successfully utilized for predicting the devolatilization reaction even at extremely high heating rates that are achieved in industrial reactors.

It is also important to understand if this model can be extended to various feedstocks with different compositions of moisture, volatile matter and fixed carbon content. Therefore, for this purpose and for comparison with other models described earlier, devolatilization of the two biomass materials (CS and SG) and blends of biomass

with the two coals are analyzed further using the matrix inversion method in the following sections.

3.4.2 Kinetics of Corn Stover Devolatilization: Matrix Inversion Method

The kinetics parameters for corn stover devolatilization were obtained via the matrix inversion method by utilizing the TGA data for heating rates 20 °C/min and 40 °C/min in the inversion algorithm and the obtained parameters were then used to predict the weight loss curves at a lower heating rate of 5 °C/min.

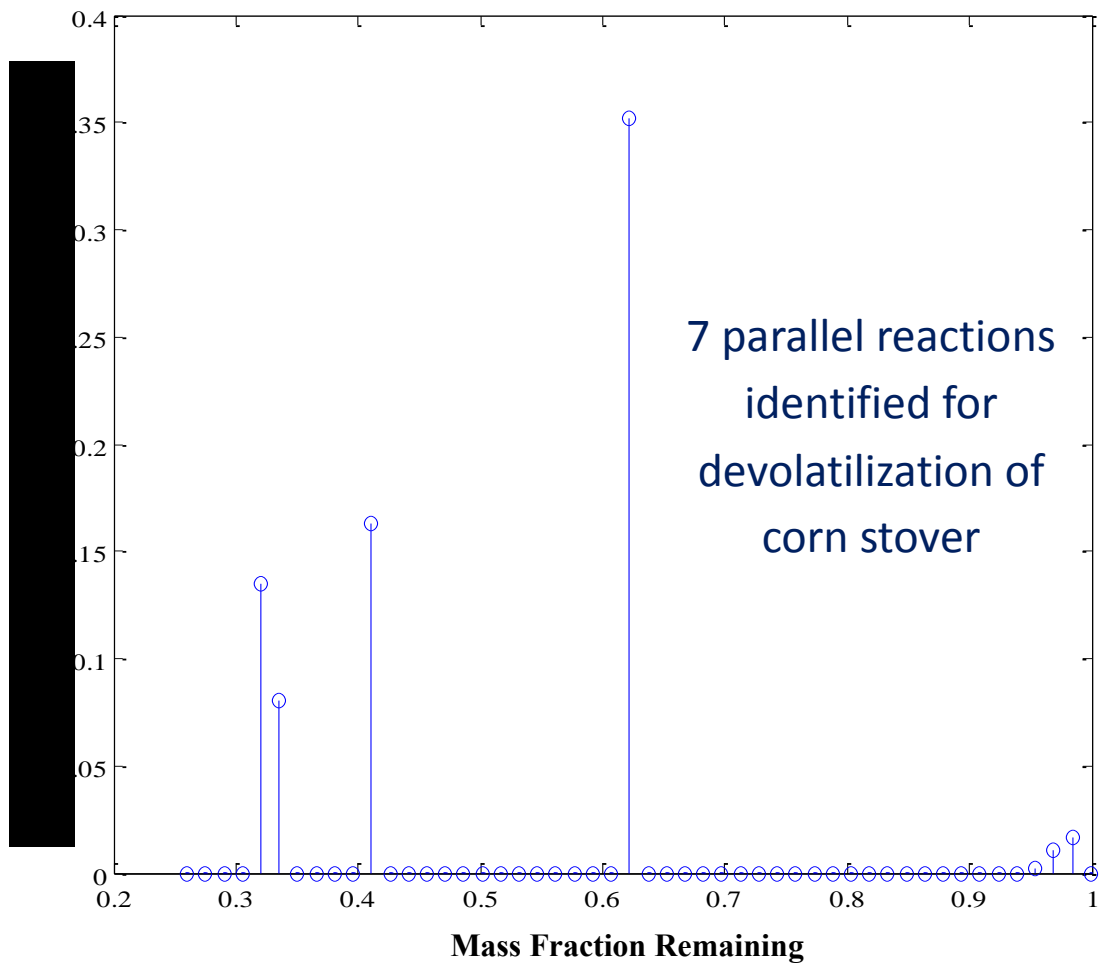


Figure 3.4.6: Mass fraction of fuel associated with each reaction during devolatilization of corn stover.

From Figure 3.4.6, it is evident that there are far fewer reactions occurring during the devolatilization of corn stover when compared to that of sub-bituminous coal. The values of $f_{i,0}$ in Figure 3.4.6 suggest that the devolatilization of corn stover can be represented by a total of 7 reactions which includes removal of moisture.

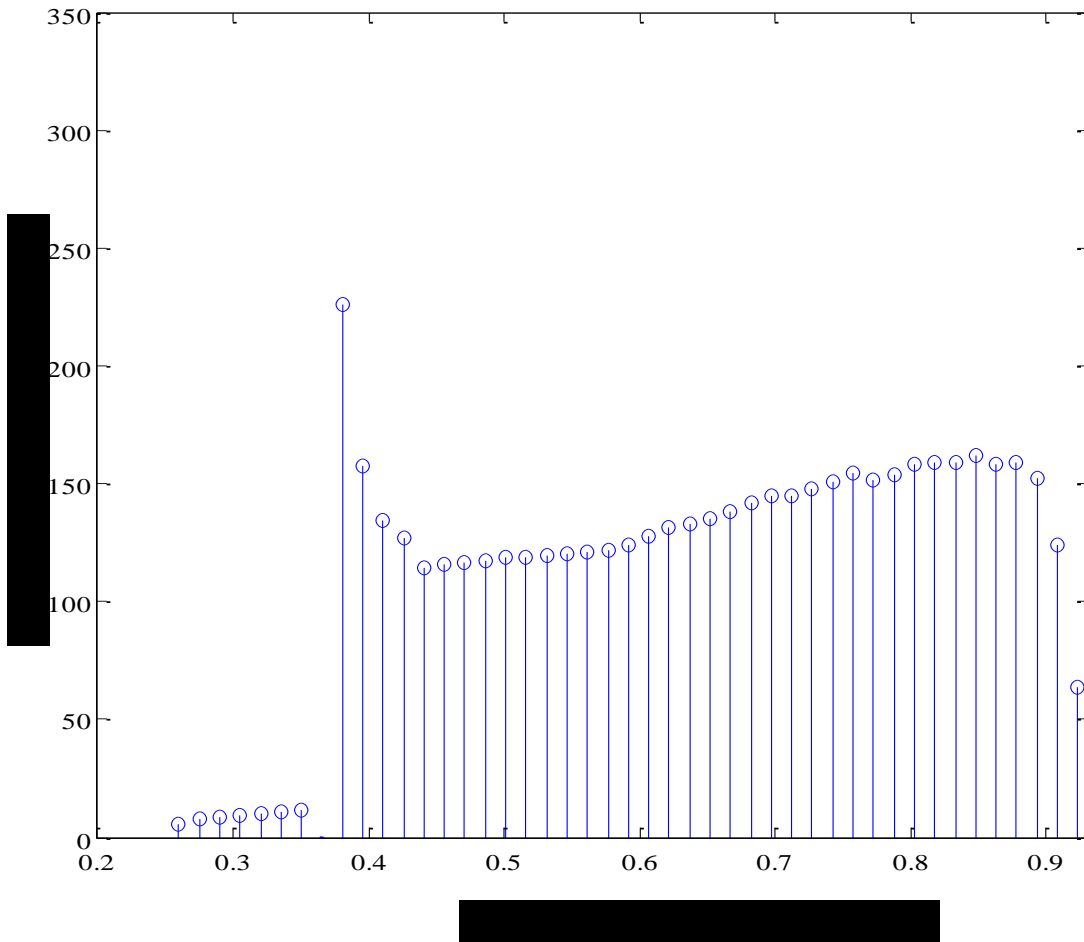


Figure 3.4.7: Plot of activation energy vs mass fraction remaining for pyrolysis of corn stover describing the values of activation energy for each parallel reaction.

The range of activation energy values obtained, 55 – 225 KJ/mol, are also comparable to the values obtained using Methods 1 and 2 described in previous sections of this chapter. Likewise, the values of pre-exponential factor have a large range of approximately $2 - 1.08E+17 \text{ min}^{-1}$.

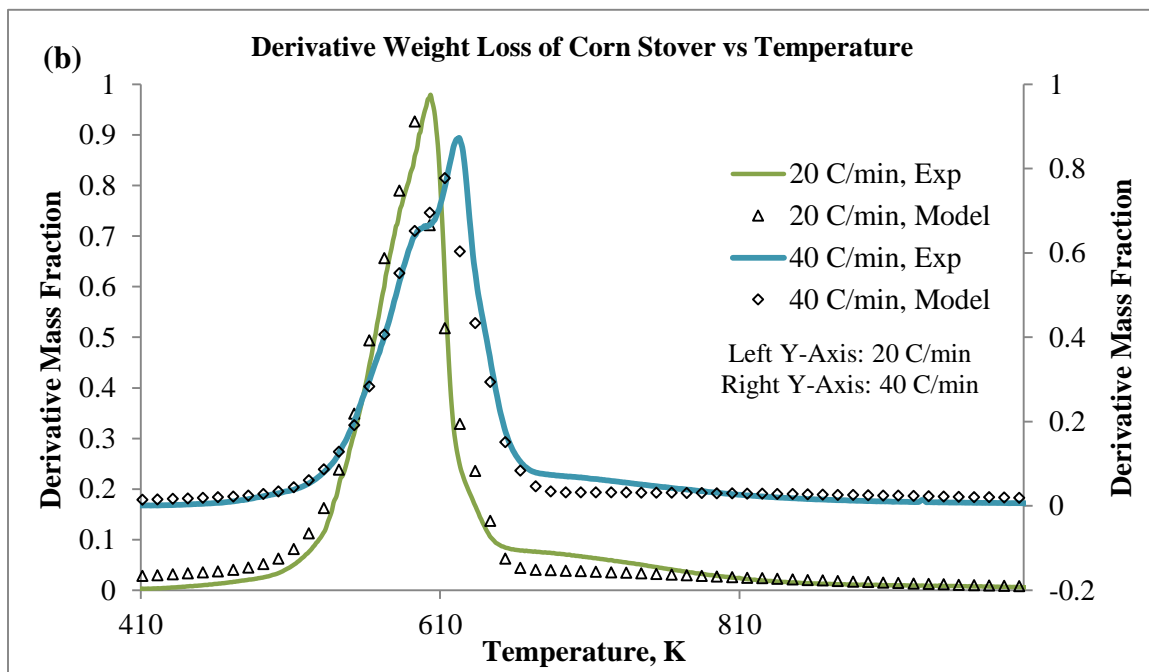
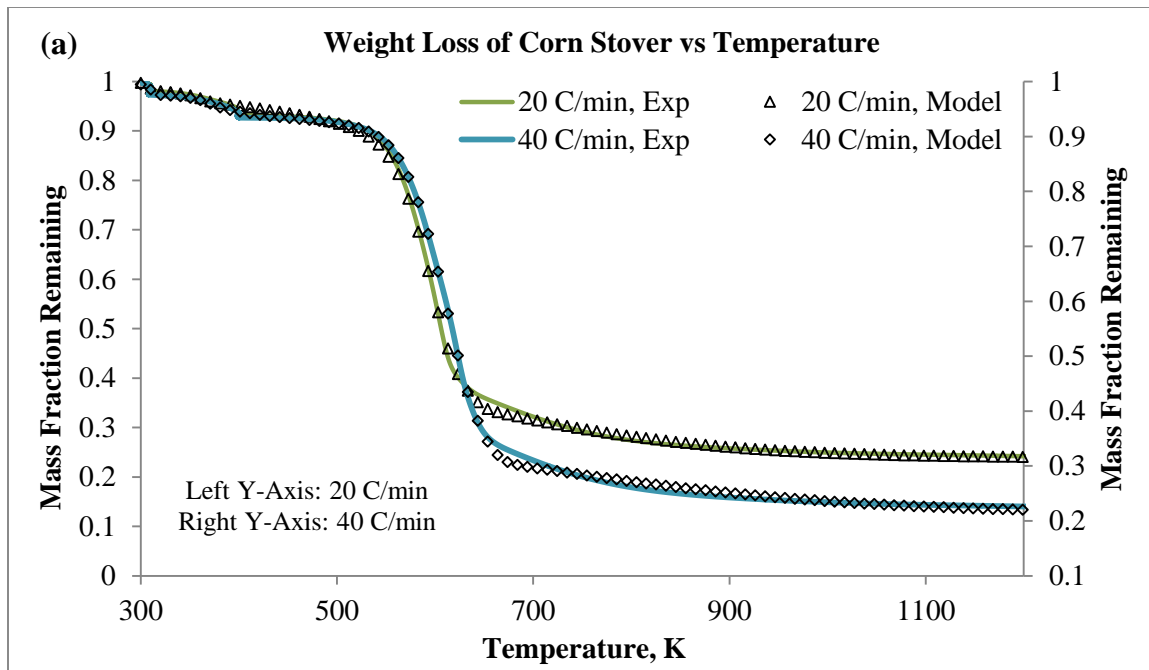


Figure 3.4.8: Comparison of experimental and predicted values for devolatilization of corn stover for two heating rates (20 °C/min and 40 °C/min) used in the matrix inversion algorithm. (a) weight Loss vs temperature, (b) derivative weight loss vs temperature.

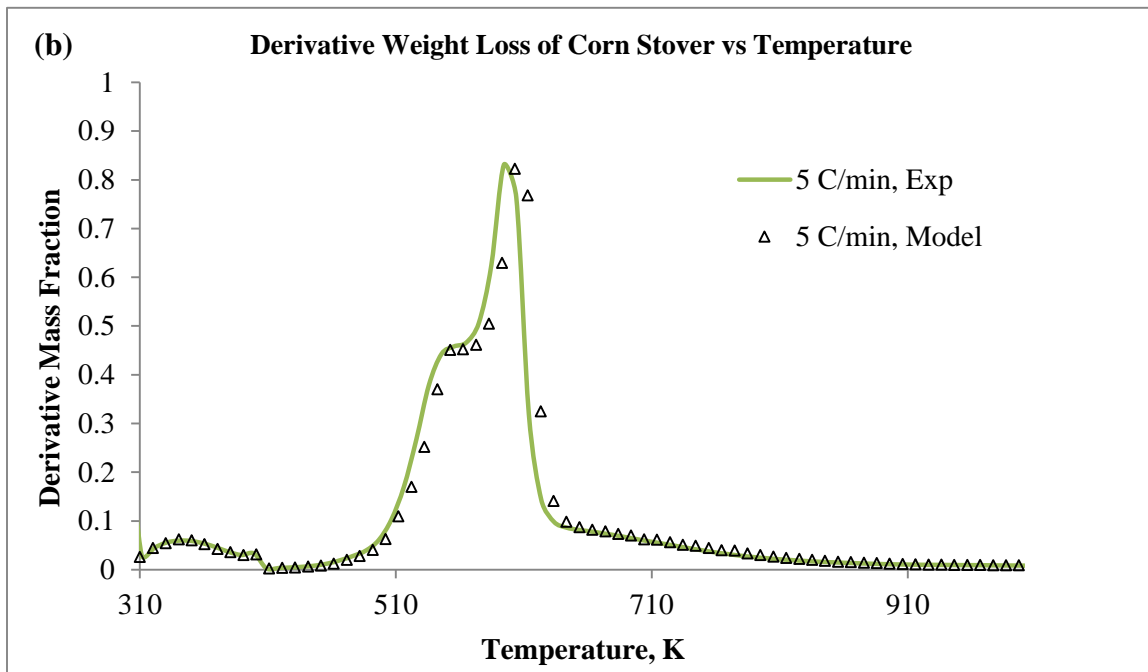
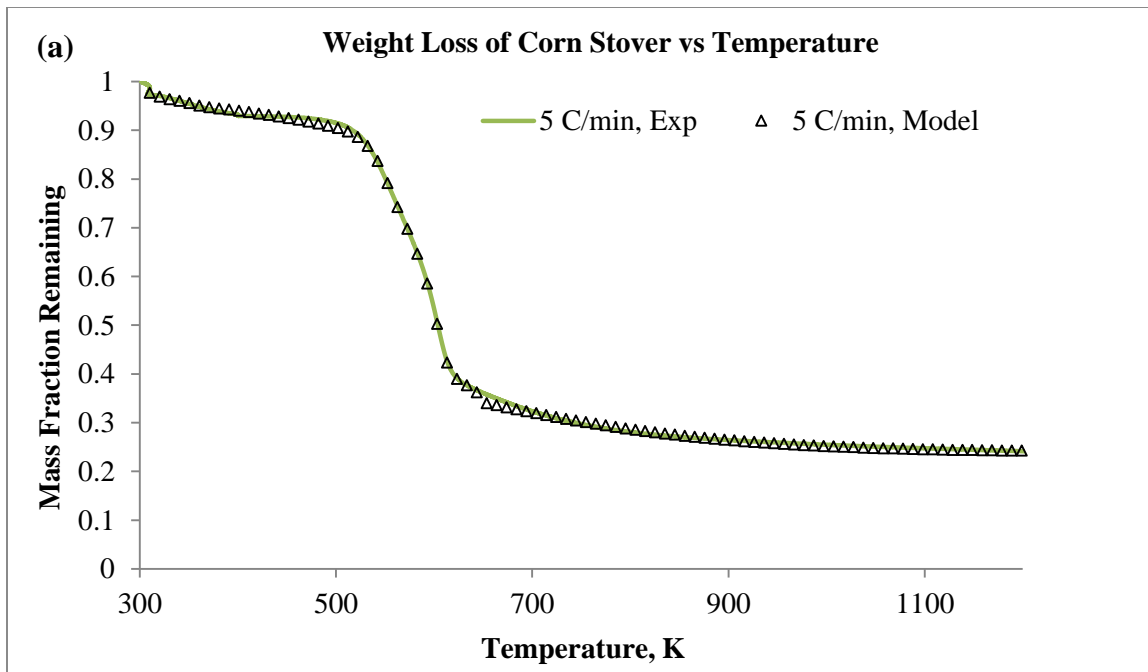


Figure 3.4.9: Comparison of experimental and predicted values for devolatilization of corn stover for the heating Rate (5 °C/min) not used in the matrix inversion algorithm. (a) weight Loss vs temperature, (b) derivative weight loss vs temperature.

From Figures 3.4.8 and 3.4.9, it is evident that this method can also be used for predicting the devolatilization kinetics of high volatile biomass materials such as corn stover.

3.4.3 Devolatilization Kinetics of 10CS90SB Blend

Once the devolatilization kinetics of single fuels were analyzed, the matrix inversion algorithm was tested on the blends of those single fuels. For illustration, the analysis of 10% corn stover blended with 90% sub-bituminous coal is discussed in this section.

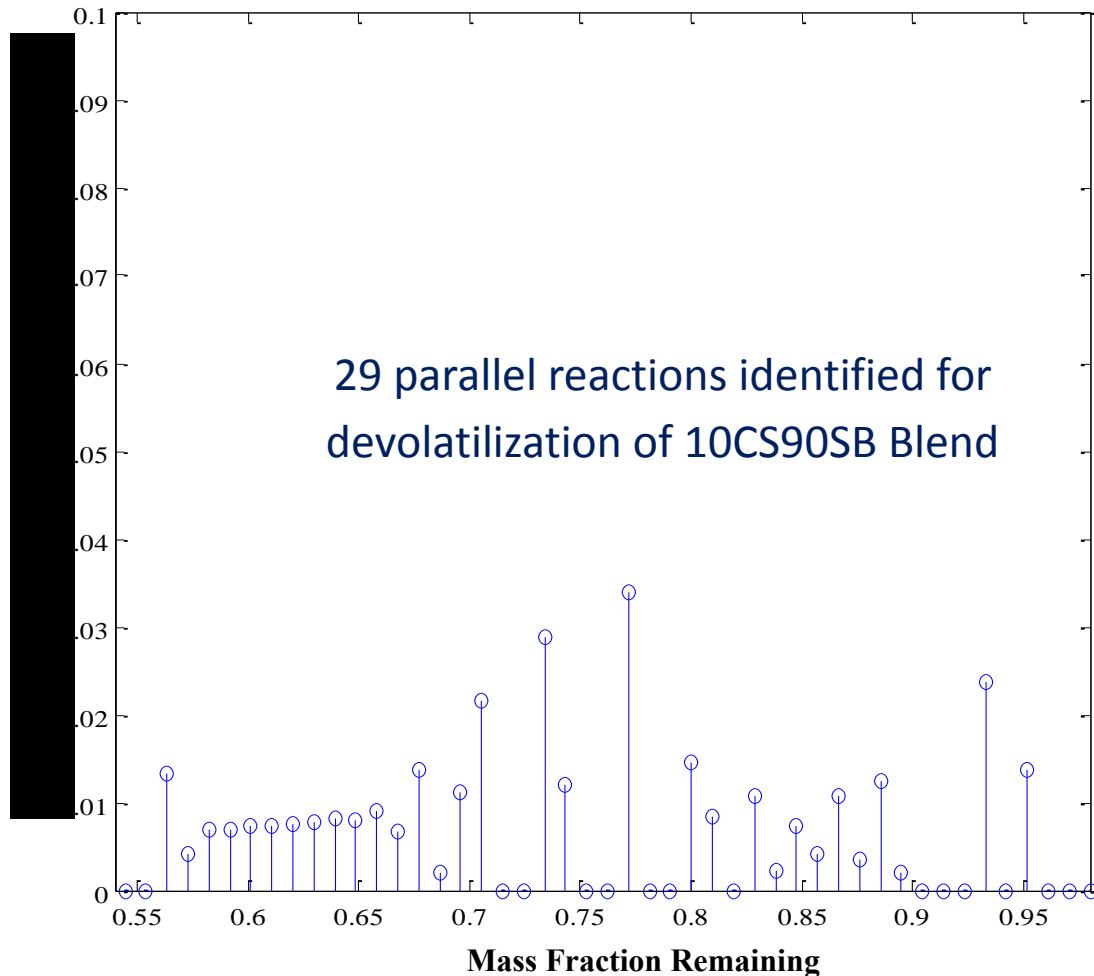


Figure 3.4.10: Mass fraction of fuel associated with each reaction during devolatilization of 10% corn stover blended with 90% DECS-38 sub-bituminous coal.

The activation energy curve for the blended feedstock follows a slightly different pattern when compared to that of the single fuels, again, indicating the fact that there are certain interactions between the single fuels during devolatilization as described in previous sections. The kinetic parameters obtained even for the blended feedstocks represent the weight loss data excellently, with errors of less than 0.5% for all heating rates. This proves the effectiveness and robustness of the matrix inversion method in representing the devolatilization of various materials when compared with other methods discussed previously.

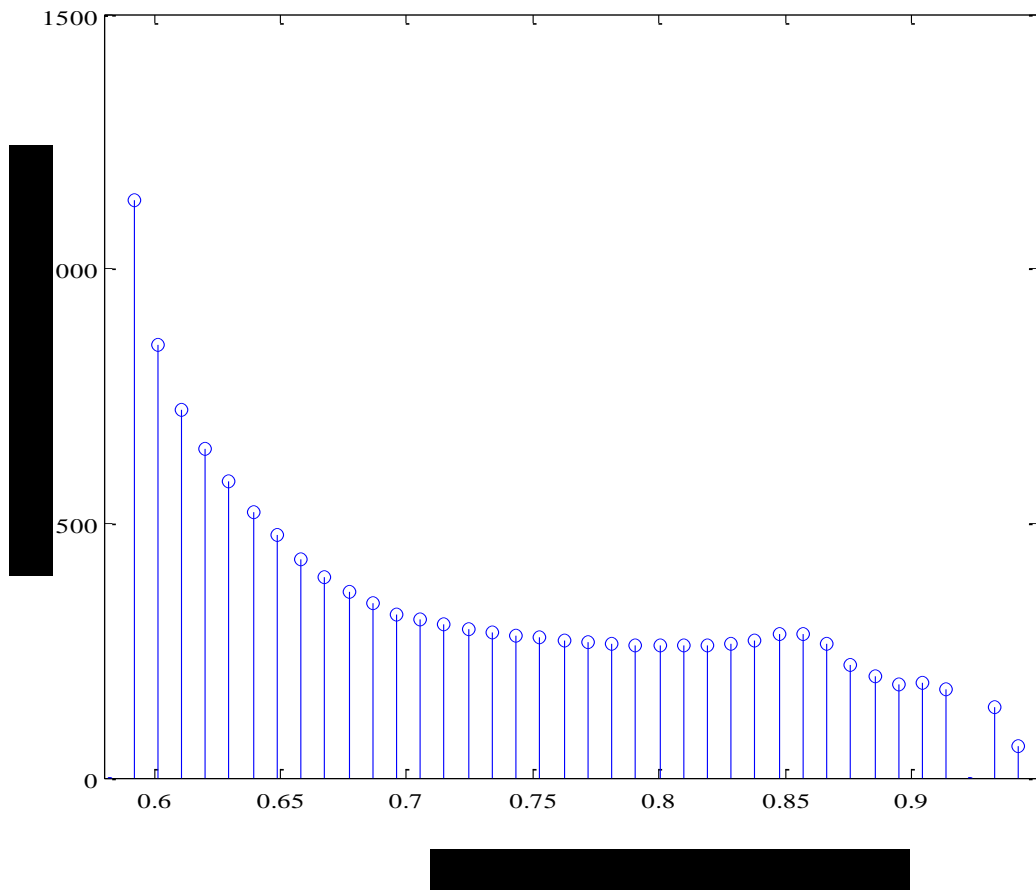


Figure 3.4.11: Plot of activation energy vs mass fraction remaining for pyrolysis of 10% corn stover-90% DECS-38 Sub-Bituminous coal describing the values of activation energy for each parallel reaction.

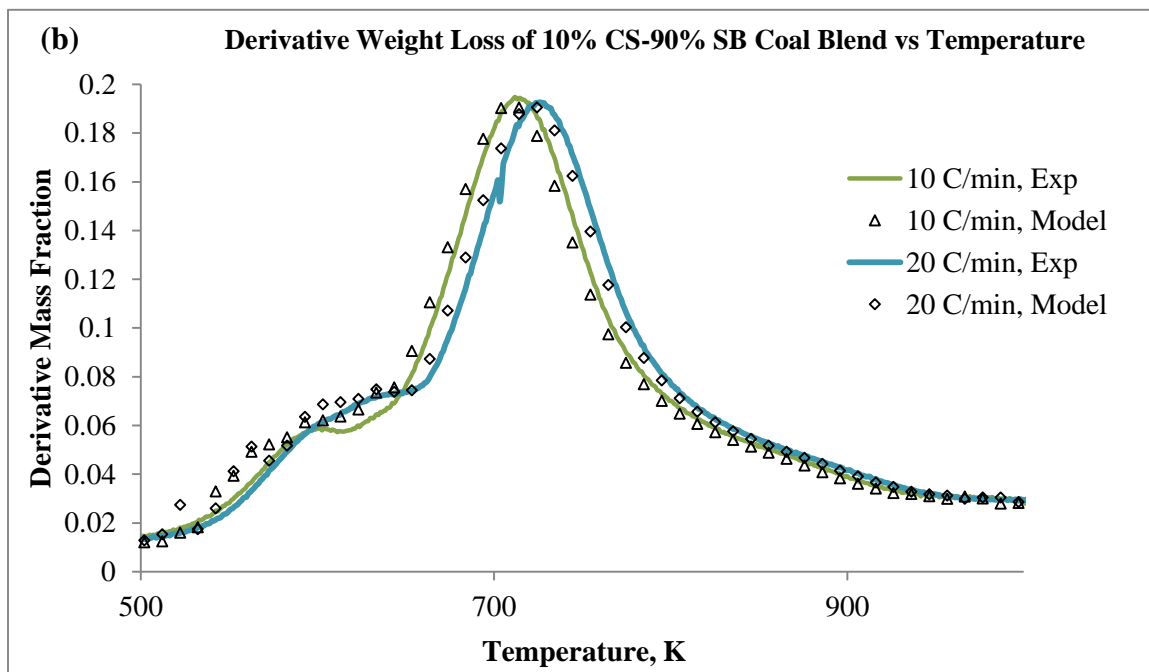
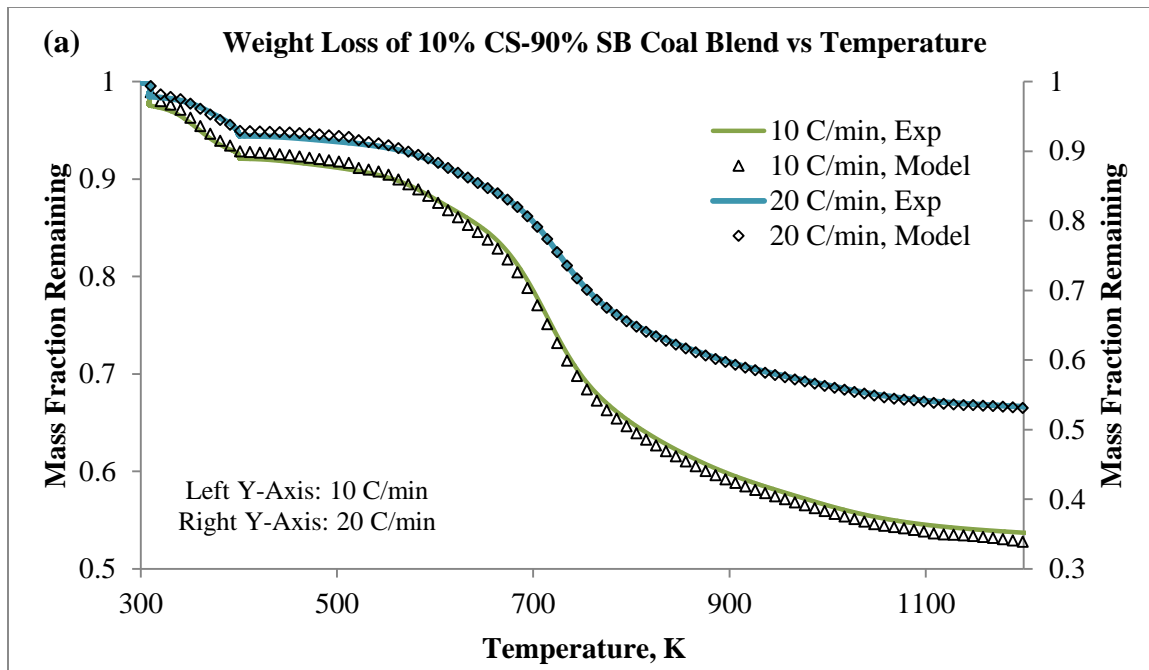


Figure 3.4.12: Comparison of experimental and predicted values for devolatilization of 10% corn stover-90% DECS-38 sub-bituminous coal for two heating rates (10 °C/min and 20 °C/min) used in the matrix inversion algorithm. (a) weight loss vs temperature, (b) derivative weight loss vs temperature.

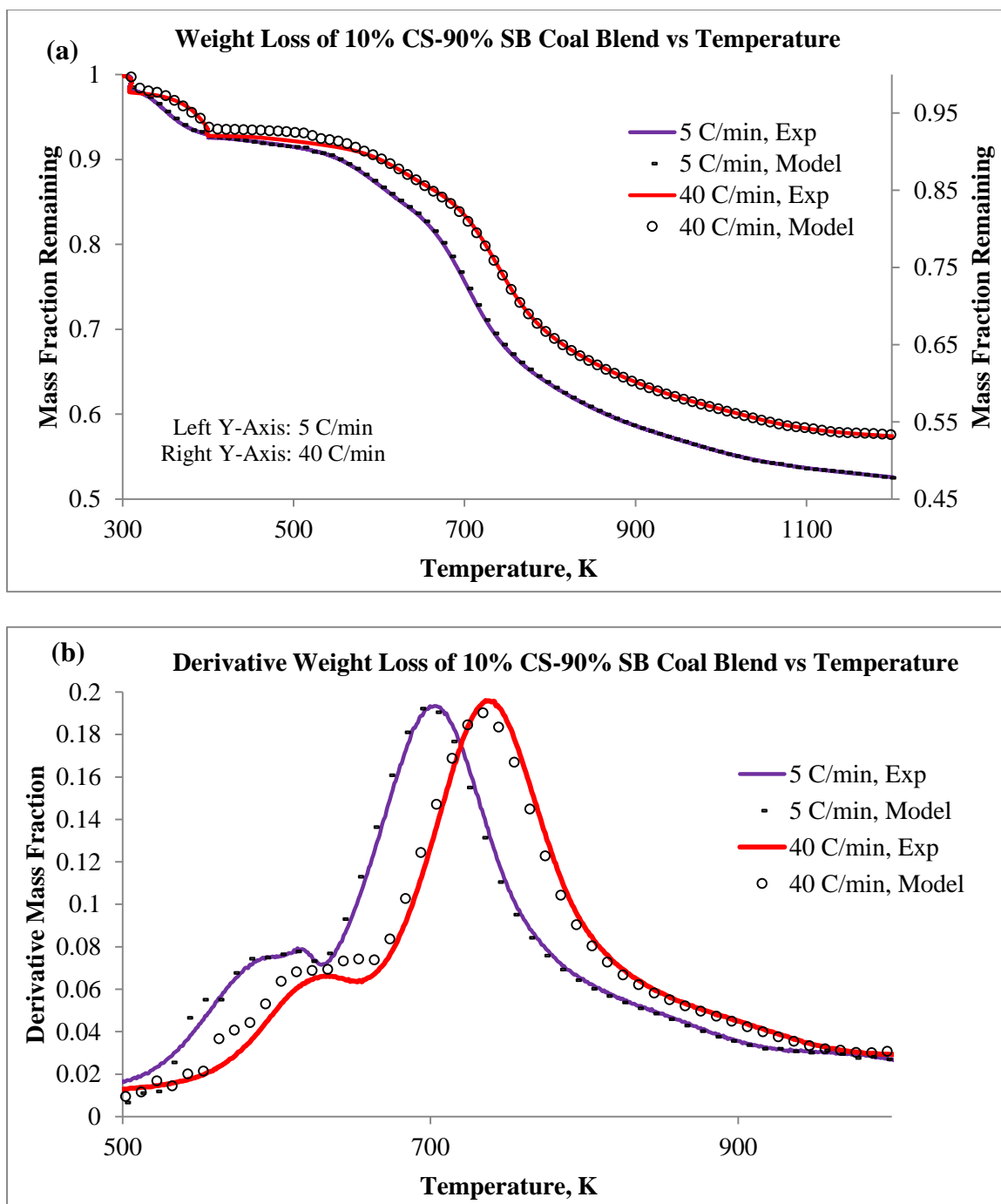


Figure 3.4.13: Comparison of experimental and predicted values for devolatilization of 10% corn stover-90% DECS-38 sub-bituminous coal blend for heating rates (5 °C/min and 40 °C/min) not used in the matrix inversion algorithm. (a) weight loss vs temperature, (b) derivative weight loss vs temperature.

Table 3.4.1: Pyrolysis kinetic parameters and number of devolatilization reactions obtained for various feedstocks using matrix inversion algorithm.

Feedstock Materials	No. of Reactions	Activation Energy Range KJ/mol	Arrhenius Constant Range sec⁻¹
DECS-38 Sub-Bituminous Coal (SB)	35	84-683	9E+5 – 5E+32
DECS-25 Lignite Coal (LG)	29	93-300	2E+8 – 2E+14
Corn Stover (CS)	7	55-226	7E+4 – 4E+13
Switchgrass (SG)	11	40-175	1E+0 – 2E+13
10% CS + 90% SB	29	75-722	2E+9 – 5E+41
30% CS + 70% SB	20	89-607	2E+7 – 5E+45
10% CS + 90% LG	25	67-356	2E+5 – 6E+15
30% CS + 70% LG	22	78-320	3E+9 – 2E+22
10% SG + 90% SB	28	112-796	2E+8-2E+51
30% SG + 70% SB	24	41-673	1E+3-8E+31
10% SG + 90% LG	28	59-237	1E+3-4E+29
30% SG + 70% LG	24	40-231	1E+0-5E+17

It is expected that the number of reactions occurring during the devolatilization of blended materials would be between those that would occur during the devolatilization of single fuels and that the number would gradually decrease with increase of high volatile matter content fuels in the blend, i.e., corn stover and switchgrass in this case. For a 10% corn stover blend with sub-bituminous coal, as shown in Figure 3.4.10, the number of devolatilization reactions is 29, while only 20 reactions were observed in 30% blend of corn stover with sub-bituminous coal as shown in Table 3.4.1.

3.5 Reactivity in CO₂ Atmosphere

For examining and comparing the results of pyrolysis and gasification reactions, the feedstock samples were subjected to heat treatment in a carbon dioxide atmosphere. Seven feedstock samples were utilized for this purpose which include both coals and blends of these coals with up to 30 % by weight of corn stover (similar to the feedstocks utilized for pyrolysis experiments). The flow rate of carbon dioxide utilized in these experiments was 100 ml/min while the heating rates varied between 5 °C/min and 40 °C/min. The feedstock samples were homogenized and placed in the TGA crucible and heated from room temperature to 1000 °C in a CO₂ atmosphere and weight loss characteristics were analyzed. The weight loss profiles thus obtained for each feedstock material were used in estimating the kinetic parameters of char-CO₂ reaction or Boudouard reaction. The weight loss profiles and DTG curves (moisture free basis) with respect temperature at a heating rate of 5 °C/min for all the feedstock materials are shown in Figures 3.5.1 and 3.5.2 respectively.

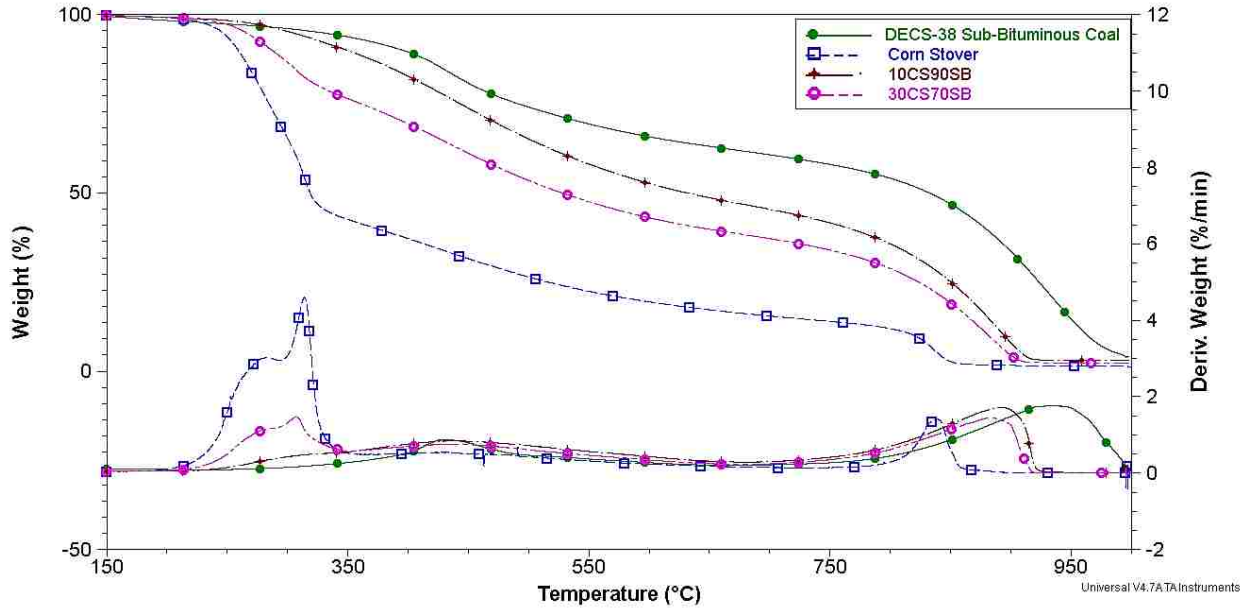


Figure 3.5.1: Weight loss profiles (Left Y-Axis) and DTG curves (Right Y-Axis) of sub-bituminous coal, corn stover and SB-CS blends at a 5 °C/min heating rate in a CO₂ atmosphere.

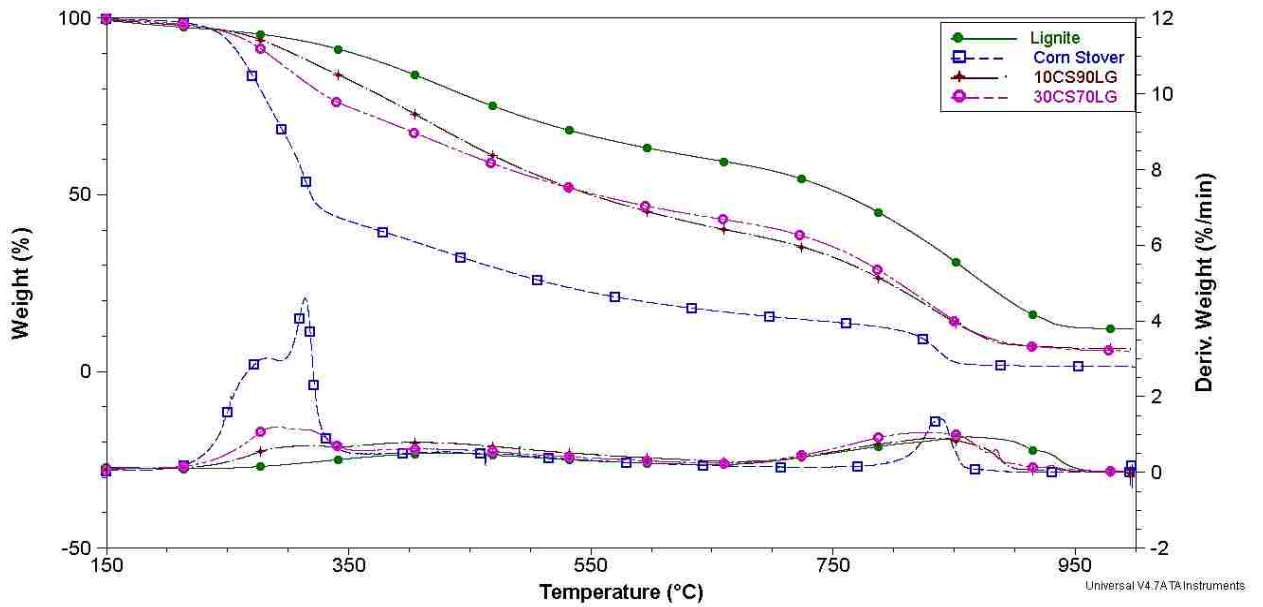


Figure 3.5.2: Weight loss profiles (Left Y-Axis) and DTG curves (Right Y-Axis) of lignite coal, corn stover and LG-CS blends at a 5 °C/min heating rate in a CO₂ atmosphere.

When compared with devolatilization of the feedstock materials utilizing a N₂ atmosphere, it can be observed that the TGA curves with respect to temperature follow a similar pattern until approximately 500 °C even when pure CO₂ is utilized as the sweeping gas. Although the mass loss rates at low temperatures are higher in pure CO₂ atmosphere, the differences are only marginal. At higher temperatures, however, a significant increase in mass loss rate is observed in pure CO₂ atmosphere. This may be understood by the stages of coal pyrolysis process. In case of 100% N₂ environment, the coal pyrolysis process has two stages: release of moisture content and devolatilization but the process of coal pyrolysis in pure CO₂ environment can be divided into three stages: moisture release, devolatilization and char gasification or Boudouard reaction with CO₂ to form CO in high temperature zone (> 500 °C) . Also, this difference may be explained due to the density difference and transport properties of these gases which are quite different (the mass of the CO₂ molecule is different from that of N₂). Moreover, the formation of char particles is larger and its surface area is also higher than that of the N₂ char particles. Hence, the weight loss observed in CO₂ environment is much higher.

3.5.1 Kinetics of Boudouard Reaction: Single Reaction Model

Using heat flow equations based on a second order partial differential equation, Kissinger [74, 87] derived an equation relating the DTA peak temperature to the rate of heating as shown in Equation 3.5.1.

$$\frac{d\left(\ln\left(\frac{H}{T_m^2}\right)\right)}{d\left(\frac{1}{T_m}\right)} = -E_a/R \quad \text{Eq. 3.5.1}$$

(Or),
$$\ln\left(\frac{H}{T_m^2}\right) = \left(-E_a/RT_m\right) + \ln\left(AR/E_a\right)$$

Where, H = rate of heating, $^{\circ}\text{C}/\text{min}$, T_m = peak temperature, E_a = energy of activation, KJ/mol .

The Kissinger equation has been widely used to determine activation energies of reactions from DTA data. The method is based on the assumption that the DTA peak temperature corresponds to the temperature of maximum reaction rate. Nevertheless, studies on metallurgical cokes and other carbons using simultaneous TG/DTG/DTA have shown that these two temperatures are very close [87].

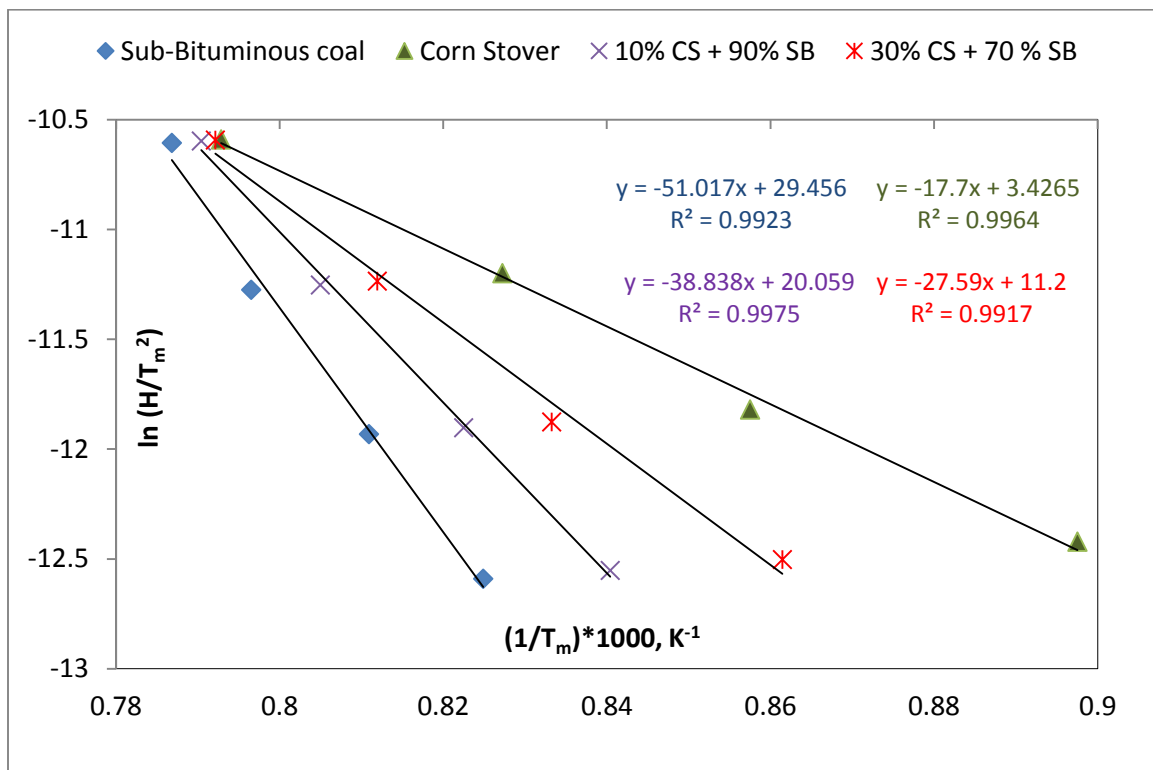


Figure 3.5.3: Plot for estimating the activation energy for Boudouard Reaction of DECS-38 sub-bituminous coal, corn stover and blends of sub-bituminous coal with corn stover at various heating rates.

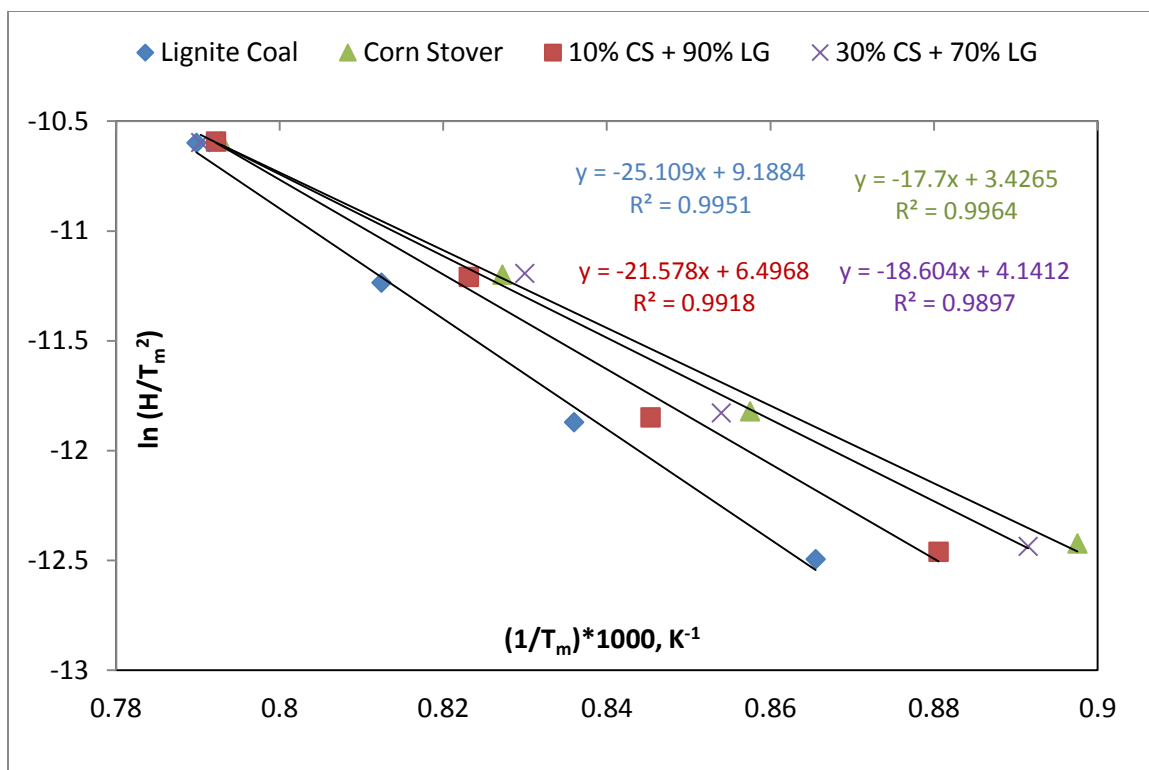


Figure 3.5.4: Plot for estimating the activation energy for Boudouard Reaction of DECS-25 lignite coal, corn stover and blends of lignite coal with corn stover at various heating rates.

Plots of $\ln(H/T_m^2)$ vs peak temperatures for coal-corn stover blends are shown in Figures 3.5.3 and 3.5.4. The activation energies and pre-exponential factors can then be obtained from the slope and intercept of each plot respectively. The kinetic analysis performed is similar to the method described in Section 3.2 for devolatilization reaction, the only difference being that at high temperatures, char gasification in CO_2 can be represented as a single reaction as opposed to several parallel reactions which was the case while estimating devolatilization kinetics. The linear fits of the obtained experimental data, with values of R^2 greater than 0.99, suggest that the Boudouard reaction follows first order kinetics and that the assumption of using maximum peak temperatures is reasonable. The kinetic parameters obtained for each material is listed in Table 3.5.1.

Table 3.5.1: Peak temperatures at various heating rates and activation energies for heat treatment of coal-corn stover blends in a CO₂ atmosphere obtained using thermogravimetric analysis.

Feedstock	Heating rate	Peak Temperature	Pre-Exponential Factor	Activation Energy
	°C/min	T _m , K	min ⁻¹	KJ/mol
Sub-Bituminous	5	1212.29	3.2E+14	424.16
	10	1233.19		
	20	1255.48		
	40	1270.97		
Lignite	5	1155.34	2.5E+05	208.76
	10	1196.19		
	20	1230.86		
	40	1266.13		
Corn stover	5	1114.17	5.4E+02	147.16
	10	1166.19		
	20	1208.86		
	40	1261.31		
10% CS + 90% SB	5	1189.91	2.0E+10	322.90
	10	1215.82		
	20	1242.30		
	40	1265.16		
30% CS + 70% SB	5	1160.81	2.0E+06	229.38
	10	1200.10		
	20	1231.64		
	40	1262.40		
10% CS + 90% LG	5	1135.67	1.4E+04	179.40
	10	1182.96		
	20	1214.87		
	40	1262.30		
30% CS + 70% LG	5	1121.67	1.2E+03	154.67
	10	1170.96		
	20	1204.87		
	40	1265.30		

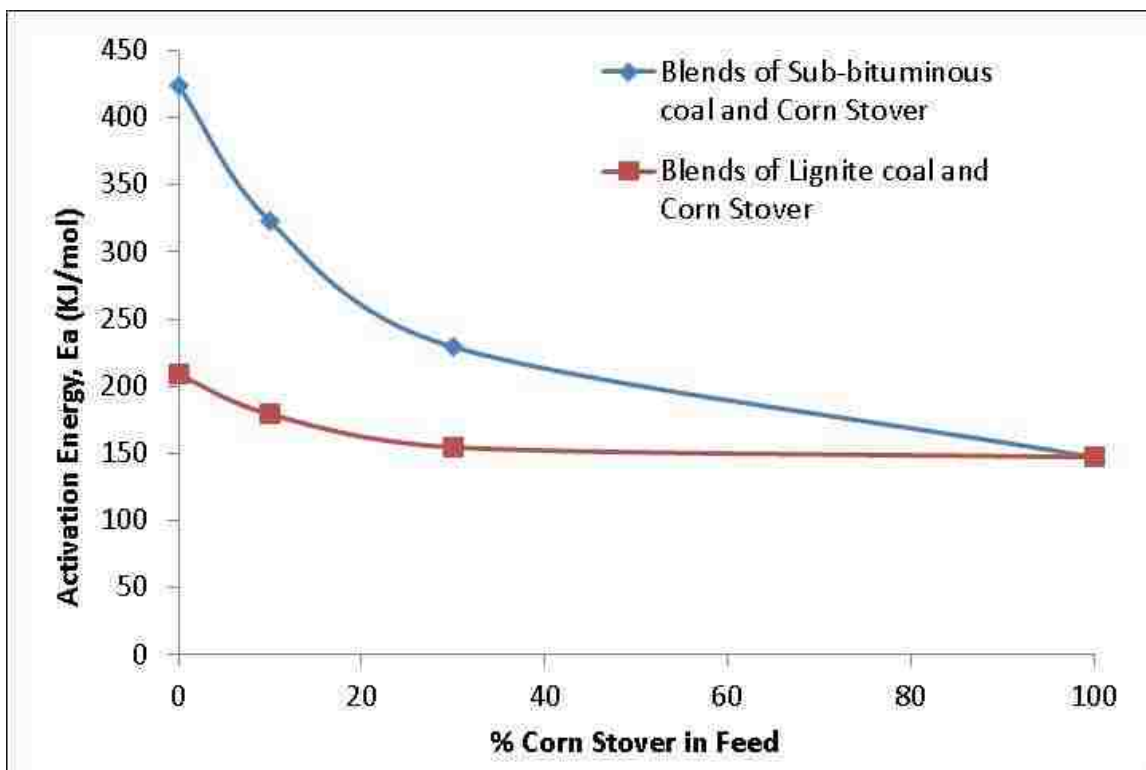


Figure 3.5.5: Variation in activation energy of Boudouard reaction with increasing percentage of corn stover in blends with sub-bituminous and lignite coals.

Values of the kinetic parameters and peak temperatures obtained, as seen from Table 3.5.1, indicate that temperature at which the char-CO₂ reaction occurs decreases with increasing percentage of corn stover in the blend. Clearly, the activation energy decreases with increasing percentage of corn stover in the feedstock as shown in Figure 3.5.5. Assessment of the kinetics indicated that while the overall range of activation energy had reduced significantly in blends with sub-bituminous coal, the amount of material reacting with the more reactive kinetics within the reaction system had increased after addition of corn stover. This indicates certain positive synergistic behavior exists between the blends. The shift in mass fraction and lowered temperature range of the reaction, all serve to confirm this hypothesis for these particular samples. A possible cause for the effect could

be the fact that the mineral content inherently present in biomass has catalytic effects which improves the CO₂ reactivity during gasification of biomass and of coal-biomass blends and that the activation energies obtained are lowered compared to those of coals, implying that biomass is a viable fuel source for co-gasification [88-90].

3.5.2 Kinetics of Boudouard Reaction: Matrix Inversion Algorithm

The single first order reaction model described in Section 3.5.1 is applicable only in the high temperature zone where only the char or fixed carbon of the solid fuel remaining after devolatilization reacts with CO₂. Hence, the model may not be able to predict the weight loss characteristics when pure CO₂ is used as the sweep gas over the full temperature range where devolatilization of the feedstock followed by char gasification occurs. To overcome this drawback and predict the weight loss of the solid feedstock reacting in a CO₂ environment, the matrix inversion algorithm (described in Section 3.3), previously utilized for accurately predicting the devolatilization reaction kinetics in an inert nitrogen atmosphere, was further extended for predicting the kinetics of any feedstock material undergoing thermal degradation in a CO₂ atmosphere. Since it has already been established that both devolatilization and char gasification can be represented with first order kinetics, utilizing this algorithm is logically viable.

For illustrative purposes, the results of the algorithm are presented for DECS-38 sub-bituminous coal. Figures 3.5.6 and 3.5.7 describe the mass loss of DECS-38 sub-bituminous coal in a CO₂ atmosphere on a dry basis, i.e., after the complete removal of moisture and letting the initial temperature for the algorithm to be 400 K. The inversion algorithm was then applied to the TGA data at various heating rates and kinetic parameters were obtained at various conversions. Similar to the results described for the pyrolysis

model, obtained kinetic parameters were then used to model the reactions at unknown heating rates that were not used in the algorithm. The obtained weight loss data was then compared with real TGA data for comparison and accuracy of the method.

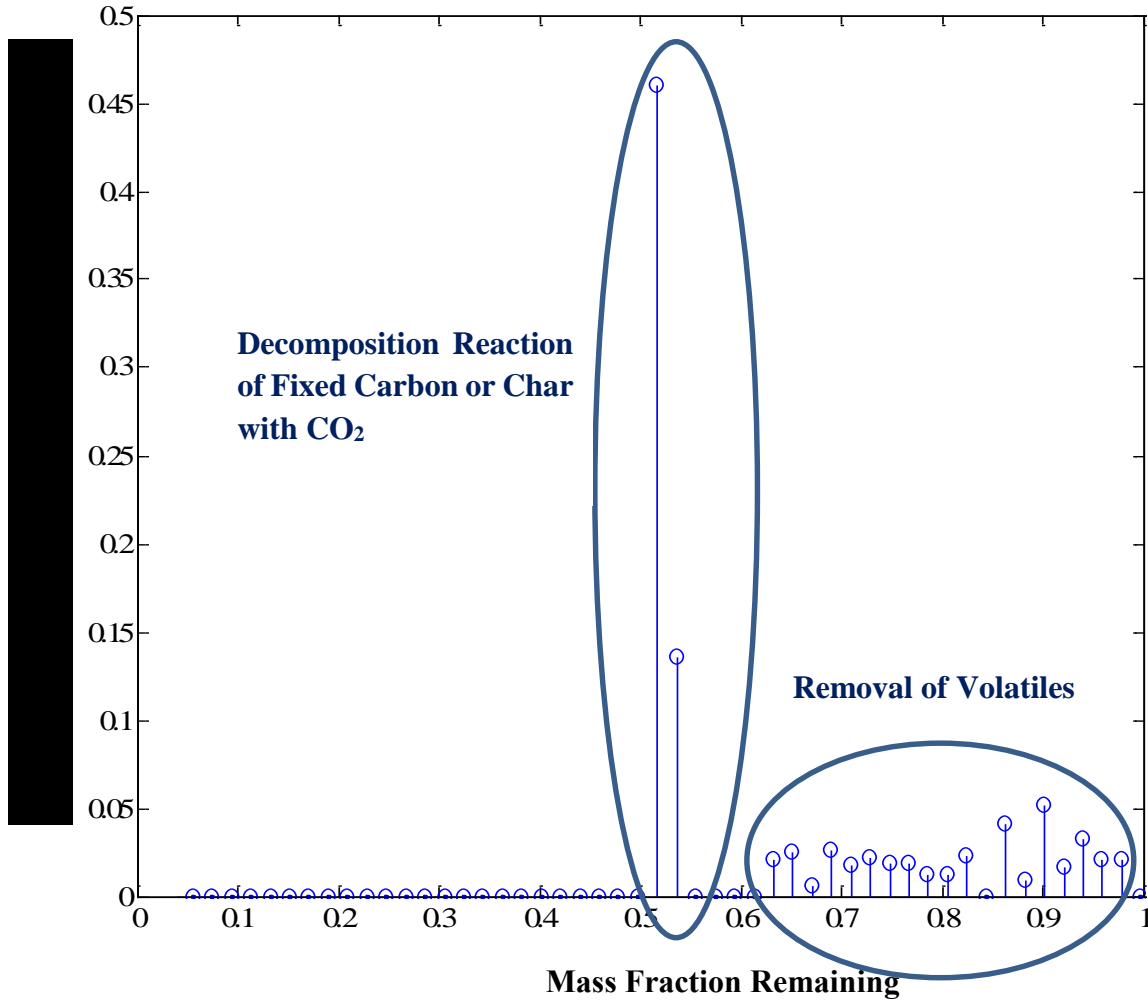


Figure 3.5.6: Stem plot of mass fraction of fuel associated with each reaction occurring during decomposition of DECS-38 sub-bituminous coal in CO₂ atmosphere obtained using DAEM (matrix inversion algorithm).

Clearly, certain differences can be observed when comparing mass loss of sub-bituminous coal in N_2 and CO_2 environments as seen from Figures 3.4.4 and 3.5.6 respectively. Two separate mass loss zones are present when the coal is decomposing in CO_2 environment as opposed to just one zone occurring during pyrolysis in N_2 atmosphere. The second region in Figure 3.5.6 where a sharp loss in mass occurs and the mass fraction of fuel associated with the decomposition reaction is high, is the region corresponding to the reaction between fixed carbon or remaining char and CO_2 .

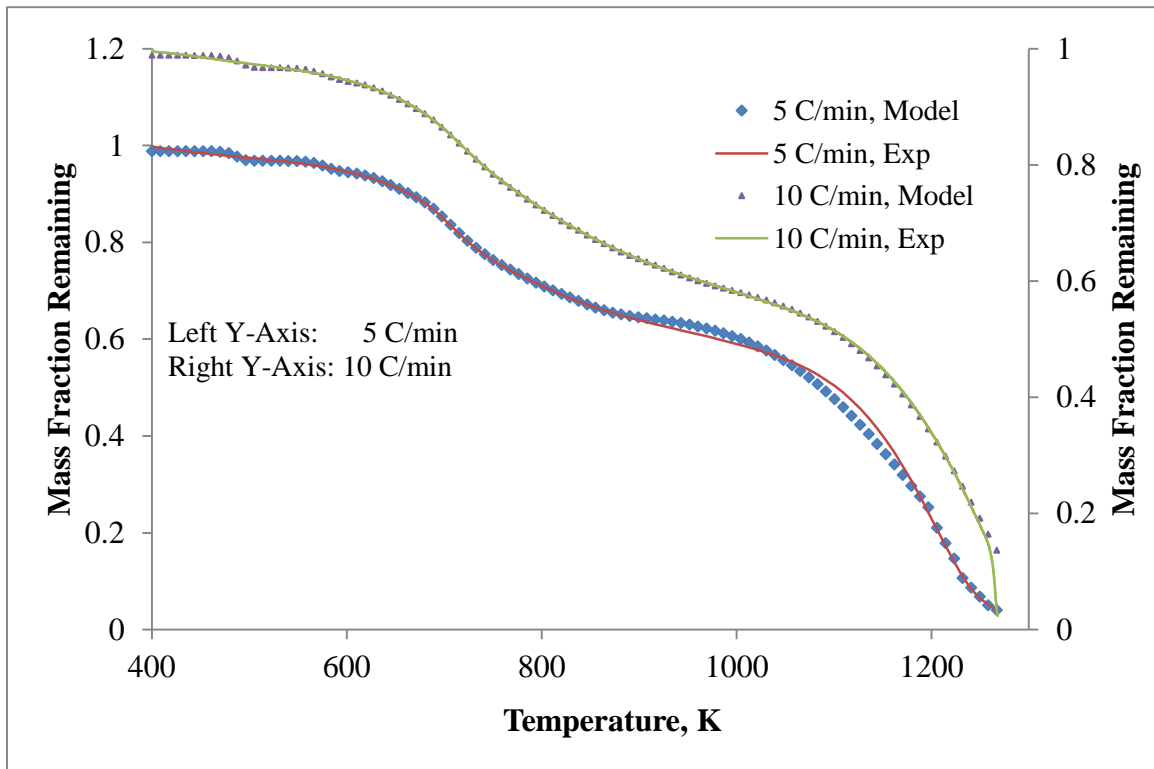


Figure 3.5.7: Comparison of experimental and predicted weight loss curves using the DAEM matrix inversion algorithm for the decomposition of DECS-38 sub-bituminous coal in a CO_2 atmosphere at heating rates of $5\text{ }^\circ\text{C}/\text{min}$ and $10\text{ }^\circ\text{C}/\text{min}$.

3.6 Conclusions

Thermogravimetric analysis has been performed on twelve feed materials, in other words, four single fuels and their blends, and the pyrolysis characteristics were analyzed. The kinetic parameters were determined for the pyrolysis reaction using a non-isothermal mode of operation and single first order reaction model at a heating rate of 5 °C/min. The lower final weight loss of sub-bituminous coal is related to the high content of fixed carbon which is not decomposed in this temperature range. Also, it can be observed that corn stover has the highest weight loss percentage. This trend is due to the high volatile content and low fixed carbon content in corn stover as compared to coals. Also, the pyrolysis temperature range decreased with an increase in the concentration of corn stover in the blends due to the fact that corn stover has a much higher weight loss rate when compared to that of the coals.

The pyrolysis of both coals can be reasonably described as a process with at least three consecutive first order reactions with distinct temperature zones while corn stover and the blends have two and four distinct temperature zones respectively, where the first-order kinetic analysis can be applied. Also, it was observed that the second thermal event during the coal pyrolysis has the highest activation energy of ~ 149 KJ/mol for DECS-38 sub-bituminous coal and ~ 78 KJ/mol for DECS-25 lignite coal. As for corn stover, the major pyrolysis region is in the temperature range of 136-350 °C where a majority (~ 77%) of the mass fraction is removed with an activation energy of ~ 104 KJ/mol. It can also be seen that the activation energies of the blends are not simply additive in nature further indicating a possibility of interactions between the individual fuels. In addition, a thorough investigation into the synergistic behavior between single fuels in the blends has been performed with the conclusion that there are definite interactions between the DECS-38

sub-bituminous coal and corn stover in the temperature range of 230-450 °C. However, in the case of blends of DECS-25 lignite coal and corn stover, minimal synergistic behavior was observed only at lower concentrations of corn stover starting at a temperature of about 320 °C and no synergistic interactions were observed during devolatilization of switchgrass blends.

Finally, three different kinetic models for pyrolysis in N₂ atmosphere have been discussed in this chapter of which the matrix inversion algorithm predicts the kinetic parameters such that the weight loss characteristics can be best represented for both single fuels as well as blends of coals and biomass materials. Also, weight loss characteristics of unknown fuel blends at unknown heating rates can be effectively predicted within 1 % error through the use of this algorithm. In addition, the weight loss characteristics of coal-biomass blends in a CO₂ environment have been compared with those of N₂ atmosphere and the kinetic parameters for the Boudouard reaction have been predicted using a single first order reaction and maximum decomposition rate at temperatures greater than 500 °C.

CHAPTER 4: EXPERIMENTAL MOVING BED GASIFICATION OF COAL-BIOMASS BLENDS

4.1 Laboratory Moving Bed Gasifier: Design and Operation

A laboratory-scale gasification system (Figure 4.1.1 (a) and Figure 4.1.1 (b)) has been designed and constructed for the purpose of gasifying the feedstock materials discussed in Chapter 2 (blends of coal and biomass). The core of the system is an updraft gasifier, where pressure and temperature profiles are measured by a pressure transducer and a set of thermocouples, respectively. Coal/biomass is fed at the top of the gasifier by means of a quick-open flange. Air/oxygen and steam is fed at the bottom of the gasifier and its rate is measured by a rotameter. The design utilizes a single condenser wherein the hot outlet gas enters a cold zone controlled using a refrigerator maintained at 5 °C so that unreacted water and other solids can be collected more efficiently ensuring that clean gas enters the gas chromatograph. The air/oxygen is sent in through the middle of the reactor so that heat coming out of the reactor can be used to preheat the air/oxygen entering the reactor ensuring better use of waste heat.

The gasifier is a 3 feet long cylindrical stainless steel modular flange assembly having an internal diameter of 1.37 inches fitted with another stainless steel tube of 0.075 inches thick on the inside to promote better heat transfer in the axial direction. An initial comparative study was also performed with an inner quartz tube of similar dimensions as that of the stainless steel tube and the outlet product gas compositions were analyzed for the gasification of both coals at various oxygen/steam ratios. A schematic representation of both reactor designs is shown in Figure 4.1.1 (c). For both reactor configurations, the inner tube is fitted with a stainless steel grate with apertures large enough to let the ash pass through but small enough to hold the feed material. The grate is connected to a mechanical

rotary linear feed-through to periodically remove ash. The bottom zone, under the grate, has another cylindrical stainless steel flange with a height of about 5 inches to collect and then discharge the ash produced in the process. The grate at the bottom of the gasifier is used not only for holding the solid particles together but also as an oxidant distributor. The oxidant, fed at the bottom of the reactor, flows along the channels and exits through the small holes along the grate, so it is distributed across the whole section of the gasifier. At the bottom, a small tube allows the use of pre-heated steam to enter the bed. Temperature profiles along the gasifier axis are measured by a set of K-type thermocouples placed within a steel protective tube. The feeding system is constituted by a conical chamber enclosed in a quick-open flange about 5 inches in height. As stated earlier, the product gas stream flows through a condenser maintained at 5 °C where the condensed liquids flow down the tubes and also capture the solid particles entrained by the gas. At the bottom, the liquid phase is discharged and collected for further analysis. Condensers, wet scrubbing, packed bed, and cartridge filters constitute the gas-cleaning system, which though not optimized, guarantees a gas sufficiently clean for gas-chromatographic analysis (GOWMAC Auto System GC equipped with thermal conductivity detector (TCD) and a packed column). Gas sampling and analysis are carried out at selected times during the whole duration of the tests. There are two possible operation modes of the gasifier, corresponding to a constant or a variable bed height. In the first modality, after ignition, the bed height is brought to the desired value and maintained constant. This is achieved by feeding the solid material at proper time intervals. Therefore, as a consequence of variations in the oxidant flow rate, the oxidant-to-fuel ratio will also vary, given that the fuel feed rate is the adjustable variable to control the (constant) bed height.

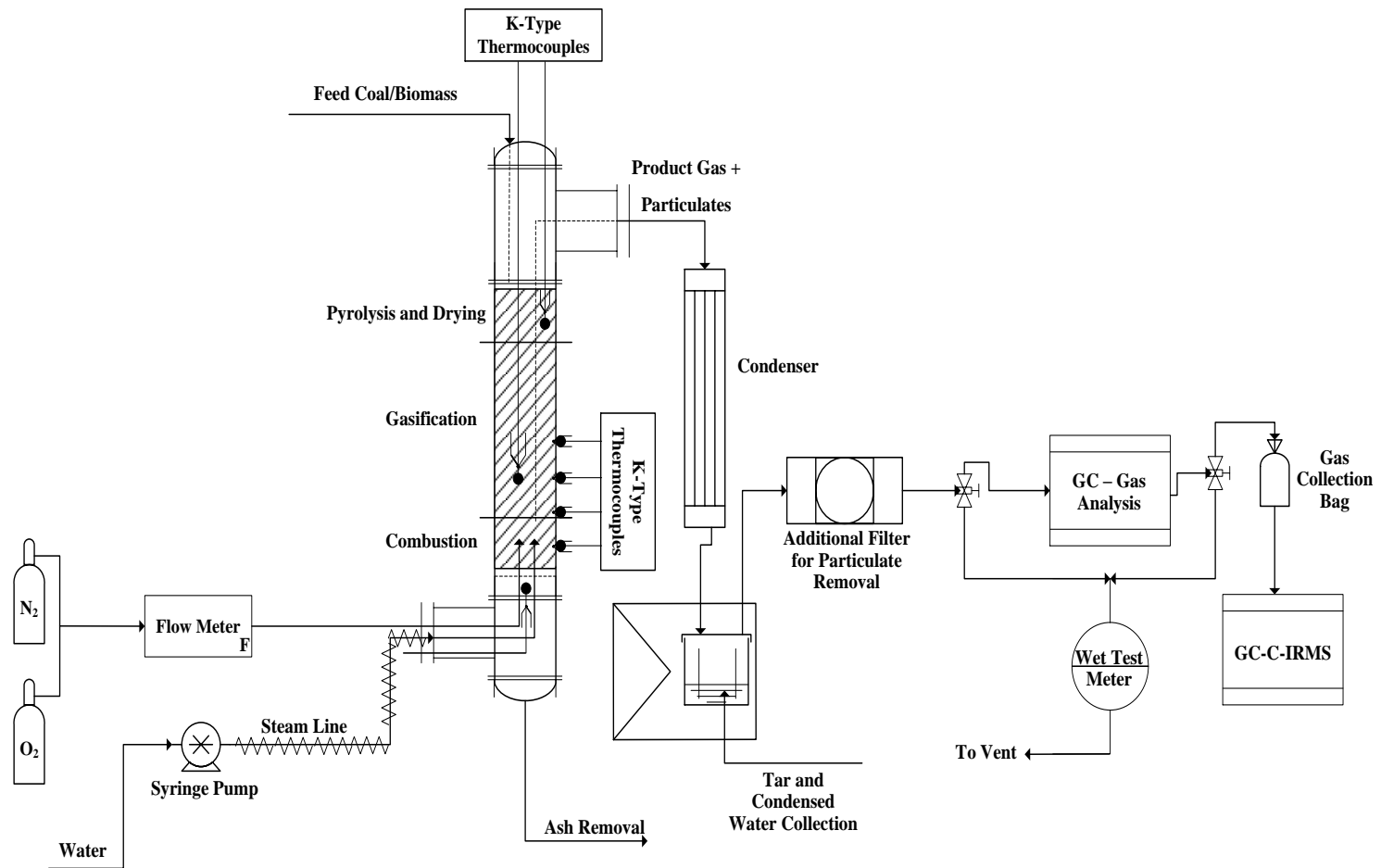


Figure 4.1.1 (a): Schematic of the laboratory scale moving bed gasification system.

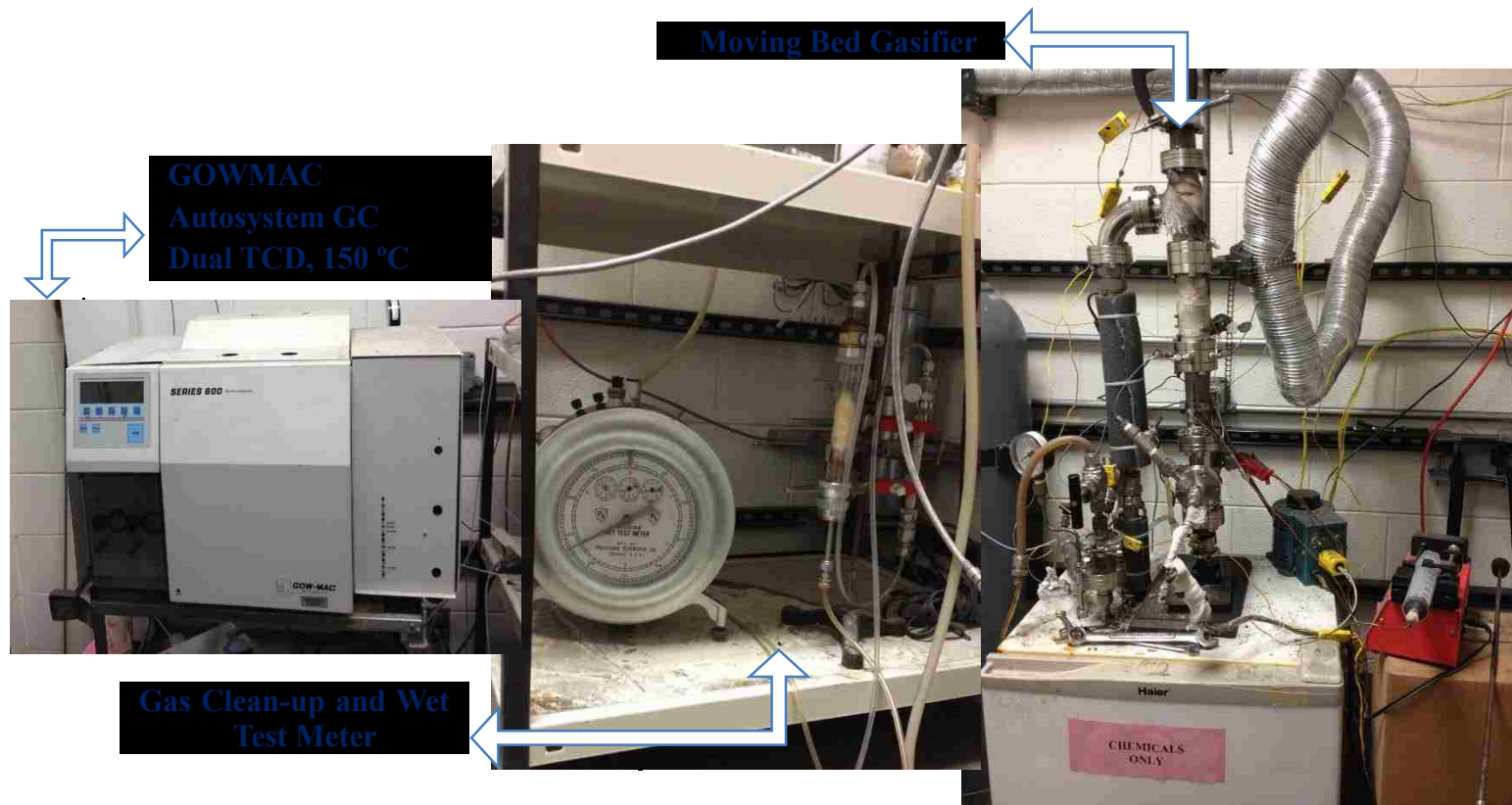


Figure 4.1.1 (b): Pictures of the laboratory scale moving bed gasification system designed and constructed for gasifying coal-biomass blends.

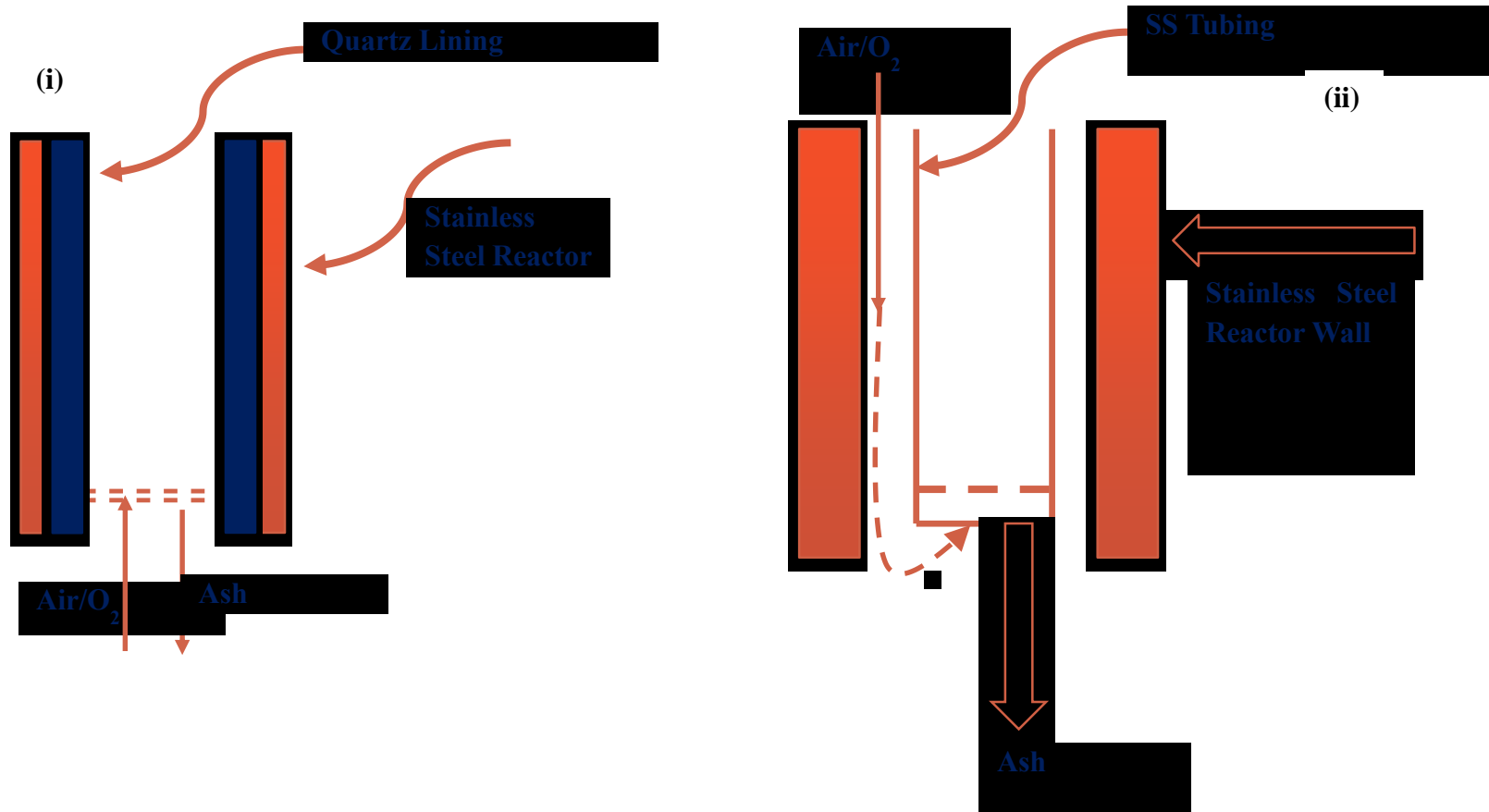


Figure 4.1.1 (c): Schematic representation of the change in reactor design: (i) original design with inner quartz lining. (ii) modified reactor design with inner stainless steel tube for better heat utilization.

The feeding process is an important aspect in the operation of fixed-bed gasifiers. The rate of feed consumption is essentially dependent on the intrinsic reactivity and the rate of oxidant supply. Sufficient feed can be added to keep the bed height at a constant value. However, as the rate of feed consumption increases with the oxidant flow rate, the feeding frequency should also be properly adjusted. In particular, a limit is expected at very high flow rates, when the feeding frequency becomes so high that a semi-continuous procedure is no longer possible. The rate of feed consumption can also be adjusted by choosing a proper rate of solid discharge at the grate, but this may be problematic for small-scale systems. Indeed, frequent solid discharge causes significant heat loss (the discharged solid is at a high temperature), with the introduction of instabilities in the gasification process.

In the second modality, gasification tests can be made for different oxidant-to-fuel ratios, thus allowing the bed height to vary. For instance, after the selection of the oxidant flow rate, the fuel feed rate can be varied and, consequently, the bed height will also vary. However, it can be understood that there is again a limit at very low fuel feed rates, when the continuous operation approaches the behavior of a batch system and the processes of drying/devolatilization, on one side, and gasification/combustion, on the other side, tend to become uncoupled.

The first step in the gasification process is the ignition of the bed. This is caused by adding small amounts of externally heated coal particles onto the grate while supplying the oxidant at low flow rates of approximately 100 ml/min to 150 ml/min. The feed material is then added onto the heated coal particles and the oxidant flow rate is increased, thus causing ignition of the bed. Once the bed is ignited, pre-heated steam is allowed to enter

the bed through the grate at the bottom. Experiments have been performed with varying oxygen flow rates ranging from 150 ml/min to 650 ml/min and varying steam flow rates of 150 ml/min to 1600 ml/min. Apart from varying the oxygen to steam ratio, tests have also been performed with varying oxygen partial pressure on DECS-38 sub-bituminous coal.

4.2 Gasification with Varying Oxygen/Steam Ratio

4.2.1 Quartz Insulation

The gasification of DECS-38 sub-bituminous coal was first carried out in the moving bed gasifier using an internal quartz insulation with varying oxygen to steam ratios. The oxygen flow rate was maintained constant at 650 ml/min while the flow rates of steam were varied from 0 to 1625 ml/min. The average composition of the product gases and the calculated energy efficiency values are provided in Tables 4.2.1 and 4.2.2 respectively.

Table 4.2.1: Average composition of product gases obtained during gasification of DECS-38 sub-bituminous coal with varying oxygen to steam ratios.

Feedstock Weight, g	Average Composition of Product Gases, %							
	H ₂ O:O ₂	H ₂ :CO	CO:CO ₂	(H ₂ +CO):CO ₂	H ₂ %	CO %	CH ₄ %	CO ₂ %
75	0.00	0.14	0.90	1.02	5.39%	39.52%	1.43%	44.02%
115	1.00	0.37	0.78	1.07	12.35%	33.57%	1.35%	42.93%
110	1.50	0.48	0.72	1.08	15.09%	30.26%	1.31%	42.16%
85	2.00	0.81	0.49	0.88	17.31%	21.36%	1.58%	41.81%
235	2.50	0.91	0.47	0.90	18.23%	20.12%	1.29%	40.78%

Table 4.2.2: Calculated energy efficiency during gasification of DECS-38 sub-bituminous coal with varying oxygen to steam ratios.

H₂O:O₂	Max H₂:CO	Max CO:CO₂	Energy Input (KJ)	Energy Output (KJ)	Efficiency %
0.00	0.15	1.03	1504	378	27.9%
1.00	0.55	0.82	2614	953	42.9%
1.50	0.59	0.74	2499	1067	49.8%
2.00	0.90	0.46	1990	676	40.4%
2.50	1.20	0.46	5437	1922	40.4%

Once the composition of the product species is obtained, the gross heating value of the gases and the energy conversion efficiency of the gasifier can be calculated using the following equations [33, 91].

$$GHV_{gases} = \sum_i GHV_i X_i \quad \text{Eq. 4.2.1}$$

where, GHV_i is the gross heating value in kJ/m^3 and X_i is the mole fraction of the fuel gases, $i = \text{CO, CH}_4$ and H_2 .

$$\eta_{gas} =$$

$$\frac{GHV_{gases}}{[N_{fuel} * GHV_{fuel} + N_{steam} * 18\{\lambda + 4.18(373 - 298)\}]} \quad \text{Eq. 4.2.2}$$

where, N_{fuel} and N_{steam} correspond to the moles of fuel and steam supplied, respectively, to the gasifier and λ is the enthalpy of vaporization. GHV_{fuel} is the gross heating value of the fuel in kJ/kg and η_{gas} is the energy conversion efficiency.

Figures 4.2.1 through 4.2.3 describe the results obtained during the gasification of sub-bituminous coal for varying steam to oxygen ratios. As seen from Figure 4.2.1, the increase in the amount of steam fed to the gasifier at constant oxygen flow rate (increased atoms of hydrogen supplied to the gasifier) results in an increase in the hydrogen percentage and a decrease in the percentage of carbon monoxide and carbon dioxide. The amount of methane produced should also increase with the steam supplied to gasifier. However, as the amount of methane produced during all the experiments was less than 2 %; it was difficult to establish a trend for methane using the obtained data.

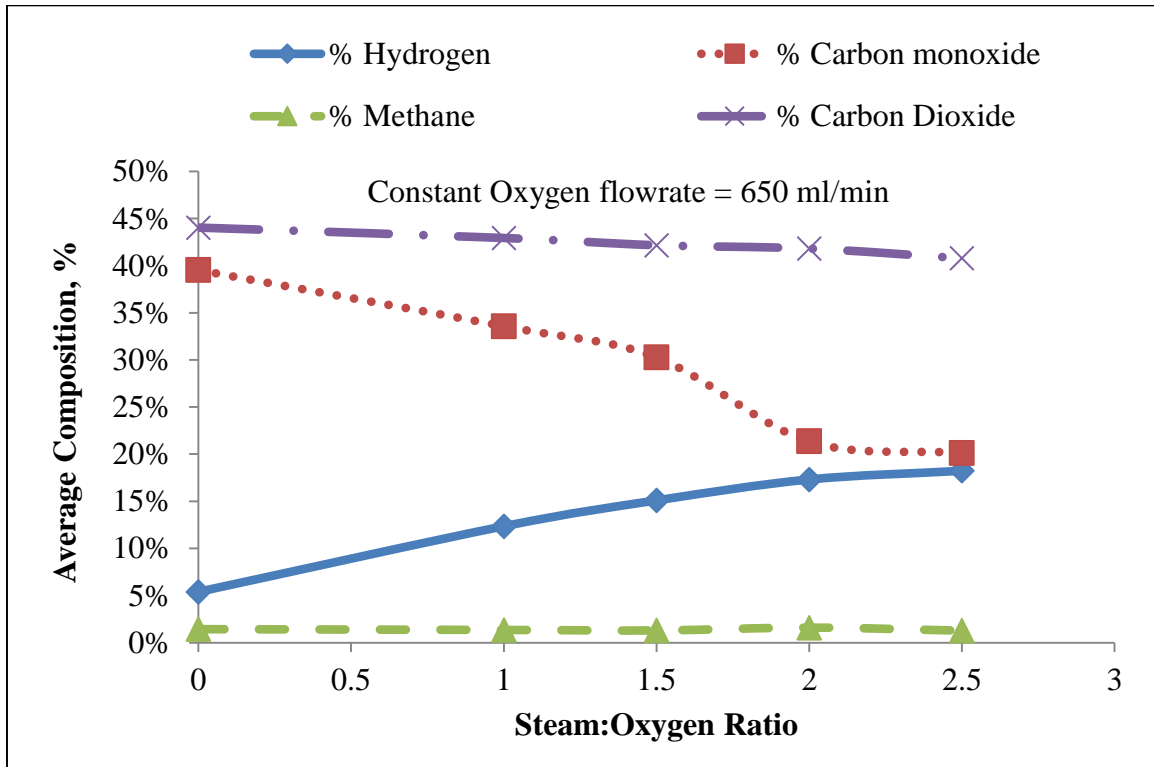


Figure 4.2.1: Average compositions of the product gases obtained during gasification of sub-bituminous coal with varying steam to oxygen ratios.

When experiments were performed with a steam to oxygen ratio above 2.5 in the non-externally heated moving-bed gasifier, the combustion zone at the bottom of gasifier was extinguished in a very short period of time. Increasing steam flow rates to higher values imply decreasing the oxygen supplied to the gasifier. Thus, the exothermic reaction heat is not sufficient to maintain self-sustained reaction. Figure 4.2.2, using the data from the same experiment, shows that the ratio of carbon monoxide to carbon dioxide in the product stream decreases with an increase of steam supplied to the gasifier. Similarly, the ratio of syngas produced to the amount of carbon dioxide produced, increases up to a certain value of steam to oxygen ratio (Steam:O₂ = 1.5) and then decreases. This is due to the reason that the production of carbon monoxide diminishes with increasing steam ratio.

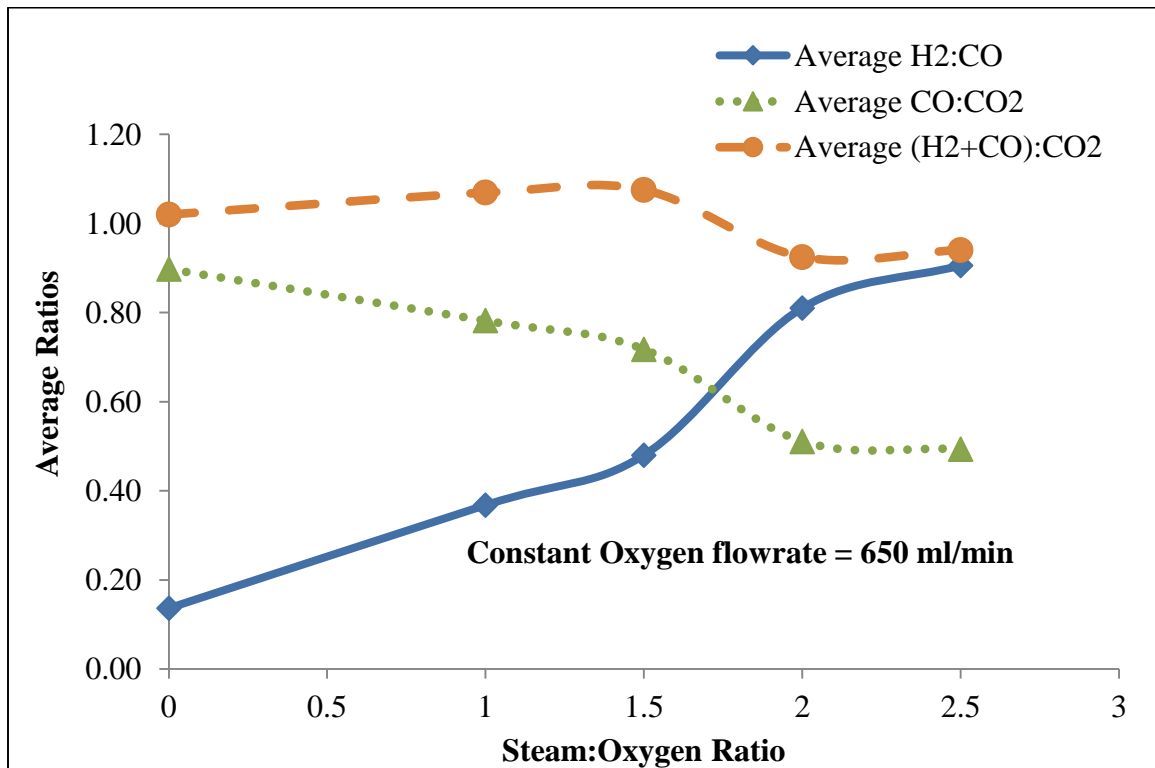


Figure 4.2.2: Average ratios of the product gases obtained during gasification of sub-bituminous coal with varying steam to oxygen ratios.

It can be observed from Figure 4.2.3. that the energy conversion efficiency, as described in Equation 4.2.2, increases up to a steam ratio of 1.5 and then decreases with higher steam ratios. The highest energy conversion efficiency obtained is approximately 50 % at a steam ratio of 1.5. The efficiency decreases for steam ratios above 1.5 since the exothermic zone at the bottom of the bed is either no longer available or that the endothermic zone is much more prevalent at higher steam ratios.

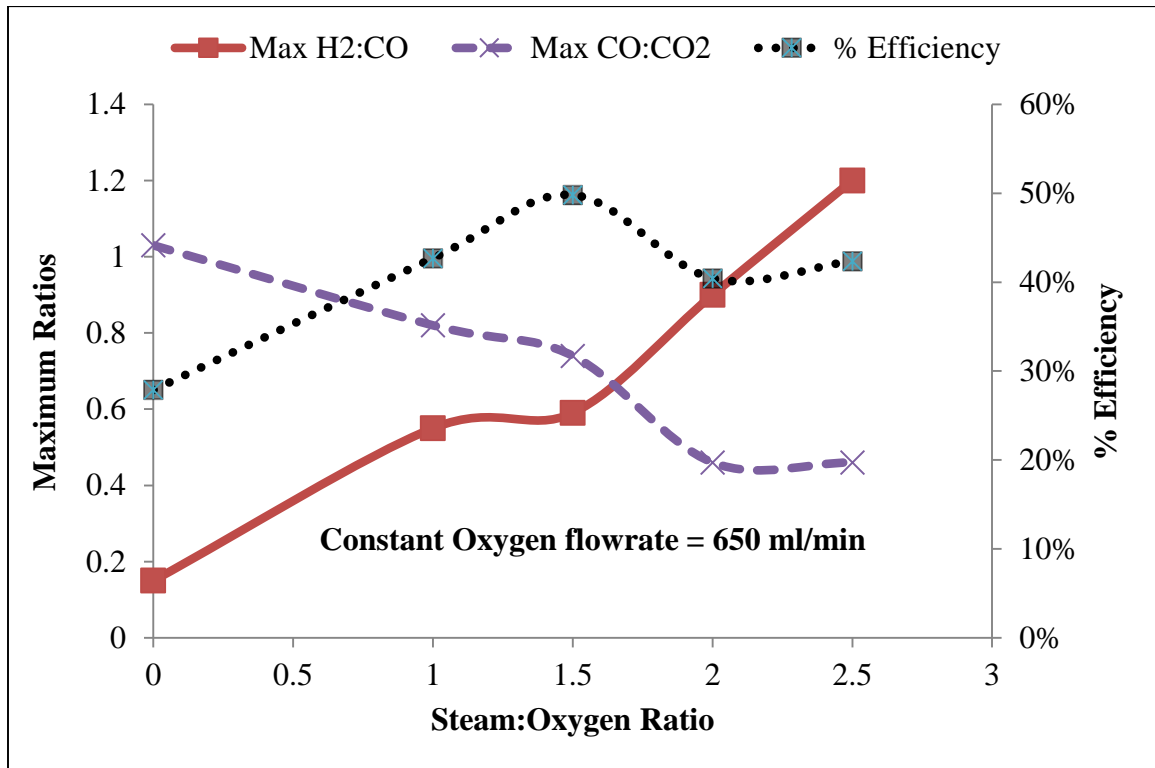


Figure 4.2.3: Maximum ratios of the product gases and efficiency obtained during gasification of sub-bituminous coal with varying steam to oxygen ratios.

4.2.2 Stainless Steel Reactor: Gasification of Coal Feedstocks

As stated earlier in Section 4.1, a comparative study on the effectiveness of using an inner stainless steel tubing in place of quartz tubing was performed at various oxygen/steam ratios for DECS-38 sub-bituminous coal. These tests were conducted to improve the heat transfer in the axial direction and thereby improve the useful product gas composition in the outlet gas stream and the overall efficiency of the gasifier. The product gas compositions and efficiency at various O₂/steam ratios for gasification of sub-bituminous coal are presented in Tables 4.2.3 (a) and (b).

Table 4.2.3 (a): Average composition of product gases obtained during gasification of sub-bituminous coal at varying O₂/steam ratios in the stainless steel moving bed gasifier.

Material	Operating Conditions				Average Product Gas Compositions			
	Air	O ₂	Steam	Steam :O ₂	H ₂ %	CO %	CH ₄ %	CO ₂ %
ml/min	ml/min	ml/min						
DECS-38 Sub- Bituminous Coal		650	0	0	12.85%	32.96%	3.50%	41.71%
		650	325	0.5	20.53%	31.27%	3.21%	41.69%
		650	650	1	24.39%	26.13%	3.09%	41.68%
		650	1300	2	26.65%	21.63%	2.53%	42.66%
	1400	300	0.00	0	4.94%	5.90%	0.00%	13.92%
	1400	300	150	0.5	5.27%	5.48%	0.00%	13.83%
	1400	300	300	1	5.95%	5.01%	0.00%	13.68%
	1400	300	600	2	7.35%	4.48%	0.28%	13.51%

Table 4.2.3 (b): Average ratios of desired product gases and calculated energy efficiency during gasification of sub-bituminous coal at varying O₂/steam ratios in the stainless steel moving bed gasifier.

Material	Operating Conditions			Average Ratios of Product Gases			Efficiency %
	Air	O ₂	Steam	H ₂ :CO	CO:CO ₂	Syngas /CO ₂	
	ml/min	ml/min	ml/min				
DECS-38 Sub- Bituminous Coal		650	0.00	0.39	0.79	1.10	47.2%
		650	325	0.66	0.75	1.24	45.9%
		650	650	0.93	0.63	1.21	53.6%
		650	1300	1.23	0.51	1.13	58.3%
	1400	300	0.00	0.84	0.42	0.78	19.6%
	1400	300	150	0.96	0.40	0.78	21.0%
	1400	300	300	1.19	0.37	0.80	23.1%
	1400	300	600	1.64	0.33	0.88	23.9%

Clearly, with an increase in the concentration of steam in the gasifier the trends of the product gas compositions are similar to those obtained using an inner quartz lining. However, it must be noted here that the percentage of hydrogen generated at same operating conditions is much higher due to the increase in bed temperature (complete consumption of oxygen which was not achieved when using a quartz insulation)) and transfer of heat upwards in the axial direction and thus, better heat utilization which improved the overall efficiency by at least 20% when the steam concentration was at its maximum in the gasifier. Also, unlike the quartz insulation where the efficiency increased

only until a certain point and the maximum steam/O₂ ratio that could be utilized was 1.5, in this experimental set-up, the efficiency increased steadily until a steam/O₂ ratio of 2:1. In addition, the ratios of H₂/CO, CO/CO₂ and syngas/CO₂, which dictate the quality of the product gas, are markedly higher as compared with the previous experimental set-up. Hence, the current experimental set-up was utilized for analyzing the product gas trends during the gasification of various blends of coals and biomass materials. Once it was established that utilizing an inner stainless steel lining improves the overall energy efficiency of the gasifier and quality of syngas produced, the process was repeated for the gasification of lignite coal. The product gas compositions and energy efficiency at various O₂/steam ratios for gasification of lignite coal are presented in Tables 4.2.3 (c) and (d).

Table 4.2.3 (c): Average composition of product gases obtained during gasification of lignite coal at varying O₂/steam ratios in the stainless steel moving bed gasifier.

Material	Operating Conditions				Average Product Gas Compositions			
	Air ml/min	O ₂ ml/min	Steam ml/min	Steam:O ₂	H ₂ %	CO %	CH ₄ %	CO ₂ %
DECS-25 Lignite Coal		650	0	0	12.40	35.73	2.39%	45.97
		650	325	0.5	16.14	34.43	1.95%	46.37
		650	650	1	20.81	27.58	1.73%	45.47
		650	1300	2	25.83	22.03	0.95%	45.90
	1400	300	0.00	0	4.37%	7.65%	0.00%	14.95
	1400	300	150	0.5	6.45%	7.45%	0.00%	14.72
	1400	300	300	1	8.20%	6.98%	0.00%	14.80
	1400	300	600	2	11.37	5.60%	0.00%	14.20

Table 4.2.3 (d): Average ratios of product gases and energy efficiency during gasification of lignite coal at varying O₂/steam ratios in the stainless steel moving bed gasifier.

Material	Operating Conditions			Average Ratios of Product Gases			Efficiency %
	Air	O ₂	Steam	H ₂ :CO	CO:CO ₂	Syngas /CO ₂	
	ml/min	ml/min	ml/min				
DECS-25 Lignite Coal		650	0.00	0.35	0.78	1.05	58.1%
		650	325	0.47	0.74	1.09	55.2%
		650	650	0.75	0.61	1.06	58.8%
		650	1300	1.17	0.48	1.04	61.9%
	1400	300	0.00	0.57	0.51	0.80	31.1%
	1400	300	150	0.87	0.51	0.94	35.9%
	1400	300	300	1.17	0.47	1.03	41.7%
	1400	300	600	2.03	0.39	1.19	52.1%

4.2.3 Stainless Steel Reactor: Blends with Corn Stover

Corn Stover was blended with both coals at various percentages, the maximum composition being 30% by weight of corn stover. Blending higher concentrations of corn stover (> 30% by weight was not feasible) resulted in the reactions inside the gasifier being extinguished due to low temperatures achieved at the bottom of the gasifier. The blends of both coals with corn stover were gasified at various O₂/steam ratios and air/steam ratios and the product gas trends analyzed accordingly. Tables 4.2.4 and 4.2.5 provide an insight

into these compositions and the effect that addition of corn stover to coal had on the quality of gases produced.

For blends of both coals with corn stover (Tables 4.2.4 and 4.2.5), it may be observed that with an increase in the inlet steam:O₂ ratio, the composition of H₂ in the outlet stream increases, composition of CO decreases while CO₂ remains constant in all experiments indicating that Boudouard reaction (Equation 1.8.4), water gas reaction (Equation 1.8.5) and water gas shift reaction (Equation 1.8.7) are taking precedence. For instance, addition of 10 % by weight of corn stover to pure sub-bituminous coal and varying the O₂:steam ratios from 2:1 to 0.5:1 results in a significant increase in the fraction of hydrogen in the dry product gas from approximately 19 % to 26 % while the percentage of carbon monoxide decreases from approximately 32 % to 22 % whereas the fraction of carbon dioxide remains fairly constant at approximately 43 %. In other words, the ratio of H₂/CO increases with the addition of steam to the gasifier. This can be attributed to the fact that addition of excess steam to the gasifier lowers the temperatures which favors the conversion of char to CO and H₂ and the generated CO is converted to CO₂ and more H₂ through water gas shift reaction [92]. The gas compositions can also be compared by increasing the corn stover percentage in the blend, and holding the O₂:steam ratio constant. An increase in corn stover percentage yields lower hydrogen and carbon monoxide while increasing the carbon dioxide yield in the product gas (Figure 4.2.4 (a)). For illustration, at a steam:O₂ ratio of 2:1, the fraction of carbon monoxide decreases from 21 % to 13 % , hydrogen percentage decreases from 27 % to 17 % while carbon dioxide increases from 42 % to 56 % when corn stover is increased from 0 % to 30 % in blends with sub-bituminous coal. This observed effect is significant with confidence intervals greater than 95%.

Table 4.2.4: Average composition of product gases and energy efficiency obtained during gasification of blends of sub-bituminous coal and corn stover at varying O₂/steam ratios in the lab scale stainless steel moving bed gasifier.

Material	Operating Conditions				Average Product Gas Compositions				Average Ratios of Product Gases			$\eta_{\text{gas}} \%$	
	Air	O ₂	Steam	Steam:O ₂	H ₂ %	CO %	CH ₄ %	CO ₂ %	H ₂ :CO	CO:CO ₂	Syngas/CO ₂		
	ml/min	ml/min	ml/min										
90% SB + 10% CS		650	325	0.5	19.41%	31.94	6.79%	43.29%	0.61	0.74	1.19	48.5%	
		650	650	1	23.19%	26.58	6.18%	43.69%	0.87	0.61	1.14	51.1%	
		650	1300	2	26.11%	22.17	5.46%	43.13%	1.18	0.51	1.12	53.3%	
	1400	300	150	0.5	4.54%	3.36%	0.00%	13.91%	1.35	0.24	0.57	20.5%	
	1400	300	300	1	6.57%	5.45%	0.07%	14.17%	1.21	0.38	0.85	44.6%	
	1400	300	600	2	7.83%	6.18%	0.17%	14.59%	1.27	0.42	0.96	48.2%	

Table 4.2.4 (contd.): Average composition of product gases and energy efficiency obtained during gasification of blends of sub-bituminous coal and corn stover at varying O₂/steam ratios in the lab scale stainless steel moving bed gasifier.

80% SB + 20% CS		650	325	0.5	13.79%	25.34	6.01%	48.17%	0.54	0.53	0.81	20.3%
		650	650	1	15.64%	22.56	5.94%	47.43%	0.69	0.48	0.81	32.4%
		650	1300	2	24.43%	20.11	5.83%	47.11%	1.21	0.43	0.82	37.1%
	1400	300	150	0.5	4.59%	4.74%	0.11%	13.50%	0.97	0.35	0.69	23.1%
	1400	300	300	1	7.23%	5.92%	0.00%	13.80%	1.22	0.43	0.95	47.1%
	1400	300	600	2	7.45%	6.11%	0.00%	13.73%	1.22	0.45	0.99	50.4%
70% SB + 30% CS		650	325	0.5	12.19%	18.13	5.08%	56.67%	0.67	0.32	0.54	21.0%
		650	650	1	14.27%	15.73	4.29%	56.79%	0.91	0.28	0.53	25.0%
		650	1300	2	16.93%	13.09	4.00%	56.17%	1.29	0.23	0.53	28.6%
	1400	300	150	0.5	4.34%	3.25%	0.00%	14.86%	1.33	0.22	0.51	25.3%
	1400	300	300	1	7.18%	5.28%	0.00%	15.44%	1.36	0.34	0.81	41.3%
	1400	300	600	2	8.91%	6.21%	0.00%	15.13%	1.44	0.41	1.00	43.5%

Table 4.2.5: Average composition of product gases and energy efficiency obtained during gasification of blends of lignite coal and corn stover at varying O₂/steam ratios in the lab scale stainless steel moving bed gasifier.

Material	Operating Conditions				Average Product Gas Compositions				Average Ratios of Product Gases			$\eta_{\text{gas}} \%$
	Air	O ₂	Steam	Steam:O ₂	H ₂ %	CO %	CH ₄ %	CO ₂ %	H ₂ :CO	CO:CO ₂	Syngas/CO ₂	
	ml/min	ml/min	ml/min									
90% LG + 10% CS		650	325	0.5	14.14%	32.18	7.21%	46.45%	0.44	0.69	1.00	41.4%
		650	650	1	17.73%	27.20	6.03%	46.20%	0.65	0.59	0.97	49.4%
		650	1300	2	20.19%	21.64	5.81%	46.05%	0.93	0.47	0.91	58.3%
	1400	300	150	0.5	6.30%	8.00%	0.00%	13.66%	0.79	0.59	1.05	35.9%
	1400	300	300	1	10.87%	8.62%	0.00%	13.26%	1.26	0.65	1.47	57.2%
	1400	300	600	2	13.83%	9.81%	0.00%	13.01%	1.41	0.75	1.82	64.6%

Table 4.2.5 (contd.): Average composition of product gases and energy efficiency obtained during gasification of blends of lignite coal and corn stover at varying O₂/steam ratios in the lab scale stainless steel moving bed gasifier.

80% LG + 20% CS		650	325	0.5	13.41%	23.93	7.43%	51.12%	0.56	0.47	0.73	36.2%
		650	650	1	16.43%	20.68	6.22%	51.94%	0.79	0.40	0.71	42.3%
		650	1300	2	18.78%	18.14	5.19%	51.74%	1.04	0.35	0.71	48.0%
	1400	300	150	0.5	6.64%	8.38%	0.00%	12.71%	0.79	0.66	1.18	37.5%
	1400	300	300	1	11.94%	7.73%	0.00%	13.33%	1.55	0.58	1.48	52.8%
	1400	300	600	2	13.98%	6.14%	0.00%	13.48%	2.28	0.46	1.49	61.1%
70% LG + 30% CS		650	325	0.5	12.92%	17.14	6.93%	60.93%	0.75	0.28	0.49	29.2%
		650	650	1	15.18%	15.14	6.51%	61.17%	1.00	0.25	0.50	34.5%
		650	1300	2	18.01%	12.39	5.06%	61.11%	1.45	0.20	0.50	38.4%
	1400	300	150	0.5	5.22%	5.69%	0.00%	14.76%	0.92	0.39	0.74	29.1%
	1400	300	300	1	12.03%	12.94	0.00%	11.65%	0.93	1.11	2.14	64.1%
	1400	300	600	2	13.73%	14.05	0.00%	14.34%	0.98	0.98	1.94	66.5%

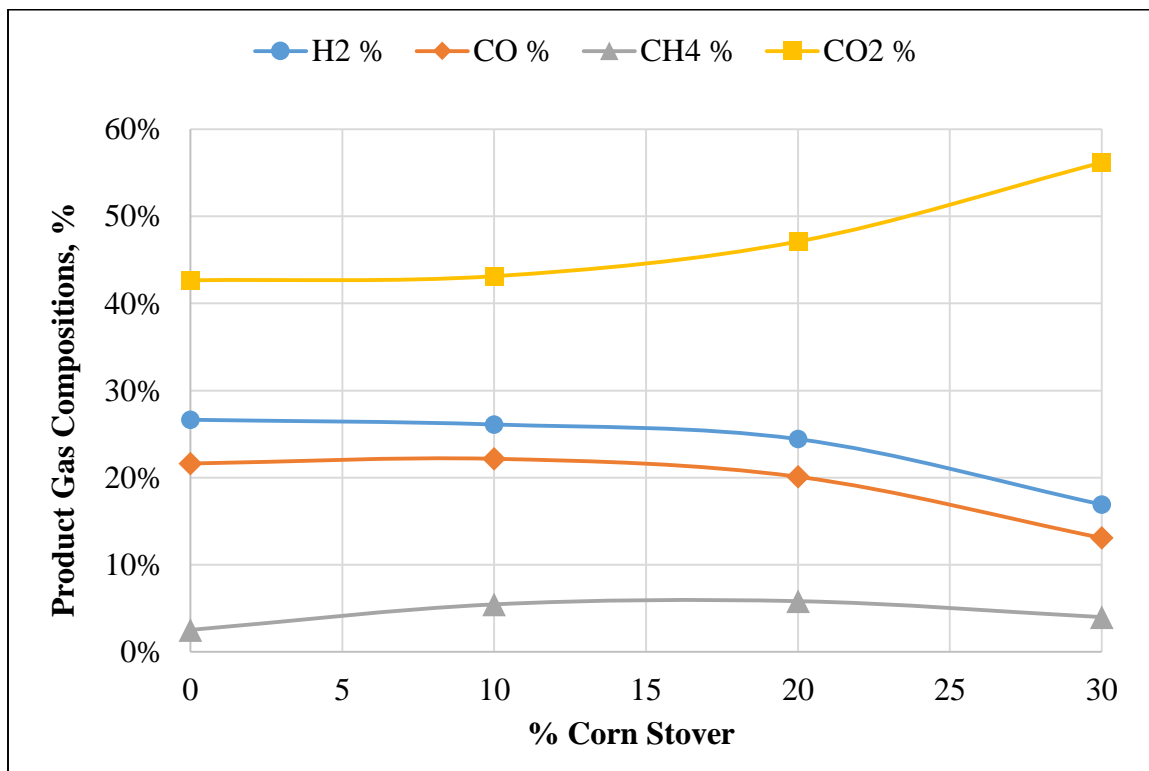


Figure 4.2.4 (a): Effect of increasing percentage of corn stover on the product gas compositions in its blends with DECS-38 Sub-Bituminous coal (Steam/O₂ = 2).

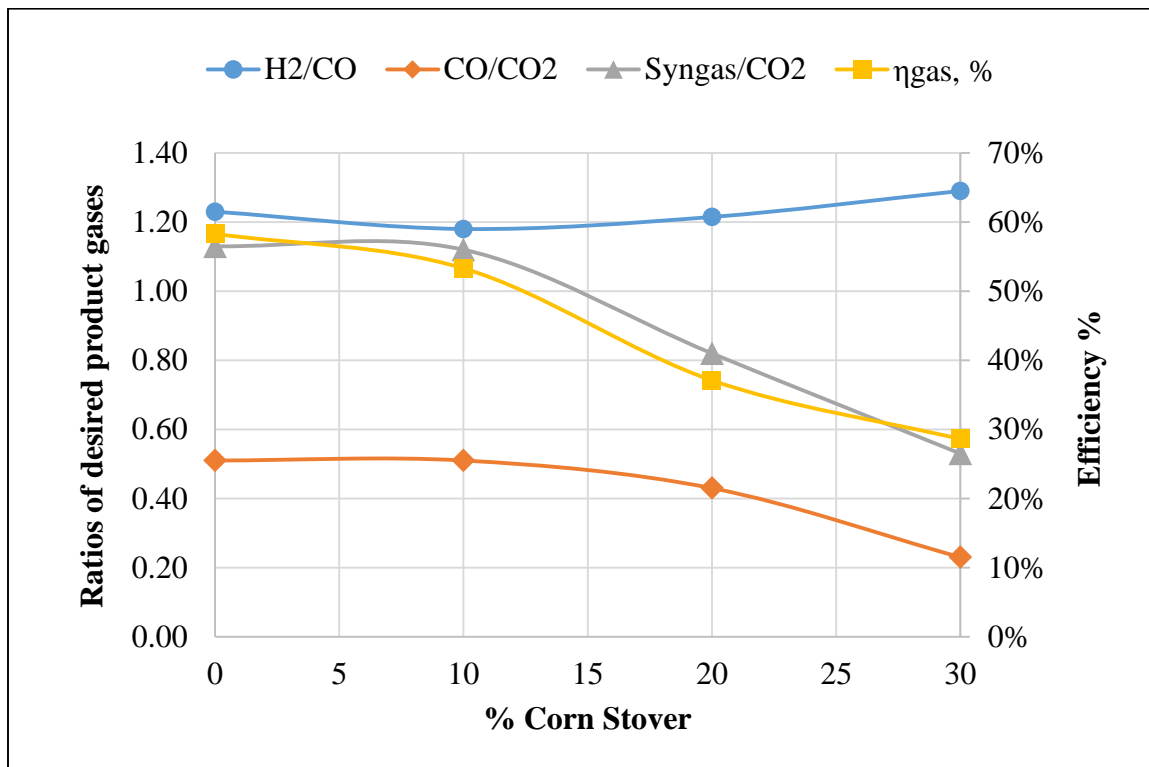


Figure 4.2.4 (b): Effect of increasing percentage of corn stover on the desired product gas ratios and efficiency in its blends with DECS-38 Sub-Bituminous coal (Steam/O₂ = 2).

4.2.4 Stainless Steel Reactor: Blends with Switchgrass

The gasification of blends of both coals with switchgrass was also performed under similar conditions as that of corn stover and the results were compared for compositions and efficiencies obtained as shown in Tables 4.2.6 and 4.2.7. Under similar experimental conditions, the product gas compositions obtained with switchgrass blends follow trends that are in comparison with corn stover blends. However, it can be clearly observed that the overall energy efficiencies obtained are much lower than that of blends with corn stover. This is due to the fact that much higher fraction of carbon dioxide is generated during gasification of these blends. A possible reason for this could be the fact that removal of higher percentage of volatile matter from switchgrass during pyrolysis may be resulting in char with higher void fraction due to which the interaction with incoming steam is reduced, thereby, generating more carbon dioxide through combustion in the bottom zone of the gasifier.

Table 4.2.6: Average composition of product gases obtained during gasification of blends of sub-bituminous coal and switchgrass at varying O₂/steam ratios in the lab scale stainless steel moving bed gasifier.

Feed	Process Conditions				Ratio of Product Gases			Average Product Gas Compositions				$\eta_{\text{gas}} \%$	
	Air ml/min	O ₂ ml/min	Steam ml/min	Steam/ O ₂	H ₂ :CO	CO:CO ₂	Syngas:CO ₂	H ₂ %	CO %	CH ₄ %	CO ₂ %		
90% SB + 10% SG													
		650	325	0.5	0.61	0.63	1.02	17.76%	28.91	5.21%	45.86%	27.1%	
		650	650	1	0.89	0.53	1.00	21.78%	24.35	5.75%	46.02%	30.4%	
		650	1300	2	1.15	0.49	1.05	26.32%	22.83	4.68%	46.62%	53.5%	
		1400	300	150	0.5	0.96	0.28	0.55	4.15%	4.32%	0.00%	15.49%	17.3%
		1400	300	300	1	1.15	0.28	0.61	5.04%	4.38%	1.18%	15.45%	25.7%
		1400	300	600	2	1.50	0.26	0.65	6.19%	4.12%	1.78%	15.93%	29.8%

Table 4.2.6 (contd.): Average composition of product gases obtained during gasification of blends of sub-bituminous coal and switchgrass at varying O₂/steam ratios in the lab scale stainless steel moving bed gasifier.

80% SB + 20% SG												
		650	325	0.5	0.72	0.37	0.63	14.16%	19.72	5.42%	53.68%	23.5%
		650	650	1	1.01	0.32	0.63	16.60%	16.45	4.50%	52.11%	30.7%
		650	1300	2	1.22	0.28	0.62	18.11%	14.88	4.65%	53.57%	33.3%
	1400	300	150	0.5	0.73	0.23	0.40	3.01%	4.14%	0.00%	17.68%	16.4%
	1400	300	300	1	0.92	0.25	0.47	3.96%	4.33%	0.70%	17.58%	24.8%
	1400	300	600	2	1.05	0.26	0.53	4.87%	4.65%	0.00%	17.98%	28.9%
70% SB + 30% SG												
		650	325	0.5	0.65	0.26	0.33	10.34%	16.00	5.73%	62.52%	21.8%
		650	650	1	0.82	0.23	0.43	11.89%	14.50	4.28%	62.03%	26.8%
		650	1300	2	1.31	0.16	0.46	13.09%	10.02	4.78%	63.43%	28.3%
	1400	300	150	0.5	0.43	0.32	0.46	3.19%	7.43%	0.00%	23.18%	14.8%
	1400	300	300	1	0.64	0.29	0.47	4.61%	7.21%	0.00%	24.91%	22.1%
	1400	300	600	2	0.71	0.29	0.50	4.98%	7.01%	0.00%	24.13%	27.7%

Table 4.2.7: Average composition of product gases obtained during gasification of blends of lignite coal and switchgrass at varying O₂/steam ratios in the lab scale stainless steel moving bed gasifier.

Feed	Process Conditions				Ratio of Product Gases			Average Product Gas Compositions				$\eta_{\text{gas}} \%$
	Air ml/min	O ₂ ml/min	Steam ml/min	Steam/ O ₂	H ₂ :CO	CO:CO ₂	(H ₂ +CO):CO ₂	H ₂ %	CO %	CH ₄ %	CO ₂ %	
90% LG + 10% SG												
		650	325	0.5	0.55	0.56	0.87	16.63%	30.05	5.96%	53.65%	37.1%
		650	650	1	0.72	0.46	0.80	17.55%	24.41	5.62%	52.58%	50.7%
		650	1300	2	0.82	0.43	0.78	18.38%	22.38	4.82%	52.07%	59.0%
	1400	300	150	0.5	0.78	0.40	0.72	5.75%	7.33%	0.00%	18.22%	30.3%
	1400	300	300	1	0.84	0.37	0.68	5.91%	7.01%	0.00%	18.99%	33.1%
	1400	300	600	2	0.88	0.38	0.71	6.08%	6.91%	0.00%	18.19%	38.0%

Table 4.2.7 (contd.): Average composition of product gases obtained during gasification of blends of lignite coal and switchgrass at varying O₂/steam ratios in the lab scale stainless steel moving bed gasifier.

80% LG + 20% SG												
		650	325	0.5	0.60	0.30	0.48	11.52%	19.05	5.44%	63.23%	34.4%
		650	650	1	0.94	0.24	0.46	14.49%	15.34	4.00%	64.18%	36.7%
		650	1300	2	1.23	0.20	0.44	15.68%	12.74	4.51%	64.06%	46.5%
	1400	300	150	0.5	0.72	0.25	0.43	3.29%	4.55%	0.00%	18.41%	24.1%
	1400	300	300	1	0.70	0.38	0.65	4.37%	6.24%	0.00%	16.32%	34.9%
	1400	300	600	2	0.72	0.44	0.76	5.15%	7.18%	0.00%	16.18%	39.7%
70% LG + 30% SG												
		650	325	0.5	0.44	0.21	0.30	6.35%	14.34	3.51%	69.80%	20.1%
		650	650	1	0.67	0.18	0.30	8.53%	12.81	3.00%	70.94%	21.9%
		650	1300	2	0.78	0.16	0.29	9.13%	11.69	3.00%	71.14%	25.5%
	1400	300	150	0.5	0.59	0.22	0.34	2.02%	3.44%	0.00%	15.89%	14.6%
	1400	300	300	1	0.58	0.23	0.36	2.48%	4.30%	0.00%	18.90%	19.0%
	1400	300	600	2	0.59	0.26	0.42	2.96%	5.00%	0.00%	18.92%	23.0%

4.3 Gasification with Varying Oxygen Partial Pressure

The gasification of sub-bituminous coal was carried out with varying oxygen partial pressures by introducing nitrogen into the feed stream. Steam was not used in these experiments. Three types of experiments were performed:

1. Varying the oxygen percentage in the feed stream (40 %, 60 % and 100 %) at a constant total flow rate of 650 ml/min.
2. Varying the oxygen percentage in the feed stream (21 %, 40 % and 60 %) at a constant total flow rate of 1400 ml/min.
3. Varying the total flow rate of the inlet gas stream and thus the oxygen fraction (40 %, 60 %, 80 % and 100 %) at a constant oxygen flow rate of 650 ml/min.

Average product gas compositions and efficiencies obtained during gasification with varying oxygen partial pressures are shown in Tables 4.3.1 and 4.3.2 respectively.

Table 4.3.1: Average composition of product gases obtained during gasification of sub-bituminous coal with varying oxygen partial pressures.

			Average Values, %					
Total Flow Rate, ml/min	% N ₂	% O ₂	CO:CO ₂	(H ₂ +CO):CO ₂	H ₂ %	CO %	CH ₄ %	CO ₂ %
650	60	40	0.59	0.66	1.61%	12.70%	0.31%	21.53%
650	30	70	0.62	0.70	3.18%	23.99%	1.27%	38.84%
650	0	100	0.90	1.02	5.39%	39.52%	1.43%	44.02%
1400	78	21	0.62	0.62	0.00%	7.20%	0.00%	11.59%
1400	60	40	1.42	1.60	2.67%	20.65%	0.95%	14.58%
1400	40	60	1.59	1.79	3.86%	31.63%	1.12%	19.88%
1625	60	40	2.16	2.39	2.75%	25.11%	0.38%	11.64%
1083.33	40	60	1.26	1.42	3.59%	28.87%	0.67%	22.90%
812.5	20	80	1.00	1.11	3.86%	32.17%	1.00%	32.33%
650	0	100	0.90	1.02	5.39%	39.52%	1.43%	44.02%

Table 4.3.2: Calculated energy efficiency during gasification of sub-bituminous coal with varying oxygen partial pressures.

Total Flow rate, ml/min	% N₂	% O₂	Max CO:CO₂	Energy Input (KJ)	Energy Output (KJ)	Efficiency
650	60	40	0.77	2591	226	8.7%
650	30	70	0.79	2082	315	15.1%
650	0	100	1.03	1504	378	25.2%
1400	78	21	1.37	1295	120	9.3%
1400	60	40	1.88	2591	735	28.4%
1400	40	60	2.27	2637	895	33.9%
1625	60	40	3.12	3170	1136	35.8%
1083.33	40	60	1.79	2036	591	29.1%
812.5	20	80	1.71	2128	543	25.5%
650	0	100	1.03	1504	378	25.2%

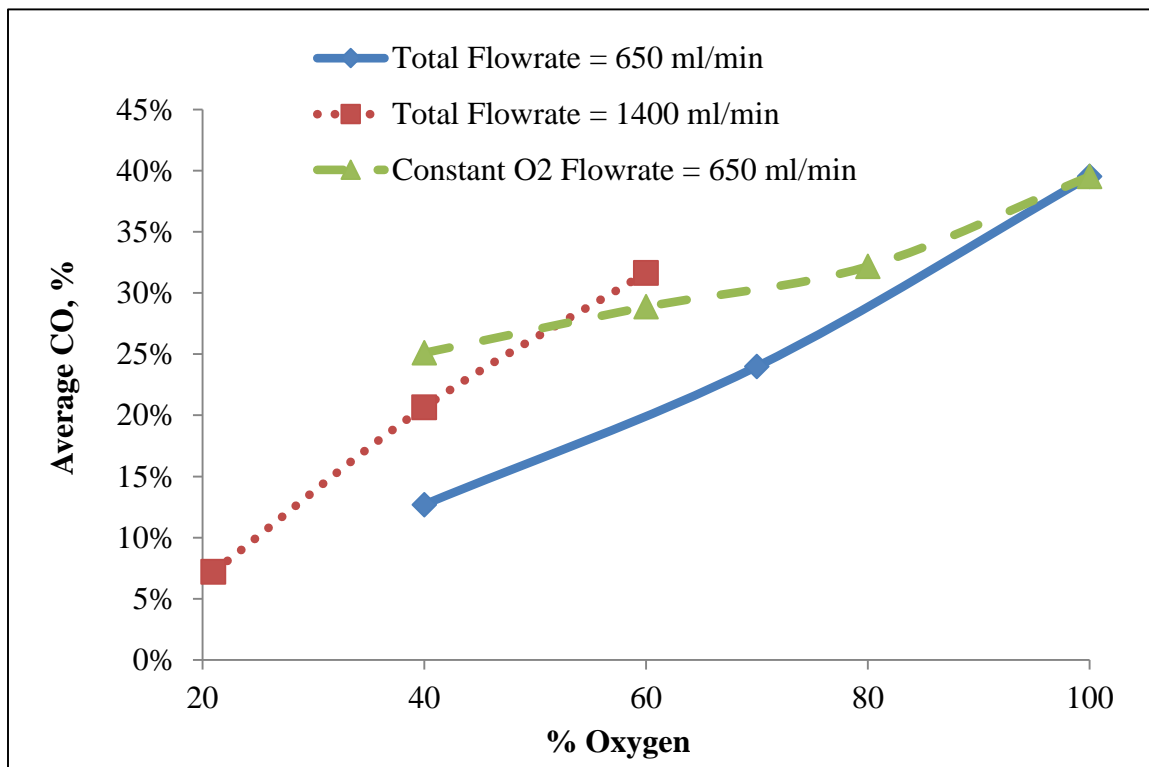


Figure 4.3.1: Average carbon monoxide concentration in exit stream obtained during gasification of sub-bituminous coal with varying oxygen partial pressures.

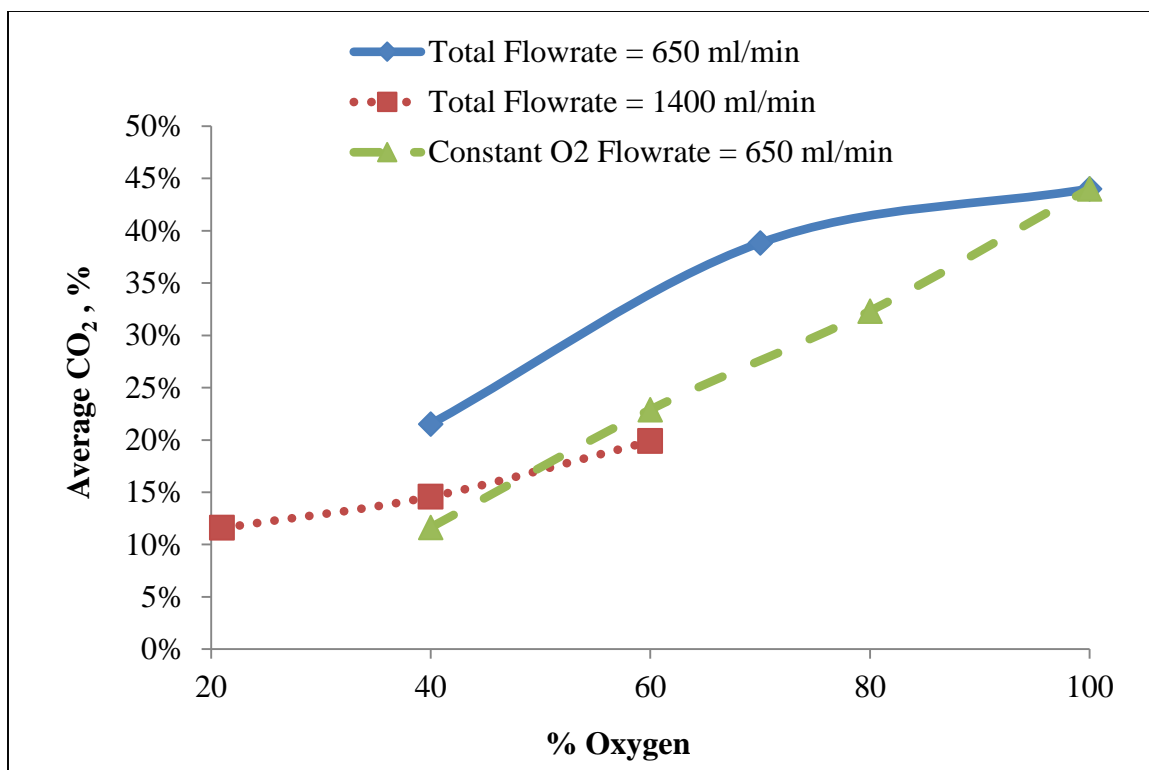


Figure 4.3.2: Average carbon dioxide concentration in exit stream during gasification of sub-bituminous coal with varying oxygen partial pressures.

From Figures 4.3.1 and 4.3.2, it can be observed that the average carbon monoxide and carbon dioxide concentrations in the gasifier exit stream increase with increasing oxygen percentage in the feed gas stream. The average composition values vary not only as a function of the partial pressure of oxygen but also vary as a function of the total flow rate of the feed stream. As the total flow rate of the inlet gas stream is increased, the concentrations of carbon monoxide and carbon dioxide in the product gas increase for the same oxygen percentage in the feed stream. For example, if the feed stream contains 40 % oxygen and 60 % nitrogen, the percentage of carbon monoxide in the product gas is 12.7 % for a total inlet gas flow rate of 650 ml/min, 20.65 % for a total inlet gas flow rate of 1400 ml/min and 25.11 % for a total inlet gas flow rate of 1625 ml/min. This is believed to

be caused because higher gas feed stream flow rate can propagate heat axially upwards at a much faster rate, causing the coal particles to react with oxygen at a higher rate.

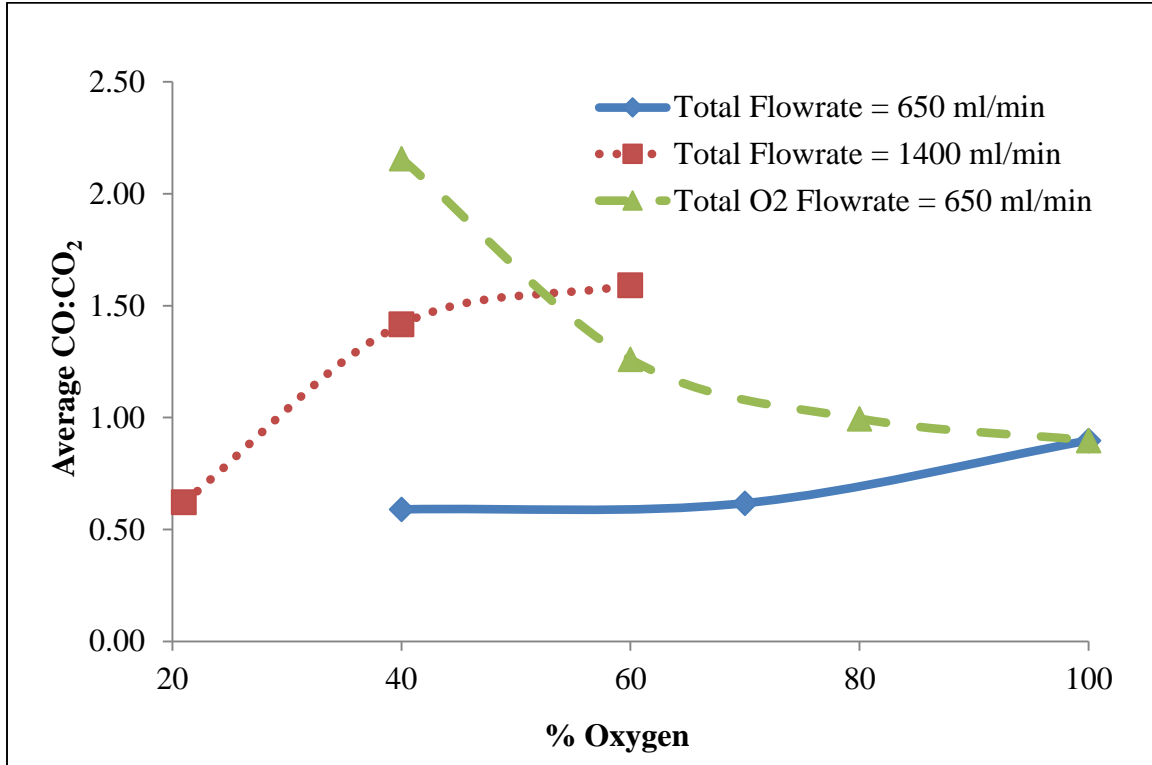


Figure 4.3.3: Average CO:CO₂ ratios in the exit gas stream obtained during gasification of sub-bituminous coal with varying oxygen partial pressures.

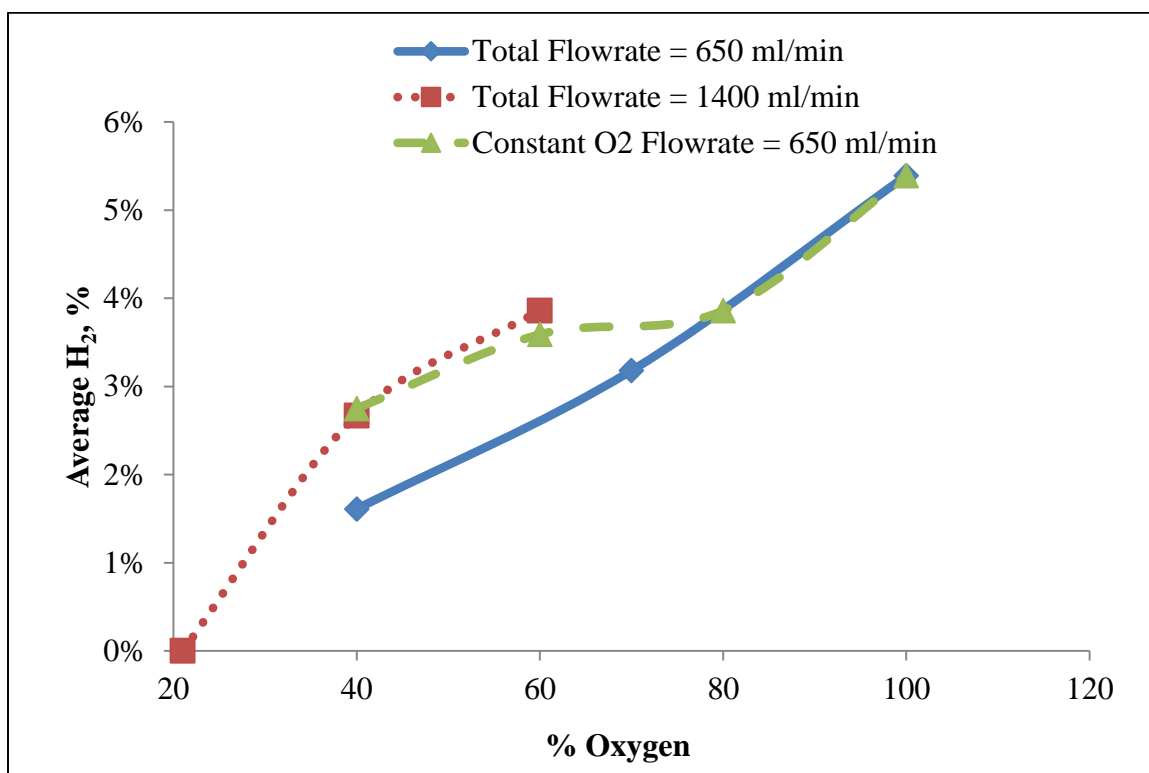


Figure 4.3.4: Average hydrogen concentration obtained during gasification of sub-bituminous coal with varying oxygen partial pressures.

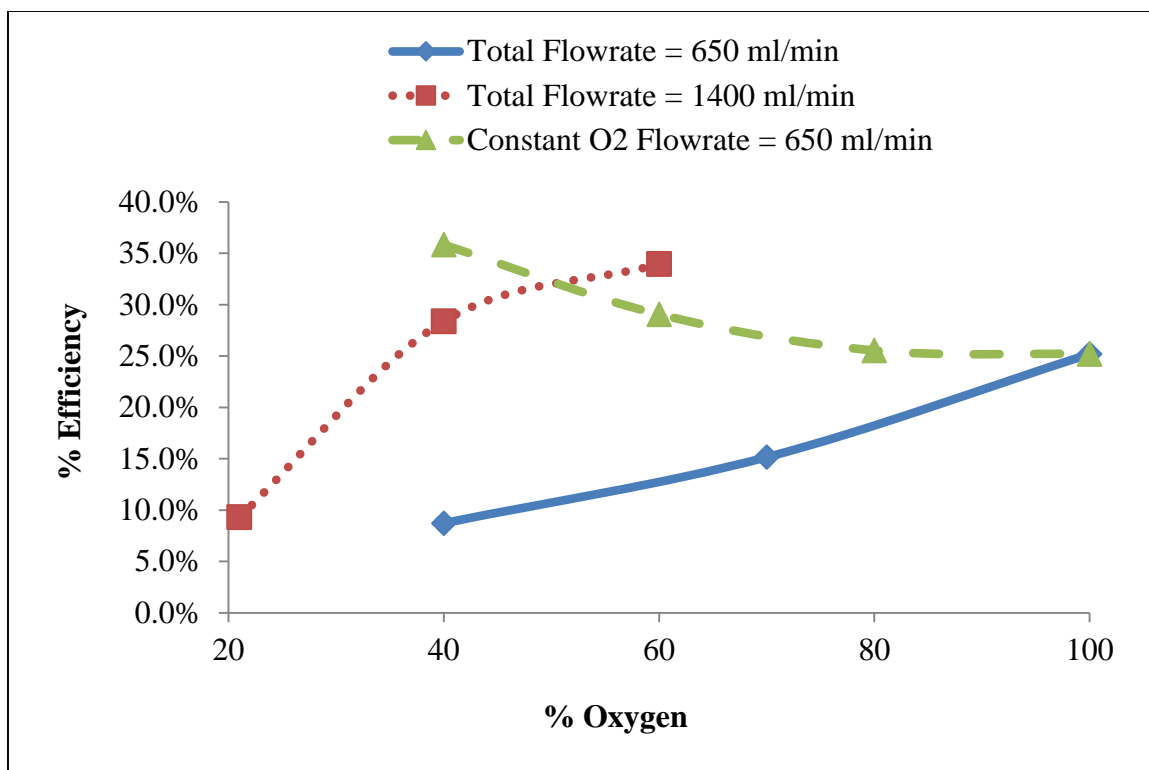


Figure 4.3.5: Energy conversion efficiency obtained during gasification of sub-bituminous coal with varying oxygen partial pressures.

Since these set of experiments were conducted in the absence of steam, it can be inferred that hydrogen would be present only in small amounts in the product gas stream. The percentage of hydrogen in the outlet gas stream was a function of the oxygen partial pressure in the feed gas stream as well as the total flow rate of the feed gas stream and followed the same trends as observed for carbon monoxide and carbon dioxide. The efficiency of the gasification reaction increased with increase in the inlet gas flow rate and oxygen partial pressure for the same reason that more heat was believed to be carried upwards to produce higher BTU value gas. Based on the above experimental results, the optimal gasification conditions in the laboratory scale moving bed gasifier are:

1. Using pure oxygen and steam in the inlet gas stream, the highest energy conversion efficiency obtained is approximately 50 % at a steam to oxygen ratio of 1.5.
2. Using a mixture of nitrogen and oxygen in the feed gas stream, the inlet gas stream flow rate of 1625 ml/min and oxygen percentage of 40 % provides the highest energy conversion efficiency and a max CO: CO₂ ratio of approximately 3:1.
3. The bed temperature range during the gasification of sub-bituminous coal was generally observed to be between 600 °C and 800 °C for the experiments with varying steam ratios and between 800 °C and 1000 °C for the experiments with varying oxygen partial pressures.

4.4 Gasification of Briquettes

The gasification of four different briquette types was also studied in the moving bed reactor under different oxygen to steam and air to steam ratios. The 4 briquette types are as follows:

1. EM-SD: Clean coal from Emerald Mine (EM), Pennsylvania blended with 20% by weight of kiln dried eastern white pine (*pinus strobus*) sawdust/shavings (SD) from sawmill (Turman Lumber Company) in Hillsville, Virginia. The coal was crushed and screened to 1.0 mm top size and air dried for 1 week to 1.6% moisture before briquetting while the sawdust was screened to 1.2 mm top size before oven drying to reduce the moisture content from approximately 11% to 0.2%.

2. EM-SD-G97: The briquettes obtained by blending Emerald Mine clean coal and pine sawdust were then coated with a wood derived chemical resin (G97). The coating was performed by dipping the briquettes in resin which was heated to approximately 300 °F.
3. EB-CS: Raw coal from Eagle Butte Mine (EB), Wyoming blended with 20% by weight of corn stover (CS) obtained from Piedmont Bioproducts, VA. The raw coal was crushed and screened to 1.0 mm top size and air dried for 1 week and oven dried for 48 hours at 105 °C to reduce the moisture content to 1.7%. Corn stover, on the other hand, was processed in a knife mill across a 3/16” screen and was blended with the coal without drying.
4. EB-CS-G97: The blends of EB and CS were then coated with G97 resin as described above and used as feed for the moving bed gasifier.

The wood derived resin coating was used for strengthening the briquettes which would be helpful during transportation of the blended feedstocks from a preparation plant to the gasification facility if the process were to be expanded to a large scale commercial facility. The idea is that the addition of resin would be helpful to hold the briquettes together without modifying the briquette properties and gasification characteristics. Experiments have been performed at atmospheric pressure with varying oxygen flow rates ranging from 300 ml/min (Air flow rate of 1400 ml/min equates to approximately 300 ml/min of oxygen) to 650 ml/min and varying steam flow rates of 150 ml/min to 1300 ml/min, the results of which would be discussed in the following sections. A ratio of 2:1

(steam:O₂) was chosen because beyond this, the endothermic zone was prevalent inside the gasifier and the gasification of the feedstocks was not sustained.

4.4.1 Product Gas Analysis: Briquette Gasification

The gasification of the four types of briquettes was carried out in the moving bed gasifier with varying oxygen to steam ratios. The oxygen flow rate was constant at 650 ml/min while the flow rates of steam were varied from 0 to 1625 ml/min. In order to obtain a baseline for this analysis, different known concentrations of the product gases (H₂, CO, CH₄ and CO₂) were first analyzed to obtain the times at which their respective peaks were occurring. A plot of volume % versus peak area gives the calibration curve for obtaining the concentrations of the product gases. The average composition of the product gases is calculated using a calibration curve for each species. Once the composition of the product species is obtained, the gross heating value of the gases and the energy conversion efficiency of the gasifier can be calculated. The average composition of the product gases and the calculated energy efficiency values are provided in Tables 4.4.1 through 4.4.4.

Figures 4.4.1 through 4.4.5 describe the product gas compositions obtained during the gasification of EM-SD briquettes as an example. All the briquettes follow similar trends in the product gas compositions with the average values being different. As seen from Figure 4.4.1, the increase in the amount of steam fed to the gasifier at constant oxygen flow rate, implies increased atoms of hydrogen supplied to the gasifier. This results in a gradual increase in the hydrogen percentage. Also, the percentage of carbon monoxide increases with increasing steam concentration. This is due to the fact that the reaction of solid carbon or char with steam (Water gas reaction) and char with carbon dioxide (Boudouard Reaction) are predominant. These reactions are endothermic in nature and are favored at

high temperatures $> 900\text{ }^{\circ}\text{C}$ as described earlier. The combustion of solid carbon at the bottom of the gasifier results in a highly exothermic reaction releasing carbon dioxide initially. As the temperature inside the gasifier increases and attains a steady value of around $900\text{ }^{\circ}\text{C}$, the char present reacts with the carbon dioxide generated from combustion and thus results in an increased concentration of carbon monoxide and decreased carbon dioxide in the producer gas.

Table 4.4.1: Average Composition of Product Gases Obtained During Gasification of EM-SD Briquettes with Varying Oxygen to Steam Ratios

Feed	Process Conditions				Ratio of Product Gases			Average Product Gas Compositions				η_{gas} %	
	Air ml/min	O ₂ ml/min	Steam ml/min	Steam/ O ₂	H ₂ :CO	CO:CO ₂	Syngas:CO ₂	H ₂ %	CO %	CH ₄ %	CO ₂ %		
EM-SD		650	325	0.50	0.56	0.20	0.31	6.71%	12.00%	3.63%	59.94%	16.70%	
		650	450	0.70	0.56	0.21	0.33	6.75%	12.12%	3.98%	57.82%	18.71%	
		650	650	1.00	0.58	0.22	0.35	6.86%	11.86%	4.29%	53.50%	20.12%	
		650	975	1.50	0.59	0.32	0.50	9.63%	16.27%	6.39%	51.32%	26.10%	
		650	1300	2.00	0.61	0.39	0.62	11.20%	18.25%	9.37%	47.14%	28.12%	
		1400	300	150	0.50	0.68	0.59	0.99	4.59%	6.74%	0.00%	11.50%	25.98%
		1400	300	300	1.00	0.90	0.64	1.22	6.23%	6.92%	0.00%	10.80%	31.40%
		1400	300	600	2.00	1.05	0.66	1.36	7.45%	7.11%	0.00%	10.73%	43.04%

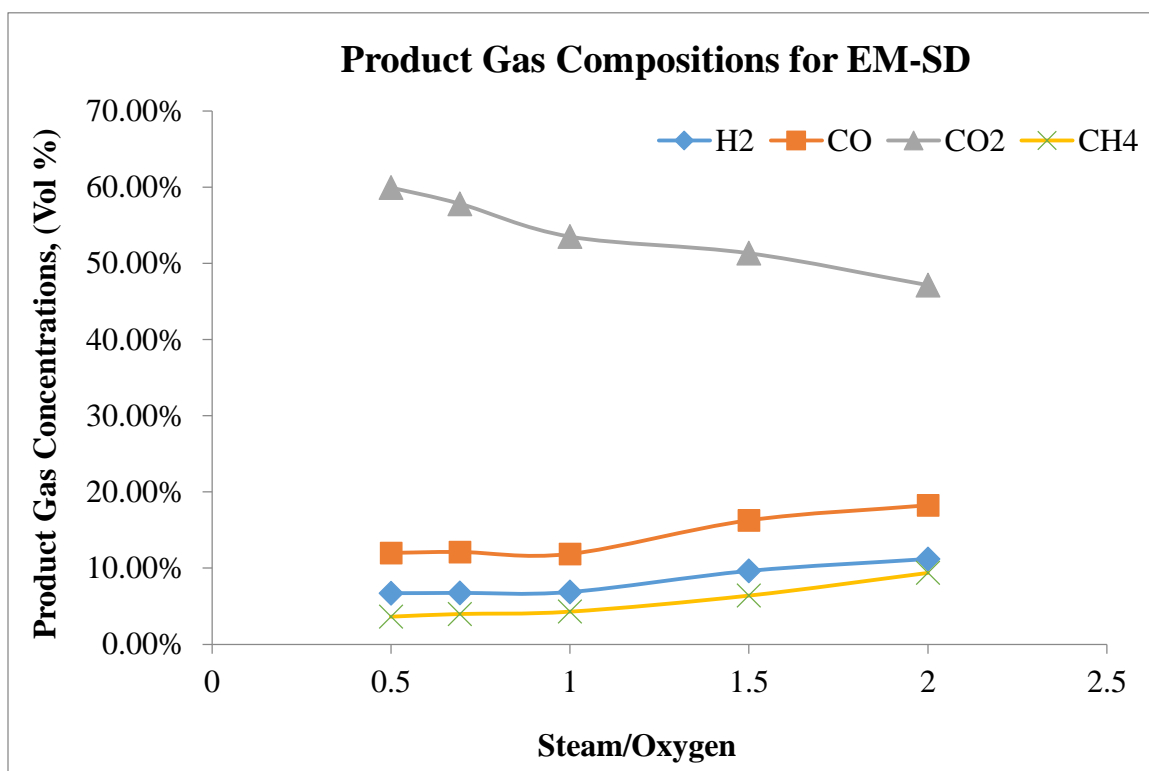


Figure 4.4.1: Average compositions of the product gases obtained during gasification of EM-SD briquettes with varying steam to oxygen ratios.

Experiments with a steam to oxygen ratio of greater than 2.0 were also performed, but they resulted in the bed being extinguished in a very short period of time. Increasing steam flow rates to very high values implies decreasing the oxygen supplied to the gasifier. Thus, the exothermic reaction of carbon and oxygen which supplies the necessary heat for the gasification reaction to proceed is not favored resulting in temperatures not high enough for hydrogen to be stripped from steam. Hence, no gasification reaction occurred at higher flow rates of steam.

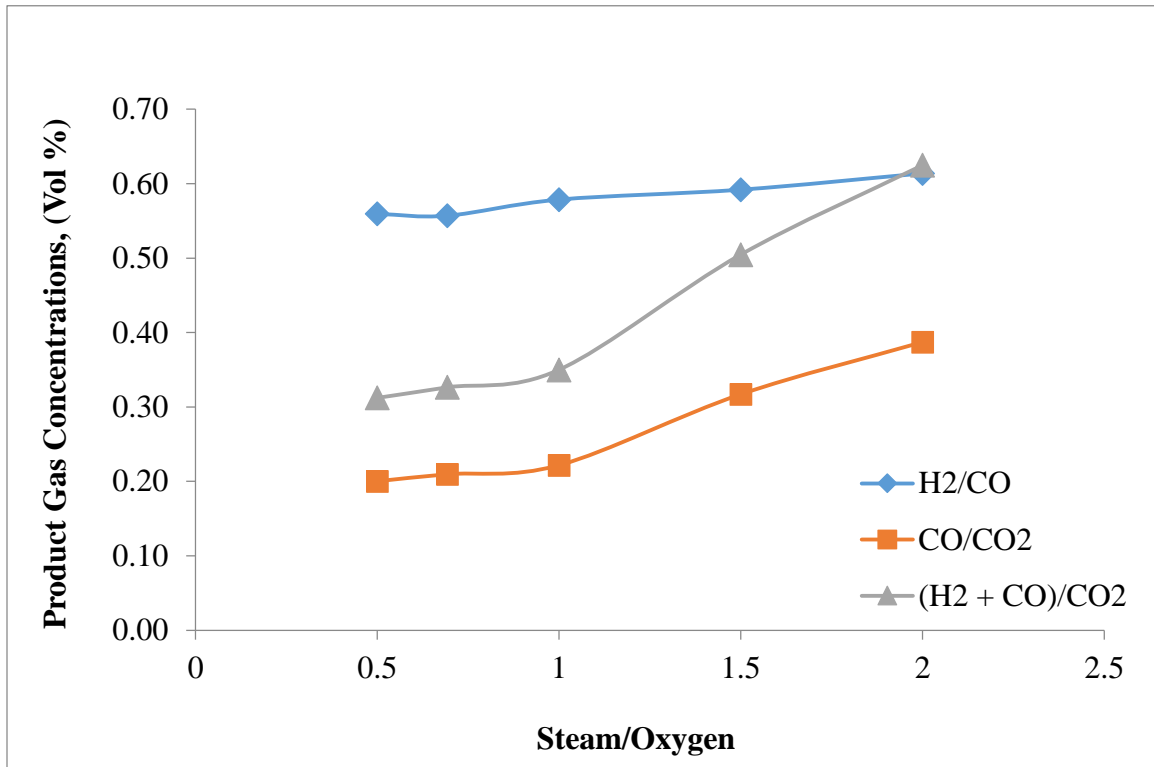


Figure 4.4.2: Average ratios of the product gases obtained during gasification of EM-SD briquettes with varying steam to oxygen ratios.

It is necessary to operate the gasifier at a nominal oxygen/carbon ratio. Even though high oxygen concentration results in increased carbon conversion, too much oxygen results in complete combustion and does not favor the production of syngas which will lower the

heating value of the producer gas. A comparison of the product gas compositions was also made by replacing oxygen with air as the gasifying agent. Air at much higher flow rate (1400 ml/min or 300 ml/min of O₂) was introduced to improve the heat transfer axially upward through the reactor so that char a higher temperature falls into the gasifying zone. These experimental runs were performed to verify if the cold gas efficiencies improve with increasing steam concentrations.

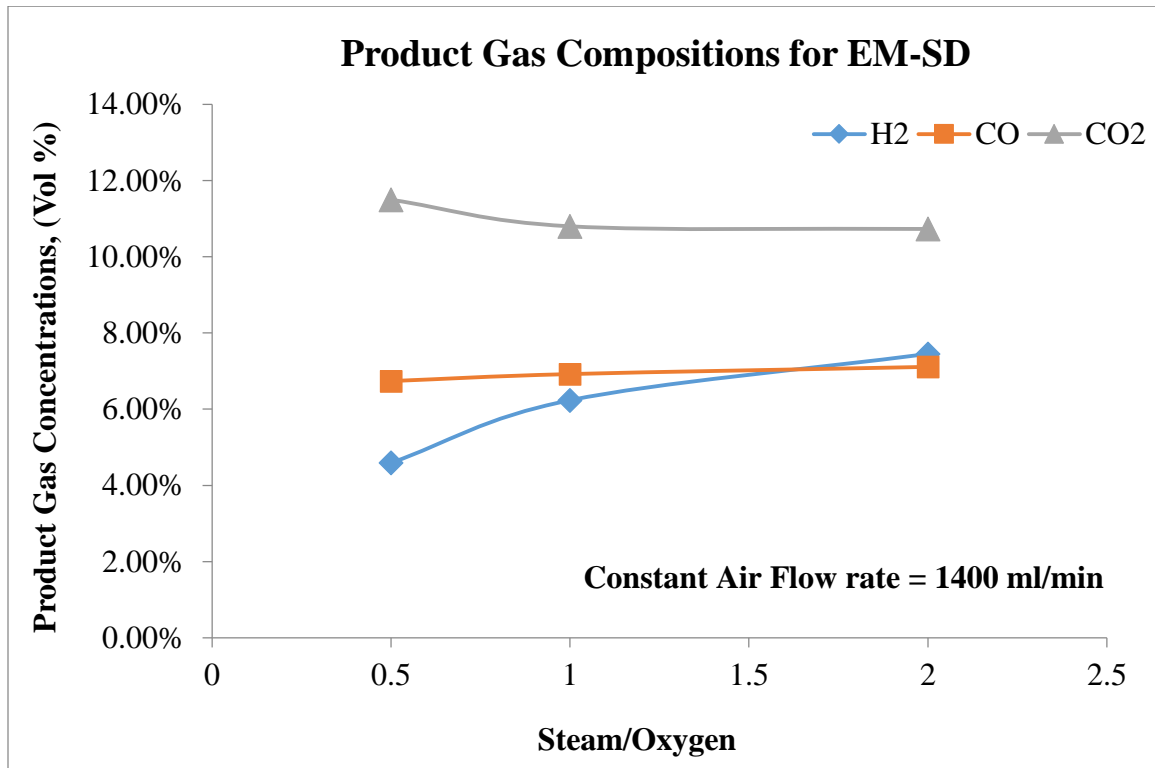


Figure 4.4.3: Average compositions of the product gases obtained during gasification of EM-SD briquettes with varying steam to oxygen ratios at a constant air flow rate of 1400 ml/min.

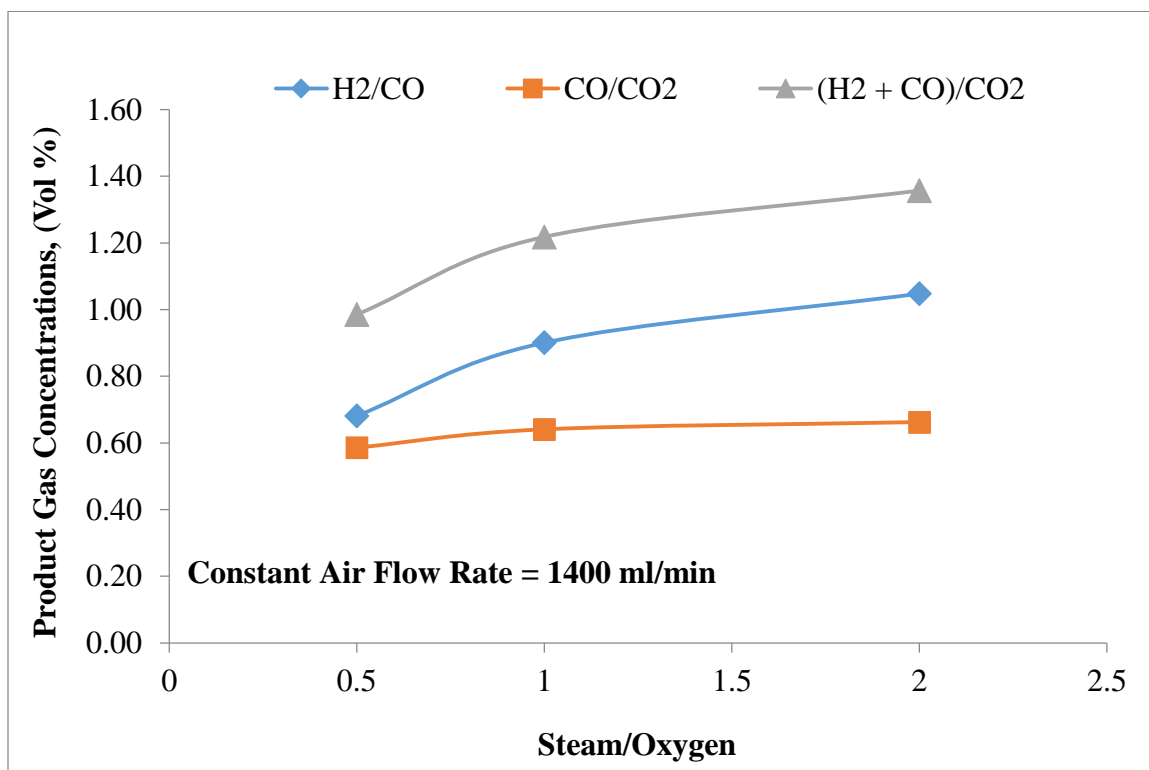


Figure 4.4.4: Average ratios of the product gases obtained during gasification of EM-SD briquettes with varying steam to oxygen ratios.

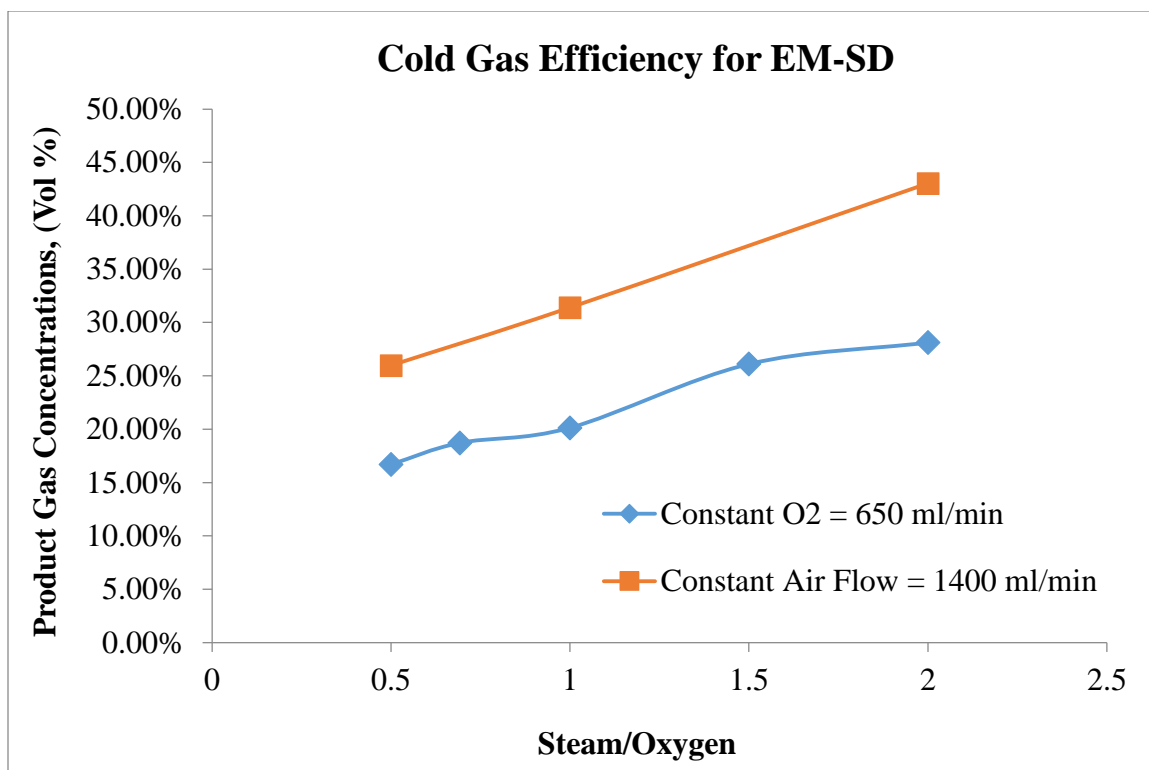


Figure 4.4.5: Comparison of cold gas efficiencies for gasification of EM-SD briquettes

From Figures 4.4.3 through 4.4.5, it can be clearly seen that the addition of air as the gasifying agent resulted in an increased H_2/CO , CO/CO_2 and syngas/ CO_2 ratio thereby improving the maximum cold gas efficiency from 28 % to 43 % as a consequence of lower CO_2 concentration in the product gas. It must be noted here that the product gas also contains unreacted nitrogen from air (~1100 ml/min) and the average product gas compositions are actual values and not normalized. On the addition of resin G-97 to the briquettes of EM-SD, it was observed that although slightly higher concentrations of hydrogen and carbon dioxide were obtained at any given steam/ O_2 ratio, the efficiencies were almost the same and the addition of the resin did not improve the product gas concentrations drastically.

Table 4.4.2: Average Composition of Product Gases Obtained During Gasification of EM-SD-G97 Briquettes with Varying Oxygen to Steam Ratios

Feed	Process Conditions				Average Ratio of Desired Gases			Average Product Gas Compositions				Efficiency %	
	Air ml/min	O ₂ ml/min	Steam ml/min	Steam:O ₂	H ₂ / CO	CO:CO ₂	(H ₂ +CO):CO ₂	H ₂ %	CO %	CH ₄ %	CO ₂ %		
EM-SD-G97		650	325		0.50	0.51	0.19	0.29	6.06%	11.77%	5.04%	61.29%	16.86%
		650	450	0.70	0.62	0.19	0.31	7.14%	11.52%	5.46%	60.04%	18.67%	
		650	650	1.00	0.69	0.25	0.42	10.13%	14.65%	6.15%	58.38%	25.44%	
		650	975	1.50	0.71	0.27	0.47	11.18%	15.64%	6.32%	57.14%	26.91%	
		650	1300	2.00	0.72	0.33	0.58	13.32%	18.44%	7.40%	55.09%	27.91%	
		1400	300	150	0.50	0.68	0.46	0.77	4.01%	5.91%	0.00%	12.83%	20.50%
		1400	300	300	1.00	1.10	0.57	1.19	6.98%	6.34%	0.00%	11.21%	32.38%
		1400	300	600	2.00	1.26	0.70	1.59	8.95%	7.11%	0.00%	10.13%	47.65%

Table 4.4.3: Average Composition of Product Gases Obtained During Gasification of EB-CS Briquettes with Varying Oxygen to Steam Ratios.

Feed	Process Conditions				Average Ratio of Desired Gases			Average Product Gas Compositions				Efficiency %	
	Air ml/min	O ₂ ml/min	Steam ml/min	Steam:O ₂	H ₂ / CO	CO:CO ₂	(H ₂ +CO):CO ₂	H ₂ %	CO %	CH ₄ %	CO ₂ %		
EB-CS		650	325	0.50	0.56	0.30	0.47	10.53%	18.67%	3.55%	61.80%	20.84%	
		650	450	0.70	0.58	0.33	0.52	11.45%	19.74%	3.53%	59.47%	24.94%	
		650	650	1.00	0.60	0.42	0.67	14.19%	23.68%	3.72%	56.52%	34.12%	
		650	975	1.50	0.73	0.45	0.78	17.45%	24.03%	3.72%	53.41%	39.27%	
		650	1300	2.00	0.79	0.50	0.90	19.47%	24.80%	3.81%	49.20%	45.48%	
		1400	300	150	0.50	0.79	0.66	1.18	6.64%	8.38%	0.00%	12.71%	36.78%
		1400	300	300	1.00	1.23	0.79	1.76	11.94%	9.73%	0.00%	12.33%	51.89%
		1400	300	600	2.00	1.38	0.97	2.30	13.98%	10.14%	0.00%	10.48%	63.50%

Table 4.4.4.: Average Composition of Product Gases Obtained During Gasification of EB-CS-G97 Briquettes with Varying Oxygen to Steam Ratios

Feed	Process Conditions				Average Ratio of Desired Gases			Average Product Gas Compositions				Efficiency %	
	Air ml/min	O ₂ ml/min	Steam ml/min	Steam:O ₂	H ₂ / CO	CO:CO ₂	(H ₂ +CO):CO ₂	H ₂ %	CO %	CH ₄ %	CO ₂ %		
EB-CS-G97		650	325		0.50	0.85	0.26	0.49	12.80%	14.99%	3.76%	57.07%	20.45%
		650	450	0.70	0.89	0.28	0.53	14.42%	16.15%	3.84%	57.41%	27.39%	
		650	650	1.00	0.98	0.30	0.59	16.74%	17.07%	4.83%	57.58%	35.28%	
		650	975	1.50	1.05	0.34	0.69	19.12%	18.27%	4.15%	54.26%	40.81%	
		650	1300	2.00	1.35	0.37	0.87	24.63%	18.30%	4.06%	49.55%	50.43%	
		1400	300	150	0.50	0.92	0.45	0.85	5.22%	5.69%	0.00%	12.76%	31.69%
		1400	300	300	1.00	1.10	0.94	1.97	12.03%	10.94%	0.00%	11.65%	55.32%
		1400	300	600	2.00	1.33	1.07	2.49	14.73%	11.05%	0.00%	10.34%	64.75%

The briquettes of EB-CS and EB-CS-G97 were also gasified under similar operating conditions. A comparison of EM-SD and EB-CS determines that the blends of EB-CS are much more reactive when compared to blends of EM-SD. This can be seen in the fact that the concentrations of syngas are much higher in blends with CS and therefore the cold gas efficiencies are also much higher at any given steam/O₂ ratio. Likewise, the addition of resin even in the case of EB-CS did not alter the product gas compositions and efficiencies to a great extent.

CHAPTER 5: SOURCE APPORTIONMENT OF CARBON USING STABLE CARBON ISOTOPE ANALYSIS

5.1 Introduction

Stable carbon isotope analysis, a unique analytical technique, has been utilized for distinguishing and quantifying the individual contributions of coal and biomass feedstock materials in the generation of carbon containing gases during the gasification of their blends. For this purpose, two different biomass samples, namely, corn stover (CS) and switchgrass (SG), were physically blended up to 30 % by weight with two coals, namely, DECS-38 sub-bituminous coal (SB) and DECS-25 lignite coal (LG). The blended samples were then gasified in a moving bed gasifier operating at atmospheric pressure and varying O₂/steam ratios. The ratio of CO/CO₂ in the product gas decreased with decreasing O₂/steam ratio and increasing amount of biomass in the blends. Gasifying at a constant O₂/steam ratio with increasing percentage of biomass in the feedstock, resulted in an increasing trend of $\delta^{13}\text{C}$ (‰) values for the carbon containing product gases. An increase in the concentration of oxygen in the feed stream at a constant biomass percentage leads to the depletion of ¹³CO and enrichment of ¹³CO₂ in the blends with corn stover while an enrichment of both ¹³CO and ¹³CO₂ was observed in blends with switchgrass. For blends with corn stover, there exists the possibility of a carbon isotope equilibrium between CO and CO₂ only at temperatures over 1000 °C at an O₂:steam ratio of 2:1 and corn stover percentage not exceeding 20 % while for blends with switchgrass, the gases are not in isotopic equilibrium. Based on isotope mass balance considerations, for the operating conditions utilized, the contribution of corn stover was in the range of 1 % - 40 % for CO generation and 6 % - 69 % for CO₂ generation. Switchgrass, on the other hand, contributed up to 53 % for CO generation and only 46 % for CO₂ generation [93].

As discussed earlier in Chapter 1, biomass feedstocks have the potential to neutralize the effect of atmospheric greenhouse gas emissions. Therefore, it is imperative to quantify the contribution of these biomass feedstocks in the generation of greenhouse gases. Stable carbon isotope analysis is one such technique that can be utilized to obtain the source from which these gases are generated during co-processing of different feedstocks [94-97].

5.2 Theory

Stable carbon isotope composition is determined as the ratio of $^{13}\text{C}/^{12}\text{C}$ in a substance relative to Pee Dee Belemnite (PDB), a cretaceous marine fossil having an anomalously high $^{13}\text{C}/^{12}\text{C}$ ratio, which is an internationally established reference standard for the stable isotope composition of carbon in natural materials. Carbon isotope ratios are commonly reported using delta notation (as $\delta^{13}\text{C}$ values) in parts per thousand (per mil, ‰) [94, 95, 98-104] as shown in Equation 5.2.1.

$$\delta^{13}\text{C} = \left(\frac{\left(\frac{^{13}\text{C}}{^{12}\text{C}} \right)_{\text{Sample}}}{\left(\frac{^{13}\text{C}}{^{12}\text{C}} \right)_{\text{Standard}}} - 1 \right) \times 1000 \text{ ‰} \quad \text{Eq. 5.2.1}$$

Most plants can be divided into three groups based on the photosynthetic pathway by which they fix carbon [105-107]:

1. C_3 : Almost 95 % of the plants on earth fall under this category. They fix carbon dioxide by the Calvin cycle and have $\delta^{13}\text{C}$ values that generally range between -23 and -34 ‰. Examples of these plants include temperate shrubs and trees, and grasses.

2. C₄: These plants fix carbon dioxide by the Hatch-Slack cycle. Their $\delta^{13}\text{C}$ values are less negative and range between -8 and -16 ‰. Plants like corn, switchgrass and warm weather grasses, predominantly, belong to this category.
3. CAM: The third group of plants fix carbon dioxide by the Crassulacean Acid Metabolism pathway, and have $\delta^{13}\text{C}$ values that are intermediary compared with C₃ and C₄ plants.

Fossil fuels such as coal and oil are made primarily of C₃ plant material and are depleted in ¹³C relative to the atmosphere, because they were originally formed from living organisms [108, 109]. Therefore, the carbon from fossil fuels that is returned to the atmosphere through combustion is depleted in ¹³C when compared to atmospheric carbon dioxide. The values of $\delta^{13}\text{C}$ vary by measurable amounts for different carbonaceous materials depending on their carbon source, fixation pathway, environment of formation and post depositional history. These values differ by about 10-15 ‰ for coal and biomass materials with the $\delta^{13}\text{C}$ for coal being more negative than that of biomass. This means that the carbon contained in coal is richer in ¹²C, as is the case with all fossil fuels. Surprisingly, the carbon isotope composition of coal typically does not vary much with increasing coal rank which implies that significant fractionation does not occur during its decomposition [110].

Most of the previous works involving coal co-processing that utilizes isotope mass spectrometry are related to the sourcing of coal-bitumen or coal-oil co-processing or gasification of carbon composite materials [98-101, 110, 111]. Steer et al. studied the efficacy of Highvale coal and Suncor bitumen co-processing using this technique and

provided a valid isotope mass balance method to quantify the amount of coal incorporated in each distillate fraction of their liquefaction process [101]. The synthetic oil generated from their process had intermediate isotope ratios which were directly proportional to the amount of coal incorporated in the feedstock. Lancet et al. determined the individual contributions of various coal/petroleum feedstocks under varied conditions and demonstrated that stable carbon isotope analysis can be a quantitative tool to independently assess the relative reactions of carbonaceous feedstocks during co-processing [99, 100, 111]. In these studies, the isotope ratios of product gas samples were not obtained directly; instead, a forced carbon balance was utilized to obtain information on the gas products. These studies concluded that during actual co-processing, considerable bond breaking occurs. Because ^{13}C - ^{12}C bonds are slightly stronger than ^{12}C - ^{12}C , heavier organic residues like tar and vacuum bottoms were presumed to be enriched in ^{13}C while lighter hydrocarbon gas products were enriched in ^{12}C relative to the feed. Therefore, the isotope ratios in such cases would never be intermediate to the parent sources. Further complications may arise if isotope ratios in product materials change over time depending on the extent of the reactions. For cases in which the generation of light hydrocarbons such as methane is very low and when isotopic mass balances are not affected in a huge way, the isotope analysis would still be very useful for envisaging product trends that occur during co-processing. Thomas et al. performed isotope ratio mass spectrometry to study the gasification of carbon composites manufactured from the co-processing of coal tar pitch fibers and petroleum pitch matrix. They observed that heat treating the composite produced changes in the carbon isotope composition of the reactant which may be due to different $\delta^{13}\text{C}$ values for the product gas and solid phases. Partially gasifying the carbon composites

lowered their $\delta^{13}\text{C}$ values by about 4 ‰ due to the loss of ^{12}C enriched gases such as methane and that the $\delta^{13}\text{C}$ values for the composites change as function of gasification temperature. Also, the products had intermediate $\delta^{13}\text{C}$ values compared with the parent materials and hence, reactions occurring during co-processing were easily distinguishable [110].

This chapter describes the utilization of stable carbon isotope analysis for distinguishing and quantifying the individual contributions of coal and biomass feedstocks towards the generation of carbonaceous product gases, in particular, CO and CO₂. Although this application has been available for many years and used mostly in bio-geochemical studies, very limited information is available in literature with regards to this particular analysis for blends of coal and biomass. Experimental data obtained by this method can provide valuable information for analyzing the interactions and synergy between the feedstocks and also for process modeling and optimization of production methods.

5.3 Experimental

5.3.1 Materials

For the purpose of this work, two different biomass samples, namely, corn stover (CS) and switchgrass (SG) were blended individually up to 30 % by weight with two different ranks of coals, namely, sub-bituminous coal (SB) and lignite coal (LG). The proximate and elemental analysis of all the feedstock samples used in this study were listed earlier in Chapter 2. These feedstocks were then gasified in a moving bed gasifier operating at atmospheric pressure and varying O₂/steam ratios. Gasification of blends of higher percentages of biomass (in excess of 30 % by weight) was not possible for the conditions at which the gasifier was operated since biomass is a low density, low heating value fuel

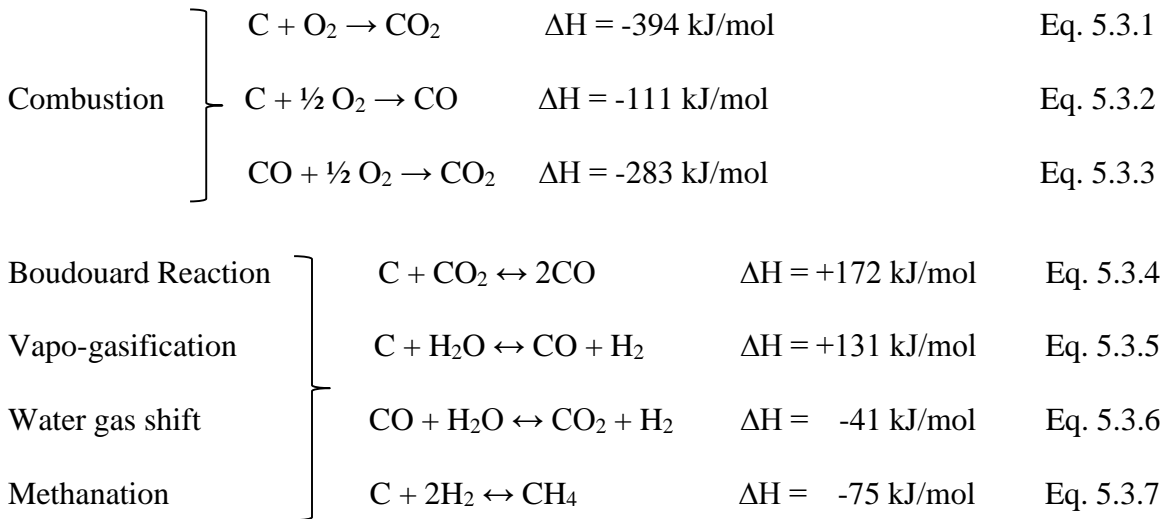
and addition of more biomass would make the gasification process less efficient. Hence, a maximum of 30 % by weight of biomass was chosen for this process.

5.3.2 Process Parameters and Reactions

The gasification of the feedstock materials was performed at atmospheric pressure using three different volumetric ratios of O₂:steam (0.5, 1.0 and 2.0) which correspond to an O₂:steam mass ratio of 1.0, 2.0 and 4.0, respectively. One hundred grams of solid feedstock was gasified during each experimental run. The oxygen flow rate was maintained constant at 650 ml/min while the flow rate of steam was maintained between 325 ml/min to 1300 ml/min and the corresponding product gas compositions obtained. The O₂/solid feedstock mass ratio was, therefore, constant at 0.625 while the corresponding steam/solid feedstock mass ratios were 0.624, 0.312 and 0.156, respectively. For the purpose of discussion, the O₂:steam ratios are further presented as volumetric ratios.

An increase in the O₂:steam ratio was seen to result in an increase in the gasification temperature. Since, the gasification was performed auto-thermally, it was necessary that the percentages of oxygen and steam were varied in such a way so as to not let the endothermic zone dominate. Therefore, a minimum O₂:steam ratio of 0.5:1 was utilized, below which endothermic zone would prevail and the gasification would not proceed further. The product gas compositions (response variables) were analyzed in two ways: (1) by varying the O₂:steam ratios at constant biomass wt% and, (2) by varying the biomass wt % at constant O₂:steam ratios (treatment factors). Each experimental run was replicated 5 times (n=5) and average product gas compositions were obtained within 95% confidence interval. A list of all the treatment factors and response variables along with values of standard deviations for product gas compositions is provided in Table 5.3.1.

In any gasifier, char gasification takes place following coal pyrolysis. The remaining carbonaceous solids from the pyrolysis reactions are further oxidized through heterogeneous reactions with carbon dioxide, carbon monoxide, steam, oxygen, and hydrogen. The major reactions that occur during the gasification process are described in Equations 5.3.1 through 5.3.7.



Sensible heating of the hot gas provides the heat required for the two endothermic gasification reactions given by Equations 5.3.4 and 5.3.5. These are responsible for most of the gasification products like hydrogen and carbon monoxide. Equation 5.3.6, known as the water gas shift reaction, is an exothermic reaction and has an effect on the H₂/CO ratio of the gasification product which is very important when the gas is used for synthesis in downstream processes such as Fischer-Tropsch synthesis. High conversion of CO and steam to CO₂ and H₂ is favored at low temperatures. The reaction of char with hydrogen to produce methane proceeds at a very slow rate except at very high pressures which is not the case in this study and hence very low concentrations of methane are observed in all the experiments that were performed.

5.3.3 Apparatus

The laboratory-scale updraft gasification system, described in Chapter 4, was designed and constructed for this study. The gasifier is a 3 feet long cylindrical stainless steel modular flange assembly having an internal diameter of 1.37 inches fitted with another stainless steel tube of 0.075 inches thick on the inside to promote better heat transfer in the axial direction. Temperature profiles along the gasifier axis are measured by a set of K-type thermocouples placed within a steel protective tube.

Coal/biomass is fed at the top of the gasifier by means of a quick-open flange while oxygen and steam are fed from the bottom of the gasifier at atmospheric pressure. The design utilizes a single condenser wherein the hot outlet gas at a temperature of approximately 120 °C enters a cold zone maintained at a temperature of about 10 °C so that unreacted water and other solids can be removed efficiently ensuring that clean product gas which is a mixture of hydrogen, carbon monoxide, carbon dioxide and small amounts of methane, is analyzed using a GOW-MAC Series 600 Auto System GC equipped with a dual thermal conductivity detector (TCD). Nitrogen was used as the carrier gas for the isothermal separation of diatomic hydrogen using a packed HAYESEP Q 60/80 column (4 feet), while helium was used for the isothermal separation of all other carbonaceous gases using a packed HAYESEP N 60/80 column (9 feet). Both carrier gases were regulated at 30 ml/min and analytes were detected every 6 minutes. The temperature of the thermal conductivity detector was maintained constant at 150 °C while the columns were constant at 140 °C.

The first step in the gasification process is the ignition of the bed by adding small amounts of externally heated charcoal particles onto the gasifier bed while supplying the

oxidant at a low flow rate of approximately 100 ml/min to 150 ml/min. The feed material is then added onto the charcoal particles and the oxidant flow rate is increased, causing ignition of the bed. Once the bed is ignited, pre-heated steam enters the bed from the bottom of the gasifier. The outlet of the GC is connected to a 500 cc TEDLAR gas sampling bag using a two-way valve. Once the oxygen in the product gas stream is depleted, the valve is opened so that the product gases are collected in the sampling bag. The collected gases are then analyzed for their isotopic composition using GC-C-IRMS.

The GC-C-IRMS analyses were performed using a modified Thermo Fisher Trace GC Ultra connected to a Delta^{PLUS}XP isotope ratio mass spectrometer by GC Isolink interface. All carbonaceous compounds eluting from the GC column (30 m Carboxen 1010 PLOT column) were oxidized to CO₂ in a capillary combustion reactor maintained at 1030 °C. Helium, flowing at 0.5 ml/min, was used as the carrier gas while the temperature of the GC was ramped at a rate of 10 °C/min from 50 °C to 150 °C and held at that temperature for 30 minutes. The product gas samples from the gasifier were loaded onto the GC using 50 µL gas tight syringes through a PVT injector held at 200 °C in split/splitless mode at a split ratio of 30:1. All isotope analyses were performed in duplicate to provide an estimate for precision and the standard deviation obtained for all δ¹³C values was less than ± 0.2 ‰ (n = 5).

Table 5.3.1: Product Gas Compositions for CO and CO₂ Produced During the Gasification of Various Coal/Biomass Blends at Different O₂/Steam Ratios

Operating Conditions		Average Gasifier Product Gas Composition, % (σ values calculated for n = 5)												
O ₂ :Steam		Pure Sub-Bituminous Coal						Pure Lignite Coal						
		CO (σ)		CO ₂ (σ)		CO/CO ₂		CO (σ)		CO ₂ (σ)		CO/CO ₂		
2.0		31.27% (1.51)		41.69% (1.24)		0.75		34.43% (2.02)		46.37% (1.15)		0.74		
1.0		26.13% (1.13)		41.68% (1.33)		0.63		27.58% (1.93)		45.47% (1.29)		0.61		
0.5		21.63% (1.28)		42.66% (1.41)		0.51		22.03% (1.58)		45.90% (1.17)		0.48		
O ₂ :Steam	Biomass Wt %	SB + CS			SB + SG			LG + CS			LG + SG			
		CO	CO ₂	CO/CO ₂	CO	CO ₂	CO/CO ₂	CO	CO ₂	CO/CO ₂	CO	CO ₂	CO/CO ₂	
2.0	10%	31.94%	43.29%	0.74	28.91%	45.86%	0.63	32.18%	46.45%	0.69	30.05%	53.65%	0.56	
1.0		26.58%	43.69%	0.61	24.35%	46.02%	0.53	27.20%	46.20%	0.59	24.41%	52.58%	0.46	
0.5		22.17%	43.13%	0.51	22.83%	46.62%	0.49	21.64%	46.05%	0.49	22.38%	52.07%	0.43	
		σ (CO)	σ (CO ₂)		σ (CO)		σ (CO ₂)		σ (CO)		σ (CO ₂)		σ (CO)	
2.0		1.09	2.15		1.38		2.18		1.65		1.98		1.61	
1.0		1.71	1.24		2.11		2.27		2.01		1.43		1.88	
0.5		1.13	1.78		1.93		2.82		2.23		2.07		1.72	
2.0	20%	25.34%	48.17%	0.53	19.72%	53.68%	0.37	23.93%	51.12%	0.47	19.05%	63.23%	0.30	
1.0		22.56%	47.43%	0.48	16.45%	53.11%	0.32	20.68%	50.94%	0.40	15.34%	64.18%	0.24	
0.5		20.11%	47.11%	0.43	14.88%	53.57%	0.28	18.14%	51.74%	0.35	12.74%	64.06%	0.20	
		σ (CO)	σ (CO ₂)		σ (CO)		σ (CO ₂)		σ (CO)		σ (CO ₂)		σ (CO)	
2.0		2.02	1.26		1.99		2.29		2.10		1.23		2.63	
1.0		1.78	1.69		2.52		1.98		2.79		1.95		2.42	
0.5		1.91	1.17		1.44		1.26		2.59		1.47		2.59	

Table 5.3.1 (contd.): Product Gas Compositions for CO and CO₂ Produced During the Gasification of Various Coal/Biomass Blends at Different O₂/Steam Ratios

O ₂ :Steam	Biomass Wt %	SB + CS			SB + SG			LG + CS			LG + SG		
		CO	CO ₂	CO/CO ₂	CO	CO ₂	CO/CO ₂	CO	CO ₂	CO/CO ₂	CO	CO ₂	CO/CO ₂
2.0	30%	18.13%	56.67%	0.32	16.00%	62.52%	0.26	17.14%	60.93%	0.28	14.34%	69.80%	0.21
1.0		15.73%	56.79%	0.28	14.50%	62.03%	0.23	15.14%	61.17%	0.25	12.81%	70.94%	0.18
0.5		13.09%	56.17%	0.23	10.02%	63.43%	0.16	12.39%	61.11%	0.20	11.69%	70.14%	0.16
		σ (CO)	σ (CO ₂)		σ (CO)	σ (CO ₂)	σ (CO)	σ (CO ₂)	σ (CO)	σ (CO ₂)	σ (CO)	σ (CO ₂)	
2.0		2.14	2.29		2.87	1.93	1.29	1.97	2.10	1.93			
1.0		2.08	1.98		2.61	2.18	1.85	1.38	1.72	1.77			
0.5		1.92	1.26		2.06	2.22	2.27	2.11	1.66	2.03			

176

Table 5.3.2: $\delta^{13}\text{C}$ values of various feedstock materials

Feedstock	$\delta^{13}\text{C}$, ‰
DECS-38 Sub-Bituminous Coal	-25.31
DECS-25 Lignite Coal	-24.71
Corn Stover	-11.05
Switchgrass	-11.13
Pine	-24.62
Poplar	-23.93

Table 5.3.3: Carbon Isotope Ratios for CO and CO₂ Produced During the Gasification of Various Coal/Biomass Blends at Different O₂/Steam Ratios

O ₂ /St	Biomass Wt %	$\delta^{13}\text{C}$, ‰ (σ values calculated for n = 5)															
		Pure Sub-Bituminous Coal								Pure Lignite Coal							
-	0%	CO		St. Dev (σ)		CO ₂		St. Dev (σ)		CO		St. Dev (σ)		CO ₂		St. Dev (σ)	
		-25.36		0.11		-23.46		0.21		-24.75		0.17		-23.26		0.19	
		SB + CS				SB + SG				LG + CS				LG + SG			
		CO	(σ)	CO ₂	(σ)	CO	(σ)	CO ₂	(σ)	CO	(σ)	CO ₂	(σ)	CO	(σ)	CO ₂	(σ)
2.0	10%	-24.47	0.15	-17.90	0.14	-22.59	0.09	-20.91	0.08	-24.61	0.07	-17.37	0.07	-23.58	0.13	-20.85	0.05
1.0		-24.04	0.11	-20.51	0.07	-23.02	0.13	-21.11	0.17	-24.38	0.04	-22.23	0.14	-24.21	0.09	-21.13	0.06
0.5		-23.91	0.18	-21.04	0.20	-23.38	0.12	-21.35	0.05	-24.06	0.06	-23.96	0.04	-24.52	0.11	-21.28	0.12
2.0	20%	-23.47	0.16	-16.92	0.18	-20.35	0.09	-20.19	0.05	-23.72	0.10	-16.19	0.09	-22.49	0.07	-19.74	0.08
1.0		-22.34	0.08	-19.51	0.09	-21.78	0.06	-20.49	0.04	-23.42	0.19	-20.81	0.20	-24.00	0.10	-20.13	0.09
0.5		-21.26	0.16	-20.38	0.09	-22.81	0.13	-20.65	0.13	-23.23	0.15	-22.74	0.06	-24.40	0.04	-20.34	0.07
2.0	30%	-21.56	0.22	-16.73	0.13	-17.84	0.14	-18.90	0.04	-22.43	0.14	-15.24	0.02	-19.16	0.12	-18.44	0.05
1.0		-20.72	0.12	-18.97	0.06	-20.43	0.09	-19.15	0.08	-21.88	0.09	-17.96	0.09	-22.89	0.06	-19.07	0.11
0.5		-19.54	0.17	-20.17	0.06	-22.10	17	-19.26	0.05	-20.99	0.05	-22.28	0.02	-23.88	0.08	-19.54	0.07

5.4 Results and Discussion

The product gas compositions of CO and CO₂ for all experimental runs are shown in Table 5.3.1. A major fraction of the product gas contains hydrogen, and methane is also formed in small quantities (CH₄ < 5 % of total product gas for all experiments). Since hydrogen and methane are not analyzed using stable isotope analysis, their compositions are not listed in Table 5.3.1.

The $\delta^{13}\text{C}$ values for all the feedstock samples used in this analysis are listed in Table 5.3.2. For sourcing applications in co-processing, it is necessary that the co-processing feedstocks, which in this case are coal and biomass, have sufficiently different carbon isotope ratios. The idea is that, two isotopically different materials undergoing thermal degradation in a closed system would generate products that would have an isotopic signature intermediary to the parent materials, thus, reflecting the relative amounts of each material utilized. As it can be seen from Table 5.3.2, sub-bituminous coal and lignite coal are similar in isotope composition (-25.31 and -24.71 ‰) as are corn stover and switchgrass (-11.05 and -11.13 ‰). The difference in the carbon isotope ratios is relatively large between the coals and corn stover/switchgrass when compared to that of softwoods like pine and poplar which have isotopic compositions of -24.62 and -23.93 ‰ respectively, similar to that of the coals. This is due to the fact that fossil fuels and most woody biomass materials belong to a similar class of biological material (i.e., C₃ plants) as discussed earlier. Therefore, corn stover and switchgrass were chosen to be mixed with the coals in different proportions in this study. Under the GC experimental method used, carbon monoxide elutes around 318 seconds after injection followed by methane and carbon dioxide at 606 seconds and 1350 seconds respectively as shown in Figure 5.4.1. The

amount of methane generated is relatively low, in the range of approximately 2-4 % of the total product gas, and hence it is difficult to quantify its isotopic signature without the injection volume being too large. This would require pre-concentration of methane from the sample gas and heavy water tracer tests may be used in such cases to determine the origin of methane [112] which is out of the scope of this work. Therefore, the IRMS analysis is limited to CO and CO₂ which are the major carbon containing gases produced.

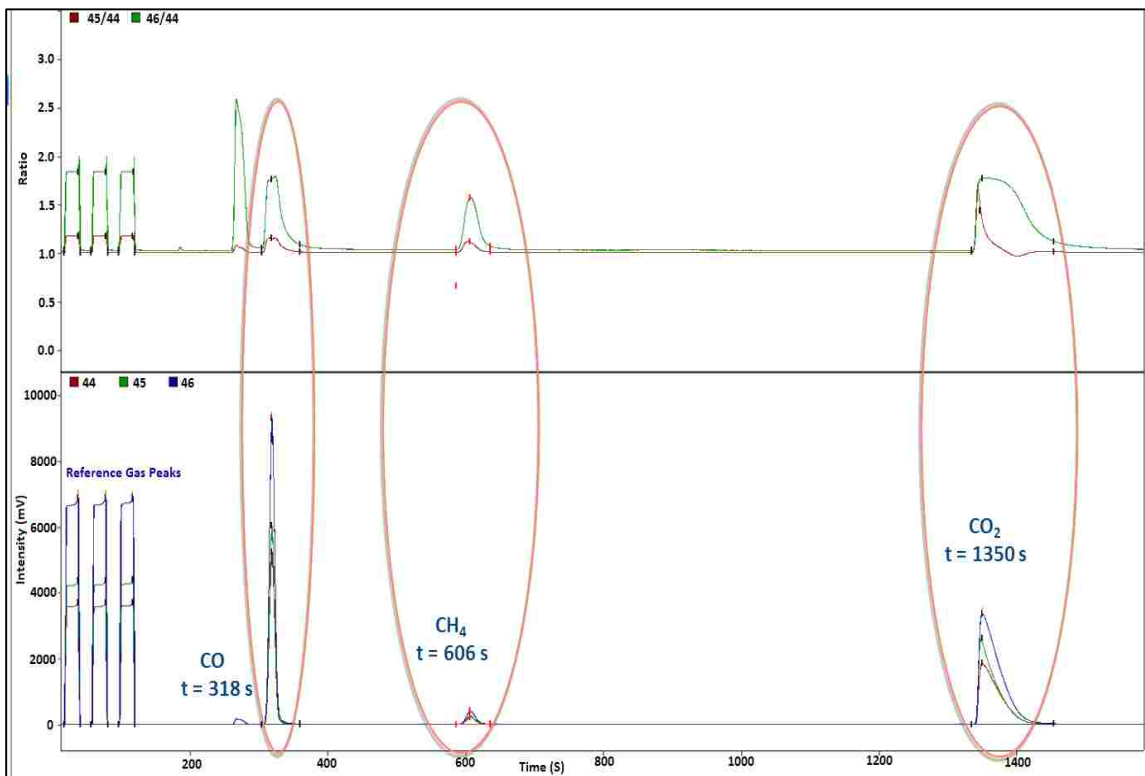


Figure 5.4.1: Typical GC-C-IRMS Chromatogram of the Gasification Products. CO elutes at t = 318 s followed by CH₄ at 606 s and CO₂ at 1350 s

The $\delta^{13}\text{C}$ values of the gaseous products (i.e., CO and CO₂) were analyzed as described in Section 5.3.3 and they are listed in Table 5.3.3. The isotope values of CO from the gasification of each pure source coal are extremely close to the isotope values of the

parent materials and are only slightly more negative by about 0.3 ‰. On the contrary, CO₂ under same gasification conditions is enriched in ¹³C by about 2 ‰ when compared with the source coals. This can be caused due to the effect of isotopic fractionation occurring during gasification. These shifts in isotopic values can be used in the estimation of isotopic equilibrium temperatures and compare them to the actual temperatures attained in the gasifier so as to verify the presence of an isotopic equilibrium between the gaseous compounds.

5.4.1 Blends with Corn Stover

For blends of both coals with corn stover, from Table 5.3.1, it may be observed that with a decrease in O₂:steam ratio, the composition of CO decreases while CO₂ remains constant in all experiments indicating that Boudouard reaction (Equation 5.3.4), water gas reaction (Equation 5.3.5) and water gas shift reaction (Equation 5.3.6) may be taking precedence. For instance, in blends of sub-bituminous coal and corn stover, holding the percentage of corn stover constant at 30 % and varying the O₂:steam ratios from 2:1 to 0.5:1 results in a significant drop in the fraction of carbon monoxide in the dry product gas from approximately 18 % to 13 % whereas the fraction of carbon dioxide remains fairly constant at approximately 56 %. In other words, the ratio of CO/CO₂ decreases with the addition of steam to the gasifier. This can be attributed to the fact that addition of excess steam to the gasifier lowers the temperatures which favors the conversion of CO to CO₂ through water gas shift reaction. The gas compositions can also be compared by increasing the corn stover percentage in the blend, and holding the O₂:steam ratio constant. An increase in corn stover percentage yields lower carbon monoxide while increasing the carbon dioxide yield in the product gas. Considering an O₂:steam ratio of 2:1, the fraction

of carbon monoxide decreases from 32 % to 18 % while carbon dioxide increases from 42 % to 56 % when corn stover is increased from 0 % to 30 % in blends with sub-bituminous coal. This observed effect is significant with confidence intervals greater than 95%. The P-values were calculated by performing an analysis of variance (ANOVA) of the obtained product gas compositions with respect to varying O₂:steam ratios and varying corn stover percentages in the blended feedstock (Section 5.5).

Similar trends are observed in blends of corn stover with lignite coal. A comparison of corn stover blends with sub-bituminous and lignite coal suggests that the ratio of CO/CO₂ is slightly lower in lignite blends. This is because, addition of corn stover to both coals reduces the amount of char reacting in the gasifier and in the presence of excess oxygen, the generation of CO₂ is favored. Also, a possible reason for this effect could be the fact that blends of lignite coal with corn stover have a lower hydrogen content. This results in lower energy content material which burns or combusts readily in the presence of oxygen to emit more CO₂ as compared to blends of sub-bituminous coal and corn stover. This result is also in accordance with the average CO₂ emission factors supplied by U.S Energy Information Administration which states that anthracite emits the largest amount of CO₂ followed by Lignite, Sub-Bituminous and Bituminous [[113](#), [114](#)].

To support the fact that addition of corn stover to the coals affects the product gas compositions, the carbon isotope composition of the gaseous products CO and CO₂ are plotted with respect to the amount of corn stover in the two feedstocks (Figures 5.4.2 and 5.4.3). With an increase in the amount of corn stover in the feed, gasification at a constant O₂:steam ratio results in a steady increase in the carbon isotope composition of the carbon containing gases, or the product gas becomes isotopically heavier during gasification. On

the contrary, the isotope values for decreasing O₂:steam ratios at any constant corn stover percentage results in CO being enriched and CO₂ being depleted in ¹³C. The implication is that carbon from both sources (coals and corn stover) is contributing in the generation of CO and CO₂. Although all blends follow a similar trend, distinctions are observed in the isotopic signatures. For example, in blends of corn stover with sub-bituminous coal, the CO in the product gas is enriched in ¹³C compared to pure coal by a maximum of about 6 ‰ whereas CO₂ is only enriched by about 3 ‰ when 30 % corn stover is added and gasified at an O₂:steam ratio of 0.5:1 while there is only an increase of about 4 ‰ in CO and 1 ‰ in CO₂ when corn stover is blended with lignite coal and treated under similar conditions. This indicates that corn stover is more readily converted to CO in the presence of sub-bituminous coal than lignite coal at lower O₂:steam ratios. Although the gas composition data in Table 5.3.1 shows that the difference in the CO compositions are very little between the two coals, the isotope analysis provides better distinctions in comparing the interactions between corn stover and coals.

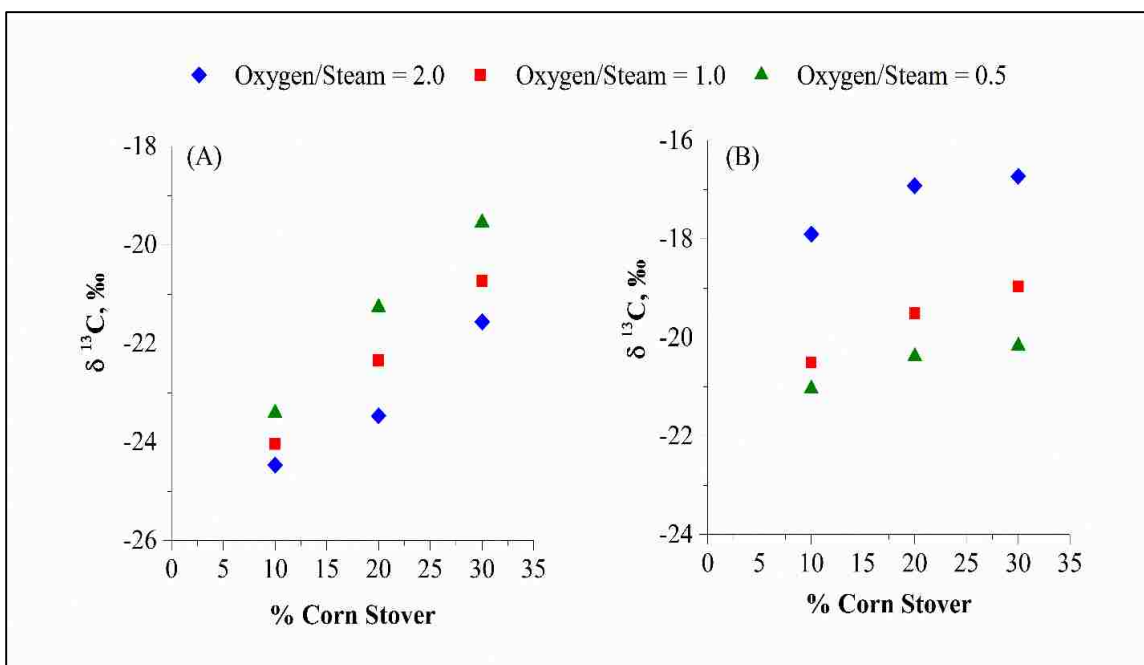


Figure 5.4.2: Effect of increasing percentage of corn stover and varying oxygen/steam ratios on the isotopic signatures of product gases in its blends with DECS-38 Sub-Bituminous coal. (A) Isotopic Signature of CO, (B) Isotopic Signature of CO₂.

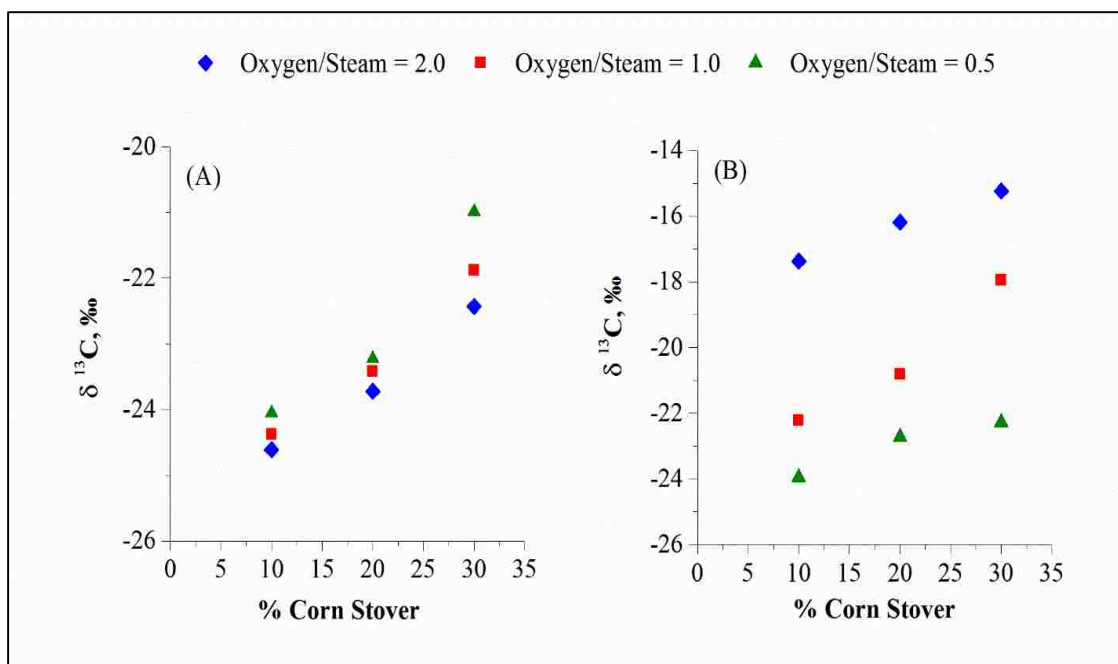


Figure 5.4.3: Effect of increasing percentage of corn stover and varying oxygen/steam ratios on the isotopic signatures of product gases in its blends with DECS-25 Lignite coal. (A) Isotopic Signature of CO, (B) Isotopic Signature of CO₂.

On the other hand, at higher O₂:steam ratio of 2:1, as an illustration, in blends of corn stover and sub-bituminous coal, CO₂ is enriched in ¹³C compared to pure coal by a maximum of 7 ‰ at an O₂:steam ratio of 2:1 (30 % corn stover blend) whereas CO is only enriched by 4 ‰, a decrease by about 2 ‰ when compared with lower O₂:steam ratio of 0.5:1. The isotope values of CO₂ in blends of corn stover with sub-bituminous coal are slightly lower in δ ¹³C value (17.90 ‰, -16.92 ‰, -16.73 ‰) than CO₂ generated from the blends with lignite coal (-17.37 ‰, -16.19 ‰, -15.24 ‰) at a 2:1 O₂:steam and corn stover percentages of 10, 20 and 30 % respectively. When compared, CS blends with each of the coals do not show much variation in δ ¹³C (CO) values even with change in O₂/steam ratio at lower percentages of corn stover, but the differences are clearly evident at higher loadings of corn stover. However, the same cannot be said for CO₂ whose isotope value is

enriched in ^{13}C with increasing O_2 :steam ratio at any blend percentage of corn stover. This indicates that at higher O_2 :steam ratios, corn stover is more readily converted to CO_2 while most of the CO is generated via coal. The results shown in Table 5.3.3, thus indicate that corn stover is definitely contributing towards the generation of these gases and a probable interactions may be existing between the blended feedstock materials.

5.4.2 Blends with Switchgrass

As in the case of corn stover, blends of both coals with switchgrass follow similar trends in the generation of the carbonaceous gases although the CO/CO_2 ratios are much lower in blends with switchgrass implying higher carbon dioxide generation when compared with corn stover at any constant O_2 :steam ratio or blend percentage (Table 5.3.1). The exact reason for this occurrence is speculative but the removal of higher percentage of volatile matter from switchgrass during pyrolysis may be resulting in char with higher void fraction due to which the interaction with incoming steam is reduced, thereby, generating more carbon dioxide through combustion in the bottom zone of the gasifier. The isotopic signature (Table 5.3.3) of the carbonaceous gases produced during the gasification of coal-switchgrass blends is shown in Figures 5.4.4 and 5.4.5. The results obtained show similar trends when compared with coal-corn stover blends (Figure 5.4.6), that is, the isotope values increase with increasing percentage of switchgrass in the feedstock at any constant O_2 /steam ratio. An interesting observation is that, based on the isotope results, the affinity of switchgrass towards the production of CO increases with increasing O_2 :steam ratio in the feed stream. The shift in isotope values is only about 1-1.5 ‰ at lower switchgrass percentages (10 % and 20 %), whereas, the difference increases to about 5 ‰ when the switchgrass percentage in the blends is 30 %. This is contrary to the results obtained for

corn stover where in the isotope values for CO increase at a constant rate with increasing steam concentration in the feed stream and the shift in isotope values is only about 1 ‰ even at higher percentages of corn stover. This may be due to the fact that switchgrass inherently has higher volatile content when compared to corn stover which evolves at higher temperatures causing a shift in the isotopic abundance of CO.

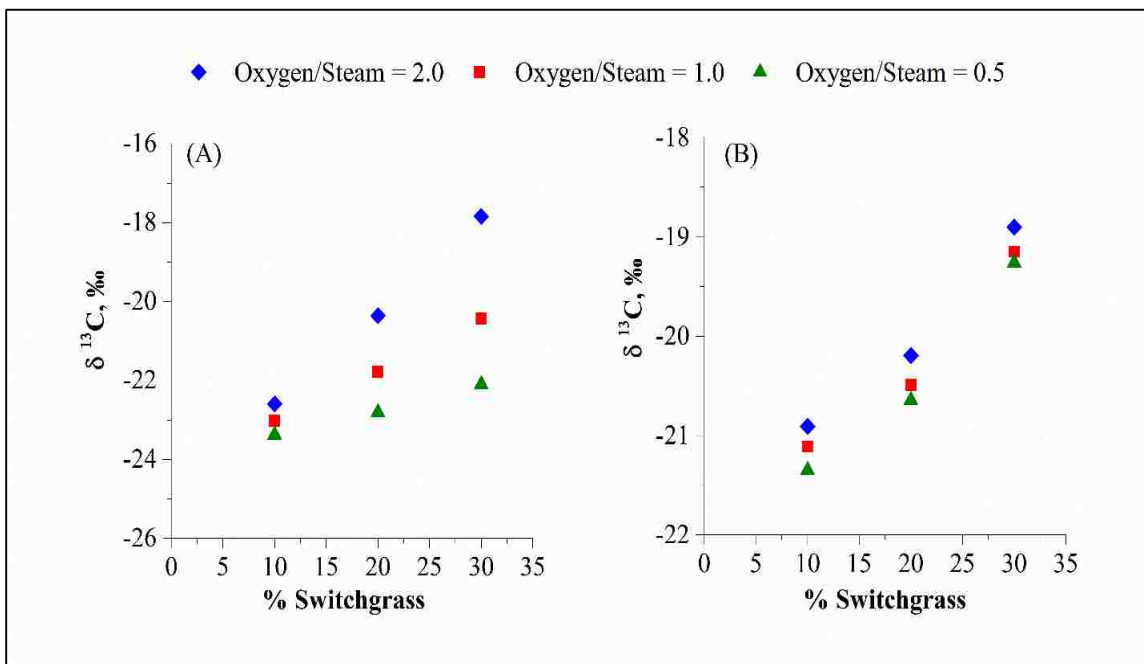


Figure 5.4.4: Effect of increasing percentage of switchgrass and varying oxygen/steam ratios on the isotopic signatures of product gases in its blends with DECS-38 sub-bituminous coal. (A) Isotopic Signature of CO, (B) Isotopic Signature of CO₂.

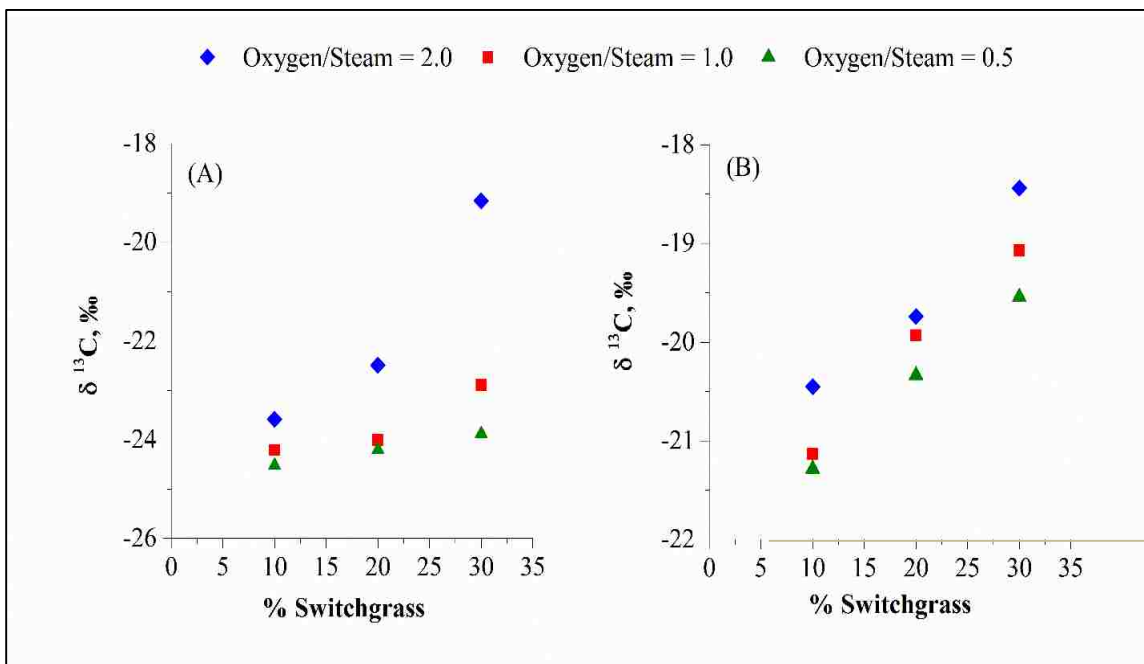


Figure 5.4.5: Effect of increasing percentage of switchgrass and varying oxygen/steam ratios on the isotopic signatures of product gases in its blends with DECS-25 lignite coal. (A) Isotopic Signature of CO, (B) Isotopic Signature of CO₂.

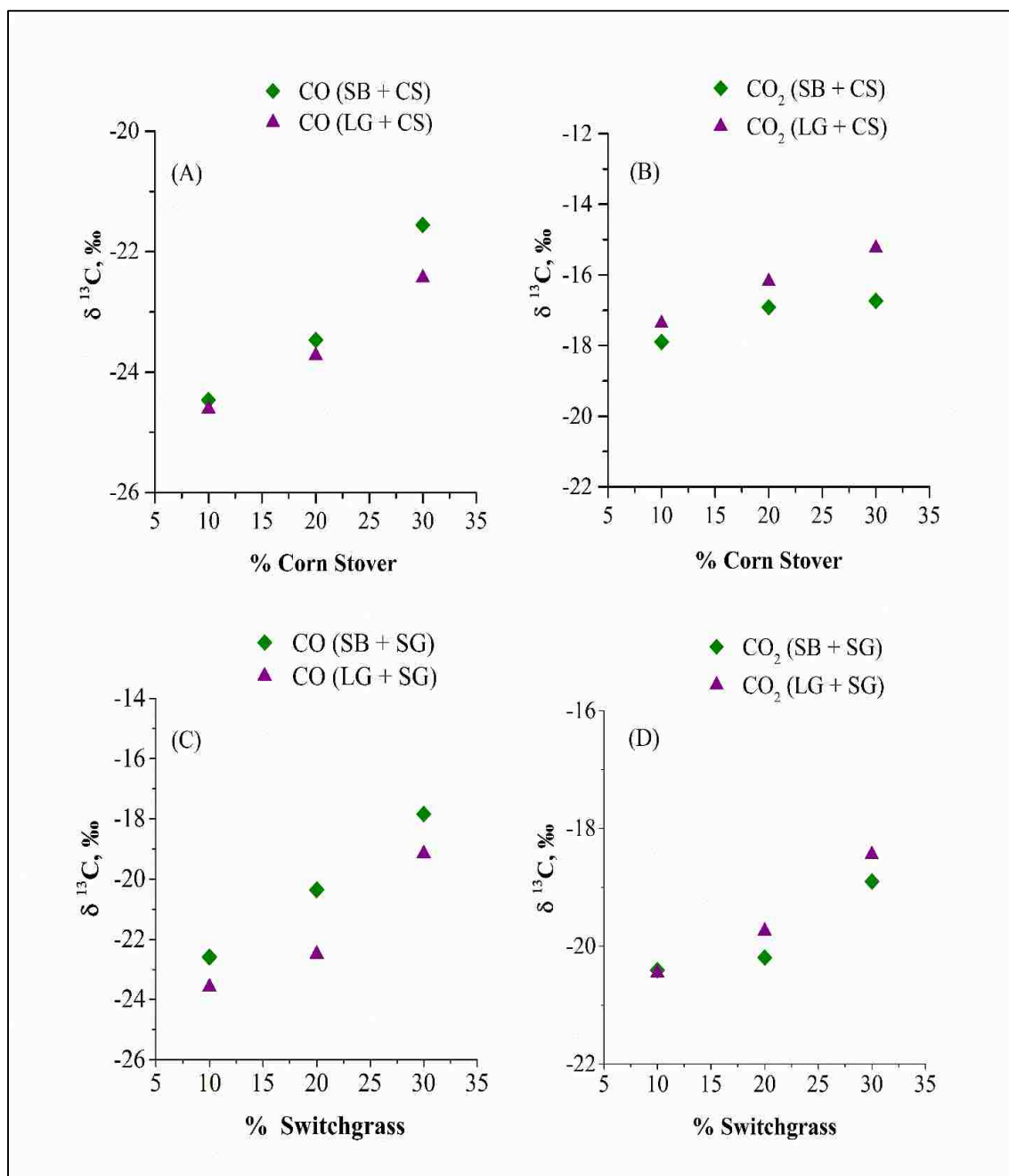


Figure 5.4.6: Comparison of isotopic signatures at an O₂:steam ratio of 2:1, (A) and (B): Blends with Corn Stover, (C) and (D): Blends with Switchgrass

5.5 Statistical Significance of Experimental Data

Analysis of variance (ANOVA) was performed on the experimental results using Design Expert[®] 9.0 software to analyze the statistical significance of the data and also verify the effect of the treatment factors (% Biomass and O₂/steam ratio) on the response variables (% CO, % CO₂, CO/CO₂ ratio, $\delta^{13}\text{C}$ (CO) and $\delta^{13}\text{C}$ (CO₂)). The advantage of using ANOVA lies in the fact that multiple factors affecting a system's performance can be analyzed simultaneously using all the experimental data, rather than analyzing one factor at a time [115]. Typically, linear or quadratic equations are used for estimating the relationship between treatment factors and response variables while the coefficients are estimated using a least-squares fit of the experimental data. The p-value determines the probability of a particular case that the coefficient for a specific term does not have a significant effect. In other words, a small p-value (generally less than 0.05) indicates that the individual terms in the model have a significant effect on the response and p-values larger than 0.1 indicate that the specific term is insignificant and does not have any effect on the response. In Table 5.5.1, p-values are provided for the whole model and also for each specific term of the model used. These p-values indicate that both the treatment factors have a significant effect on the percentage of CO generated during gasification of all the feedstocks (very low p-values \ll 0.05), but, the ratio of O₂/steam does not have a significant effect on the percentage of CO₂ that is generated (p-values \gg 0.05). Similarly, very low p-values (\ll 0.05) have been obtained for the other response variables (CO/CO₂, $\delta^{13}\text{C}$ (CO) and $\delta^{13}\text{C}$ (CO₂)) indicating that the desired output variables are significantly influenced by a change in the process variables. R-squared values obtained for different models have also been provided in Table 5.5.1. These values are close to 1 in most cases and thus, indicate a very good fit of the suggested models.

Table 5.5.1: Analysis of Variance (ANOVA) for Models Generated Based on Experimental Data and Estimating the Statistical Significance (P-Values) Between Treatment Factors and Response Variables.

Feedstock	Treatment Factors	Response Variables									
		% CO		% CO ₂		CO/CO ₂		δ ¹³ C (CO)		δ ¹³ C (CO ₂)	
		P-Value		P-Value		P-Value		P-Value		P-Value	
SB + CS	Suggested Model	Quadratic	< 0.0001	Quadratic	< 0.0001	Quadratic	< 0.0001	2FI	< 0.0001	Quadratic	< 0.0001
	A - % CS	< 0.0001		< 0.0001		< 0.0001		< 0.0001		< 0.0001	
	B – O₂/Steam	< 0.0001		0.7596		< 0.0001		0.0003		0.0008	
	AB	0.0014		0.0802		0.0009		0.0015		0.0132	
	A²	< 0.0001		< 0.0001		< 0.0001		-		0.0018	
	B²	0.0348		0.7675		0.0682		-		0.7042	
	R-Squared	0.9937		0.9960		0.9936		0.9831		0.9620	
LG + CS	Suggested Model	Quadratic	< 0.0001	Quadratic	< 0.0001	Quadratic	< 0.0001	Linear	0.0002	Linear	< 0.0001
	A - % CS	< 0.0001		< 0.0001		< 0.0001		< 0.0001		0.0027	
	B – O₂/Steam	< 0.0001		0.7253		< 0.0001		0.0275		< 0.0001	
	AB	0.0016		0.1244		0.0064		-		-	
	A²	0.0017		< 0.0001		0.0033		-		-	
	B²	0.0483		0.9149		0.1390		-		-	
	R-Squared	0.9887		0.9979		0.9843		0.9410		0.9671	

Table 5.5.1 (contd.): Analysis of Variance (ANOVA) for Models Generated Based on Experimental Data and Estimating the Statistical Significance (P-Values) Between Treatment Factors and Response Variables.

Feedstock	Treatment Factors	Response Variables									
		% CO		% CO ₂		CO/CO ₂		δ ¹³ C (CO)		δ ¹³ C (CO ₂)	
		P-Value		P-Value		P-Value		P-Value		P-Value	
SB + SG	Suggested Model	Linear	< 0.0001	Quadratic	< 0.0001	Linear	< 0.0451	Quadratic	< 0.0001	Quadratic	< 0.0001
	A - % SG	< 0.0001		< 0.0001		0.0229		< 0.0001		0.0003	
	B – O₂/Steam	0.0006		0.7388		0.0492		< 0.0001		0.0018	
	AB	-		0.8713		-		< 0.0001		0.5420	
	A²	-		< 0.0001		-		0.1234		0.0017	
	B²	-		0.0076		-		0.0209		0.4035	
	R-Squared	0.9601		0.9985		0.9523		0.9996		0.9992	
LG + SG	Suggested Model	2FI	< 0.0001	Linear	< 0.0001	2FI	< 0.0001	2FI	0.0015	2FI	< 0.0001
	A - % SG	< 0.0001		< 0.0001		< 0.0001		0.0023		< 0.0001	
	B – O₂/Steam	0.0005		0.9270		0.0014		0.0189		0.0002	
	AB	0.0391		-		0.0250		0.0106		0.0021	
	R-Squared	0.9544		0.9885		0.9671		0.9440		0.9978	

5.6 Isotope Equilibrium

The generation of CO and CO₂ during gasification can therefore be explained via two possible theories (Tables 5.3.1 and 5.3.3). One possibility is that there might be an existence of a partial isotopic equilibrium between CO₂ and CO according to the following isotope exchange reaction:



These two gases, CO and CO₂ could be produced in isotope equilibrium or they may form due to the gasification of solid carbon and re-equilibrate isotopically in the gasifier according to Equation 5.6.1. Using the observed $\delta^{13}\text{C}$ values for CO₂ and CO and the carbon isotope fractionation factor reported as a function of temperature by Richet et al [104, 116-118], apparent equilibrium temperatures (AET) for the isotope exchange reaction can be estimated. Based on the values of fractionation factor for CO-CO₂ isotope exchange provided by Richet et al.[116, 118], with an increase in temperature, the difference between the $\delta^{13}\text{C}$ values of CO₂ and CO decreases.

An increase in the O₂:steam ratio implies an increase in the gasification temperature. For blends of corn stover with both coals, only when the percentages of corn stover in the blend are lower (10 % and 20 %) and high temperatures in excess of 1000 °C at an O₂:steam ratio of 2:1 are attained in the gasifier, there exists the potential for an isotopic equilibrium between CO and CO₂ as the observed average gasifier temperatures are close to the calculated isotopic equilibrium temperatures (Table 5.6.1). For lower gasifier temperatures (i.e., lower O₂:steam ratios) and higher corn stover loadings (30 %), the calculated apparent equilibrium temperature deviates from the observed gasifier temperatures. Moreover, the difference in $\delta^{13}\text{C}$ values between CO₂ and CO increases with

increasing temperatures which is opposite in direction to the expected trend of convergence in carbon isotope composition as temperature increases. Thus, an isotope exchange equilibrium does not exist.

The carbon isotope results may be explained by two chemical reactions: 1) Boudouard reaction (Equation 5.3.4) and 2) Water Gas Shift reaction (Equation 5.3.6). Boudouard reaction is endothermic by nature, therefore from thermodynamics, the formation of CO would result in a decrease in temperature of the gasification zone. This reduction in temperature would, therefore, favor the water gas shift reaction which is exothermic by nature and high conversions of CO and steam to CO₂ and H₂ can be obtained. From the product gas compositions shown in Table 5.3.1 and maximum gasifier temperatures shown in Table 5.6.1, the ratio of CO/CO₂ decreases with decreasing temperature (decreasing O₂:steam ratios) for corn stover blends and therefore, the relationship between CO-CO₂ proceeds via the kinetic conversion of CO to CO₂ and no isotope exchange is occurring between CO and CO₂ in these chemical reactions.

A similar argument may be made for interpreting the carbon isotope composition of CO and CO₂ in blends with switchgrass. As shown in Table 5.3.3 and Figures 5.4.4 and 5.4.5, although CO is enriched in ¹³C with increasing temperature at a given percentage of switchgrass, and the variation in the δ¹³C values of CO₂ is minimal (i.e., the difference in δ ¹³C values of CO₂ and CO is decreasing with increasing temperatures), the calculated isotopic equilibrium temperatures from CO and CO₂ are unreasonably high (Table 5.6.1). Also, the data from the product gas composition (Table 5.3.1) of the gasifier shows that the ratio of CO/CO₂ decreases with decreasing temperature which is in conjunction with the results obtained for corn stover blends. The calculated AETs for all sample blends are much

higher than the actual gasifier temperatures and from Table 5.6.1, it is evident that the temperatures achieved in the gasifier are far from equilibrium and therefore, isotopic equilibrium is not achieved even with blends of switchgrass.

Table 5.6.1: Comparison of Isotopic Equilibrium Temperatures of CO₂-CO Product Gases and Experimental Gasifier Temperatures

O₂:Steam	% CS Added to SB	Temperature, °C		% CS Added to LG	Temperature, °C	
		Gasifier	Equilibrium		Gasifier	Equilibrium
2		1055.4	1089.8		1081.3	1029.5
1	10	900.8	> 1300	10	1010.9	> 1300
0.5		853.5	> 1300		912.9	> 1300
2		1029.3	1090.6		1041.5	1002.9
1	20	894.1	> 1300	20	890.9	> 1300
0.5		825.6	> 1300		852.1	> 1300
2		900.7	1143.1		883.2	1078.2
1	30	867.8	> 1300	30	826.2	> 1300
0.5		803.3	> 1300		739.7	> 1300
O₂:Steam	% SG Added to SB	Temperature, °C		% SG Added to LG	Temperature, °C	
		Gasifier	Equilibrium		Gasifier	Equilibrium
2		1010.6	> 1300		1037.3	> 1300
1	10	962.1	> 1300	10	995.2	> 1300
0.5		901.1	> 1300		908.1	> 1300
2		959	> 1300		927.7	> 1300
1	20	933	> 1300	20	847.3	> 1300
0.5		879.1	> 1300		811.3	> 1300
2		912.8	> 1300		882.1	> 1300
1	30	899.7	> 1300	30	733.4	> 1300
0.5		823.5	> 1300		680.9	> 1300

5.7 Carbon Sourcing

To interpret the amount of each parent source incorporated into the carbon containing gases, the following expression has been utilized:

$$(\delta^{13}\text{C } X)_{\text{Biomass}} + (\delta^{13}\text{C } X)_{\text{Coal}} = \delta^{13}\text{C}_{\text{Product}} \quad \text{Eq. 5.7.1}$$

And, $X_{\text{Biomass}} + X_{\text{Coal}} = 1$ Eq. 5.7.2

Where, X is the fraction of parent material incorporated into product gas.

Therefore,
$$\left(\% \text{ Biomass Carbon} = \frac{\delta^{13}\text{C}_{\text{Product}} - \delta^{13}\text{C}_{\text{Biomass}}}{\delta^{13}\text{C}_{\text{Biomass}} - \delta^{13}\text{C}_{\text{Coal}}} \right) \quad \text{Eq. 5.7.3}$$

For this analysis, it is assumed that the $\delta^{13}\text{C}$ values of the parental material and the gaseous products are equivalent over the course of the experiment, i.e., no isotope fractionation occurs during the reaction [101, 119]. The contribution of each parent material in the generation of CO and CO₂ is shown in Figure 5.7.1. The results of this analysis suggest that the contribution of biomass in the generation of both CO and CO₂ is greater in blends with sub-bituminous coal as compared with blends of lignite coal. Using Equation 5.7.3, it can be clearly seen, that the addition of biomass has had a definite impact in the generation of carbon containing gases. If no interactions are present between biomass and coals, then the resultant product gas mixture would have isotope values that are closer to the source coal and enriched in ¹²C. As this is not occurring, it may be suggested that the synergy between corn stover and coals is higher at higher O₂:steam ratios (2:1), with corn stover contributing almost up to 60 % and 70 % with respect to the generation of CO₂ in its blends with sub-bituminous coal and lignite coal respectively, while, the blends of switchgrass with coals contribute only about 45 % at the same O₂:steam ratio (2:1). At lower O₂:steam

ratios (0.5:1), however, the contribution of switchgrass (43 % in blends with SB and 38 % in blends with LG) is higher than corn stover (36 % in blends with SB and 18 % in blends with LG) with respect to the generation of CO_2 . Considering the generation of CO, the contribution of corn stover is maximum at an O_2 :steam ratio of 0.5:1 (40 % and 27 % in blends with SB and LG respectively) while the contribution from switchgrass is maximum at a 2:1 ratio of O_2 :steam (53 % and 41 % in blends with SB and LG respectively). These comparisons are being made at 30 % biomass blend ratios where the contribution of biomass towards the generation of CO and CO_2 is the highest. These results are particularly important to know during co-gasification of coal/biomass blends as one of the major reasons for blending biomass with coal is to mitigate the emission of greenhouse gases. Moreover, the interpretation of these data would only help in process modeling and optimization of co-gasification processes. Ultimately, the usage of the data from this analysis depends on the end product one would like to achieve by heat treating or chemical conversion of coal/biomass blends.

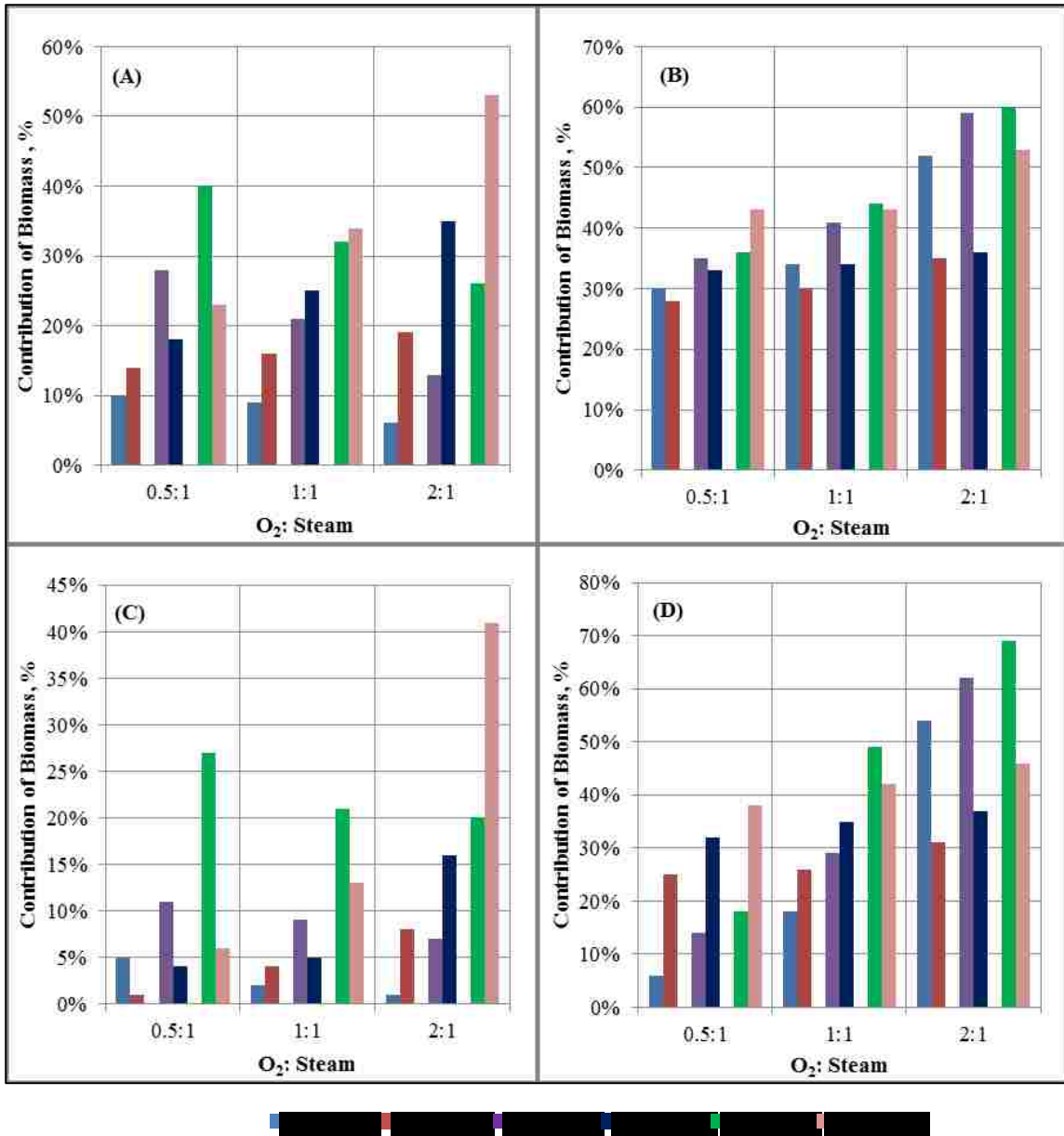


Figure 5.7.1: Individual contribution of each biomass source towards generation of product gases at different O₂/steam ratios. (A) Contribution in the generation of CO in blends with sub-bituminous coal, (B) Contribution in the generation of CO₂ in blends with sub-bituminous coal, (C) Contribution in the generation of CO in blends with lignite coal, and (D) Contribution in the generation of CO₂ in blends with lignite coal.

CHAPTER 6: CONCLUSIONS AND FUTURE WORK

The research objectives and tasks stated in Section 1.10 of Chapter 1 were successfully performed and some of the conclusions of this work along with recommendations for future research are described in this chapter.

6.1 Conclusions

The main objective of this work was to investigate the thermochemical conversion of blends of coal and biomass to create an alternative technology for offsetting the load on the usage of fossil fuels in producing energy. A comprehensive literature survey suggested a lot a knowledge gaps for co-gasification of coal-biomass blends in a moving bed gasifier and inconsistency in predicting kinetic parameters, synergistic interactions and weight loss characteristics for devolatilization of blended feedstocks. Therefore, a thorough investigation of pyrolysis kinetic models was conducted in this work. In addition, gasification characteristics of the single fuels as well as blended feedstocks were evaluated with an emphasis on improving the producer gas composition. Also, source apportionment of the blended feedstocks in generating carbonaceous gases was evaluated using a unique analytical technique which utilizes the difference in the carbon isotope compositions of coal and biomass. Based on the research work performed, some of the major conclusions and contributions are enlisted:

1. The thermal decomposition characteristics of pure coals (DECS-38 Sub-Bituminous Coal and DECS-25 Lignite Coal), pure biomass feedstocks (Corn Stover and Switchgrass) and coal-biomass blends (each biomass feedstock was blended with each coal feedstock in weight ratios of 10%, 20% and 30% respectively) were evaluated at various heating rates ranging between 5 °C/min and

40 °C/min using non-isothermal thermogravimetric analysis. These coals were chosen based on economic considerations, their low sulfur content, and high percentage of carbon present since the ultimate goal is to gasify these blends in a moving bed reactor for the production of syngas that can be used as feedstock for downstream processes such as Fischer-Tropsch Synthesis used for producing liquid fuels. Also, keeping in view of the overall gasification process, blends of higher percentages of biomass (in excess of 30 % by weight) was not possible for the conditions at which the gasifier was operated since biomass is a low density, low heating value fuel and addition of more biomass would make the gasification process less efficient. Hence, a maximum of 30 % by weight of biomass was chosen for this work. Two different environments comprising of an inert nitrogen atmosphere and a non-inert carbon dioxide atmosphere were utilized respectively and the weight loss profiles of each feedstock material were evaluated with respect to temperature.

2. The weight loss profiles in the N₂ atmosphere illustrate that the thermal evolution profiles of the single fuels are different from that of the blends. The thermal evolution profiles of sub-bituminous coal (SB) and lignite coal (LG) display only one major peak over a wide temperature distribution, ~ 152-814 °C for SB and ~ 175-818 °C for LG whereas the thermal decomposition profile for corn stover (CS) falls in a much narrower band than that of the coals, ~ 226-608 °C and the maximum weight loss rate of CS is almost an order of magnitude higher than both coals. Also, the maximum weight loss rate of LG is much lower than that of SB. This can be attributed to the fact that the volatile matter or the immobile phase present in LG

coal are bonded together with much higher molecular bond energy than that of SB coal and hence will be removed with a slower rate at similar temperatures.

3. For blends of CS and SB, the first peak occurs at a maximum peak temperature of approximately 326-330 °C representing the devolatilization of CS (evolution of hemicellulose and cellulose components) while the second peak occurs at a maximum peak temperature of 419-430 °C representing the devolatilization of SB. Similar trends are observed for blends of CS and LG with maximum peak temperatures ranging from 318-336 °C for the devolatilization of CS and 411-423 °C for the devolatilization of LG. Also, it can be observed that the maximum weight loss rate (%/min) for the CS devolatilization profile increased with increasing concentration of CS in the blends and vice versa for the coal devolatilization profile, without an apparent change in the shape and position of the peaks when compared to that of the single fuels. Also, the change in the maximum devolatilization rate is not linear with the increase in corn stover percentage indicating the possibility of interactions between the blended fuels.
4. The thermal evolution profiles of switchgrass and blends of both coals with switchgrass during devolatilization were also evaluated. The weight loss curves follow a similar pattern as that of blends with corn stover. The devolatilization interval for switchgrass starts around 175 °C with the decomposition of hemicellulose and ends around 650 °C with the slow decomposition of lignin. When compared with blends of corn stover, a clear distinction in the DTG profiles can be observed. For these blends of coals and switchgrass, three different peaks are clearly observed, where the low temperature peaks can be attributed to the

decomposition of switchgrass while the high temperature peak is for the decomposition of coals. This is different from those observed in blends with corn stover, where the two low temperature peaks merge which is an indication that some components in coal are interacting with corn stover in the low temperature range of around 220 °C-380 °C. A clear distinction in the hemicellulose and cellulose peaks is observed when switchgrass is blended with coal. This suggests that no significant interactions are occurring and that the two components are decomposing separately.

5. The non-linearity in the evolution of volatile matter with increasing percentage of corn stover in the blends verifies the possibility of synergistic behavior in the blends with sub-bituminous coal where deviations from the predicted yield ranging between 2% -7% were observed whereas very little deviations (1% - 3%) from predicted yield were observed in blend with lignite coal indicating no significant interactions with corn stover. Similar to corn stover blends, the blends containing switchgrass also show a clear increase in the amount of volatile matter with increasing percentage of switchgrass in the blend. However, clearly, the deviations from the predicted and experimental yield is minimal suggesting that no significant interactions are present during devolatilization of blends of coals and switchgrass.
6. When compared with devolatilization of the feedstock materials utilizing a N₂ atmosphere, the TGA curves with respect to temperature follow a similar pattern until approximately 500 °C even when pure CO₂ is utilized as the sweeping gas. Although the mass loss rates at low temperatures are higher in pure CO₂ atmosphere, the differences are only marginal. At higher temperatures, however, a

significant increase in mass loss rate is observed in pure CO₂ atmosphere. This may be understood by the stages of coal pyrolysis process. In case of 100% N₂ environment, the coal pyrolysis process has two stages: release of moisture content and devolatilization but the process of coal pyrolysis in pure CO₂ environment can be divided into three stages: moisture release, devolatilization and char gasification or Boudouard reaction with CO₂ to form CO in high temperature zone (> 500 °C) . Also, this difference may be explained due to the density difference and transport properties of these gases which are quite different (the mass of the CO₂ molecule is different from that of N₂). Moreover, the formation of char particles is larger and its surface area is also higher than that of the N₂ char particles. Hence, the weight loss observed in CO₂ environment is much higher.

7. Three different kinetic models for pyrolysis in N₂ atmosphere have been discussed and compared, of which, the matrix inversion algorithm predicts the kinetic parameters such that the weight loss characteristics can be best represented for both single fuels as well as blends of coals and biomass materials. Also, weight loss characteristics of unknown fuel blends at unknown heating rates can be effectively predicted within 1 % error through the use of this algorithm. The weight loss characteristics of coal-biomass blends in a CO₂ environment have been compared with those of N₂ atmosphere and the kinetic parameters for the Boudouard reaction have been predicted using a single first order reaction and maximum decomposition rate at temperatures greater than 500 °C. The distributed activation energy model has also been utilized to predict the weight loss of the feedstocks in a CO₂

atmosphere over the whole temperature range of the experimental procedure (~35 °C to 1000 °C).

8. A laboratory-scale moving gasification system has been designed and constructed for the purpose of gasifying the feedstock materials. The efficiency and product gas compositions obtained reveal that utilizing an inner stainless steel tubing better promotes heat transfer upwards in the axial direction when compared to utilizing a quartz insulation. The trends of the product gas compositions are similar to those obtained using an inner quartz lining. However, the percentage of hydrogen generated at same operating conditions is much higher due to the increase in bed temperature (complete consumption of oxygen which was not achieved when using a quartz insulation) and transfer of heat upwards in the axial direction and thus, better heat utilization which improved the overall efficiency by at least 20% when the steam concentration was at its maximum in the gasifier. Also, unlike the quartz insulation where the efficiency increased only until a certain point and the maximum steam/O₂ ratio that could be utilized was 1.5, in this experimental set-up, the efficiency increased steadily until a steam/O₂ ratio of 2:1. In addition, the ratios of H₂/CO, CO/CO₂ and syngas/CO₂, which dictate the quality of the product gas, are markedly higher as compared to the experimental design utilizing an inner quartz lining.
9. Using pure oxygen and steam in the inlet gas stream, energy conversion efficiencies greater than 50 % were obtained for blends of both coals with corn stover at a steam to oxygen ratio of 2:1. Also, replacing pure oxygen with air as the gasifying agent greatly improved the H₂:CO ratios (greater than 2:1 in some cases) and overall

efficiency in blends with corn stover. This is due to the fact that the addition of air at a much higher flow rate than oxygen promoted the heat transfer axially along the gasifier, resulting in better temperature distribution and hence, promoting the reaction char with steam. In contrast, blends with switchgrass are not very effective with respect to the overall gasification characteristics. This could be speculated to be because of the fact that no synergy and interactions exist in blends with switchgrass and addition of switchgrass to a coal source may not be very effective from the viewpoint of generating high quality producer gas for downstream operations (Fischer-Tropsch synthesis, etc.).

10. Using a mixture of nitrogen and oxygen in the feed gas stream, the inlet gas stream flow rate of 1625 ml/min and oxygen percentage of 40 % provides the highest energy conversion efficiency and a max CO: CO₂ ratio of approximately 3:1. The bed temperature range during the gasification of sub-bituminous coal was generally observed to be between 600 °C and 800 °C for the experiments with varying steam ratios and between 800 °C and 1000 °C for the experiments with varying oxygen partial pressures.
11. An effective method has been utilized for analyzing and distinguishing the individual contributions of coal and biomass towards the generation of carbonaceous gases using the differences in their carbon isotope ratios. The gasification of these blends was performed at varying O₂/steam ratios in a moving bed gasifier and the generated carbon gases were effectively analyzed using stable carbon isotope ratio mass spectrometry. It was observed that an increase in the amount of biomass in the feed led to a steady increase in the isotopic value of the

carbon containing gases, implying that the product gas becomes isotopically heavier during gasification. This is also an indication of probable synergistic effects between the blended materials.

12. Furthermore, the correlation between the $\delta^{13}\text{C}$ values and gasifier temperatures suggests that CO/CO₂ ratio proceeds via a kinetic mechanism rather than an isotopic exchange. The amount of each parent material utilized for the generation of the product gases was calculated using a simple mixing equation. The addition of biomass had a definite impact in the generation of carbon containing gases. For blends with corn stover, higher O₂:steam ratios result in the contribution of almost up to 70% of carbon from corn stover in the generation of CO₂, while, the blends of switchgrass with coals prove to be much effective at lower oxidant ratios with respect to the generation CO₂ and vice versa for the generation of CO. Finally, it can be stated that the data obtained utilizing this unique analytical technique would provide valuable insights not only pertaining to the synergy between the blended feedstock materials but also towards process modeling, optimization and reaction pathways in the field of co-gasification of coal and biomass.

6.2 Recommendations for Future Work

Based on the research work performed and current technology status of coal-biomass blends gasification, the following recommendations are suggested for future work with excellent avenues for research improvements in this field:

1. The work performed in this research involved the utilization of two coal ranks and two biomass sources. It is a known fact that each carbonaceous feedstock varies

greatly in its physical and chemical properties. Hence, a mechanistic model needs to be developed and evaluated to provide a database of the availability of various biomass feedstocks and segregate these based on their properties which may be useful during scaling up of the process.

2. For improving upon the devolatilization models suggested in this research, future work can involve utilization of thermogravimetric analysis coupled with other analytical techniques such as mass spectrometry or infra-red spectroscopy (TGA-MS or TGA-FTIR) so that specific models pertaining to each component evolving during the devolatilization stage can be evaluated. The kinetic models coupled with component-specific models would be extremely useful in moving this research to the next stage.
3. Also, evaluating the morphology, surface characteristics and microstructure of both coal chars as well as chars of coal-biomass blends is recommended due to the fact that difference in these properties of chars is believed to contribute towards better understanding the gasification characteristics of blended feedstocks. Coal char, generally, has a more packed cluster structure while biomass char is more amorphous. This is expected to result in distinct gasification characteristics due to differences in vapor diffusion rates within the char particles. Therefore, the reactivities differ significantly. Evaluation of these properties would be extremely useful for mathematically modeling the gasification process.
4. ASPEN process models and hydrodynamic models (1-D and 2-D) congregating all the processes during gasification need to be developed and evaluated. The stable

carbon isotope analysis utilized in this work, also, needs to be incorporated into process models to better understand reaction pathways. It is important to mathematically model the moving bed gasification results to establish the effects of mass, heat and momentum. In addition, a thorough investigation pertaining to energy balances around a gasification plant needs to be performed. The new data should account for different operating conditions and biomasses to have enough points to cover the whole range and variability that wants to be modelled.

5. In the research work undertaken, the main focus was on studying the kinetics of pyrolysis and evaluating the producer gas compositions in a moving bed gasifier. To further this research towards developing an alternative source for production of liquid fuel, downstream operations such as Fischer-Tropsch synthesis coupled with water gas shift reactors to adjust the concentration of hydrogen and carbon monoxide need to be studied. A process involving the combination of coal-biomass blends gasification and these downstream processes needs to be developed and evaluated for its viability.
6. Finally, a thorough investigation into the costs and economics involved in the process of gasifying coal-biomass blends as a source for next generation alternative energy technology needs to be evaluated if the process is to be commercially viable.

APPENDIX A: MATLAB CODES USED FOR ESTIMATING KINETIC PARAMETERS

In Appendix A, all the MATLAB codes used for estimating the kinetic parameters of devolatilization are presented. Firstly, the codes used for estimating the weight loss profiles using the Gaussian distribution method are presented. Secondly, the elaborate codes used for the matrix inversion algorithm are presented. Any comments preceded by % are part of a description and do not actually belong to the code.

A.1 Distributed Activation Energy Model: Gaussian Distribution of Activation Energy

% DAEM using Miura's method

```
function Vmodel = miura2()
```

```
clear;
```

```
clc;
```

```
format short
```

```
global E T1 T2 T3 T4 alpha beta H1 H2 H3 H4
```

```
alpha = exp(16.209);
```

```
beta = 0.068;
```

% Heating rate, C/min

```
H1 = 5;
```

```
H2 = 10; H3 = 20; H4 = 40;
```

% Initial Temperature, K

```
To = 400.5;
```

```
[E] = xlsread('SBrates_miura.xls','Data','A5:A24'); % Obtained Activation Energy, KJ/mol
```

```
[Vexp] = xlsread('SBrates_miura.xls','Data','g5:g24'); % Exp weight loss
```



```

n = size(E);

[T1] = xlsread('SBrates_miura.xls','Data','c5:c24');
[T2] = xlsread('SBrates_miura.xls','Data','d5:d24');
[T3] = xlsread('SBrates_miura.xls','Data','e5:e24');
[T4] = xlsread('SBrates_miura.xls','Data','f5:f24');

z1 = zeros(size(E));
z2 = zeros(size(E));
z3 = zeros(size(E));
z4 = zeros(size(E));

Ko = zeros(size(E));

int1 = zeros(size(E));
int2 = zeros(size(E));
int3 = zeros(size(E));
int4 = zeros(size(E));

Vmodel = zeros(size(E));
for i=1:size(E)

    z1(i) = quadgk(@temp, To, T1(i));
    z2(i) = quadgk(@temp, To, T2(i));
    z3(i) = quadgk(@temp, To, T3(i));
    z4(i) = quadgk(@temp, To, T4(i));

```

```

Ko(i) = alpha*exp(E(i)*beta) ;
int1(i) = -(Ko(i)/H1)*z1(i);
int2(i) = -(Ko(i)/H2)*z2(i);
int3(i) = -(Ko(i)/H3)*z3(i);
int4(i) = -(Ko(i)/H4)*z4(i);
Vmodel(i)= quadgk(@integral,0,E(i));
End

plot(T1,Vexp,'-r',T2,Vexp,'-b',T3,Vexp,'-g',T4,Vexp,'-c',
T1,Vmodel,'or',T2,Vmodel,'ob',T3,Vmodel,'og', T4,Vmodel,'oc')

title('Comparison of Experimental and Calculated V/Vf for Sub-Bituminous Coal')
xlabel('Temperature, K')
ylabel('V/Vf')
legend('5 C/min', '10 C/min','20 C/min','40 C/min')

function y = temp(T)
global E
for i=1:size(E)
y=exp(-E(i) *1000./(8.314*T)); % The exponential term
end

function p = integral(X)
global E

% Parameters obtained from logistic distribution
fo = 0.000298051;

```

```

A=0.84114;
w=123.06867;
Ec=267.37791;
p = zeros(size(E));
for i=1:size(E)
    p =(((fo + (A/(1.2533*w))*exp(-2*((X-Ec)/w).^2)))));
end

```

The same code is used for determining the weight loss profiles of all feedstock materials by inputting the required data sets of those particular feedstocks.

A.2 Matrix Inversion Algorithm

The codes presented here are shown for DECS-38 sub-bituminous coal only as an illustration. The same codes are used for estimating the kinetic parameters of all other feedstocks, both single fuels as well as blended feedstocks, by inputting the appropriate TGA data sets at different heating rates.

1. Matmodel2: This code uses the inversion algorithm described in Chapter 2 and calculates the values of activation energy, pre-exponential factor and initial mass fraction of each reaction occurring during devolatilization. This code is a part of several other codes used in the calculation of these kinetic parameters. Both real TGA data and simulated data can be used in this code.

```
function c= Matmodel2(T1,T2,B,Tr,xx,B1,B2,T0)
```

```
% T1 and T2 are the temperature data sets corresponding to the values of X
```

```

% for the specified number of reactions.

% B1 and B2 are the heating rates corresponding to T1 and T2

% Tr is the reduced set of temperature data selected for the calculation of PE.

% B is the heating rate corresponding to Tr

% xx is the set of X values chosen by specifying the number of reactions

warning off

options2=optimset('MaxIter',100000,'TolFun',1e-4,'TolX',1e-
4,'MaxFunEvals',100000);

% This defined the error tolerance of the calculations

n=length(T1); % This specifies how many calculations there will be for E and PE

for i=1:n

E(i)=fminbnd('AEerror2',0,1200,options2,T1(i),T2(i),T0,B1,B2);

% This applies the built-in solver 'FMINBND' to the program 'AEerror2' with the
% specified parameters. The minimum and maximum values of E that can be found
by iteration

% are 0 and 1200 respectively. Options2 defines the tolerance of the iteration.

PE(i)=Ai2(E(i),T1(i),T2(i),T0,B1,B2);

```

```
% This uses the code Ai2 with the specified parameters to calculate the value of PE
using the calculated value of E
```

```
PE(1)=0.0000001; % Initial guess for PE
```

```
chi_check20(i)=chi(E(i),PE(i),T1(i),T0,B,B2);
```

```
chi_check100(i)=chi(E(i),PE(i),T2(i),T0,B,B2);
```

```
% the above two commands provide a check of the matrix  $\Psi$ .
```

```
end
```

```
check=[chi_check20' chi_check100']
```

```
a=isfinite(PE'); % This find all the finite values of PE
```

```
PE=PE(a);
```

```
E=E(a);
```

```
q=length(Tr); % reduces no of data points in TGA set
```

```
npoints=q;
```

```
nn=length(E);
```

```
Tr1i=Tr;
```

```
for i=1:npoints
```

```
for j=1:nn
```

```

term1(j)=quad(@term,T0,Tr1i(i),[],[],E(j));
chi1(i,j)=exp((-PE(j)/B)*(term1(j)));
chi1(i,nn+1)=1;
chi_1(i,j)=chi(E(j),PE(j),Tr1i(i),T0,B,B2); %Uses the code 'chi' to create  $\chi$ 
chi_1(i,nn+1)=1;
end
end

% The above loop creates the chi matrix using the obtained E and PE. The function
'term'
% represents the temperature integral.

options3=optimset('TolX',10);
f0=lsqnonneg(chi_1,xx) %This uses matrix inversion to calculate the values of f0.
m=100;
T=linspace(T0,1167,m);
for i=1:m
for j=1:nn
term1(j)=quad(@term,T0,T(i),[],[],E(j));

chi2(i,j)=exp((-PE(j)/B1)*(term1(j)));
chi2(i,nn+1)=1;
chi_2(i,j)=chi(E(j),PE(j),T(i),T0,B,B2); % Uses the code 'chi' to create  $\chi$ 
chi_2(i,nn+1)=1;

```

```
end
```

```
end
```

```
% This loop creates the chi matrix for the other heating rate.
```

```
[length(f0) length(E') length(PE')];
```

```
E(n+1)=0;PE(n+1)=0;
```

```
% This defined the last E and PE values as 0 since they represent ash.
```

```
c=[f0 E' PE'];
```

```
% The final output of this code. These are the values of f0, E and PE for each  
reaction.
```

2. AError2: This function solves each term of the temperature integral defined in Chapter 3 using the inbuilt EXPINT function.

```
function error = AError2(E,T1,T2,T0,B1,B2)
```

```
% This uses the EXPINT function to find the integral from X to inf of exp(-t)/t dt
```

```
R=8.314; % Universal gas constant in j/molK
```

```
% Each term in the temperature integral is defined here.
```

```
first=T0*exp(-E*1000/(R*T0));
```

```

aa=E*1000/(R*T0);
bb=exp(-aa)/aa;
second=(-E*1000/R)*expint(aa);
third=T1*exp(-E*1000/(R*T1));
cc=E*1000/(R*T1);
dd=exp(-cc)/cc;
fourth=(E*1000/R)*expint(cc);
fifth=first;
sixth=second;
seventh=T2*exp(-E*1000/(R*T2));
ee=E*1000/(R*T2);
ff=exp(-ee)/ee;
eighth=(E*1000/R)*expint(ee);
ls=(1/B1)*(first-second-third+fourth); %LHS of EQ 2.17
rs=(1/B2)*(fifth-sixth-seventh+eighth); %RHS of EQ 2.17
error = sqrt((1-rs/ls)^2);

```

3. A_{i2} : The value of pre-exponential factor is estimated using this code by combining Eq. 3.3.6 through Eq. 3.3.10 of Chapter 3.

```

function y = Ai2(E,T1,T2,T0,B1,B2)
R=8.314; % Universal gas constant in j/molK
% terms in Eq 3.26

```



```

first=T0*exp(-E*1000/(R*T0));
aa=E*1000/(R*T0);
bb=exp(-aa)/aa;
second=(E*1000/R)*expint(aa);
third=T1*exp(-E*1000/(R*T1));
cc=E*1000/(R*T1);
dd=exp(-cc)/cc;
fourth=(E*1000/R)*expint(cc);
Ai=-B1/(first-second-third+fourth);
y=Ai;

```

4. Chi: This code calculates the matrix Ψ described in Chapter 3.

```

function error = chi(E,PE,T2,T0,B1,B2);

% This uses the approximation for integral from X to inf of exp(-t)/t dt to
% create the matrix chi.

A=PE;

R=8.314; % Universal gas constant in j/molK

first=T0*exp(-E*1000/(R*T0));
aa=E*1000/(R*T0);bb=exp(-aa)/aa;
second=(E*1000/R)*expint(aa);

third=T2*exp(-E*1000/(R*T2));

```

```

cc=E*1000/(R*T2);dd=exp(-cc)/cc;
fourth=(E*1000/R)*expint(cc);
rhs=(A/B1)*(first-second-third+fourth);
error = exp(rhs);

```

5. Term:

% This code simply defines the exponential term 'exp(-E/RT)

```

function y=term(T,E)
y=exp(-E*1000./(8.314*T)); % The exponential term

```

6. Orates: The TGA curves for known and unknown heating rates are created using this code. The kinetic parameters obtained using Matmodel.m are used as inputs to this code. The matrix Ψ is created and mass fraction remaining is obtained by multiplying with mass fraction associated with each reaction.

```

function z=orates(f0,T0,E,PE,b,Tup,m)
% b is the heating rate in K/min
% Tup is the maximum temperature that the curve should reach
% m is the number of points on the curve

B=b/60; %K/sec
s=size(E');

```

```

nn=s(:,1);
T=linspace(T0,Tup,m); % This selects a number of evenly spaced temperature
points
for i=1:m
for j=1:nn
term1(j)=quad(@term,T0,T(i),[],[],E(j));
chi2(i,j)=exp((-PE(j)/B)*(term1(j)));
chi2(i,nn+1)=1;
end
end
% This loop creates the matrix chi using kinetic and temperature data

M=chi2*f0
z=[T' M]

x=z(:,1);y=100.*z(:,2);
deriv=-diff(y)./diff(x) % This calculates the discreet derivatives of the data sets
x=x(2:length(x));
hold on
plot(x,deriv,'m--') % This plots the derivative curve on the same axes
ylabel('Derivative Mass Fraction Remaining')
plot(T,M,'b.') % This plots the TGA curve

```

7. Pyrolysis: This code applies the DAEM algorithm to actual TGA data. Data from any two heating rates can be used as input to this code.

```
function c = pyrolysis()

clear;

clc;

% Heating Rates, C/min

b1=5;

b2=40;

B1=b1/60; % heating rate K/sec

B2=b2/60; % heating rate K/sec

T0=300; % Initial temp

R=8.314; %j/molK

nrxns=50;

rnTGA=100;

% Real TGA data for lower heating rate

[TT1,Temp1,alldata] = xlsread('SBrates.xls','5 C min','d154:d18220'); % Temp
Data

[x1,MF1,alldata] = xlsread('SBrates.xls','5 C min','h154:h18220'); % Weight loss
data

% Real TGA data for higher heating rate

[TT2,Temp2,alldata] = xlsread('SBrates.xls','40 C min','d167:d6726');

[x2,MF2,alldata] = xlsread('SBrates.xls','40 C min','h167:h6726');
```

```
Tr1=linspace(TT1(1),TT1(length(TT1)),rnTGA)'; % reducing TGA points
```

```
Tr2=linspace(TT2(1),TT2(length(TT2)),rnTGA)'; % reducing TGA points
```

```
Xr1=interp1q(TT1,x1,Tr1);
```

```
Xr1(1)=0.998;
```

```
Xr2=interp1q(TT2,x2,Tr2);
```

```
Xr2(1)=0.998;
```

```
Xr2(end)=0.56;
```

```
% %Initial and end values need to be specified to allow calculations
```

```
TT1=Tr1;
```

```
TT2=Tr2;
```

```
x1=Xr1
```

```
x2=Xr2
```

```
x1(length(x1))=x1(length(x1)-1);
```

```
X=linspace(0.998,0.56,nrxns)' % Choosing conversions
```

```
T1=interp1q(flipud(x1),flipud(TT1),X);
```

```
T2=interp1q(flipud(x2),flipud(TT2),X);
```

```

plot(T1,X,'go')

hold on

plot(T2,X,'ro')

plot(TT1,x1,'g')

plot(TT2,x2,'r')

deriv1=-100*diff(x1)./diff(TT1)

Tt1=TT1(2:length(TT1));

deriv2=-100*diff(x2)./diff(TT2)

Tt2=TT2(2:length(TT2));

plot(Tt1,deriv1,'g')

plot(Tt2,deriv2,'r')

Xtga=x1; % Data for either heating rate may be used to calculate E and PE

data3=Matmodel2(T1,T2,B1,Tr1,Xtga,B1,B2,T0) % Applying DAEM algorithm
to data

f0=data3(:,1)

E=data3(:,2)

PE=data3(:,3)

c=[f0 E PE];

% Plotting kinetic parameters as a function of conversion

f0=f0(1:50);

```

```
X=X(1:50);  
figure(2);  
stem(X,f0)  
xlabel('Mass Fraction Remaining');  
ylabel('f0, Mass Fraction of Fuel Associated with Reaction');
```

```
E=E(1:50); X=X(1:50);  
figure(3);  
stem(X,E)  
xlabel('Mass Fraction Remaining');  
ylabel('E (KJ/mol)');
```

```
PE=PE(1:50);  
X=X(1:50);  
figure(4);hold on  
stem(X,PE,'b')  
xlabel('Mass Fraction Remaining');  
ylabel('A (/sec)');
```

8. Pyrolysis1: This code is used for estimating the weight loss profiles at unknown heating rates not used in the algorithm. The kinetic parameters obtained for real TGA data at known heating rates using previous codes are used as inputs to this code.

```
function c = pyrolysis1()
```

```
% nrxns is the number of points at which to calculate the kinetics, or the number of  
reactions
```

```
% rnTGA is the number of points that the TGA data should be reduced to
```

```
% nTGA is the number of points that orates.m uses to create the data
```

```
% b1 and b2 are the heating rates used in K/min
```

```
clear;
```

```
clc;
```

```
b1=10;
```

```
b2=20;
```

```
B1=b1/60;
```

```
B2=b2/60;
```

```
T0=300;
```

```
R=8.314; % Universal gas constant in j/molK
```

```
nTGA=100;
```

```
rnTGA=100;
```

```
f0= [0.54894922    0.00370381    0.021526785    0.007376867    0.006970187  
      0.026344887    0.016856559    0.011701375    0.022369799    0.012156829
```


0.022985722	0.019675679	0.007490796	0.042997369	0.003156278
0.027915627	0.011575587	0.0097363	0.014827114	0.004765505
0.010518342	0.008007697	0.008804414	0.008575667	0.00905741
0.008390065	0.009093133	0.00779559	0.009968905	0.007247496
0.011794159	0.005119809	0.008592462	0.012718192	0.030654896

0]';

E = [293.810372 523.6464203 439.7116109 4.85895261 92.83742045

66.94006184 59.85523809 223.0812877 1199.999906 24.80397376

41.08870387 100.0708152 119.5127056 182.4481902 197.6091577

243.7077374 262.3374918 305.2370132 330.345946 356.970629

382.4309661 403.9481959 410.872351 398.9204904 376.3977433

350.659064 328.0705123 305.8166101 284.0888109 263.640219

245.7139639 230.57669 216.8757918 200.5473982 141.6867706];

PE= [1.00E-07 6.34E+87 1.45E+73 0.026853079 1.11335E+12

34108032.39 1896602.687 1.18E+28 1.20E+156 1.795308473

18.96809319 612261.6267 15991778.85 3.93468E+11 4.2429E+12

4.97E+15 8.43E+16 5.16E+19 2.06E+21 9.46E+22

3.14E+24 4.80E+25 6.35E+25 4.05E+24 5.06E+22

4.04E+20 5.55E+18 8.62E+16 1.57E+15 3.71694E+13

1.34296E+12 74485045041 5207872042 278720029.2 38041.67707];

% Kinetic Parameters obtained using known heating rates

```
data1=orates(f0,T0,E,PE,B1*60,1200,nTGA); % Generates TGA data at heating  
rate B1
```

```
TT1=data1(:,1); x1=data1(:,2); % Defines temperature and weight percent data sets
```

```
data2=orates(f0,T0,E,PE,B2*60,1200,nTGA); % Generates TGA data at heating  
rate B2
```

```
TT2=data2(:,1); x2=data2(:,2); % Defines temperature and weight percent data  
sets
```

```
c = [data1 data2]; % Temperature and weight loss data at unknown heating rates
```

```
deriv1=-100*diff(x1)./diff(TT1)
```

```
Tt1=TT1(2:length(TT1))';
```

```
deriv2=-100*diff(x2)./diff(TT2)
```

```
Tt2=TT2(2:length(TT2))';
```

```
plot(Tt1,deriv1,'g')
```

```
plot(Tt2,deriv2,'r')
```

REFERENCES

1. Abhijit Bhagavatula, *Hydrogenation of Naphthalene and Coal Tar Distillate over Ni/Mo/Al₂O₃ Catalyst in a Trickle Bed Reactor*, in *Department of Chemical Engineering*. 2009, West Virginia University.
2. Sumesh Sukumara, *A Multidisciplinary Techno-Economic Decision Support Tool for Validating Long-Term Economic Viability of Biorefining Processes*, in *Chemical and Materials Engineering*. 2014, University of Kentucky: Lexington, KY, USA.
3. Qixiang Xu, *Investigation of Co-Gasification Characteristics of Biomass and Coal in Fluidized Bed Gasifiers*, in *Chemical and Process Engineering*. 2013, University of Canterbury: Christchurch, NZ.
4. Y. Feng, B. Xiao, K. Goerner, G. Cheng, and J. Wang, *Influence of Particle Size and Temperature on Gasification Performance in Externally Heated Gasifier*. *Smart Grid and Renewable Energy*, 2011. **2**(2): p. 158-164.
5. C. J. Campbell, *Oil Shock*. *Energy World*, 1996. **240**: p. 7-12.
6. S. A. Korpela, *Oil Depletion in the World*. *Current Science*, 2006. **91**(9): p. 1148-1152.
7. S. Lee, Speight, J. G., and Loyalka, S. K., *Handbook of Alternative Fuel Technologies*. 2007, Boca Raton: : CRC Press, c2007.
8. Murray Silk, Mark Ackiewicz, John Anderson, and Olayinka Ogunsola, *Overview of Fundamentals of Synthetic Ultraclean Transportation Fuel Production*, in *Ultraclean Transportation Fuels*. 2007, American Chemical Society: Washington, DC.
9. U.S. EIA. *U.S. Coal Supply and Demand, 2009 Review*. 2010; Available from: http://www.eia.gov/energyexplained/index.cfm?page=coal_home#tab2.
10. *Potential Contributions of Bio-Energy to the World's Future Energy Demand*. 2007, International Energy Agency (IEA): Paris, France.
11. T. M. Letcher, *Future Energy: Improved, Sustainable and Clean Options for Our Planet*. 1st ed. 2008, Oxford, U.K: Elsevier Ltd.
12. Aime Tchapda and Sarma Pisupati, *A Review of Thermal Co-Conversion of Coal and Biomass/Waste*. *Energies*, 2014. **7**(3): p. 1098-1148.
13. *Annual Energy Outlook 2013 with Projections to 2040*, U.S.E.I.A. (EIA), Editor. 2013: Washington, DC, USA.

14. *21st Century Coal Advanced Technology and Global Energy Solution*. 2013, International Energy Agency (IEA): Paris, France.
15. *World Energy Outlook 2013*. 2013, International Energy Agency (IEA). Paris, France.
16. M. Balat, *Influence of Coal as an Energy Source on Environmental Pollution*. Energy Sources, Part A: Recovery, Utilization, and Environmental Effects, 2007. **29**(7): p. 581-589. DOI: 10.1080/15567030701225260.
17. C. Di Blasi, *Modeling Chemical and Physical Processes of Wood and Biomass Pyrolysis*. Progress in Energy and Combustion Science, 2008. **34**(1): p. 47-90. DOI: 10.1016/j.pecs.2006.12.001.
18. Ke Liu., Chunshan Song., and Velu Subramani., *Hydrogen and Syngas Production and Purification Technologies*. 2010, John Wiley and Sons, Inc.
19. Ruksana Moreea-Taha, *Modelling and Simulation for Coal Gasification*, in *IEA Coal Research*. 2000. p. 50.
20. Prabir Basu, *Biomass Gasification and Pyrolysis: Practical Design and Theory*. 2010, Elsevier Inc.
21. Eric D. Larson Thomas G. Kreutz, Guangjian Liu, Robert H. Williams, *Fischer-Tropsch Fuels from Coal and Biomass*, in *25th Annual International Pittsburgh Coal Conference*. 2008: Pittsburgh, Pennsylvania, USA.
22. Guangjian Liu, Eric D. Larson, Robert H. Williams, Thomas G. Kreutz, and Xiangbo Guo, *Making Fischer–Tropsch Fuels and Electricity from Coal and Biomass: Performance and Cost Analysis*. Energy & Fuels, 2010. **25**(1): p. 415-437. DOI: 10.1021/ef101184e.
23. Stanislav V. Vassilev, David Baxter, Lars K. Andersen, and Christina G. Vassileva, *An Overview of the Chemical Composition of Biomass*. Fuel, 2010. **89**(5): p. 913-933. DOI: <http://dx.doi.org/10.1016/j.fuel.2009.10.022>.
24. S. Van Loo, Koppejan, J., *The Handbook of Biomass Combustion and Co-Firing*. 2008, London-Sterling (VA): Earthscan. 442 p.
25. Robert. C. Brown, *Biorenewable Resources: Engineering New Products from Agriculture*. 1 ed. 2003: Blackwell Publishing.
26. Rohan Fernando, *Co-Gasification and Indirect Co-Firing of Coal and Biomass*. 2009.
27. *America's Energy Future Panel on Alternative Transportation Fuels, Liquid Transportation Fuels from Coal and Biomass: Technological Status, Costs, and Environmental Impacts*. 2009, Washington, D.C.: The National Academic Press.

28. S Schuck, *Biomass as an Energy Source*. Int. J. Environ. Stud., 2006. **63**(6): p. 823-835.
29. Peter McKendry, *Energy Production from Biomass (Part 1): Overview of Biomass Bioresource technology*, 2002. **83**(1): p. 37-46. DOI: [http://dx.doi.org/10.1016/S0960-8524\(01\)00118-3](http://dx.doi.org/10.1016/S0960-8524(01)00118-3).
30. M. Sami, K. Annamalai, and M. Wooldridge, *Co-Firing of Coal and Biomass Fuel Blends*. Progress in Energy and Combustion Science, 2001. **27**(2): p. 171-214. DOI: [http://dx.doi.org/10.1016/S0360-1285\(00\)00020-4](http://dx.doi.org/10.1016/S0360-1285(00)00020-4).
31. R.D. Perlack, Stokes, B.J. (Leads), *U.S. Billion-Ton Update: Biomass Supply for a Bioenergy and Bioproducts Industry*. 2011, U.S. Department of Energy. : Oak Ridge National Laboratory, Oak Ridge, TN. p. 227
32. *Biomass Combined Heat and Power: Catalog of Technologies* September 2007: U.S. Environmental Protection Agency p. 122.
33. Gerardo Gordillo, Kalyan Annamalai, and Nicholas Carlin, *Adiabatic Fixed-Bed Gasification of Coal, Dairy Biomass, and Feedlot Biomass Using an Air–Steam Mixture as an Oxidizing Agent*. Renewable Energy, 2009. **34**(12): p. 2789-2797. DOI: 10.1016/j.renene.2009.06.004.
34. Colomba Di Blasi, Gabriella Signorelli, and Giuseppe Portoricco, *Countercurrent Fixed-Bed Gasification of Biomass at Laboratory Scale*. Industrial and Engineering Chemistry Research, 1999. **38**(7): p. 2571-2581.
35. D.L. Klass, *Biomass for Renewable Energy, Fuels, and Chemicals*. 1998, San Diego: Academic Press.
36. M.J Prins, J.P Krzysztow, and F.J.J.G. Janssen, *From Coal to Biomass Gasification: Comparison of Thermodynamic Efficiency*. Energy, 2007. **32**: p. 1248-1259.
37. Jiachuan Bu, *Kinetic Analysis of Coal and Biomass Co-Gasification with Carbon Dioxide*. 2009, West Virginia University.
38. B. Sven and J. Martina, *Carbon Dioxide Capture and Storage—Liability for Non-Permanence under the Unfccc*. Int. Environ. Agreem. Polit. Law Econ., 2006. **6**: p. 173-186.
39. A. Stangeland, *A Model for the CO₂ Capture Potential*. Int. J. Greenh. Gas Control, 2007. **1**: p. 418-429.
40. A.G. Collot, Y. Zhuo, D.R. Dugwell, and . R. Kandiyoti, *Co-Pyrolysis and Co-Gasification of Coal and Biomass in Bench-Scale Fixed Bed and Fluidised Bed Reactors*. Fuel, 1999. **78**: p. 667-679.

41. Rohan Fernando, *Fuels for Biomass Co-Firing*, in *IEA Coal Research*. 2005: London, UK. p. 37.
42. Olayinka Ogunsola and Isaac Gamwo, *Ultraclean Transportation Fuels*. Vol. 959. 2007: American Chemical Society.
43. Richard C. Baliban, Josephine A. Elia, and Christodoulos A. Floudas, *Toward Novel Hybrid Biomass, Coal, and Natural Gas Processes for Satisfying Current Transportation Fuel Demands, 1: Process Alternatives, Gasification Modeling, Process Simulation, and Economic Analysis*. *Ind. Eng. Chem. Res.*, 2010. **49**: p. 7343–7370.
44. Burtron H. Davis, *Fischer-Tropsch Synthesis: Overview of Reactor Development and Future Potentialities*. Prepr. Pap.-Am. Chem. Soc., Div. Fuel Chem. , 2003. **48**(2).
45. M. Ojeda, R. Nabar, A. U. Nilekar, A. Ishikawa, M. Mavrikakis, and E. Iglesia, *Co Activation Pathways and the Mechanism of Fischer-Tropsch Synthesis*. *Journal of Catalysis*, 2010. **272**(2): p. 287-297. DOI: DOI 10.1016/j.jcat.2010.04.012.
46. Ragnar Warnecke, *Gasification of Biomass: Comparison of Fixed Bed and Fluidized Bed Gasifier*. *Biomass and Bioenergy*, 2000. **18**: p. 489-497.
47. Christopher Higman and Maarten van der Burgt, *Gasification*. 2007.
48. A. K. Sadhukhan, P. Gupta, T. Goyal, and R. K. Saha, *Modelling of Pyrolysis of Coal-Biomass Blends Using Thermogravimetric Analysis*. *Bioresource technology*, 2008. **99**(17): p. 8022-6. DOI: 10.1016/j.biortech.2008.03.047.
49. S Dutta, C.Y Wen, and R.J. Belt, *Reactivity of Coal and Char: In Carbon Dioxide Atmosphere*. *Industrial and Engineering Chemistry Process Design and Development*, 1977. **16**(1): p. 20-30.
50. J. L. Figueiredo and J. A. Moulijn, *Carbon and Coal Gasification: Science and Technology*. *Nato Asi Series Series E, Applied Sciences*. 1986, Dordrecht ; Boston: Martinus Nijhoff : Distributors for the U.S. and Canada, Kluwer Academic Publishers, Hingham, MA. 655 p.
51. A Kristiansen, *Understanding Coal Gasification*, in *IEA Coal Research*. 1996: London, UK.
52. D.B. Anthony and J.B. Howard, *Coal Devolatilization and Hydrogasification*. *AIChE*, 1976. **22**(4): p. 625-656.
53. Federica Lippi Enrico Biagini, Luigi Petarca, Leonardo Tognotti, *Devolatilization Rate of Biomasses and Coal-Biomass Blends: An Experimental Investigation*. *Fuel*, 2002. **81**: p. 1041-1050.

54. Yiping Wang Junqing Cai, Limin Zhou, Qunwu Huang, *Thermogravimetric Analysis and Kinetics of Coal/Plastic Blends During Co-Pyrolysis in Nitrogen Atmosphere*. Fuel Processing Technology, 2008. **89**: p. 21-27.
55. Edwige Sima-Ella, Gang Yuan, and Tim Mays, *A Simple Kinetic Analysis to Determine the Intrinsic Reactivity of Coal Chars*. Fuel, 2005. **84**(14-15): p. 1920-1925. DOI: 10.1016/j.fuel.2005.03.022.
56. A. W. Coats and J. P. Redfern, *Kinetic Parameters from Thermogravimetric Data*. Nature, 1964. **201**(491): p. 68-69.
57. S. Yaman and H. Haykiri-Acma, *Synergy in Devolatilization Characteristics of Lignite and Hazelnut Shell During Co-Pyrolysis*. Fuel, 2007. **86**(3): p. 373-380. DOI: 10.1016/j.fuel.2006.07.005.
58. T. Hatakeyama and F.X Quinn, *Thermal Analysis – Fundamentals and Applications to Polymer Science*. 1999, Chichester.: John Wiley and Sons. .
59. Christopher Higman and Maarten van der Burgt, *Gasification*. 2008, Elsevier Inc
60. S. S. Idris, N. Abd Rahman, K. Ismail, A. B. Alias, Z. Abd Rashid, and M. J. Aris, *Investigation on Thermochemical Behaviour of Low Rank Malaysian Coal, Oil Palm Biomass and Their Blends During Pyrolysis Via Thermogravimetric Analysis (Tga)*. Bioresource technology, 2010. **101**(12): p. 4584-92. DOI: 10.1016/j.biortech.2010.01.059.
61. Yanqiu Sun, Arnab Mukherjee, Oleksandr Kuznetsov, Ryan Thaner, Lawrence B. Alemany, and W. E. Billups, *Functionalization by Reductive Alkylation and Mapping of a Sub-bituminous Coal by Energy Dispersive X-Ray Spectroscopy*. Energy & Fuels, 2011. **25**(4): p. 1571-1577. DOI: 10.1021/ef200106g.
62. M. Jeguirim and G. Trouve, *Pyrolysis Characteristics and Kinetics of Arundo Donax Using Thermogravimetric Analysis*. Bioresource technology, 2009. **100**(17): p. 4026-31. DOI: 10.1016/j.biortech.2009.03.033.
63. J. Cai, Y. Wang, L. Zhou, and Q. Huang, *Thermogravimetric Analysis and Kinetics of Coal/Plastic Blends During Co-Pyrolysis in Nitrogen Atmosphere*. Fuel Processing Technology, 2008. **89**(1): p. 21-27. DOI: 10.1016/j.fuproc.2007.06.006.
64. H. B. Vuthaluru, *Investigations into the Pyrolytic Behaviour of Coal/Biomass Blends Using Thermogravimetric Analysis*. Bioresource technology, 2004. **92**(2): p. 187-195. DOI: 10.1016/j.biortech.2003.08.008.
65. Akinwale O. Aboyade, Johann F. Görgens, Marion Carrier, Edson L. Meyer, and Johannes H. Knoetze, *Thermogravimetric Study of the Pyrolysis Characteristics and Kinetics of Coal Blends with Corn and Sugarcane Residues*. Fuel Processing Technology, 2013. **106**: p. 310-320. DOI: 10.1016/j.fuproc.2012.08.014.

66. E. Biagini, F. Lippi, L. Petarca, and L. Tognotti, *Devolatilization Rate of Biomasses and Coal-Biomass Blends: An Experimental Investigation*. Fuel, 2002. **81**(8): p. 1041-1050.
67. S. Yaman and H. Haykiri-Acma, *Interaction between Biomass and Different Rank Coals During Co-Pyrolysis*. Renewable Energy, 2010. **35**(1): p. 288-292. DOI: 10.1016/j.renene.2009.08.001.
68. C. Meesri and B. Moghtaderi, *Lack of Synergetic Effects in the Pyrolytic Characteristics of Woody Biomass/Coal Blends under Low and High Heating Rate Regimes*. Biomass & Bioenergy, 2002. **23**(1): p. 55-66. DOI: Pii S0961-9534(02)00034-X
69. A.K. Sadhukhan, Gupta, P., Saha, R.K., *Modeling and Experimental Studies on Pyrolysis of Biomass Particles*. Journal of Analytical and Applied Pyrolysis, 2008. **81**: p. 183-192.
70. P. Ahuja, S. Kumar, and P.C. Singh, *A Model for Primary and Heterogeneous Secondary Reactions of Wood Pyrolysis*. Chemical Engineering Technology, 1996. **19**: p. 272-282.
71. W.D. Jong, Nola, G.Di., Venneker, B.C.H., Spliethoff, H., Wojtowicz, M.A., *TG-FTIR Pyrolysis of Coal and Secondary Biomass Fuels: Determination of Pyrolysis Kinetic Parameters for Main Species and NO_x Precursors*. Fuel, 2007. **86**: p. 2367-2376.
72. C.A. Koufopoulos, Papayannakos, N., *Modeling of the Pyrolysis of Biomass Particles: Studies on Kinetics Thermal and Heat Transfer Effects*. Canadian Journal of Chemical Engineering, 1991. **69**: p. 907-915.
73. L. Zhou, Wang, Y., Huang, Q., Cai, J., *Thermogravimetric Characteristics and Kinetics of Plastic and Biomass Blends Co-Pyrolysis*. Fuel Processing Technology, 2006. **87**: p. 963-969.
74. Homer E Kissinger, *Reaction Kinetics in Differential Thermal Analysis*. Analytical Chemistry, 1957. **29**(11): p. 1702-1706.
75. Eli S. Freeman and Benjamin Carroll, *The Application of Thermoanalytical Techniques to Reaction Kinetics: The Thermogravimetric Evaluation of the Kinetics of the Decomposition of Calcium Oxalate Monohydrate*. The Journal of Physical Chemistry, 1958. **62**(4): p. 394-397. DOI: 10.1021/j150562a003.
76. A. Jerez, *A Modification to the Freeman and Carroll Method for the Analysis of the Kinetics of Non-Isothermal Processes*. Journal of Thermal Analysis, 1983. **26**(2): p. 315-318.
77. J. Feroso, B. Arias, M. V. Gil, M. G. Plaza, C. Pevida, J. J. Pis, and F. Rubiera, *Co-Gasification of Different Rank Coals with Biomass and Petroleum Coke in a*

- High-Pressure Reactor for H(2)-Rich Gas Production*. Bioresource technology, 2010. **101**(9): p. 3230-5. DOI: 10.1016/j.biortech.2009.12.035.
78. S Gopalakrishnan and R Sujatha, *Comparative Thermoanalytical Studies of Polyurethanes Using Coats-Redfern, Broido and Horowitz-Metzger Methods* Der Chemica Sinica, 2011. **2**(5): p. 103-117.
79. Shabbar Syed, Rana Qudaih, Ilham Talab, and Isam Janajreh, *Kinetics of Pyrolysis and Combustion of Oil Shale Sample from Thermogravimetric Data*. Fuel, 2011. **90**(4): p. 1631-1637. DOI: <http://dx.doi.org/10.1016/j.fuel.2010.10.033>.
80. Abhijit Bhagavatula, Gerald Huffman, Naresh Shah, and Rick Honaker, *Evaluation of Thermal Evolution Profiles and Estimation of Kinetic Parameters for Pyrolysis of Coal/Corn Stover Blends Using Thermogravimetric Analysis*. Journal of Fuels, 2014: p. 1-12. DOI: 10.1155/2014/914856.
81. Z. Li, C. Liu, Z. Chen, J. Qian, W. Zhao, and Q. Zhu, *Analysis of Coals and Biomass Pyrolysis Using the Distributed Activation Energy Model*. Bioresource technology, 2009. **100**(2): p. 948-52. DOI: 10.1016/j.biortech.2008.07.032.
82. Kouichi Miura and Taisuke Maki, *A Simple Method for Estimating $F(E)$ and $K_0(E)$ in the Distributed Activation Energy Model*. Energy and Fuels, 1998. **12**: p. 864-869.
83. C. P. Please, M. J. McGuinness, and D. L. S. McElwain, *Approximations to the Distributed Activation Energy Model for the Pyrolysis of Coal*. Combustion and Flame, 2003. **133**(1-2): p. 107-117. DOI: [http://dx.doi.org/10.1016/S0010-2180\(02\)00554-0](http://dx.doi.org/10.1016/S0010-2180(02)00554-0).
84. Stuart A. Scott, John S. Dennis, John F. Davidson, and Allan N. Hayhurst, *Thermogravimetric Measurements of the Kinetics of Pyrolysis of Dried Sewage Sludge*. Fuel, 2006. **85**(9): p. 1248-1253. DOI: <http://dx.doi.org/10.1016/j.fuel.2005.11.003>.
85. S. A. Scott, J. S. Dennis, J. F. Davidson, and A. N. Hayhurst, *An Algorithm for Determining the Kinetics of Devolatilisation of Complex Solid Fuels from Thermogravimetric Experiments*. Chemical Engineering Science, 2006. **61**(8): p. 2339-2348. DOI: <http://dx.doi.org/10.1016/j.ces.2005.11.002>.
86. Fadeela Saloojee, *Kinetics of Pyrolysis and Combustion of South African Coal Using the Distributed Activation Energy Model*, in *Faculty of Engineering and Built Environment*. 2011, University of Witwatersrand: Johannesburg.
87. H. Barkia, L. Belkbir, and S. A. A. Jayaweera, *Thermal Analysis Studies of Oil Shale Residual Carbon*. Journal of Thermal Analysis and Calorimetry, 2004. **76**(2): p. 615-622. DOI: 10.1023/B:JTAN.0000028040.16844.40.

88. Wenkui Zhu, Wenli Song, and Weigang Lin, *Catalytic Gasification of Char from Co-Pyrolysis of Coal and Biomass*. Fuel Processing Technology, 2008. **89**(9): p. 890-896. DOI: <http://dx.doi.org/10.1016/j.fuproc.2008.03.001>.
89. D. Vamvuka, E. Karouki, and S. Sfakiotakis, *Gasification of Waste Biomass Chars by Carbon Dioxide Via Thermogravimetry. Part I: Effect of Mineral Matter*. Fuel, 2011. **90**(3): p. 1120-1127. DOI: <http://dx.doi.org/10.1016/j.fuel.2010.12.001>.
90. Thinesh Vittee, *Determination of Kinetics of Char Reactivity with Carbon Dioxide Using Thermogravimetry and the Distributed Activation Energy Model*. 2012, University of Witwatersrand: Johannesburg.
91. Mandar Kulkarni and Rajive Ganguli, *Moving Bed Gasification of Low Rank Alaska Coal*. Journal of Combustion, 2012.
92. Qixiang Xu, Shusheng Pang, and Tana Levi, *Reaction Kinetics and Producer Gas Compositions of Steam Gasification of Coal and Biomass Blend Chars, Part 1: Experimental Investigation*. Chemical Engineering Science, 2011. **66**(10): p. 2141-2148. DOI: <http://dx.doi.org/10.1016/j.ces.2011.02.026>.
93. Abhijit Bhagavatula, Gerald Huffman, Naresh Shah, Christopher Romanek, and Rick Honaker., *Source Apportionment of Carbon During Gasification of Coal-Biomass Blends Using Stable Carbon Isotope Analysis*. Fuel Processing Technology, 2014. **128**: p. 83-93. DOI: <http://dx.doi.org/10.1016/j.fuproc.2014.06.024>.
94. A. J. Buczynska, B. Geypens, R. Van Grieken, and K. De Wael, *Stable Carbon Isotopic Ratio Measurement of Polycyclic Aromatic Hydrocarbons as a Tool for Source Identification and Apportionment--A Review of Analytical Methodologies*. Talanta, 2013. **105**: p. 435-50. DOI: 10.1016/j.talanta.2012.10.075.
95. D. E. Matthews and J. M. Hayes, *Isotope-Ratio-Monitoring Gas Chromatography-Mass Spectrometry*. Analytical Chemistry, 1978. **50**(11): p. 1465-1473. DOI: Doi 10.1021/Ac50033a022.
96. Tomoaki Okuda, Hidetoshi Kumata, Hiroshi Naraoka, and Hideshige Takada, *Origin of Atmospheric Polycyclic Aromatic Hydrocarbons (PAHs) in Chinese Cities Solved by Compound-Specific Stable Carbon Isotopic Analyses*. Organic Geochemistry, 2002. **33**(12): p. 1737-1745. DOI: [http://dx.doi.org/10.1016/S0146-6380\(02\)00180-8](http://dx.doi.org/10.1016/S0146-6380(02)00180-8).
97. Carole McRae, Cheng-Gong Sun, Colin E. Snape, Anthony E. Fallick, and Duncan Taylor, *$\delta^{13}C$ Values of Coal-Derived PAHs from Different Processes and Their Application to Source Apportionment*. Organic Geochemistry, 1999. **30**(8, Part 2): p. 881-889. DOI: [http://dx.doi.org/10.1016/S0146-6380\(99\)00072-8](http://dx.doi.org/10.1016/S0146-6380(99)00072-8).
98. S. H. Bottrell, P. K. K. Louie, K. D. Bartle, N. Taylor, S. Wallace, W. Kemp, and W. Steedman, *Differentiation of Forward and Back Reactions During Co-*

- Processing of Coal and Petroleum by Isotope Mass Balance Analysis*. Fuel, 1990. **69**(10): p. 1332-1333. DOI: Doi 10.1016/0016-2361(90)90300-F.
99. M. S. Lancet, R. A. Winschel, and F. P. Burke, *Stable Carbon Isotope Analysis of Coprocessing Materials*. Abstracts of Papers of the American Chemical Society, 1991. **202**: p. 71.
100. M. S. Lancet, R. A. Winschel, and F. P. Burke, *Stable Carbon-Isotope Analysis of Coprocessing Materials*. Fuel, 1993. **72**(8): p. 1209-1217. DOI: Doi 10.1016/0016-2361(93)90332-V.
101. J. G. Steer, T. Ohuchi, and K. Muehlenbachs, *Efficacy of Coal-Bitumen Co-Processing as Determined by Isotopic Mass Balance Calculations*. Fuel Processing Technology, 1987. **15**: p. 429-438. DOI: Doi 10.1016/0378-3820(87)90064-6.
102. H. Craig, *Isotopic Standards for Carbon and Oxygen and Correction Factors for Mass-Spectrometric Analysis of Carbon Dioxide*. Geochimica Et Cosmochimica Acta, 1957. **12**(1-2): p. 133-149. DOI: Doi 10.1016/0016-7037(57)90024-8.
103. J. Hoefs and E. Usdowski, *C¹³/C¹² Fractionation and Kinetics of CO₂ Absorption by Hydroxide Solutions*. Fortschritte Der Mineralogie, 1987. **65**: p. 76-81.
104. Alain Brasseur, Diano Antenucci, Jean-Marie Bouquegneau, Antoinette Coëme, Patrick Dauby, René Létolle, Marc Mostade, Pierre Pirlot, and Jean-Paul Pirard, *Carbon Stable Isotope Analysis as a Tool for Tracing Temperature During the El Tremedal Underground Coal Gasification at Great Depth*. Fuel, 2002. **81**(1): p. 109-117. DOI: [http://dx.doi.org/10.1016/S0016-2361\(01\)00114-4](http://dx.doi.org/10.1016/S0016-2361(01)00114-4).
105. S. A. Robinson and S. P. Hesselbo, *Fossil-Wood Carbon-Isotope Stratigraphy of the Non-Marine Wealden Group (Lower Cretaceous, Southern England)*. Journal of the Geological Society, 2004. **161**: p. 133-145. DOI: Doi 10.1144/0016-764903-004.
106. R. F. Follett, K. P. Vogel, G. E. Varvel, R. B. Mitchell, and J. Kimble, *Soil Carbon Sequestration by Switchgrass and No-Till Maize Grown for Bioenergy*. Bioenergy Research, 2012. **5**(4): p. 866-875. DOI: DOI 10.1007/s12155-012-9198-y.
107. A. Bechtel, R. Gratzner, R. F. Sachsenhofer, J. Gusterhuber, A. Lucke, and W. Puttmann, *Biomarker and Carbon Isotope Variation in Coal and Fossil Wood of Central Europe through the Cenozoic*. Palaeogeography Palaeoclimatology Palaeoecology, 2008. **262**(3-4): p. 166-175. DOI: DOI 10.1016/j.palaeo.2008.03.005.
108. Prakash K. Singh, M. P. Singh, P. K. Prachiti, M. S. Kalpana, C. Manikyamba, G. Lakshminarayana, Alok K. Singh, and A. S. Naik, *Petrographic Characteristics and Carbon Isotopic Composition of Permian Coal: Implications on Depositional Environment of Sattupalli Coalfield, Godavari Valley, India*. International Journal

- of Coal Geology, 2012. **90–91**(0): p. 34-42. DOI: <http://dx.doi.org/10.1016/j.coal.2011.10.002>.
109. M. J. Whiticar, *Stable Isotope Geochemistry of Coals, Humic Kerogens and Related Natural Gases*. International Journal of Coal Geology, 1996. **32**(1–4): p. 191-215. DOI: [http://dx.doi.org/10.1016/S0166-5162\(96\)00042-0](http://dx.doi.org/10.1016/S0166-5162(96)00042-0).
110. K. M. Thomas, F. Dillon, S. Bottrell, P. K. K. Louie, and K. D. Bartle, *The Use of C^{13}/C^{12} Isotope Mass-Spectrometry in the Study of the Gasification of Carbon Composite-Materials*. Carbon, 1993. **31**(2): p. 273-277. DOI: Doi 10.1016/0008-6223(93)90032-6.
111. R. A. Winschel, F. P. Burke, and M. S. Lancet, *Application of Stable Carbon Isotope Analysis to Continuous Coal Oil Coprocessing*. Abstracts of Papers of the American Chemical Society, 1990. **200**: p. 62.
112. Anne Dufaux, Bénédicte Gaveau, René Létolle, Marc Mostade, Marianne Noël, and Jean-Paul Pirard, *Heavy Water Tracing Test in the Underground Coal Gasification Process at Thulin*. Fuel, 1990. **69**(11): p. 1454-1456. DOI: [http://dx.doi.org/10.1016/0016-2361\(90\)90129-E](http://dx.doi.org/10.1016/0016-2361(90)90129-E).
113. J. C. Quick, *Carbon Dioxide Emission Factors for US Coal by Origin and Destination*. Environmental Science & Technology, 2010. **44**(7): p. 2709-2714. DOI: Doi 10.1021/Es9027259.
114. B.D Hong and E.R Slatick, *Carbon Dioxide Emission Factors for Coal in Energy Information Administration, Quarterly Coal Report*,. 1994: Washington, DC, August 1994. p. 1-8.
115. Shayan Karimipour, Regan Gerspacher, Rajender Gupta, and Raymond J. Spiteri, *Study of Factors Affecting Syngas Quality and Their Interactions in Fluidized Bed Gasification of Lignite Coal*. Fuel, 2013. **103**(0): p. 308-320. DOI: <http://dx.doi.org/10.1016/j.fuel.2012.06.052>.
116. P. Richet, Y. Bottinga, and M. Javoy, *Review of Hydrogen, Carbon, Nitrogen, Oxygen, Sulfur, and Chlorine Stable Isotope Fractionation Among Gaseous Molecules*. Annual Review of Earth and Planetary Sciences, 1977. **5**: p. 65-110. DOI: DOI 10.1146/annurev.ea.05.050177.000433.
117. M. Sato, T. Mori, Y. Shimoike, K. Nagao, and K. Notsu, *Carbon Isotope Systematics of CO_2 , CO and CH_4 in Fumarolic Gases from Satsuma-Iwojima Volcanic Island, Japan*. Earth Planets and Space, 2002. **54**(3): p. 257-263.
118. Y. Bottinga, *Calculated Fractionation Factors for Carbon and Hydrogen Isotope Exchange in the System Calcite-Carbondioxide-Graphite-Methane-Hydrogen-Water Vapor* Geochimica Et Cosmochimica Acta, 1969. **33**: p. 49-64.

119. M. Schoell, *The Hydrogen and Carbon Isotopic Composition of Methane from Natural Gases of Various Origins*. *Geochimica Et Cosmochimica Acta*, 1980. **44**(5): p. 649-661. DOI: Doi 10.1016/0016-7037(80)90155-6.

VITA

NAME: ABHIJIT BHAGAVATULA

PLACE OF BIRTH

Hyderabad, India

EDUCATION

- *Master of Science, Chemical Engineering, West Virginia University, Morgantown, WV, USA*
- *Bachelor of Technology, Chemical Engineering, Vellore Institute of Technology, Vellore, India*

CERTIFICATIONS/HONORS

- *Engineer-in-Training, West Virginia*
- *Toyota Lean Systems Student Certification, University of Kentucky*
- *Invited Reviewer for Journal of Mechanical Engineering Research*

PUBLICATIONS/ORIGINAL CONTRIBUTIONS

- *Evaluation of Thermal Evolution Profiles and Estimation of Kinetic Parameters for the Pyrolysis of Coal/Corn Stover Blends Using Thermogravimetric Analysis, Abhijit Bhagavatula*, Gerald Huffman, Naresh Shah, Rick Honaker, **Journal of Fuels**, Volume 2014, Article ID 914856, 12 pages, <http://dx.doi.org/10.1155/2014/914856>.*
- *Source Apportionment During Gasification of Coal-Biomass Mixtures Using GC-C-IRMS, Abhijit Bhagavatula*, Gerald Huffman, Naresh Shah, Christopher Romanek, Rick Honaker, **Fuel Processing Technology**, Volume 128 (2014), 83-93. <http://dx.doi.org/10.1016/j.fuproc.2014.06.024>.*
- *Comparison of Various Activation Energy Models for Estimating the Pyrolysis Kinetic Parameters of Coal-Biomass Blends, Accepted, In Press, **Bioresource Technology**.*
- *Effect of Operating Conditions on the Product Gas Compositions during Gasification of Various Coal-Biomass Blends in a Moving Bed Gasifier, Submitted Under Review, **Bioresource Technology**.*

SELECTED CONFERENCE PROCEEDINGS

- *Detailed Kinetic Modeling and Simulation of Coal/Corn Stover Mixtures in a Moving Bed Gasifier, 2013 AIChE Annual Conference, San Francisco.*
- *Modeling of Pyrolysis and Boudouard Reactions of Various Coals, Biomasses and Coal-Biomass Blends Using Thermogravimetric Analysis, Experimental Moving Bed Gasification System and Stable Carbon Isotope Ratio Mass Spectroscopy, 2012 AIChE Annual Conference, Pittsburgh.*
- *Modeling of pyrolysis and Boudouard reactions of various coals, biomasses and coal-biomass blends using thermogravimetric analysis and stable carbon isotope ratio mass spectroscopy, 2012 ICHME-Gasification 11 Conference, Cagliari, Italy.*
- *Modeling of pyrolysis and Boudouard reactions of various coals, biomasses and coal-biomass blends using thermogravimetric analysis, 243rd ACS National Meeting and Exposition, San Diego, March, 2012.*
- *Kinetics of the Hydrotreatment of Coal Tar Distillates in a Trickle Bed Reactor, International Coal Conference, Pittsburgh, September, 2008.*